



UNIVERSIDADE FEDERAL DE SANTA CATARINA
CENTRO TECNOLÓGICO
PROGRAMA DE PÓS-GRADUAÇÃO EM ENGENHARIA MECÂNICA

Marcos Paulo Nostrani

**DEVELOPMENT OF A DIGITAL ELECTRO HYDROSTATIC ACTUATOR FOR
APPLICATION IN AIRCRAFT FLIGHT CONTROL SURFACES**

Florianópolis

2020

Marcos Paulo Nostrani

**DEVELOPMENT OF A DIGITAL ELECTRO HYDROSTATIC ACTUATOR FOR
APPLICATION IN AIRCRAFT FLIGHT CONTROL SURFACES**

Tese submetido(a) ao Programa de Pós-Graduação em Engenharia Mecânica da Universidade Federal de Santa Catarina para a obtenção do título de Doutor em Engenharia Mecânica.

Orientador: Prof. Victor Juliano De Negri, Dr. Eng.

Coorientador: Prof. Anders Petter Krus, Dr. Eng.

Florianópolis

2020

Ficha de identificação da obra elaborada pelo autor,
através do Programa de Geração Automática da Biblioteca Universitária da UFSC.

Nostrani, Marcos Paulo
Development of a Digital Electro Hydrostatic Actuator
for Application in Aircraft Flight Control Surfaces /
Marcos Paulo Nostrani ; orientador, Victor Juliano De
Negri, coorientador, Anders Petter Krus, 2021.
192 p.

Tese (doutorado) - Universidade Federal de Santa
Catarina, Centro Tecnológico, Programa de Pós-Graduação em
Engenharia Mecânica, Florianópolis, 2021.

Inclui referências.

1. Engenharia Mecânica. 2. Digital Hydraulics. 3.
Hydraulic Actuators. 4. Aviation Actuators. 5. Aircraft
Control Surfaces. I. De Negri, Victor Juliano. II. Krus,
Anders Petter. III. Universidade Federal de Santa
Catarina. Programa de Pós-Graduação em Engenharia Mecânica.
IV. Título.

Marcos Paulo Nostrani

**DEVELOPMENT OF A DIGITAL ELECTRO HYDROSTATIC ACTUATOR FOR
APPLICATION IN AIRCRAFT FLIGHT CONTROL SURFACES**

Esta Tese foi julgada adequada para obtenção do Título de “Doutor em Engenharia”, e aprovada em sua forma final pelo Programa de Pós-Graduação em Engenharia Mecânica.

Florianópolis, 12 de fevereiro de 2021.

Prof. Luiz Carlos Sandoval Góes, Dr. Eng. - Relator.
Instituto Tecnológico de Aeronáutica

Prof. Amir Antônio Martins de Oliveira Júnior, Dr. Eng.
Universidade Federal de Santa Catarina

Prof. Eduardo André Perondi, Dr. Eng.
Universidade Federal do Rio Grande do Sul

Certificamos que esta é a **versão original e final** do trabalho de conclusão que foi julgado adequado para obtenção do título de doutor em Engenharia Mecânica.

Prof. Paulo de Tarso Rocha de Mendonça, Dr. Eng.
Coordenador do Programa

Prof. Victor Juliano De Negri, Dr. Eng.
Orientador – Universidade Federal de Santa Catarina

Florianópolis, 12 de fevereiro de 2021.

Este trabalho é dedicado a todos aqueles que estiveram envolvidos na sua realização: amigos, familiares e, principalmente, aos meus queridos pais, meu irmão e minha namorada.

AGRADECIMENTOS

Gostaria de agradecer primeiramente aos meus pais, por tudo que eles proporcionaram durante toda a minha vida, por me fornecerem todo o apoio durante a realização desta tese de doutorado, sempre me incentivando a nunca desistir, por todo o amor que me deram ao longo de toda minha vida, nunca deixando nada faltar, os quais sou eternamente grato pela pessoa a qual sou hoje.

Ao meu irmão Daniel e minha cunhada Bianca, por toda a amizade e companheirismo.

A minha namorada Débora, por todo apoio e companheirismo, estando sempre ao meu lado, mesmo quando estive ausente durante o doutorado sanduíche, sempre incentivando-me a fazer o meu melhor e nunca desistir, principalmente nos momentos difíceis.

Ao professor Victor Juliano De Negri, por toda dedicação e envolvimento em sua orientação no desenvolvimento desta tese, sempre colaborando com dicas e sugestões. Também por toda a amizade em todos estes anos que venho trabalhando em seu laboratório - LASHIP, na qual cresci muito profissionalmente como engenheiro e como pessoa. Muito obrigado por todas as oportunidades que o senhor me deu.

Ao meu grande amigo Luiz Alberto Galaz Mamani (*in memoriam*), por toda a sua ajuda durante a minha formação acadêmica e no meu desenvolvimento pessoal, pois sem ele eu não seria o engenheiro que sou hoje.

Aos meus amigos do LASHIP, Ivan, Artur Tozzi, Andrei, Nicodemos, Thales, Vinícius, João Pedro, Gabriel, Talles, Gregori, Nelson, Henri, Heitor, Henrique, Ruham, Túlio, Luana, Mateus, Pedro Henrique, Thomas, Rodrigo, Paulista, Tiago, Guilherme, Felipe, Paulo e tantos outros por todo apoio e amizade ao longo deste trabalho. Pelos concelhos e conversas durante os momentos bons e difíceis. Viva ao café do LASHIP.

Dentre os meus amigos do LASHIP, gostaria de dar um agradecimento especial ao Ivan Mantovani, Artur Tozzi, Pedro Henrique, Ruham Victor, Vinicius Vígolo, por toda a parceria e ajuda nos momentos bons e difíceis da elaboração desta tese. Por todo o comprometimento na construção da bancada experimental, na qual sem a ajuda de vocês eu não teria conseguido.

Aos amigos que fiz na Suécia enquanto estava no período de doutorado sanduíche, Viktor, Samuel, Alejandro, Ingo, Katharina, Peter, e tantos outros por toda amizade e companheirismo enquanto estive em seu país.

Ao professor Petter Krus, pela sua coorientação no desenvolvimento desta tese, por ter me recebido de braços abertos quanto estive em seu laboratório FLUMES da Universidade de Linköping - Suécia. Obrigado pela volta no NSX.

A empresa Saab AB por ter me proporcionado a ida até à Suécia e ter acreditado em meu trabalho.

Ao engenheiro Alessandro Dell'amico, por ter me recebido junto a empresa Saab AB e ter acreditado em minha pesquisa enquanto estive em seu país.

Ao CISB por ter me proporcionado a oportunidade de bolsa para poder fazer meu doutorado sanduíche na Suécia.

Gostaria de agradecer a empresa HYDAC e seus colaboradores Rodrigo, Cristiano e Tina, pela ajuda e fornecimento dos componentes hidráulicos para a construção da bancada de testes.

Gostaria de agradecer à empresa MEDAL Bombas e seus colaboradores Eduardo Dalla Lana, Seu Emerson e todos aqueles que estiveram envolvidos, no desenvolvimento e doação das bombas para a bancada. Muito obrigado.

A Nova Motores Elétricos pelo fornecimento dos motores elétricos.

Ao Programa de Pós-Graduação em Engenharia Mecânica da Universidade Federal de Santa Catarina.

O presente trabalho foi realizado com apoio da Coordenação de Aperfeiçoamento de Pessoal de Nível Superior – Brasil (CAPES) – Código de Financiamento 001

RESUMO

Mediante a crescente conscientização global para a redução das emissões de gases do efeito estufa, a indústria aeronáutica vem buscando soluções mais eficientes que possam ser aplicadas em suas aeronaves visando a economia de combustível. Com a demanda crescente pelo transporte aéreo, essa busca por sistemas mais eficientes aumentou consideravelmente, dando origem a conceitos como *More Electric Aircraft*, que visa a substituição dos sistemas hidráulicos e pneumáticos por sistemas puramente elétricos. No entanto, a baixa relação peso potência, alta confiabilidade, boa resposta dinâmica faz com que a tecnologia dos atuadores hidráulicos seja amplamente utilizada no controle das superfícies primárias e secundárias de controle de voo. Porém, os sistemas hidráulicos são conhecidos pela sua baixa eficiência energética, a qual é causada pelas técnicas de controle restritivo que estrangulam a passagem de fluido em orifícios de controle, e também pelos vazamentos internos nos componentes. Com o intuito de melhorar a eficiência dos sistemas hidráulicos, a hidráulica digital surge como uma nova alternativa tecnológica, onde o controle é realizado por técnicas não restritivas, através do uso de componentes hidráulicos em paralelo ou através da hidráulica de chaveamento rápido. Mediante isto, esta tese de doutorado visa o desenvolvimento de uma nova solução de atuador hidráulico para aplicação em aeronáutica utilizando hidráulica digital. A solução desenvolvida visa o uso de uma bomba digital, válvulas *on/off* e cilindros multi-câmaras. Esta solução foi denominada de *Digital Electro Hydrostatic Actuator* - DEHA em alusão aos *Electro Hydrostatic Actuators* - EHA. Para o projeto do DEHA, foi desenvolvida uma metodologia para a determinação da quantidade necessária de câmaras para o cilindro e o número de módulos binários para a bomba digital. Assim, um cilindro de quatro câmaras e uma bomba digital com três módulos binários foram utilizadas, resultando em 43 diferentes velocidades para o atuador. Com a definição do cilindro e da bomba digital, o atuador foi otimizado para um perfil de velocidades desejado utilizando um algoritmo de otimização. Para verificar a viabilidade da solução proposta, um modelo matemático utilizando os *softwares* MATLAB/Simulink e Hopsan foi elaborado. Além disso, um modelo para o EHA e outro para o SHA (*Servo Hydraulic Actuator*) foram elaborados para comparação de resultados e aferição das eficiências. Com o intuito de validar o modelo matemático, uma bancada de testes foi construída no Laboratório de Sistemas Hidráulicos e Pneumáticos - LASHIP da UFSC, onde diferentes experimentos foram realizados. Os resultados obtidos mostram que o DEHA consegue controlar a posição com erro em regime permanente de 0.27×10^{-3} m e com eficiência energética da ordem de 54%, sendo 29 vezes maior que o SHA e 1.2 vezes maior que o EHA, o que demonstra que o DEHA pode ser uma solução promissora para o desenvolvimento de atuadores hidráulicos mais eficientes.

Palavras-chave: Hidráulica digital. Atuadores hidráulicos. Atuadores para aviação, Superfícies de controle de aeronaves.

RESUMO EXPANDIDO

Introdução

Com o aumento do consumo de combustíveis provenientes de fontes não renováveis nas últimas décadas, o impacto causado por essa ação é uma das maiores preocupações de ambientalistas e governos. De acordo com Lotfalipour *et al.* (2010), a combustão de combustíveis fósseis é o maior contribuinte para as emissões de CO₂. No setor da aviação, Gössling (2010) cita que este é responsável por cerca de 1,6 a 2,2% das emissões globais de CO₂, o que significa cerca de 13% do total de emissões desse gás apenas de fontes de transporte. Terrenoire *et al.* (2019) destacam que, no ano de 2017, os voos mundiais produziram cerca de 859 milhões de toneladas de CO₂.

Atualmente, a tecnologia moderna de propulsão de aeronaves é baseada, quase que exclusivamente, no uso de motores de combustão interna (SLIWINSKI *et al.*, 2017), principalmente porque os combustíveis fósseis possuem alta densidade de energia. Devido a isto, com o desenvolvimento de sistemas aeronáuticos mais eficientes, como por exemplo os sistemas hidráulicos, é possível a redução do tamanho de componentes como trocadores de calor e tubulações, onde a combinação destas ações pode ter impacto significativo na aeronave contribuindo para um menor consumo de combustível, reduzindo as emissões de gases do efeito estufa como o CO₂.

Em aeronaves, um dos sistemas mais importantes para o controle de voo é o sistema hidráulico. Este, segundo Moir & Seabridge (2008), foi implementado pela primeira vez na aviação no início dos anos 30, tendo a vantagem de ser uma maneira eficiente de transmitir energia, onde movimentos de baixa energia do cockpit podem ser transferidos para locais de alta demanda energética (MOIR & SEABRIDGE, 2008). Esses locais são normalmente representados pelas superfícies de controle primárias e secundárias. No entanto, os sistemas hidráulicos também podem ser implementados em trens de pouso, portas de carga e sistema de direção (WARD, 2017). Porém, uma das desvantagens do uso de sistemas hidráulicos é a baixa eficiência energética, decorrente das perdas causadas pelas características de controle de pressão e vazão, que normalmente são fornecidas ao estrangular o escoamento através de orifícios de controle (controle dissipativo) e por vazamentos internos. As superfícies de controle são extremamente importantes para o bom funcionamento da aeronave em voo e, por esse motivo, os sistemas hidráulicos são uma parte essencial e a melhoria de sua eficiência energética pode trazer ganhos significativos não apenas na economia de combustível, mas também na redução do sistema de refrigeração do fluido hidráulico e tubulações.

Uma das alternativas para o melhoramento da eficiência energética dos sistemas hidráulicos é a utilização da hidráulica digital. Esta tecnologia vem ganhando espaço na comunidade acadêmica nas últimas décadas, onde estudos vem demonstrando o seu potencial para a redução do consumo de energia (UUSITALO *et al.*, 2009; WINKLER *et al.*, 2010; NOSTRANI, 2015; NOSTRANI *et al.*, 2017). Entretanto, a sua aplicação em aviação ainda está em fase embrionária, onde podem se citar os trabalhos de Belan (2018) e Dell'amico *et al.* (2018).

A partir dos benefícios que a hidráulica digital pode trazer para a redução do consumo energético de sistemas hidráulicos, nesta tese de doutorado objetiva-se o desenvolvimento de um atuador hidráulico para a aplicação em sistemas de controle de voo de aeronaves. Para isso, a solução proposta utiliza a combinação de bomba digital e cilindros multi-câmaras para o controle de velocidade e posição. Com a utilização de uma bomba digital, as perdas energéticas por vazamento interno são minimizadas. Isto acontece devido à quando uma aeronave está em voo de cruzeiro, o atuador permanece a maior parte do tempo parado. Assim, as vazões dos módulos binários de uma bomba digital são direcionadas para o reservatório a baixa pressão.

Para a projeto do atuador utilizando hidráulica digital, diretrizes foram elaboradas para o dimensionamento dos componentes (áreas do cilindro multi-câmaras e deslocamentos volumétricos da bomba digital). Além disso, um modelo matemático considerando as principais dinâmicas envolvidas dos componentes utilizados, como válvulas, cilindro e bomba, foi elaborado. Estes componentes modelados se baseiam nos utilizados na bancada experimental, a qual foi desenvolvida para a validação do modelo matemático.

Objetivos

O objetivo principal desta tese de doutorado é o desenvolvimento de um atuador hidráulico, utilizando princípios de hidráulica digital, para o controle de superfícies primárias e secundárias de controle de voo. O atuador proposto visa o uso de uma bomba digital para a unidade de conversão primária de energia, válvulas *on/off* para a unidade de limitação e controle, e para a unidade de conversão secundária um cilindro hidráulico multi-câmaras.

Com a implementação da hidráulica digital no atuador proposto, a eficiência energética pode ser aumentada com o uso de técnicas de controle de vazão e pressão não resistivas, o que proporciona a melhora do consumo de combustível da aeronave.

Como objetivos específicos tem-se, o desenvolvimento de diretrizes para o dimensionamento do atuador, a construção de um modelo matemático utilizando os softwares

MATLAB/Simulink e Hopsan, com o intuito de verificar a viabilidade do atuador desenvolvido, e por fim, a construção de uma bancada de testes para validação do modelo matemático.

Metodologia

Para a obtenção das informações existentes sobre as principais configurações de sistemas hidráulicos digitais em estudo, como também os principais sistemas de atuação de superfícies de controle de aeronaves, foram utilizados livros e artigos científicos que abordam estes temas.

Um modelo matemático utilizando os softwares MATLAB/Simulink e Hopsan foi desenvolvido para a verificação do comportamento dinâmico do atuador proposto e assim, analisar a viabilidade de sua aplicação.

Como auxílio para a validação do modelo matemático, uma bancada de testes foi desenvolvida. A partir dos resultados obtidos pela bancada, com o auxílio de um computador e um sistema de aquisição de dados, os resultados obtidos pelos experimentos foram comparados com o modelo matemático proposto, onde foi constatada a validação do mesmo.

Resultados e discussões

Com a análise das diferentes combinações de áreas que podem ser utilizadas em um cilindro multi-câmaras, dois conceitos de áreas diferentes foram elaborados. O primeiro conceito está relacionado com a área resultante, a qual é a soma das áreas de todas as câmaras que estão aumentando de volume, tanto para o movimento de avanço quanto no de recuo. As câmaras que geram a área resultante podem ser conectadas às câmaras que estão diminuindo de volume, o que promove a operação em modo regenerativo. Quando o cilindro multi-câmaras está em modo regenerativo, o segundo conceito de área é utilizado. Este, está relacionado à área equivalente, que na qual é a área resultante subtraída do valor da área da câmara que está em modo regenerativo.

A partir do uso dos conceitos de áreas resultantes e equivalentes, uma equação que correlaciona todas as possibilidades de áreas que podem ser utilizadas em um cilindro de n câmaras, onde n é um número par (2, 4, 6, 8 ...), foi desenvolvida. Com a combinação desta equação com a equação das diferentes combinações de bombas em uma bomba digital, é possível determinar o número de diferentes velocidades que o atuador desenvolvido pode proporcionar. Com isto, é possível calcular quantas câmaras o cilindro deve ter, ou o número de bombas na bomba digital, dependendo dos requisitos de projeto.

Para a obtenção dos parâmetros para o atuador digital (tamanho das áreas e deslocamentos volumétricos), um algoritmo de otimização foi desenvolvido utilizando a função

fmincon presente na biblioteca do software MATLAB. Esta função leva em consideração, as máximas e mínimas velocidades do atuador, a máxima carga externa e as pressões nas câmaras.

O atuador desenvolvido foi denominado de DEHA – *Digital Electro Hydrostatic Actuator*, em alusão ao EHA - *Electro Hydrostatic Actuator*, onde as bombas e o cilindro compreendem o atuador. O DEHA é composto por um cilindro multi-câmaras de quatro câmaras para a unidade de conversão secundária, oito válvulas *on/off* e quatro válvulas de retenção para a unidade de limitação e controle. A unidade de conversão primária é composta por uma bomba digital, a qual é composta por três módulos binários constituídos de três válvulas *on/off*, três válvulas de retenção, três bombas de deslocamento fixo e três válvulas de alívio para questões de segurança.

Com a obtenção dos parâmetros para o atuador digital, um modelo matemático foi desenvolvido considerando as principais dinâmicas dos componentes hidráulicos, os quais foram utilizados na bancada de testes.

A partir dos resultados obtidos, foi constatado que os resultados do modelo matemático apresentam comportamento semelhante aos resultados obtidos experimentalmente, tanto para a posição, quando para as pressões nas câmaras do atuador. Em regime permanente, o erro de posição atingido é de cerca de 0.27×10^{-3} m. As pressões nas câmaras do cilindro apresentam variações em relação aos resultados obtidos pelo modelo e experimentalmente. Estas variações estão associadas com as diferenças entre as dinâmicas de cada válvula utilizadas na bancada de testes e as modelas no modelo matemático, visto que as válvulas reais podem apresentar diferenças na sua fabricação. Além disso, o atrito do cilindro pode ocasionar as diferenças na pressão, visto que o atrito apresenta um comportamento não linear, a qual o modelo de atrito aplicado pode não representar tais não linearidades com precisão.

Com a validação do modelo matemático, o mesmo foi utilizado para a aferição da eficiência energética do DEHA. Além disso, mais dois modelos matemáticos foram desenvolvidos, um para o SHA – *Servo Hydraulic Actuator* e outro para o EHA, com o intuito de comparação de eficiências. Ademais, o SHA e o EHA são, atualmente, os atuadores hidráulicos mais aplicados em aeronaves.

Os resultados para a eficiência energética mostram que o DEHA é 29 vezes mais eficiente que o SHA e 1,2 vezes mais que o EHA. Em outros termos, o SHA dissipa 44 vezes mais energia do que o EHA e 52 vezes mais que o DEHA. A alta eficiência do DEHA é atribuída às reduções das perdas energéticas que ocorrem nos módulos binários da bomba digital quando o atuador não está se movendo, pois nesta condição, a vazão é direcionada para o reservatório,

que está praticamente a mesma pressão da sucção das bombas, o que reduz o diferencial de pressão e conseqüentemente o vazamento interno das bombas. No caso do SHA, para as mesmas condições, a bomba de deslocamento volumétrico variável opera com baixo deslocamento volumétrico, apenas suprindo o vazamento das servo válvulas, porém a alta pressão. Para o EHA, os resultados são semelhantes ao DEHA, onde para uma situação com o atuador parado, as perdas energéticas principais ocorrem devido ao vazamento interno da bomba.

Com os resultados obtidos pelo DEHA, fica evidenciado o seu potencial para o desenvolvimento de sistemas hidráulicos mais eficientes para aplicação em aeronaves. Porém, o seu estudo está em fase inicial, onde o melhoramento dos componentes hidráulicos e a utilização de novas técnicas de controle podem melhorar seu comportamento.

Conclusão e trabalhos futuros

Nesta tese de doutorado, uma nova topologia de atuador hidráulico, baseada na utilização da tecnologia da hidráulica digital, onde as perdas energéticas por perda de carga são minimizadas através do uso de componentes hidráulicos em paralelo, foi desenvolvida.

Para o projeto do atuador digital, diretrizes para o seu dimensionamento foram elaboradas, onde foi constatado que a utilização de cilindros hidráulicos com múltiplas câmaras pode melhorar a resolução do sistema, para controle de velocidade, através do uso da regeneração entre câmaras. Porém, para a velocidade máxima, a carga máxima que o atuador pode controlar é reduzida devido à presença de uma pressão contrária ao movimento, a qual é gerada pela câmara que está sendo regenerada. No entanto, a regeneração entre câmaras permite a utilização de bombas menores, reduzindo as dimensões do sistema.

A configuração desenvolvida proporciona ao atuador 43 valores diferentes de velocidades. O atuador foi denominado DEHA – *Digital Electro Hydrostatic Actuator* em alusão aos Atuadores Eletro Hidrostáticos (*Electro Hydrostatic Actuators*), onde a bomba e o cilindro são os componentes principais.

Para o dimensionamento das áreas do cilindro e deslocamentos volumétricos da bomba digital, para que a distribuição das 43 velocidades próxima de ser linear, um algoritmo de otimização baseado em gradiente foi elaborado. Este algoritmo leva em consideração as velocidades máximas positivas e negativas, a força máxima e as pressões nas câmaras.

Para a verificação da viabilidade do controle do DEHA, um modelo matemático foi elaborado utilizando os softwares MATLAB e Hopsan. Para a sua validação, uma bancada de testes foi construída onde diversos experimentos foram realizados.

A partir dos resultados obtidos pelo modelo e pelos experimentos, foi constatado que os mesmos apresentavam boa concordância, tanto para a posição quanto para as pressões, onde o erro em regime permanente para o controle de posição é de 0.27×10^{-3} m. Os desvios nos valores das pressões podem ser relacionados ao atrito do cilindro, possibilidade da presença de ar na tubulação e diferenças nas dinâmicas das válvulas reais e nas modeladas.

Com a validação do modelo matemático, o cálculo da eficiência energética foi realizado. Além disso, mais dois sistemas foram modelados com o intuito de comparação das eficiências, sendo um EHA e um SHA (*Servo Hydraulic Actuator*). Os resultados para a eficiência energética mostram que o DEHA é 29 vezes maior do que a do SHA e 1,2 vezes maior que a do EHA. A alta eficiência e baixa dissipação de energia do DEHA é atribuída à redução de perda energética na bomba digital quando o atuador não está se movendo, pois a vazão é direcionada para o reservatório a baixa pressão, o que reduz o vazamento interno. Para o SHA, nas mesmas condições, a bomba de deslocamento volumétrico variável é colocada em um regime de baixo deslocamento volumétrico, apenas suprindo a vazamento das servo válvulas, o que acontece a alta pressão. No EHA, os resultados são semelhantes ao DEHA, onde as perdas energéticas principais ocorrem devido ao vazamento interno da bomba.

Os resultados obtidos pelo DEHA demonstram que esta configuração apresenta grande potencial para a obtenção de sistemas hidráulicos mais eficientes para aplicação em aeronaves, o que reduziria os sistemas de refrigeração do fluido hidráulico, diminuindo o seu peso, e conseqüentemente, o consumo de combustível. No entanto, a pesquisa deste tipo de atuador ainda está em fase inicial, onde o desenvolvimento de novos componentes e técnicas de controle podem melhorar o seu desempenho.

Para futuras pesquisas para o desenvolvimento do *Digital Electro Hydrostatic Actuator* - DEHA, tem-se a avaliação da aplicação de dois cilindros multi-câmaras sendo controlados pela mesma bomba digital para o controle de mais de uma superfície ao mesmo tempo, um estudo dos tempos de comutação das válvulas *on/off* para os sistemas que utilizam fontes de vazão constante, a análise da confiabilidade do sistema digital no caso de uma falha em um ou mais módulos binários ou em uma ou mais válvulas na unidade de limitação e controle, realizar um estudo das vibrações que ocorrem no sistema e desenvolver soluções para mitigar esses efeitos.

Palavras-chave: Hidráulica digital. Atuadores hidráulicos. Atuadores para aviação. Superfícies de controle aeronaves.

ABSTRACT

Through the growing global awareness to reduce greenhouse gas emissions, the aeronautical industry has been looking for more efficient solutions that can be applied in the aircraft in order to reduce fuel consumption. With the continuing growing demand for air transportation, the search for more efficient systems has increased considerably, bringing the concept called More Electric Aircraft, which aims to replace hydraulic and pneumatic systems with purely electric systems. However, the high power-to-weight ratio, high reliability, the good dynamic response makes hydraulic actuators technology widely used to control primary and secondary flight control surfaces. However, hydraulic systems are known by their low energy efficiency, which is caused by restrictive control techniques that throttle the passage of fluid through control orifices, and also by internal leakage of the components. To improve the efficiency of hydraulic systems, digital hydraulics emerges as a new technological alternative, where control is performed by non-restrictive techniques, through the use of hydraulic components in parallel or through fast switching hydraulics. Therefore, this doctoral thesis aims to develop a new hydraulic actuator solution for the application in aeronautics using digital hydraulics. The developed solution uses a digital pump, on/off valves, and a multi-chamber cylinder. The solution was called Digital Electro Hydrostatic Actuator - DEHA in reference to Electro Hydrostatic Actuators - EHA. For the DEHA design, a methodology was developed to determine the required number of chambers for the cylinder and the number of binary modulus for the digital pump. Therefore, a four-chamber cylinder and a digital pump with three binary modulus were used, resulting in 43 different velocities for the actuator. In addition, the actuator has been optimized for the desired velocity profile using an optimization algorithm. The same algorithm was used to optimize the pumps for the multi-chamber cylinder already available at the Laboratory of Hydraulic and Pneumatic Systems at UFSC. To verify the feasibility of the proposed solution, a mathematical model using the MATLAB/Simulink and Hopsan software was developed. In addition, a model for the EHA and another for the SHA (Servo Hydraulic Actuator) were developed to compare results and efficiencies. In order to validate the mathematical model, a test bench was built, where different experiments were performed. The results obtained show that DEHA is able to control the position with an error equals to 0.27×10^{-3} m in steady-state and with an energy efficiency of 54%, being 29 times higher than SHA and 1.2 times higher than EHA, which demonstrates that DEHA can be a promising solution for the development of more efficient hydraulic actuators.

Keywords: Digital hydraulics. Hydraulic actuators. Aviation actuators. Aircraft control surfaces.

FIGURES LIST

Figure 2.1 - Aircraft's main flight control surfaces.....	39
Figure 2.2 - Electro-Mechanical Actuator – EMA.	40
Figure 2.3 - Topologies of Electro-Mechanical Actuators with Nut-Screw. a) Concentric; b) Perpendicular axes; c) Parallel axes.....	42
Figure 2.4 - Boeing 787 spoiler Electro-Mechanical Actuator.....	43
Figure 2.5 - Mechanical Hydraulic Actuator with a hydraulic valve powered by a centralized hydraulic unit.	44
Figure 2.6 - Simplified model of the Servo Electric-Hydraulic Actuator.....	45
Figure 2.7 - Redundancy systems for aircraft actuators. a) Redundant surfaces; b) External redundant actuators; c) Internal redundant actuators.	45
Figure 2.8 - Electro-Hydraulic Actuator in tandem configuration.....	46
Figure 2.9 – Electro-Hydrostatic Actuators Configurations. a) FPVM; b) VPFM; c) VPVM.....	47
Figure 2.10 – Electrical Back-up Hydraulic Actuator – EBHA. a) Shared Actuator; b) Separated Actuators (Hybrid System).	49
Figure 2.11 - Airbus A380 EHA and Servo Hydraulic Actuator.....	50
Figure 3.1 - Application of variable displacement pumps in hydraulic systems. a) Hydraulic circuit; b) Vane pump with variable displacement.	52
Figure 3.2 - Classification of the switched hydraulic systems: a) Valves; b) Pumps; c) Cylinders.	54
Figure 3.3 - Switched hydraulics PWM signal: a) Signal; b) Switched on/off valve.....	55
Figure 3.4 – Step-up system: a) Hydraulic circuit; b) Electric equivalent circuit.	56
Figure 3.5 - Step-down system: a) Hydraulic circuit; b) Electric equivalent circuit.	57
Figure 3.6 - Representation of digital valves: a) Switched valve; b) Digital flow control unit - DFCU; c) Symbol of a DFCU.....	59
Figure 3.7 - Simplification of the hydraulic circuits: a) Conventional; b) Equivalent using DFCUs.	59
Figure 3.8 - Distribution of discrete flow rate outputs: a) Valves with the same size; b) In power of two; c) In Fibonacci series.	60
Figure 3.9 – Four way hydraulic valve using DFCUs.	61
Figure 3.10 – A digital hydraulic pump with three binary modulus.....	62
Figure 3.11 – Digital piston pump: a) Pump mode; b) Pump and motor mode.....	63

Figure 3.12 - Motor type digital hydraulic actuators.....	63
Figure 3.13 - Multi-chambers linear cylinders: a) Three-chambers; b) Four-chambers; c) Parallel four-chambers cylinder.....	64
Figure 3.14 – System using a digital pump and on/off valves for velocity control.....	65
Figure 3.15 – Digital hydraulic system using on/off valves and multi-chamber cylinder for force control.....	66
Figure 3.16 - Digital hydraulic system using a digital pump.	67
Figure 4.1 – Chamber combinations for a two-chamber linear cylinder. a) Symmetrical cylinder forward movement; b) Asymmetrical cylinder forward movement; c) Asymmetrical cylinder backward movement; d) Asymmetrical cylinder forward movement with the regenerative chamber.	70
Figure 4.2 – Chamber combinations on forward movement for a four-chamber cylinder. a) Without regeneration; b) Chamber B in regenerative mode; c) Chamber D in regenerative mode.	72
Figure 4.3 – Chamber combinations on backward movement for a four-chamber cylinder. a) Without regeneration; b) Chamber A in regenerative mode; c) Chamber C in regenerative mode.	73
Figure 4.4 - Chamber combinations on forward movement for a six-chamber cylinder. a) Without regeneration; b) Chamber F in regenerative mode; c) Chambers D and F in regenerative mode.	75
Figure 4.5 - Number of possible chamber combinations.....	77
Figure 4.6 - Actuator with six chambers.in parallel.	77
Figure 4.7 - Digital hydraulic pump circuit with three binary modulus.....	78
Figure 4.8 - Displacement combinations for different sizes of pumps.....	79
Figure 4.9 - Total number of velocities for different number of pumps and chambers.	80
Figure 4.10 - Limitation and control unit connected in a four-chamber cylinder.	81
Figure 4.11 – Actuator forward velocity as a function of the supply flow rate and the equivalent area.....	83
Figure 4.12 - Actuator backward velocity as a function of the supply flow rate and the equivalent area.....	84
Figure 4.13 - Velocity distribution for different actuator and pump distributions.....	87
Figure 4.14 - Actuator pressure according to velocity and regenerative area.	88
Figure 4.15 - Error between the desired and real velocity values.	90

Figure 4.16 - Optimized velocity for a linear distribution.	95
Figure 4.17 - Error between the desired and the resulting velocity for a linear distribution. ...	96
Figure 4.18 - System resolution for a linear distribution.	96
Figure 4.19 – Negative velocities as a function of the supply flow rate and the equivalent area.	97
Figure 4.20 - Positive velocities as a function of the supply flow rate and the equivalent area.	98
Figure 4.21 – Working pressure as a function of the supply flow rate and the equivalent area.	98
Figure 4.22 - Working pressure behavior for positive velocities.....	99
Figure 4.23 - Optimized velocity for a nonlinear distribution.	100
Figure 4.24 – Cylinder areas for different external loads.	101
Figure 4.25 – Pumps volumetric displacements for different external loads.....	102
Figure 5.1 – Proposed Digital Actuator – Digital Electro Hydrostatic Actuator.....	103
Figure 5.2 – Friction force test bench.	106
Figure 5.3 - Static friction force map.	106
Figure 5.4 – Normally closed digital valve.....	108
Figure 5.5 – Representation of the f factor for a seat valve.	110
Figure 5.6 - On/Off valves flow rate coefficient experiments: a) Hydraulic circuit; b) Test bench.	111
Figure 5.7 - On/Off valves flow coefficient experiments results: a) 1 to 2; b) 2 to 1.....	111
Figure 5.8 – Evaluation of the response times of the on/off valves.....	112
Figure 5.9 - Response times for the on/off valves in the limitation and control unit.	113
Figure 5.10 - - Response times for the on/off valves in the primary conversion unit.....	113
Figure 5.11 - Pumps internal leakage experiments.	116
Figure 5.12 - Pumps delivered flow rate as a function of the output pressure.....	117
Figure 5.13 - System control block diagram.....	118
Figure 5.14 - PID controller block diagram.....	118
Figure 5.15 – Velocities matrix structure.....	119
Figure 5.16 - Delay controller.....	121
Figure 5.17 - DEHA Hopsan model.....	122
Figure 5.18 - Servo Hydraulic Actuator - SHA Model.....	123
Figure 5.19 - Servo valves leakage.	124

Figure 5.20 - Variable displacement pump volumetric efficiency map.	125
Figure 5.21 - SHA model developed in Hopsan.	126
Figure 5.22 - Electro-Hydrostatic Actuator model.	127
Figure 5.23 - EHA model developed in Hopsan.	128
Figure 6.1 - Hydraulic diagram of the test bench.	131
Figure 6.2 - Test bench primary conversion unit hydraulic circuit diagram.	132
Figure 6.3 – Actuator velocities comparison for the optimization algorithm pump and the MEDAL prototype pump.	133
Figure 6.4 - Test bench primary conversion and pressurized reservoir units.	135
Figure 6.5 - Test bench limitation and control unit and the secondary conversion hydraulic. unit circuit diagram.	136
Figure 6.6 - Test bench limitation and control unit and secondary conversion unit.	137
Figure 6.7 – Schematic diagram of the control system.	138
Figure 6.8 – a) Power electronics panel; b) Booster panel.	139
Figure 6.9 - Booster control signal. a) Signal applied in the valve; b) Signal sent to the booster.	139
Figure 7.1 – Experimental and simulation velocities.	140
Figure 7.2 – Pressure in the chambers of the cylinder for positive velocities.	141
Figure 7.3 - Pressure in the chamber of the cylinder for positive velocities.	142
Figure 7.4 – Position response for position control without external load.	143
Figure 7.5 - Position error for position control without external load.	144
Figure 7.6 – Velocity signal for position control without external load.	144
Figure 7.7 – Pump valve signals for position control without external load.	145
Figure 7.8 – Output pressure in the pumps for position control without external load.	145
Figure 7.9 - VPs valves signal for position control without external load.	146
Figure 7.10 – VRs valves signal for position control without external load.	146
Figure 7.11 – Cylinder chambers pressure for position control without external load.	147
Figure 7.12 – External load.	149
Figure 7.13 – Reservoir pressure.	149
Figure 7.14 - Position response for position control with external load.	150
Figure 7.15 - Position error for position control with external load.	151
Figure 7.16 - Velocity signal for position control with external load.	151
Figure 7.17 - Pumps valves signal for position control with external load.	152

Figure 7.18 - Output pressure in the pumps for position control with external load.....	152
Figure 7.19 - VPs valves signal for position control with external load.....	153
Figure 7.20 - VRs valves signal for position control with external load.	153
Figure 7.21 - Cylinder chambers pressure for position control with external load.	154
Figure 7.22 – Position responses for the DEHA, SHA, and EHA.....	156
Figure 7.23 – Input hydraulic energy.....	157
Figure 7.24 - Output hydraulic energy.....	158
Figure 7.25 – Dissipated energy.	159
Figure 7.26 – Input, Dissipated, Output Energies. a) DEHA, b) EHA, c) SHA.....	160
Figure 7.27 - Efficiency.	161
Figure A.1 - Mechanical flight control system.	177
Figure A.2 - Mechanical actuator with a hydraulic booster.....	178
Figure A.3 - Aircraft simplified hydraulic system.....	179
Figure A.4 - More electric aircraft concept. a) Nowadays; b) Future tendencies.....	182
Figure B.1 – Representations of the bristles by the LuGre model.....	184
Figure B.2 – Friction characteristics in steady-state.....	185

TABLES LIST

Table 4.1 – Nomenclatures of the limitation and control unit valves.....	81
Table 4.2 – Cylinder areas in the distribution of a power of two series.....	83
Table 4.3 – Digital pump displacements distribution in power of two series.	83
Table 4.4 - Pumps volumetric displacement distribution, power of two, and power of three..	86
Table 4.5 - Cylinder areas distribution, power of two, and power of three.....	86
Table 4.6 - Examples of dynamic and load needs for aircraft.	92
Table 4.7 - Digital pump combinations.	93
Table 4.8 - System parameters for the optimization algorithm.	94
Table 4.9 - Optimized areas and volumetric digital pump displacements for a linear velocity. distribution.....	95
Table 4.10 - Optimized areas and volumetric pumps displacement for a nonlinear velocity distribution.....	100
Table 5.1 – Parameters for the multi-chamber cylinder.	104
Table 5.2 - Friction force model parameters.	107
Table 5.3 - On/Off valves parameters.	114
Table 5.4 – Check valve parameters.....	115
Table 5.5 – Complementary components used in the Hopsan model.	122
Table 5.6 - Parameters of the SHA.....	126
Table 5.7 - Parameters for the EHA actuator.	128
Table 6.1 - Pumps displacement for the test chamber multi-chamber cylinder.	133
Table 6.2 – Hydraulic components of the primary conversion unit.	134
Table 6.3 - Hydraulic components of the pressurized reservoir unit.....	135

LIST OF ABBREVIATIONS

ABS – Anti-Lock Brake Systems
ADP – Air Driven Pump
CISB – Brazilian Swedish Research and Innovation Center
DEHA – Digital Electro Hydrostatic Actuator
DFCU – Digital Flow Control Unit
EAHA – Electro Assisted Hydraulic Actuator
EBHA – Electrical Back-up Hydrostatic Actuator
ECU – Electronic Control Unit
EDP – Engine Driven Pump
EHA – Electro Hydrostatic Actuator
EMA - Electric Mechanical Actuator
EMI – Electromagnetic Interference
FBW – Fly-by-Wire
FCS – Flight Control System
FPVM – Fixed Pump Variable Motor
HIRF – High Intensity Radiated Field
LASHIP – Laboratory of Hydraulic and Pneumatic Systems
MDP -Motor Driven Pump
MEA – More Electric Aircraft
MP – Demand Electric Motor Driven Pump
PBW – Power-by-Wire
PTS – Power Transfer System
PWM – Pulse Width Modulation
RAT – Ram Air Turbine
SHA – Servo Hydraulic Actuator
UFSC – Federal University of Santa Catarina
VPFM – Variable Pump Fixed Motor
VPVM – Variable Pump Variable Motor

LIST OF SYMBOLS

GREEK ALPHABET

α	Flow rate coefficient	[1]
α_f	Empiric friction parameter	[1]
β_e	Equivalent Buck modulus	[Pa]
κ	Duty Cycle	[1]
ζ	Damping factor	[1]
ξ_{ch}	Damping factor of the check valves	[1]
ρ	Specific mass	[kg/m ³]
σ_0	Bristle stiffness coefficient	[N/m ²]
σ_1	Bristle damping coefficient	[N.s/m]
σ_2	Viscous coefficient	[N.s/m]
η_v	Volumetric efficiency	[1]
η	Energy efficiency	[1]
ω	Rotational frequency of the pump	[rad/s]
ω_{np}	Rotational frequency for the variable displacement pump	[rad/s]
ω_{ch}	Natural frequency of the check valves	[rad/s]
ω_p	Rotational frequency of the digital pump	[rad/s]
ω_n	Natural frequency	[rad/s]
$\omega_{n_{on}}$	Natural frequency for the opening of the on/off valves	[rad/s]
$\omega_{n_{off}}$	Natural frequency for the closing of the on/off valves	[rad/s]
ω_{np}^{EHA}	Natural frequency for the pump of the EHA	[rad/s]

LATIN ALPHABET

A_A	Area of the chamber A	[m ²]
A_B	Area of the chamber B	[m ²]

A_C	Area of the chamber C	[m ²]
A_D	Area of the chamber D	[m ²]
A_E	Area of the chamber E	[m ²]
A_F	Area of the chamber F	[m ²]
A_G	Area of the chamber G	[m ²]
A_H	Area of the chamber H	[m ²]
A_e	Equivalent area	[m ²]
A_{eb}	Equivalent area for the backward movement	[m ²]
A_{ef}	Equivalent area for the forward movement	[m ²]
A_g	Regenerative area	[m ²]
A_r	Resultant area	[m ²]
A_{rb}	Resultant area for the backward movement	[m ²]
A_{rf}	Resultant area for the forward movement	[m ²]
A_v	Area of passage of the hydraulic fluid	[m ²]
A_A^{EHA}	Area A for the EHA	[m ²]
A_B^{EHA}	Area B for the EHA	[m ²]
A_A^{SHA}	Area A for the SHA	[m ²]
A_B^{SHA}	Area B for the SHA	[m ²]
A_C^{SHA}	Area C for the SHA	[m ²]
A_D^{SHA}	Area D for the SHA	[m ²]
B	Viscous friction coefficient	[kg/s]
C_{LAB}	Leakage coefficient of the chamber A to B	[m ³ /(sPa)]
C_{LBC}	Leakage coefficient of the chamber B to C	[m ³ /(sPa)]
C_{LCD}	Leakage coefficient of the chamber C to D	[m ³ /(sPa)]
c_s	Switching cost factor	[m/s]
c_d	Discharge coefficient	[1]

dT_{min}	Minimum time interval for a valve combination change	[s]
dT_s	Sample time interval	[s]
dT_v	Time that the combination valve matrix should be recalculated	[s]
d	Closing element diameter	[m]
D	Volumetric displacement	[m ³ /rev]
D_1	Volumetric displacement of the pump 1	[m ³ /rev]
D_2	Volumetric displacement of the pump 2	[m ³ /rev]
D_3	Volumetric displacement of the pump 3	[m ³ /rev]
D_{pv}	Volumetric displacement for the variable displacement pump	[m ³ /rev]
D_p^{EHA}	Volumetric displacement for the EHA	[m ³ /rev]
e	Position error	[m]
e_t	Total velocity error	[m/s]
E_{i_DEHA}	Supplied energy for the DEHA	[J]
E_{i_SHA}	Supplied energy for the SHA	[J]
E_{i_DHA}	Supplied energy for the EHA	[J]
E_{o_DEHA}	Output energy for the DEHA	[J]
E_{o_SHA}	Output energy for the SHA	[J]
E_{o_EHA}	Output energy for the EHA	[J]
E_{input}	Supplied energy	[J]
$E_{dissipated}$	Dissipated energy	[J]
E_{output}	Output energy	[J]
f	Closing element diameter fraction coefficient	[1]
F_C	Coulomb friction	[N]
F_S	Static friction	[N]
F_{fr}	Friction force	[N]

F_L	Load force	[N]
K_P	Proportional gain	[1]
K_i	Integral gain	[1]
K_d	Derivative gain	[1]
k_v	Flow rate coefficient of the on/off valves	[m ³ /(sPa ^{0.5})]
k_{ch}	Flow rate coefficient of the check valves	[m ³ /(sPa ^{0.5})]
k_{pl}	Leakage coefficient	[m ³ /(sPa ^{0.5})]
k_{plv}	Leakage coefficient for the variable displacement pump	[m ³ /(sPa ^{0.5})]
l	Actuator length	[m]
M_T	Total mass	[kg]
m	Mass in movement	[kg]
n	Number of chambers	[1]
N	Number of supply pressures	[1]
n_{cc}	Total combinations of chambers	[1]
n_{ccb}	Total combinations of chambers for the backward movement	[1]
n_{ccf}	Total combinations of chambers for the forward movement	[1]
n_{cp}	Total combinations of pumps	[1]
n_v	Total number of different velocities	[1]
q_{VA}	Flow rate of the chamber A	[m ³ /s]
q_{VB}	Flow rate of the chamber B	[m ³ /s]
q_{VC}	Flow rate of the chamber C	[m ³ /s]
q_{VD}	Flow rate of the chamber D	[m ³ /s]
q_{VT}	Flow rate of the reservoir	[m ³ /s]
q_{VS}	Flow rate of the supplied source	[m ³ /s]
q_{vsb}	Supply flow rate for the backward movement	[m ³ /s]
q_{vsf}	Supply flow rate for the forward movement	[m ³ /s]

q_{Vn}	Nominal valve flow rate	[m ³ /s]
q_{vch}	Check valves flow rate	[m ³ /s]
q_{vpl}	Leakage flow rate of the pumps	[m ³ /s]
q_{vpr}	Real pumps flow rate	[m ³ /s]
q_{vp}	Variable displacement pump flow rate	[m ³ /s]
q_{VL}	Load flow rate	[m ³ /s]
p	Number of pumps	[1]
p_{ac}	Pre load pressure of the check valves	[Pa]
p_A	Pressure in the chamber A	[Pa]
p_B	Pressure in the chamber B	[Pa]
p_C	Pressure in the chamber C	[Pa]
p_D	Pressure in the chamber D	[Pa]
p_{HS}	High supply pressure	[Pa]
p_{LS}	Low supply pressure	[Pa]
p_L	Load pressure	[Pa]
p_{Ain}	Internal pressure	[Pa]
p_T	Reservoir pressure	[Pa]
p_W	Working pressure	[Pa]
p_A^{EHA}	Pressure in the chamber A for the EHA	[Pa]
p_B^{EHA}	Pressure in the chamber B for the EHA	[Pa]
p_A^{SHA}	Pressure in the chamber A for the SHA	[Pa]
p_B^{SHA}	Pressure in the chamber B for the SHA	[Pa]
p_C^{SHA}	Pressure in the chamber C for the SHA	[Pa]
p_D^{SHA}	Pressure in the chamber D for the SHA	[Pa]
t_{ds}	Time delay	[s]
t_{dsp}	Time delay for the primary conversion unit	[s]

t_{dsl}	Time delay for the limitation and control unit	[s]
t_s	Accommodation time	[s]
t_{SOD}	Time to energize the valve solenoid	[s]
t_{SCD}	Time to de-energize the valve solenoid	[s]
t_{SOR}	Opening valve spool dynamics	[s]
t_{SCR}	Closing valve spool dynamics	[s]
t_{PEAK}	Peak time	[s]
t_{REV}	Reverse time	[s]
U_{Dv}	Displacement control signal for the variable displacement pump	[1]
v_a	Actuator velocity	[m/s]
v_{a_maxp}	Maximum positive velocity	[m/s]
v_S	Stribeck velocity	[m/s]
v_{af}	Actuator forward velocity	[m/s]
v_{ab}	Actuator backward velocity	[m/s]
v_d	Desired velocity	[m/s]
v_{ref}	Reference velocity	[m/s]
v_r	Real velocity	[m/s]
V_{PEAK}	Peak voltage	[V]
V_{HOLD}	Hold voltage	[V]
V_{0A}	Dead volume of the chamber A	[m ³]
V_{0B}	Dead volume of the chamber B	[m ³]
V_{0C}	Dead volume of the chamber C	[m ³]
V_{0D}	Dead volume of the chamber D	[m ³]
x_{st}	Steady-state displacement	[m]
x	Vector of areas	[m ²]
x_{vmax}	Maximum opening of the on/off valves spoon	[m]

V_{HOLD}	Hold voltage	[V]
V_{PEAK}	Peak voltage	[V]
Z	Deflection of rugosity	[m]

SUMMARY

1.	INTRODUCTION	33
1.1.	CONTEXTUALIZATION	33
1.2.	OBJECTIVES	35
1.2.1.	Main objectives	35
1.2.2.	Specific objectives	35
1.3.	THESIS JUSTIFICATION AND CONTRIBUTIONS	36
1.4.	THESIS OUTLINE.....	37
2.	LITERATURE REVIEW	38
2.1.	FLIGHT CONTROL SURFACES AND ACTUATORS	38
2.1.1.	Introduction.....	38
2.2.	AIRCRAFT CONTROL ACTUATORS.....	40
2.2.1.	Electro-Mechanical Actuators – EMA.....	40
2.2.2.	Servo Electro-Hydraulic Actuators - SHA	43
2.2.3.	Electro-Hydrostatic Actuators – EHA	46
2.3.	FINAL CONSIDERATIONS ABOUT CHAPTER 2	50
3.	SWITCHED AND DIGITAL HYDRAULICS.....	52
3.1.	SWITCHED HYDRAULICS	54
3.1.1.	Step-up systems	56
3.1.2.	Step-down systems	57
3.2.	DIGITAL HYDRAULICS	58
3.2.1.	Digital valves in parallel connection.....	58
3.2.2.	Digital pumps	61
3.2.3.	Digital actuators	63
3.2.4.	Applications for digital pumps, valves, and actuators	65
3.2.5.	Final considerations about digital hydraulics	67
4.	DIGITAL ACTUATOR DESIGN	69

4.1.	SECONDARY CONVERSION UNIT	69
4.2.	PRIMARY CONVESION UNIT	78
4.3.	LIMITATION AND CONTROL UNIT	81
4.4.	ANALYSIS OF THE MULTI-CHAMBERS CYLINDERS – VELOCITY AND PRESSURE	82
4.5.	CALCULUS OF THE CYLINDER AREAS AND THE SIZE OF THE PUMPS....	88
4.6.	FINAL CONSIDERATIONS OF CHAPTER 4	102
5.	ACTUATOR MODEL	103
5.1.	DIGITAL ELECTRO HYDROSTATIC ACTUATOR MODEL - DEHA	103
5.1.1.	Cylinder model	104
5.1.1.1	Friction force model	105
5.1.2.	ON/OFF valves model.....	107
5.1.3.	Check valves model	114
5.1.4.	Digital pump model.....	115
5.1.5.	System control.....	117
5.2.	SERVO HYDRAULIC ACTUATOR MODEL – SHA	123
5.3.	ELECTRO HYDROSTATIC ACTUATOR MODEL - EHA	127
5.4.	FINAL CONSIDERATIONS ABOUT THE ACTUATOR MODEL	129
6.	TEST BENCH.....	130
6.1.	TEST BENCH PRIMARY CONVERSION UNIT	132
6.2.	LIMITATION AND CONTROL UNIT AND SECONDARY CONVERSION UNIT	136
6.3.	DATA ACQUISITION AND SYSTEM CONTROL.....	138
7.	EXPERIMENTAL AND SIMULATION RESULTS	140
7.1.	RESULTS FOR VELOCITY CONTROL	140
7.2.	RESULTS FOR POSITION CONTROL.....	142
7.3.	SYSTEM EFFICIENCY EVALUATION	155
7.4.	FINAL CONSIDERATION OF CHAPTER 7	161

8.	CONCLUSIONS	163
8.1.	FUTURE RESEARCHES	165
9.	REFERENCES.....	167
	APPENDIX A – Flight control systems.....	177
	APPENDIX B – Friction model equations.....	184
	APPENDIX C – Optimization algorithm guidelines	187
	APPENDIX D – Optimization algorithm code.....	189

1. INTRODUCTION

1.1. CONTEXTUALIZATION

With the increase in the consumption of non-renewable fuel sources in recent decades, the impact caused by this action is one of the major concerns of environmentalists and governments. According to Lotfalipour *et al.* (2010), the combustion of fossil fuels is the largest contributor to CO₂ emissions. Davis & Caldeira (2010) mention that carbon dioxide emissions, from burning fossil fuels, are the primary cause of global warming. In relation to means of transportation, Tsita & Pilavachi (2017) quote that environmental issues are one of the biggest concerns and, coupled with the fast growth of the use of cars by the population, could lead to an increase in greenhouse gas emissions. Neves *et al.* (2017) highlight that, in the economy, the transportation sector is the most outdated in reducing carbon content. Gössling (2010) quotes that the aviation sector is responsible for about 1.6 to 2.2% of global CO₂ emissions, which means about 13% of the total emissions of this gas only from transport sources. Terrenoire *et al.* (2019) quote that in the year of 2017, worldwide flights produced around 859 million tons of CO₂.

By increasing CO₂ emissions into the atmosphere, environmental awareness has set worldwide. As a result, design requirements, which aim to achieve more efficient systems, have become stricter. Due not only to the increase in greenhouse gas emissions, but also to the increase of solid particles dissolved in air, mayors of some world capitals were forced to ban, by 2025, all vehicles that use diesel as their source of fuel (TSITA & PILAVACHI, 2017). Another important statistical data shows that in 2014, European Union countries consumed 33% of their energy in the transport sector, where 94% of this amount came from petroleum sources (NEVES *et al.*, 2017). In Xylia & Silveira (2016) it is mentioned that Sweden set the goal of acquiring a fleet of independent fossil fuel vehicles until 2030.

Nowadays, modern aircraft propulsion technology is still based almost exclusively around the use of internal combustion engines (SLIWINSKI *et al.*, 2017), mainly because fossil fuels have a high energy density.

In aircraft, one of the most important system for flight control is the hydraulic system. These systems, according to Moir & Seabridge (2008), were firstly implemented in aviation in the early 1930s, having the advantage of being an efficient way to transmit power, where low-energy movements from the cockpit can be transferred to high energy demand locations (MOIR & SEABRIDGE, 2008). These locations are normally represented by the primary and secondary

control surfaces. However, the hydraulic systems can be also implemented in landing gears, cargo doors, and the steering system (WARD, 2017). Nevertheless, one of the disadvantages of using hydraulic systems is their low energy efficiency, which comes from the losses caused by the pressure and flow control characteristics, that normally are provided by throttling the flow through control orifices (dissipative control) and by internal leakages. The control surfaces are extremely important for the proper functioning of the aircraft in flight, and for this reason, the hydraulic systems are a key part and improving their energy efficiency can bring significant gains not only in fuel economy, but also in reducing the hydraulic fluid cooling system.

Nowadays, there are some researches to replace aircraft hydraulic actuators with electric actuators, generating the More Electric Aircraft - MEA concept (BENNETT *et al.*, 2010; CAO *et al.*, 2012; NAAYAGI, 2013). However, the designs developed, in most cases, still use hydraulic systems, as in the case of electro hydrostatic actuators. In this system, an electric motor is coupled directly to a hydraulic pump, which is directly coupled to the hydraulic cylinder. In this type of configuration, the actuator control is achieved by varying the volumetric displacement of the pump and/or its rotational frequency. In addition, to keep the actuator in its desired position, in solutions that use electric motors, it is necessary to keep a voltage signal applied to the electric motor. Therefore, the electric motor can balance the opposite torque generated by the load. In purely hydraulic solutions, this action is done by closing valves.

In Moir & Seabridge (2008), it is quoted that the use of hydraulic systems can bring some advantages as the use of small diameter pipes allows flexibility in the installation, and with the use of oil as a fluid, it permits the lubrication of the system. These authors also mention that overloads imposed on the hydraulic system can be resisted without major damage.

Another advantage of using hydraulic systems is the ease implementation of redundant systems, such as using parallel or tandem cylinders and sharing the main hydraulic unit for more than one actuator.

As mentioned earlier, hydraulic systems have low energy efficiency. In order to improve their efficiency, a new topic of research is gaining more space in the academic community, which is called digital hydraulics (UUSITALO *et al.*, 2009; WINKLER *et al.*, 2010; NOSTRANI, 2015; NOSTRANI *et al.*, 2017).

In the digital hydraulics, the control of flow rate and pressure is performed to reduce the main energy losses, which are caused by the pressure drop, which is mainly caused by the throttling of the flow into control orifices and internal leakages.

This reduction of the pressure drop is accomplished by using hydraulic components (valves, pumps, cylinders) in parallel arrangements, called parallel digital hydraulic systems or thought systems, that use valves switching in high frequencies, where the flow and pressure control are achieved through the acceleration and deceleration of the hydraulic fluid.

For use in electro-hydraulic positioning systems, this technology provides researchers new guidelines for designing system solutions, which have optimized energy consumption without losses in their dynamic characteristics.

However, as this is still an emergent research, there are many challenges that must be overcome for its commercial application. One of the limitations currently encountered with the use of digital hydraulics is the low response time of commercially available valves. However, research on the development of new components has been growing in recent years, including the works by Tu *et al.* (2007), Uusitalo *et al.* (2009), and Winkler *et al.* (2010).

With the emergence of digital hydraulics, the development of test benches has become an important tool for understanding the physical phenomena that occur in systems that use this type of technology. These phenomena are caused by the fast switching of valves between the high and low pressure lines.

With the support of test benches, the development of mathematical models that can predict the behavior of digital hydraulic systems in their real environments can assist designers in the process of improving such hydraulic circuits.

1.2. OBJECTIVES

1.2.1. Main objectives

Due to the low efficiency that the hydraulic systems present, which are caused by the high throttle losses regarding to the use of hydraulic components, this doctoral thesis aims to develop a hydraulic actuator, using a digital pump, on/off valves and multi-chamber cylinder, in order to control the aircraft flight control surfaces with the purpose of increased energy efficiency.

1.2.2. Specific objectives

To achieve the main objective of this doctoral thesis, aiming the use of digital hydraulic systems for application in aircraft, the following specific objectives were defined:

- Develop a digital hydraulic circuit through the use of a digital pump, on/off valves, and multi-chamber cylinder, for application in the aircraft flight control surfaces, with focus on increasing the hydraulic system efficiency;
- Develop guidelines for system sizing, number of the cylinder chambers, number of pumps and calculation of the system resultant resolution;
- Develop an analytical model, through Hopsan software, to perform the modeling of hydraulic components.
- Using Matlab/Simulink software to develop control strategies for the system;
- Develop and build an experimental test bench to study the physical effects involved in these types of systems, as well as the validation of the numerical model.
- Compare the proposed system efficiency with the conventional system and the electric hydrostatic solution.

1.3. THESIS JUSTIFICATION AND CONTRIBUTIONS

As mentioned before, the hydraulic systems are known by their low energy efficiency. However, they are commonly applied in aircraft control surfaces due to their high power/weight ratio, high reliability, and low maintenance. The justifications for the proposition of this doctoral thesis come from the necessity of increasing the aircraft hydraulic system energy efficiency, and then find new solutions that can accomplish this requirement. Moreover, by increasing the hydraulic system energy efficiency, the fuel consumption of the aircraft may be reduced, and therefore the greenhouse gas emissions. Another point to mention is, with the finishing of this doctorate thesis, it can be used to development of new hydraulic systems solutions.

The Laboratory of Hydraulic and Pneumatic Systems - LASHIP of the Federal University of Santa Catarina - UFSC is a pioneer in Brazil in the study and development of digital hydraulic systems. Additionally, in this area specifically, LASHIP over the last eight years has published, in renowned journals and congresses around the world, fifteen papers. Also, two master theses were published in 2015, two in 2018, and one in 2019. In 2018 the first doctoral thesis about this subject was published. Another factor to be highlighted is that with the research carried out in the area of digital hydraulic systems, LASHIP, and consequently UFSC, strengthened its collaboration with Sweden, through the Linköping University – FLUMES – Division of Fluid and Mechatronic Systems, where have already been carried out

three sandwich doctorate, with the support of the Brazilian Swedish Research and Innovation Center – CISB, Saab AB - Svenska Aeroplan AB, CAPES - Improvement of Higher Education Personnel and CNPq - National Council for Scientific and Technological Development.

As a contribution of this doctoral thesis, the use of a digital pump with a multi-chamber cylinder applied in aircraft can be considered an innovation, since in the literature, there are no references on the use of this type of system, neither for position or velocity control. In the literature, the application of the digital hydraulics for flight control surfaces was studied in the works of Belan *et al.* (2015) and Dell'amico *et al.* (2018), where a multi-chamber cylinder and three different pressure sources were used for force control. The use of the digital pump has been studied in Locateli *et al.* (2014a), Locateli *et al.* (2014b), Heitzig & Theissen (2011), and Theissen *et al.* (2013), where the digital pump was used for velocity control of conventional hydraulic cylinders. In Pynnttari *et al.* (2014), a parallel pump associated with on/off valves and a four-chamber cylinder was developed for velocity control.

Other contributions to this work are:

- Increase the knowledge of digital hydraulic positioning systems for parallel connections from the use of multi-chamber cylinders and digital pumps;
- With the support of the obtained results, the advantages and disadvantages of using digital hydraulics compared to conventional hydraulic systems will be established.

1.4. THESIS OUTLINE

The thesis manuscript is organized as follows. In Chapter 2, the literature review of the main flight control systems and the main flight control actuators is presented. In Chapter 3 a literature review of the main digital hydraulic systems in study nowadays is shown. Chapter 4 presents the digital hydraulic actuator in study. This chapter also presents guidelines for the design of these kinds of actuators. Chapter 5 presented the dynamic mathematical model of the proposed actuator developed in the software MATLAB/Simulink and Hopsan. In Chapter 6, the test bench developed for the experimental analysis and validation of the mathematical model is detailed. Chapter 7 shows the simulation and experimental results. Chapter 8 the conclusions of the thesis and Chapter 9, the references.

2. LITERATURE REVIEW

2.1. FLIGHT CONTROL SURFACES AND ACTUATORS

2.1.1. Introduction

In aircraft, the flight control systems (FCS) are extremely important for keeping the aircraft capable of flying in normal conditions or in failure situations. Wang *et al.* (2016) define that a flight control system is a mechanical/electrical system, which transmits the control signals that come from the pilot's commands and drives the control surfaces to realize the scheduled flight. According to Moir & Seabridge (2008), the flight control systems have made considerable advances over the years. The same authors quote that the first biplanes, the control of these aircraft were provided by warping the wings and control surfaces through wires attached to the flying controls in the cockpit. In the APPENDIX A – Flight control systems, it is presented more details about the flight control systems.

In aeronautical systems, control surfaces are of utmost importance for aircraft control under normal or emergency flight conditions. According to Moir & Seabridge (2008), the movement of an aircraft is defined in relation to its translational and rotational movement around previously defined axes, where the translational movement is that which a vehicle travels from one point in space to another and the rotational movement, in the case of aircraft, is related to three defined axes called pitch, roll, and yaw.

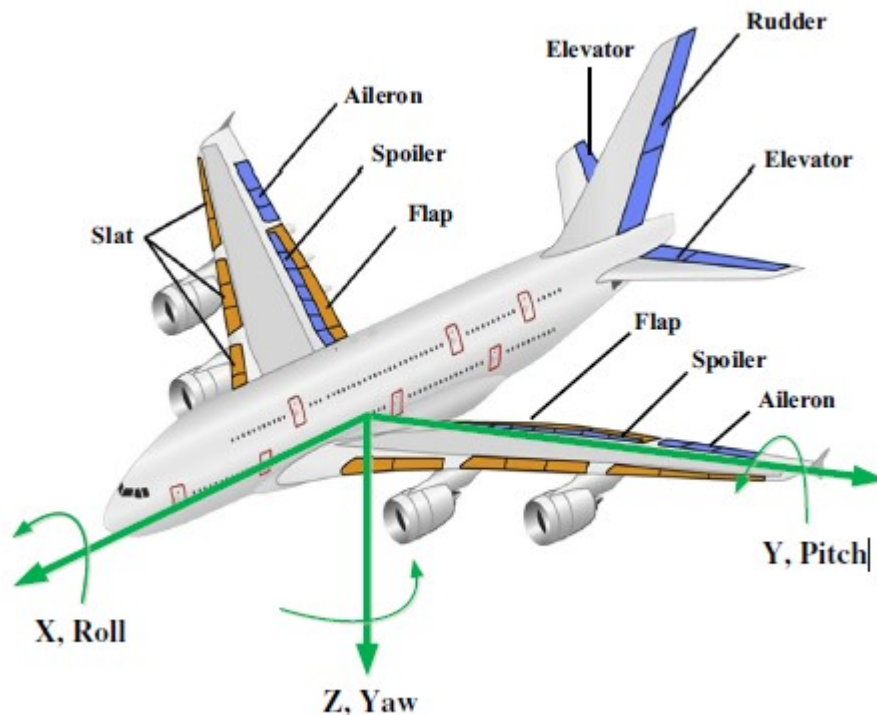
Wang *et al.* (2016) mention that an aircraft control system is composed of different types of control surfaces. According to Moir & Seabridge (2008), there are two main surfaces for the control of an aircraft, which are called primary and secondary surfaces. The primary surfaces are in charge of the main control of the aircraft, being the elevator, ailerons, and rudder. These surfaces have a critical safety aspect, where the loss of one or more flight control axis is hazardous for the aircraft (WANG *et al.*, 2016).

For the primary control surfaces, the elevators are responsible for pitch movement. This movement causes the aircraft to rotate through an imaginary axis, which connects the two ends of the wings. The ailerons perform the roll movement, which is the rotation of the aircraft along the imaginary axis, joining the nose to the tail. The rudder is responsible for the yaw movement, which is performed through the aircraft's central imaginary line (MOIR & SEABRIDGE, 2008).

The secondary flight control surfaces are responsible to modify the aerodynamic configuration of the aircraft during some flight phases (MARÉ, 2017). According to van den Bossche (2004), these surfaces are dedicated to controlling the lift of the wings. The most common secondary control surfaces are the flaps, slats, and speed-brakes.

The flap control is provided by sections of flaps installed in the two-thirds of the inboard wing trailing edges, where during the take-off and landing, the flaps rearwards and downwards in order to increase the wing area, and then, increase the wing lift, as quote Moir & Seabridge (2008) and Wang *et al.* (2016). For the slat control, this occurs by extending forwards and outwards from the wing leading edge, which also aims the increasing of wing area and camber, and therefore, the wing lift (MOIR & SEABRIDGE, 2008; WANG *et al.*, 2016). In the speed-brakes control, they are used to increase the aircraft drag and reduce the wing lift (MOIR & SEABRIDGE, 2008; WANG *et al.*, 2016). Figure 2.1 shows the main aircraft control surfaces.

Figure 2.1 - Aircraft's main flight control surfaces.



Source: Wang *et al.* (2016).

As mentioned before, the aircraft control surfaces have extreme importance for aircraft performance and safety. These surfaces must be actuated and controlled with some kind of flight control system, as purely mechanical, electro-hydraulic, fly-by-wire, power-by-wire, and so on. For the actuation of the flight control surfaces, different topologies of actuators can be

applied, as the mechanical actuators, electro-mechanical actuators, electro-hydraulic actuators, and electro-hydrostatic actuators. In Section 2.2, these kinds of actuators will be presented with more details.

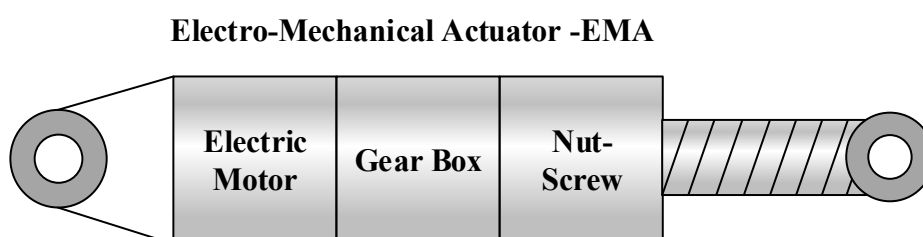
2.2. AIRCRAFT CONTROL ACTUATORS

In Section 2.1, the main flight control systems that are used to control the aircraft's primary and secondary control surfaces have been presented. For to control primary control surfaces responsible for the pitch, roll and yaw movements of the aircraft, as well as the secondary surfaces, that control the wing lifts and the aircraft drag, the signals generated by the pilot commands are converted in mechanical movements in the control surfaces by some kind of actuators. Normally, there are three main different topologies of actuators that are applied in aircraft, called Electro-Mechanical Actuators – EMA, Servo Electro-Hydraulic Actuators – SHA, and the Electro-Hydrostatic Actuators – EHA.

2.2.1. Electro-Mechanical Actuators – EMA

The Electro-Mechanical Actuator – EMA is an actuator topology that uses a DC brushless electric motor and a gearbox to drive the aircraft surface (MOIR & SEABRIDGE, 2008). According to Qiao *et al.* (2017), the EMAs can be linear or rotary type, where for the linear EMAs, the electric motor rotational frequency is converted in linear motion by a ball or a roller screw mechanism. For the rotatory EMAs, the electric motor rotation frequency is reduced through a gearbox, which is coupled to the control surface directly, or by a connection rod (QIAO *et al.*, 2017). The same authors also mention that an Electro-Mechanical Actuator is composed of a servo motor (Electric Motor), gearbox, screw mechanism (Nut-screw), and an ECU – Electronic Control Unit. Figure 2.2 shows the main schematic of an Electro-Mechanical Actuator.

Figure 2.2 - Electro-Mechanical Actuator – EMA.



Source: By the author based in Maré (2017).

Normally, for flight control, a variable-speed motor with high reliability, high power density, and acceptable heat dissipation is required (QIAO *et al.*, 2017). The gearbox is responsible to transform the high velocity low torque of the servo motor, in low velocity, and high torque to the screw mechanism, which is responsible to convert the rotary electric motor motion in linear motion with a required force (QIAO *et al.*, 2017). The Electronic Control Unit – ECU is responsible for the control of the EMA, where it receives the position, velocity, load signal by sensors installed in the EMA, for feedback the position, and limit the current (QIAO *et al.*, 2017).

According to Wang *et al.* (2016), with the development of power electronics and permanent magnets, the EMAs become very promising for flight control. For the primary control surfaces, in the mid of the 1980s, the Advanced Electro-Mechanical System EMAS program was responsible for the development of the linear EMA for the Lockheed C-141 aileron control (MARÉ, 2017). Qiao *et al.* (2017) highlight that, with the successes of the test with the C-141 actuator, other PBW systems were developed with different sizes and configurations. Nowadays, one of the most common applications for the EMAs is the actuation system of the aileron of the Airbus A320 (MARÉ, 2017).

In the secondary control surfaces, Qiao *et al.* (2017) mention that, there is a good acceptability by the manufacturer of using the Electro-Mechanical Actuator in surfaces that are less critical for safety aspects, as the flaps, slats, and spoilers. One of the feature concerns for the EMAs is the jamming of the actuator. According to Maré (2017), a lubrication fault, overheating, or damage contact surface can cause deterioration of efficiency and then, the transmission jamming. Qiao *et al.* (2017) highlight that, nowadays the EMAs are not yet mature enough for applications in primary flight control surfaces due to their jamming probability. However, the same authors quote that, in low-power applications, the EMAs can be applied. An example of the application of the Electro-Mechanical Actuators in secondary flight control surfaces is in the spoiler actuator for the Boeing 787 (MARÉ, 2017; QIAO *et al.*, 2017)

Wang *et al.* (2016) mention that the use of the Electro-Mechanical Actuator can bring some advantages as:

- Reduce flight control weight by 25%;
- Reduce maintenance by 42%;
- Reduce the mean time to repair by 50%;
- Increase the aircraft availability.

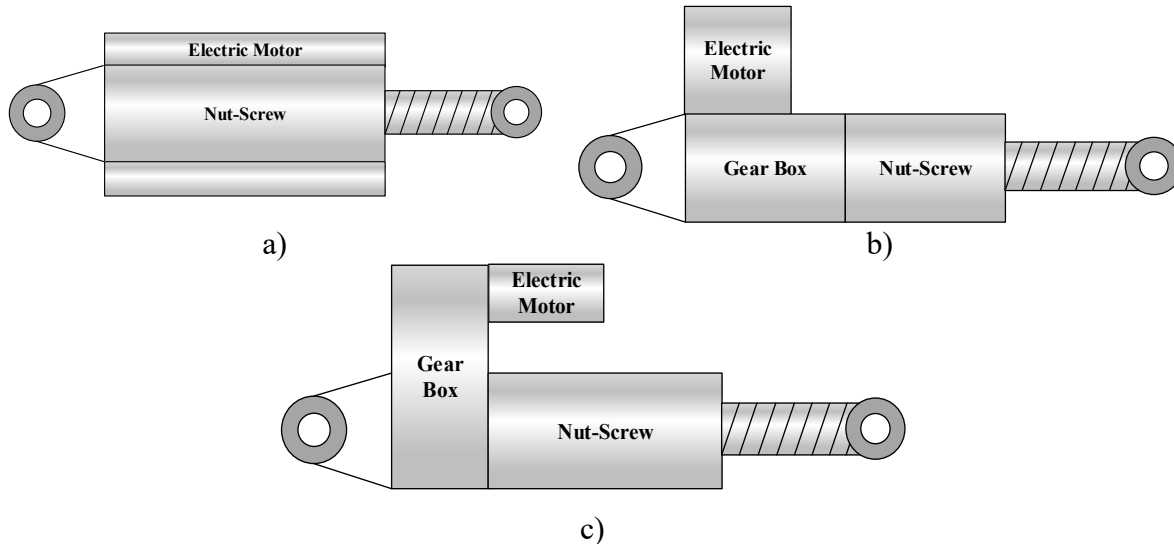
However, the same authors point out the main disadvantages, such as:

- The Jamming of the actuator;
- Sizing of the actuator.

The Electro-Mechanical Actuators have also other advantages when they are compared with the Electro-Hydraulic Actuators – EHA (these kinds of actuators will be more detailed in Section 2.2.3), as the elimination of the hydraulic circuits, which implies in a significant reduction of cost for maintenance due to the absence of wearing parts such as seals (GARCIA *et al.*, 2008).

For the implementation of the EMAs, there are some actuator arrangements based on the electric motor installation in relation to the nut-screw. Maré (2017) mentions that there are four main topologies, called in-line, concentric, perpendicular axes, and parallel axes. The in-line one was present in Figure 2.2, where in this configuration, the electric motor is assembled in the same central line of the nut-screw. In Figure 2.3, the concentric, perpendicular, and parallel axes electro-mechanical actuators are presented.

Figure 2.3 - Topologies of Electro-Mechanical Actuators with Nut-Screw. a) Concentric; b) Perpendicular axes; c) Parallel axes.



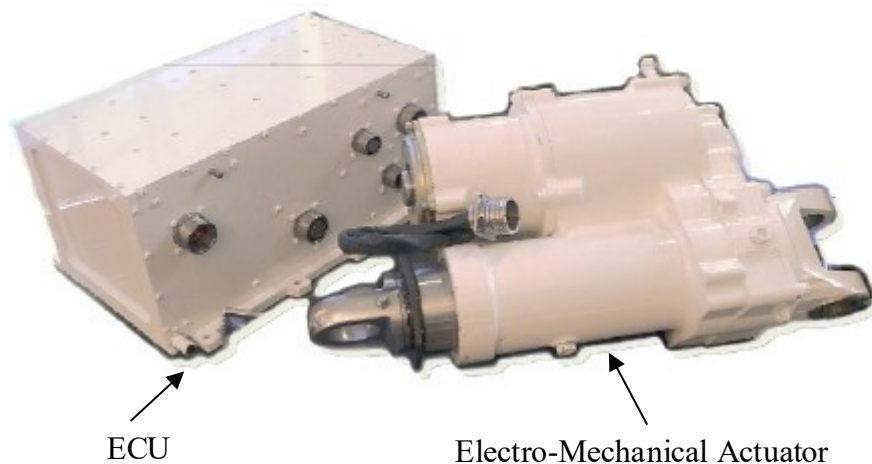
Source: By the author based in Maré (2017).

As shown in Figure 2.3a, the concentric configuration has the installation of the electric motor in a concentric way with the nut-screw. In the configurations with perpendicular and parallel axes (Figure 2.3b and c), the rotation axis of the electric motor is installed perpendicular or in parallel with the nut-screw axis, respectively. Maré (2017) quotes that, the solution with the perpendicular axis is not desirable due to the necessity of use conical gears.

However, the solutions that adopted the concentric and parallel axes configurations are well accepted, due to the reduction of the actuator total length.

Besides the applications of the Electro-Mechanical Actuators in the primary and secondary flight control surfaces, they are used in others systems of the aircraft, as the landing gears, braking systems, steering and engines (MARÉ, 2017). For an exemplification of a real EMA, Figure 2.4 shows the Boeing 787 spoiler Electro-Mechanical Actuator.

Figure 2.4 - Boeing 787 spoiler Electro-Mechanical Actuator.



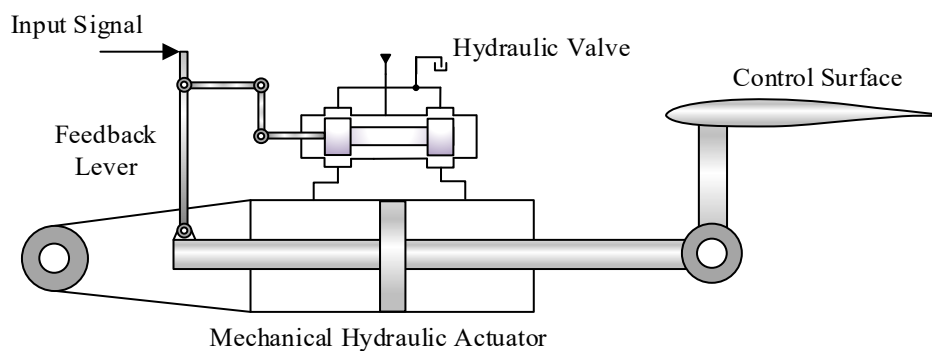
Source: Adapted from Maré (2017).

2.2.2. Servo Electro-Hydraulic Actuators - SHA

The hydraulic systems are one of the most important systems for the aircraft. They are responsible for the control of primary and secondary flight control surfaces (MOIR & SEABRIDGE, 2008), landing gears, cargo doors, steering (WARD, 2017) and so on. Alleyne & Lui (2000) point out that, the low power/weight ratio, coupled with a fast dynamic response and high rigidity are characteristics that make hydraulic systems unbeatable by other technologies. Zimmerman *et al.* (2007) quote that, the high-power density of hydraulic systems makes this technology extremely advantageous for mobile applications, where system compaction is important. For the actuation of the flight control surfaces, the Electro-Hydraulic Actuators are the most common solution applied (MÁRTON & OSSMANN, 2012). Normally, for the application of Electro-Hydraulic Actuators, the aircraft uses centralized hydraulic power units for the actuation of all actuators. According to Wang *et al.* (2016), the actuation system that used centralized hydraulic supplies was designed since 1950, to maneuver the surface movement. According to Wang *et al.* (2016), the controller of the early hydraulic actuators was mechanical, where the input signals were transmitted to a hydraulic valve through levers. When

the valve spool connects the high pressure to the actuator, it starts to move. When the actuator achieves the final position, the feedback lever closes the valve and the actuator movement stops. (WANG *et al.*, 2016). Figure 9 shows a Mechanical Hydraulic Actuator, which is powered by a centralized hydraulic power unit.

Figure 2.5 - Mechanical Hydraulic Actuator with a hydraulic valve powered by a centralized hydraulic unit.



Source: By the author based in Wang *et al.* (2016).

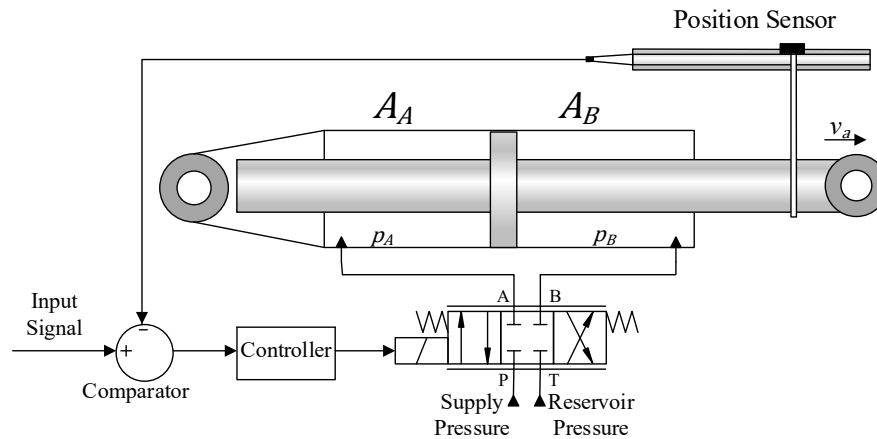
Garg *et al.* (2013) mention that, with the beginning of the jet age of civil aircraft transportation after World War II, the aircraft developed in this period as the De Havilland Comet 1, Boeing 707 were initially hydraulic controlled. The second generation of aircraft, as the Boeing 727 and 737, McDonnell Douglas DC10, Airbus A300 applied the hydro-mechanical flight control systems (GARG *et al.*, 2013).

Wang *et al.* (2016) highlight that, with the development of the Fly-By-Wire flight control systems, it was possible to implement electrical signals with hydraulic power. The same authors also quote that, the widespread use of hydraulic actuators in commercial aircraft's flight control surfaces is due to numerous advantages, such as:

- The hydraulic fluid is almost incompressible;
- High forces can be delivered by high pressure fluid;
- The high power per unit of weight and volume;
- Mechanical stiffness;
- Fast dynamic response.

When it is used a Servo Electro-Hydraulic Actuator, the control signals that came from the pilot's commands, are processed by a computer and sent electrically to the hydraulic servo-valve, which drives the actuator. In Figure 2.6, a simplified model of the Servo Electric-Hydraulic Actuator is presented.

Figure 2.6 - Simplified model of the Servo Electric-Hydraulic Actuator.



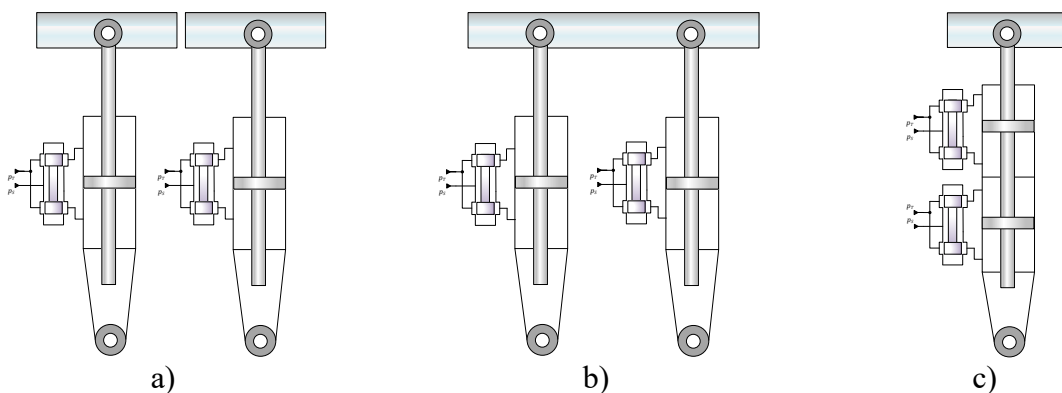
Source: By the author.

In Figure 2.6, the input signal is compared with the position sensor signal generating a position error. This error signal is sent for the controller and then for the servo valve. Once the servo valve receives the electric signal to move the actuator forward, for instance, it connects port P to the chamber A of the cylinder and the port T to the chamber B. When the cylinder achieves the desired position, the servo valve is closed.

One of the disadvantages of the servo valves used in this kind of actuator is the internal leakage, which causes energy losses. According to Maré (2017), the internal leakage of the servo valves has two different origins, in the null opening position and the pilot stage.

Another point to be mentioned about the SHAs are the possibility of implementation of redundant actuators, as can be seen in Figure 2.7.

Figure 2.7 - Redundancy systems for aircraft actuators. a) Redundant surfaces; b) External redundant actuators; c) Internal redundant actuators.

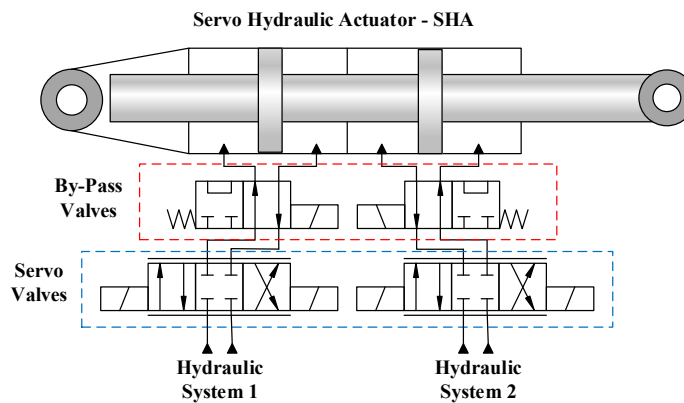


Source: By the author based in Bennett *et al.* (2012) and Belan (2018).

In Figure 2.7a, the redundancy is achieved by the use of two identical systems and in Figure 2.7b the redundancy is achieved using two parallel actuators in the same control surface.

In a case of failure of one actuator, the remained one controls the surface. In Figure 2.7c, the redundancy is internal of the actuator. This configuration was also presented in Belan (2018), as shows Figure 2.8.

Figure 2.8 - Electro-Hydraulic Actuator in tandem configuration.



Source: By the author based in Belan (2018).

In the configuration presented by Belan (2018), two servo valves are used in a tandem actuator. Both servo valves control the cylinder at the same time. In a case of failure of one servo valve, the by-pass valve is activated and the remained system controls the actuator, where the load capacity is reduced by 50%.

2.2.3. Electro-Hydrostatic Actuators – EHA

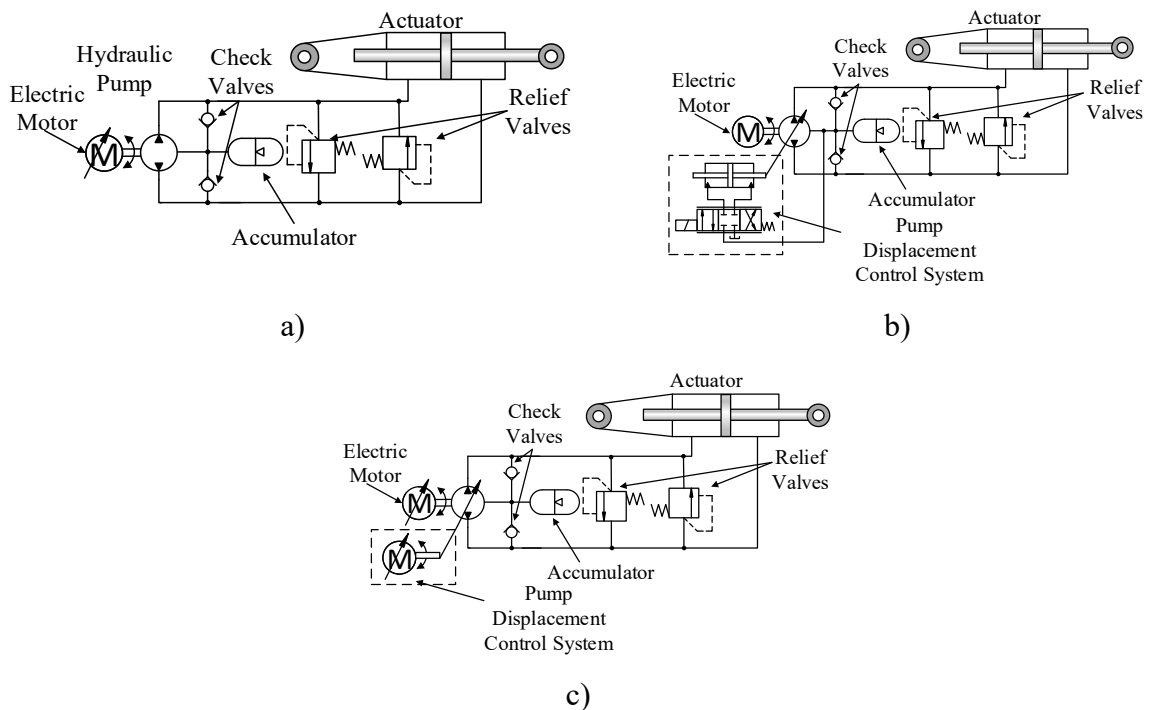
The Electro-Hydrostatic Actuators - EHA were developed to replace the hydraulic systems that use centralized power units by decentralized power units. According to van den Bossche (2006), the Electro-Hydrostatic Actuators are basically a self-contained hydraulic actuator, which is controlled by a hydraulic pump connected in a variable speed electric motor. Alle *et al.* (2012) highlight that other configurations can be used in EHAs, as variable displacement pumps with a fixed rotational frequency electric motor or a variable displacement pump with a variable rotational frequency electric motor.

For the configuration with variable rotational frequency electric motor and fixed displacement pump (FPVM), the amount of hydraulic fluid, which is directed for the cylinder's chambers, is controlled by the variation of the electric motor rotational frequency. In this arrangement, is necessary a bi-directional hydraulic pump (ALLE *et al.*, 2012). In the configuration with fixed rotational frequency electric motor and variable displacement pump (VPFM), the system is controlled by the variation of the hydraulic pump displacement. According to Wang *et al.* (2016), a servo valve and a cylinder establish the variation of the

pump displacement. Alle *et al.* (2012) quote that the control of the pump displacement can be also carried out by a servo motor. This arrangement provides better dynamic responses, however, the energy efficiency is smaller than the fixed displacement/variable rotational frequency motor and the variable displacement mechanism is complex. (ALLE *et al.*, 2012; WANG *et al.*, 2016).

In the variable displacement pump/variable rotational frequency electric motor Electro-Hydrostatic Actuators (VPVM), both pump and electric motor can be controlled independently. Thus, this configuration can provide the advantages of each system (ZHANG & ZHOU, 2010). The variable pump/variable electric motor EHAs, according to Zhang & Zhou (2010), are composed of a bi-directional variable pump, controller, sensors, hydraulic system, and the servo motors responsible to control the pump displacement and rotational frequency. Wang *et al.* (2016), mention that, although the ability to increase the system dynamics, the VPVM EHAs have a more complex structure, and thus, less reliability. This is one of the reasons for the adoption of FPVM EHAs in the More Electric Aircraft, due to its simplicity and lightness (WANG *et al.*, 2016). Figure 2.9 presents the different configurations for the EHAs.

Figure 2.9 – Electro-Hydrostatic Actuators Configurations. a) FPVM; b) VPFM; c) VPVM.



Source: By the author based in Alle *et al.* (2018) and Wang *et al.* (2016).

For the use of electro hydrostatic actuators, the development of the components that are part of them was necessary. In these kinds of actuators, high performance brushless DC

electric motors are necessary, due mainly to the flow and pressure control, which requires high power density (WANG *et al.*, 2016). In addition, Alle *et al.* (2012) quote that the electric motor is one of the most critical components for EHAs.

The hydraulic pump used in EHAs is another critical component. In conventional hydraulic systems applied in aircraft, the pumps used have large volumetric displacements in order to supply hydraulic fluid for all the actuators in a specific hydraulic circuit. For instance, in the Airbus A380, the volumetric displacement of the hydraulic pumps can achieve $47 \text{ cm}^3/\text{rev}$ (MARÉ, 2017). Another point to be mentioned is, for conventional hydraulic systems, the pumps work normally in a constant rotational frequency and output pressure, consequently, they can be optimized for these operation conditions, as quoted in Maré (2017). In Electro-Hydrostatic Actuators, the rotational frequency of the pumps is in a range of 10000 to 16000 rpm (MARÉ, 2016; ZHANG *et al.*, 2016), and the volumetric displacement is around $0.5 \text{ cm}^3/\text{rev}$ (MARÉ, 2017). In addition, the pumps need to operate in both directions of rotation and must be able to accelerate and decelerate with very low response time.

Due to the high rotational frequencies, Zhang *et al.* (2016) mention that some problems can occur during the pump operation, as the pressure pulsation, cavitation, and power losses. In addition, in cruise flight, the pump operates with very low rotational frequency, only supplying the system components leakage. In these conditions, the mechanical losses can increase significantly, due to constant change in the pump rotation direction. However, the use of hydraulic pumps with small volumetric displacements can bring some advantages for the Electro-Hydrostatic Actuators, as the capability to reach more compact systems and increase the system power density (ZHANG *et al.*, 2016).

To justify the use of the Electro-Hydrostatic Actuator, this kind of actuator have some advantages, such as (ALLE *et al.*, 2012):

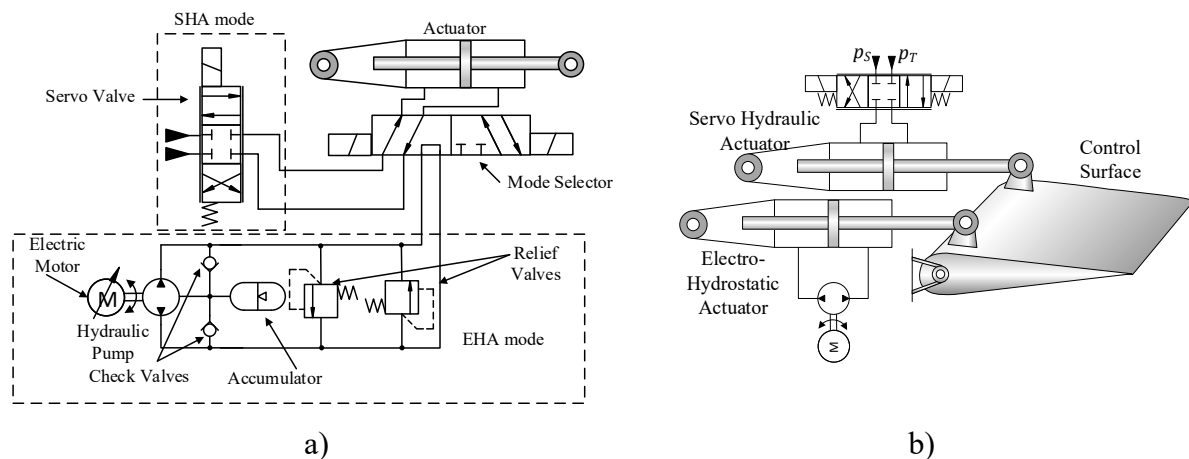
- The replacement of the centralized hydraulic systems by decentralized ones, which reduces the number of hydraulic pipes through the aircraft and consequently, the weight of the hydraulic system;
- Reduction of the maintenance cost due to the easy replacement of an EHA and case of fault;
- Reduction of energy losses due to the less use of components that throttle the flow.

The manufacturer of EHAs Moog also highlights that these actuators have a low level of noise and high values of forces can be achieved. However, the same manufacturer points out some disadvantages, as:

- The implementation in asymmetrical actuators is difficult and expensive;
- To fill the system with oil requires specialized equipment (vacuum) and strategic air bleed holes;
- The actuator remains lose when the system is powered off and then, additional components may be required to prevent undesirable actuator movements.

To exemplify the use of these kinds of actuators, the first appearance of the Electro Hydrostatic Actuator in a civil aircraft was in the Airbus A380 (van den BOSSCHE, 2006; JÄKER *et al.*, 2008; ALLE *et al.*, 2012; MARÉ, 2017). In this aircraft, during its development, two EHAs for the aileron and elevator and two EBHA (Electrical Back-up Hydrostatic Actuator) for the rudder and spoiler were developed (van den BOSSCHE, 2006). The concept of the Electrical Back-up Hydrostatic Actuator can be seen in Figure 2.10.

Figure 2.10 – Electrical Back-up Hydraulic Actuator – EBHA. a) Shared Actuator; b) Separated Actuators (Hybrid System).



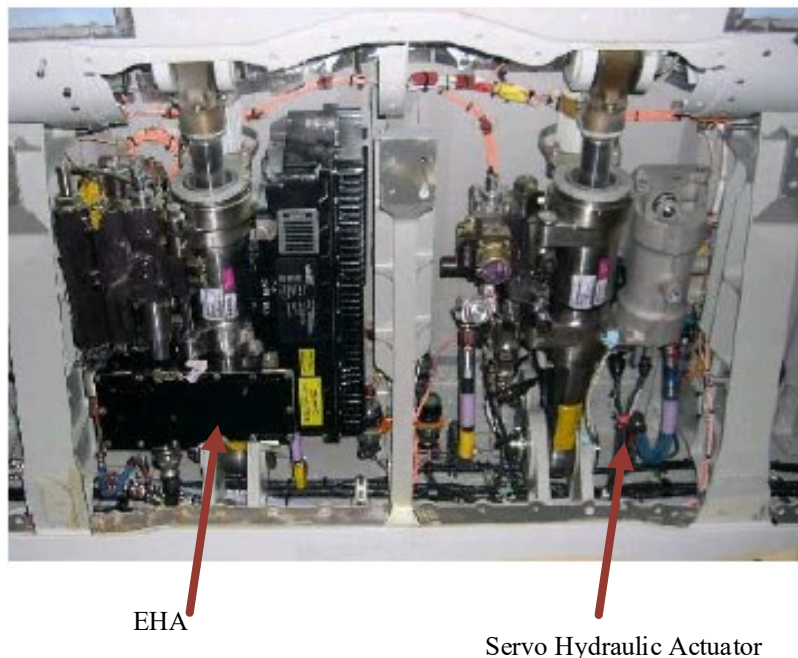
Source: a) By the author based in Maré (2017); b) By the author based in Wang *et al.* (2016).

According to Wang *et al.* (2016), the Electrical Back-up Hydrostatic Actuator is another type of EHA. They combine both systems in the same actuator, where the EHA is used as a back-up system (MARÉ, 2017). Wang *et al.* (2016) highlight that in normal mode, the servo hydraulic system controls the actuator, where the hydraulic power comes from the centralized hydraulic unit, but the use of both systems at the same time is also possible, where the system is called Electro-Assisted-Hydraulic Actuator – EAHA (MARE, 2017). With this

configuration, the reliability of the system can be increased, however, the centralized hydraulic unit is still necessary.

Figure 2.10b shows a configuration where both systems control the same flight control surface, but with separated actuators. This system is called Redundant Hybrid System (WANG *et al.*, 2016). In this conception, when the servo hydraulic actuator is active, the EHA remains in back-up mode, only following the servo hydraulic position. In case of a fault in the servo hydraulic system, the EHA controls the actuator, and therefore, the flight surface (WANG *et al.*, 2016). Figure 2.11 presents a real application of a configuration similar to the one shown in Figure 2.10.

Figure 2.11 - Airbus A380 EHA and Servo Hydraulic Actuator.



Source: van den Bossche (2006).

In Figure 2.11 it is possible to verify that the EHA takes up more space than the Servo Hydraulic Actuator. The reason for that is that all EHA components, valves, pump, and reservoir must be installed close to the actuator.

2.3. FINAL CONSIDERATIONS ABOUT CHAPTER 2

In this chapter, a review of the main flight control systems and flight control surfaces, which are implemented in aircraft, was presented. The flight control systems and the flight control surfaces have as a link element, the control actuators, which are normally, purely mechanic or electro-mechanic, purely hydraulic or electro-hydraulic.

With the development of the control electronics and its implementation together with mechanic and hydraulic actuators, the Fly-by-Wire flight control system has become the most control system used for commercial aircraft. According to Niedermeier & Lambregts. (2012), six different FBW control systems were implemented by Airbus, Boeing, Embraer, Ilyushin, Tupolev, Suchoi, and Antonov.

With the Fly-by-Wire systems and the necessity of to obtain more efficient aircraft, the More Electric Aircraft – MEA brought a new concept for the development of new aircraft topologies, where the main object is the replacement of the conventional hydraulic control system with more electric ones. Some solutions apply electro-mechanical actuators, however, some authors highlight that these kind of actuators are susceptible to jamming (WANG *et al.*, 2016; MARÉ, 2017; QIAO *et al.*, 2017), and are not mature enough for the use in primary control surfaces (QIAO *et al.*, 2017). The Electro-Hydrostatic Actuators are another alternative for the replacement of the centralized conventional hydraulic actuators, and consequently, obtain a more efficient solution. Nevertheless, they still use the principles and advantages of hydraulic systems. As mentioned in Section 2.2.2, hydraulic systems have been used in aircraft control surfaces since half of the 20th century (WANG *et al.*, 2016). Some of the reasons for that are the high power/weight ratio, high reliability, and low maintenance. However, the hydraulic systems have low energy efficiency due to the use of resistive components that throttle the flow, to control pressure and flow rate. In order to overcome the low energy efficiency of the hydraulic systems, a new conception for the design of more energy efficient hydraulic systems, with promising results, has been developed during the last decades, called digital hydraulics.

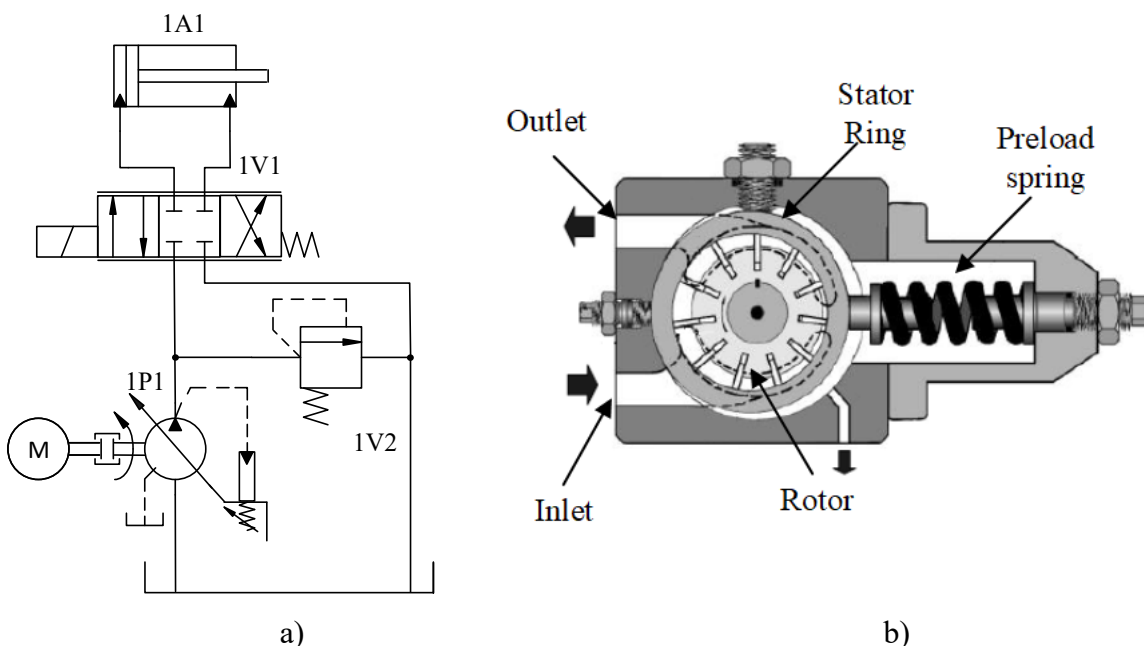
To introduce a better understanding of digital hydraulics, in Chapter 3 these systems will be presented and explained with more details.

3. SWITCHED AND DIGITAL HYDRAULICS

The application of power hydraulics is typically the most commonly used solution in systems that demand high power and low weight. von Linsingen (2013) quotes that the utilization of the hydraulic systems has the characteristics of being able to be applied in practically all kinds of activities, from mineral extraction, aerospace industry, and even in everyday situations, such as transport vehicles and civil construction. However, the use of power hydraulics typically requires the use of restrictive flow and pressure control techniques. Therefore, the use of valves that throttled the hydraulic fluid passages, increase energy dissipation due to pressure drop effects, resulting in low efficiency. Rydberg (2015) quotes that a typical efficiency for a mobile load sensing hydraulic system is around 35%. In this context, there are innumerable researches in this area with the purpose of making hydraulic systems more energy efficient. One solution to minimize energy losses due to pressure drop is to control the flow rate supplied by the hydraulic pump, controlling its volumetric displacement. According to Ivantsynova (2008), the use of actuators, which have controlled displacement, not only allows energy recovery, but also avoids fluid throttle losses.

An example of the application of hydraulic circuits using pumps with variable displacement is shown in Figure 3.1.

Figure 3.1 - Application of variable displacement pumps in hydraulic systems. a) Hydraulic circuit; b) Vane pump with variable displacement.



Source: a) By the author; b) Adapted from von Linsingen (2013).

Eggers *et al.* (2005) also highlight that the use of variable displacement pumps presents:

- Increased energy efficiency through omission of throttle losses and the possibility of energy recovery;
- Simplification of the system itself by using less components;

In the system presented in Figure 3.1, the control of the actuator is performed by throttling the flow by the valve 1V1, which causes losses through friction and internal leakages, generating heat. When no hydraulic flow is required, the pump should be setting with a low volumetric displacement. In this case, the pump flow rate should be sufficient enough only to maintain the system pressure and supply the system internal leakage. However, in low volumetric displacements, the volumetric efficiency for a variable displacement pump is degraded.

This control action avoids the flow rate through the relief valve 1V2 at high pressure. Therefore, the dissipative effects caused by the throttle losses are attenuated, increasing the system efficiency. In this context, the 1V2 relief valve is used as a safety device for the system, in the case of a failure in the pump's displacement variation control.

In addition to the solutions that employ pumps with variable displacement, in recent decades, two new technologies have drawn the attention of the academic community and industry to obtain more efficient hydraulic systems, called switched hydraulics and digital hydraulics.

Although the definition of digital hydraulics is not yet well defined among the academic community as mentioned by Belan *et al.* (2014), the most accepted definition is proposed by Linjama (2011), who mentions that digital hydraulics consists of systems that use components with actively controlled discrete output values. According to Scheidl *et al.* (2012), researches on digital hydraulic systems intensified from the beginning of the 21st century. Much of this is due to the development of fast-switching valves, compact, highly dynamic response accumulators, cylinders, and digital pumps (SCHEIDL *et al.*, 2012). According to these same authors, without the development of these components, many applications of digital hydraulics would become unviable. Scheidl *et al.* (2012) also mention that adequate modeling and simulation methods were developed to improve the understanding of the phenomena that occur in these types of systems.

For the switched hydraulics, one or more valves working at high frequency are used, being modulated by a PWM signal (LINJAMA & VILENIUS, 2008; LINJAMA, 2009; WANG

et al., 2011; BELAN *et al.*, 2014; BELAN, 2018). In digital hydraulics, the hydraulic components are connected in a parallel arrangement (Parallel Connection Technology). In this configuration, two or more hydraulic components (valves, cylinders, pumps) are connected in order to form a parallel arrangement, where the system output is given by the different interactions of the components. Systems that use parallel connections, according to Linjama & Vilenius (2008), are considered completely digital because their output has discrete values.

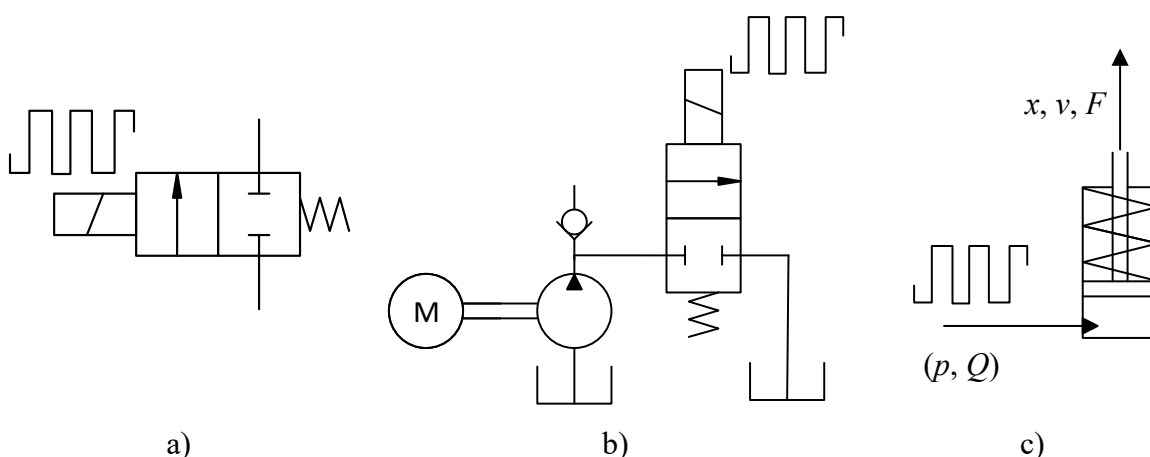
In Section 3.1, the switched hydraulics will be explained in detail, and in Section 3.2, the digital hydraulics.

3.1. SWITCHED HYDRAULICS

The switched hydraulics had one of its first industrial applications in the development of the Anti-Lock Brake Systems (ABS) (LINJAMA, 2011). Scheidl *et al.* (2013) also mention the application of variation in valve opening time in compressors and in the clutch systems in passenger cars. In the literature, since the 1960s and 1980s, some researchers can be found using switched hydraulics (Pollard, 1963; Brown, 1987; Brown *et al.*, 1988).

In switched hydraulics, there are systems that use switched valves, switched pumps, and switched cylinders, as classified by Linjama & Vilenius (2008). Figure 3.2 exemplifies the classification proposed by these authors.

Figure 3.2 - Classification of the switched hydraulic systems: a) Valves; b) Pumps; c) Cylinders.



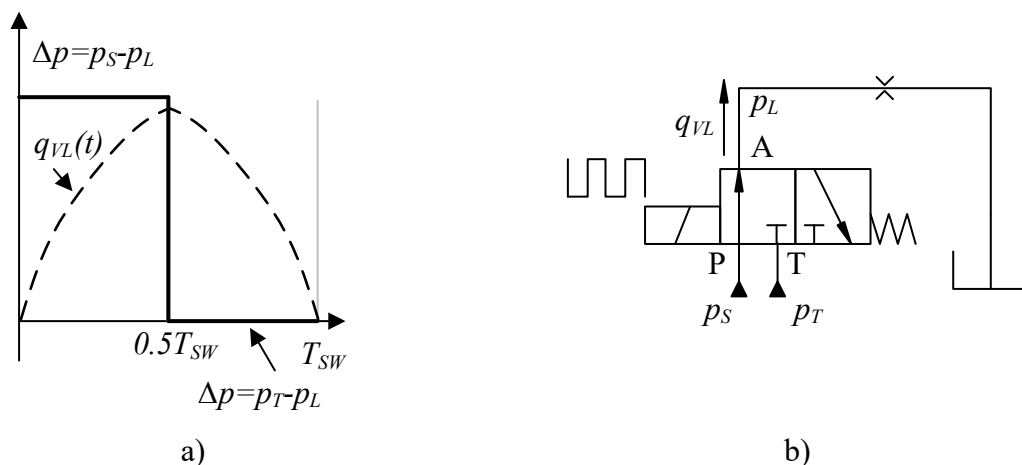
Source: Adapted from Linjama & Vilenius (2008).

According to Figure 3.2, on the switched valves (item a), a high-frequency signal is applied to the on/off valve, where the time that the valve remains open or closed is determined. For switched pumps (item b), the flow rate that the pump delivers to the system is determined

by switching the on/off valve, which directs fluid to the system or reservoir. In switched cylinders (item c), the flow rate or pressure in the control chamber has a switched behavior.

The high frequency signal, which is sent to the components, is usually a Pulse Width Modulation (PWM) type. In this type of signal, the duty cycle variation (κ) determines the system behavior. Figure 3.3 shows a PWM signal with 50% duty cycle.

Figure 3.3 - Switched hydraulics PWM signal: a) Signal; b) Switched on/off valve.



Source: By the author.

As shown in Figure 3.3 (item a), for a given switching period (T_{sw}), the on/off valve (item b) remains opened, connecting lines P to A with T blocked, and closed, connecting lines T to A with P blocked during the same time interval for a duty cycle κ equals to 50%. However, using different duty cycles, the time that the valve remains opened or closed changes. This type of control is widely used in converter-type switched hydraulic systems, such as the step-up converter and step-down converter, which will be explained in sections 3.1.1 and 3.1.2, respectively.

In recent years, research on switched hydraulic systems has grown considerably. The Laboratory of Hydraulic and Pneumatic Systems of UFSC - LASHIP has contributed to this increase, mentioning the works of De Negri *et al.* (2014), De Negri *et al.* (2015), Galloni (2015), Nostrani (2015), Nostrani *et al.* (2016) and Nostrani *et al.* (2017).

One of the limitations of switched hydraulic systems is the response time of the valves. Due to the high frequency switching of the valves, they need to have a short response time to achieve complete opening or closing in all ranges of duty cycles. For example, for a frequency of 50 Hz, the required time would be 2 ms. However, valves with this behavior are rare commercially. Linjama & Vilenius (2008) conducted studies on different response times of

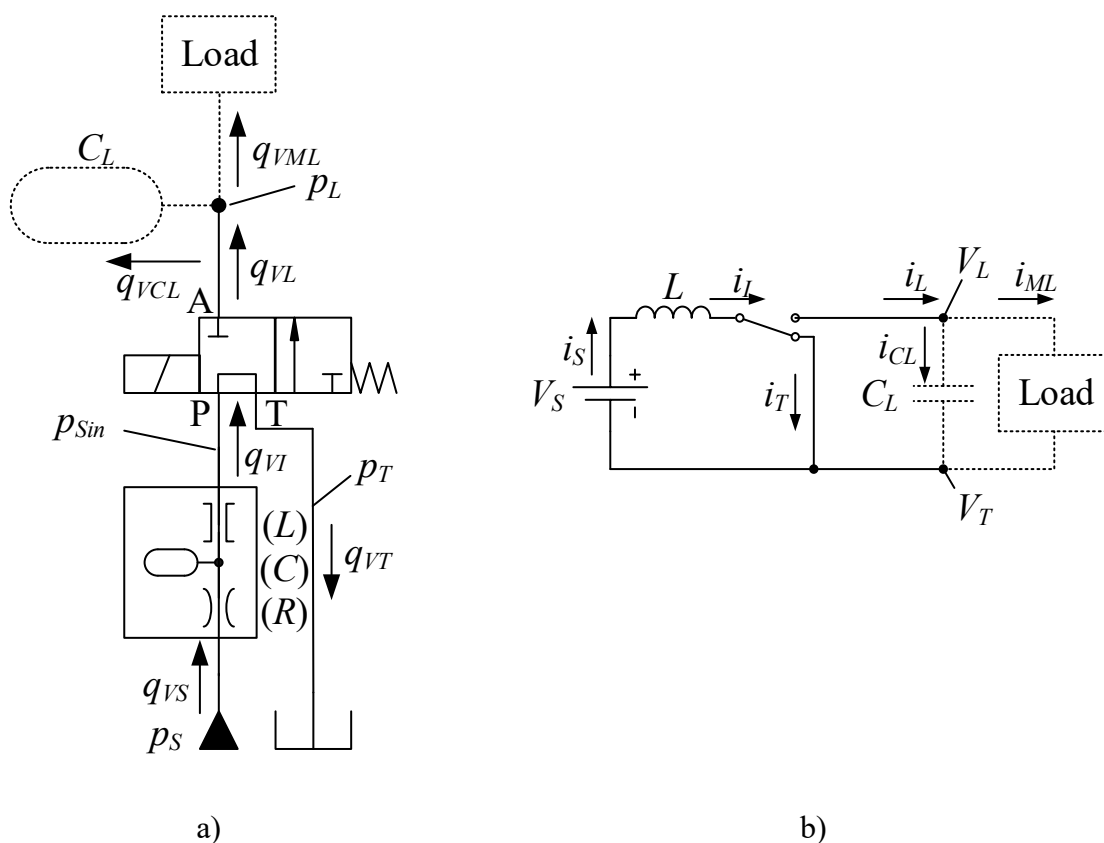
commercial valves, where an average response time of 10 ms is noted. The hydraulic component manufacturer Parker has the D1FP series proportional valves with 3.5 ms response time.

In order to overcome this limitation, studies have been elaborated for the development of valves with shorter response times, as is the case of Winkler *et al.* (2010). In this study, an externally piloted seat valve with 1 ms response time was developed. In addition to the work of Winkler *et al.* (2010), it is possible to cite the works of Wang & Li (2008), Wang & Li (2009), and Tu *et al.* (2009), where a rotary spool valve was developed.

3.1.1. Step-up systems

As mentioned in Section 3.1, the switched hydraulic systems, which apply circuits called converters, are one of the most studied systems. In these types of systems, an on/off valve associated with an inductive element, which is usually a large length, small diameter hydraulic tube, called inertance tube. In step-up converter or boost converter systems, the tube is installed before the valve, as shown in Figure 3.4.

Figure 3.4 – Step-up system: a) Hydraulic circuit; b) Electric equivalent circuit.



Source: Adapted from De Negri *et al.* (2014).

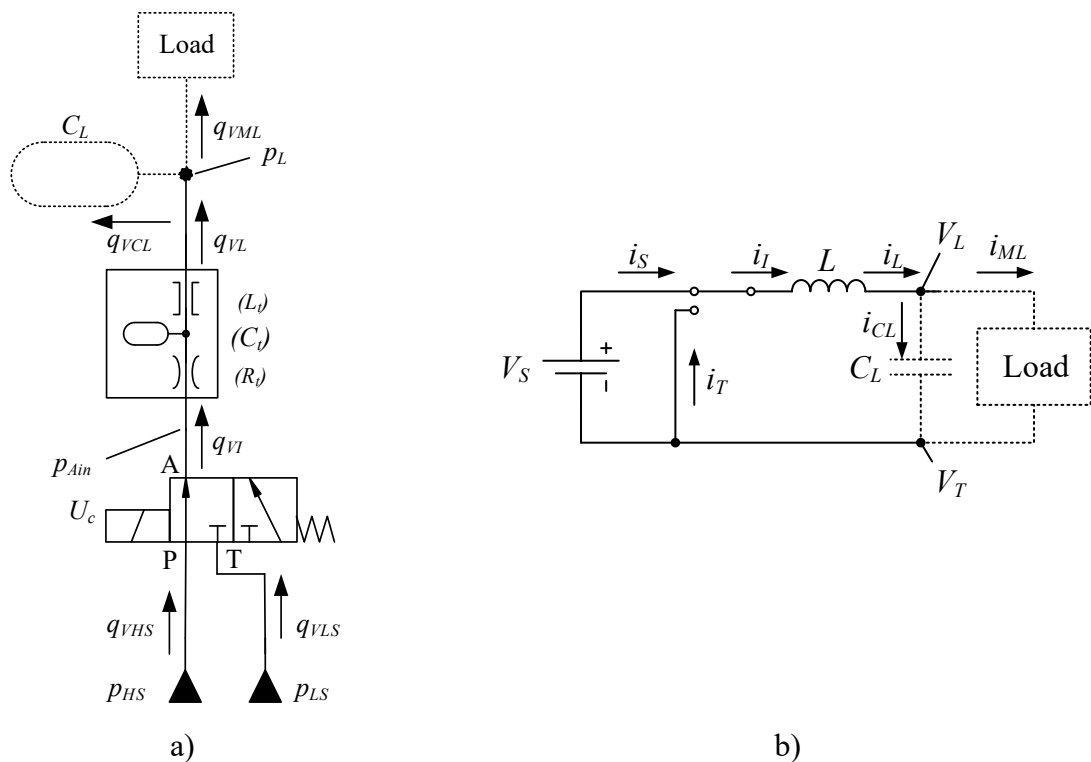
The steady-state behavior study, of this type of configuration, was originally based on switched power supplies (analogy between electrical and hydraulic systems, Figure 3.4 item b), which are widely used nowadays (De Negri *et al.*, 2014).

For the configuration shown in Figure 3.4, when the valve is activated, connecting ports P and T, and blocking port A, hydraulic fluid is accelerated within the inertance tube. By switching the valve, connecting ports P and A, and blocking T, the inertia of the mass of fluid contained in the tube compresses it, increasing the loading pressure (p_L). De Negri *et al.* (2014) make a study about this type of circuit, reaching hydraulic efficiency values around 80%.

3.1.2. Step-down systems

In the configuration of step-down switched hydraulic systems, the inertance tube is positioned after the valve, as shown in Figure 3.5.

Figure 3.5 - Step-down system: a) Hydraulic circuit; b) Electric equivalent circuit.



Source: Adapted from De Negri *et al.* (2015).

In this type of configuration, when the valve is activated, connecting ports P and A, and blocking port P, the internal pressure (p_{Ain}) increases to the high supply pressure value (p_{HS}). This action induces fluid acceleration along the inertance tube. When the valve is

switched to the other position by connecting ports T and A, and blocking P, the fluid inertia, which is contained inside the inertance tube, causes the internal pressure to fall below the low supply pressure value (p_{LS}), causing fluid suction from the low to the high pressure line (DE NEGRI *et al.*, 2015). The load pressure (p_L) can be controlled from the duty cycle variation of the PWM signal, having its value equal to p_{LS} for κ equals to zero and p_{HS} for κ equals to 1, considering zero load flow rate (q_{VL}).

The modeling of this type of system, considering the energy losses from the valve and the inertance tube, was discussed in De Negri *et al.* (2015). The authors comment that the losses from these components directly influence the system efficiency. However, with the correct selection of inertance tube parameters (length and internal diameter), it is possible to obtain efficiency values of the order of 70%.

3.2. DIGITAL HYDRAULICS

Digital hydraulics has emerged as an alternative to conventional hydraulic systems, aiming to achieve more energy efficient systems. In this type of system, the hydraulic components are connected in such a way to form parallel arrangements. According to Linjama & Vilenius (2008), digital hydraulic systems, which use parallel connections, are considered digital due to the fact that their output has discretized values.

For this type of system, there are in study nowadays, configurations of parallel connection hydraulic systems that use valves, pumps, and actuators in parallel, as mentioned in Linjama (2011) in his paper Digital Fluid Power - State of the Art.

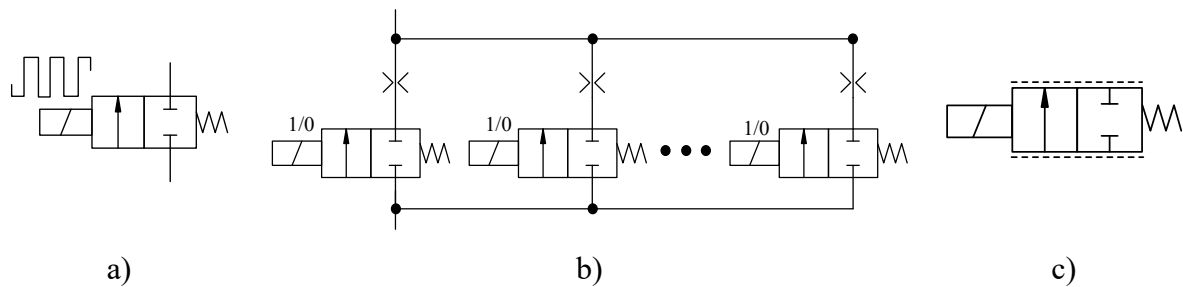
To illustrate the application of the use of digital hydraulic systems, the components will be presented according to the classification proposed in von Linsingen (2013) and used in Belan *et al.* (2014). In this case, in Section 3.2.1 the digital valves for the Limitation and Control Unit will be presented. Section 3.2.2, presents the digital pumps for the Primary Conversion Unit, and in Section 3.2.3, for the Secondary Conversion Unit, the digital actuators.

3.2.1. Digital valves in parallel connection

In this Section, the digital valves for the Limitation and Control Unit will be presented. With the emergence of digital hydraulics where the components are connected in order to form parallel connections, the number of on/off valves, which are used to obtain systems with good dynamic responses, has increased considerably. In addition, more and more researches in this area have intensified. In this context, Linjama & Vilenius (2003) propose the concept of DFCU

- Digital Flow Control Unit, which consists of an arrangement of two-way on/off valves connected in parallel. Figure 2.13 shows the representation of switched valves (item a), a DFCU (item b), and its simplified symbol (item c).

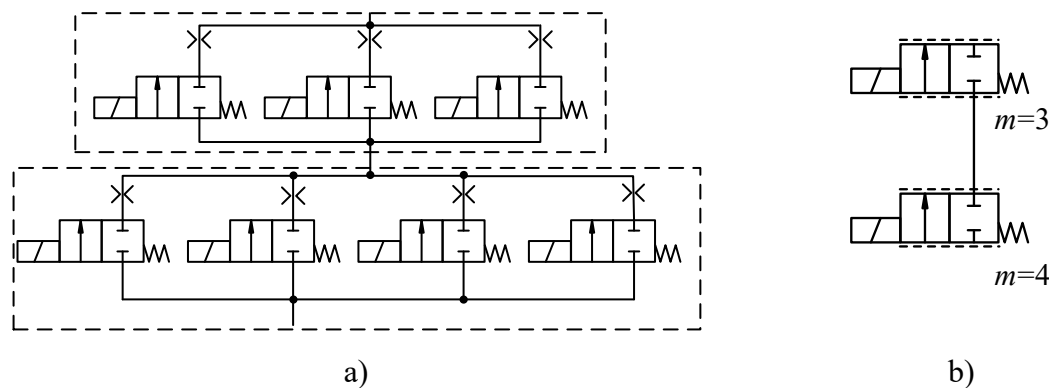
Figure 3.6 - Representation of digital valves: a) Switched valve; b) Digital flow control unit - DFCU; c) Symbol of a DFCU.



Source: Adapted from Linjama (2011).

The simplified DFCU symbol has dashed parallel lines, similar to those used in proportional valves, which are continuous lines (LINJAMA & VILENIUS, 2003). With the introduction of DFCUs, the hydraulic diagrams become more compact, as shown in Figure 3.7.

Figure 3.7 - Simplification of the hydraulic circuits: a) Conventional; b) Equivalent using DFCUs.



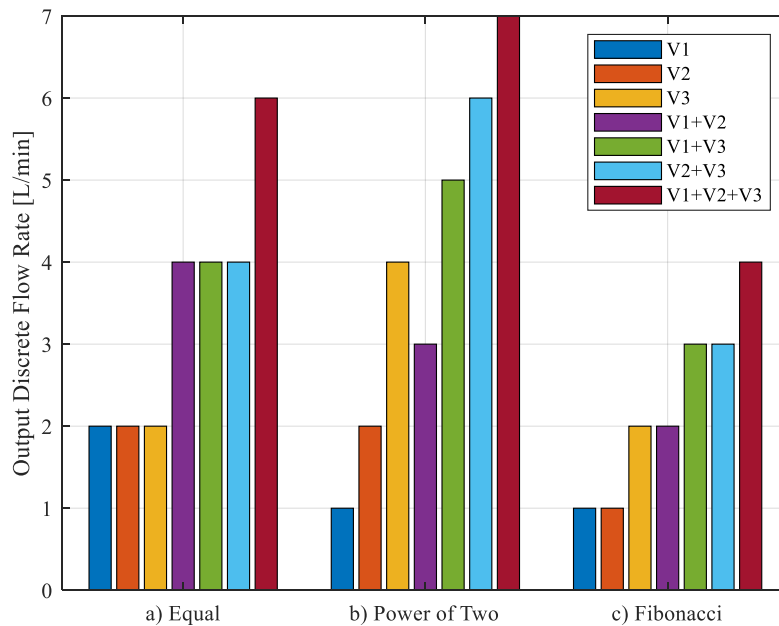
Source: By the author.

The parameter m presented in Figure 3.7b represents the number of valves contained in the DFCU, which in this case is equal to three and four, respectively.

Using a DFCU, the number of discrete flow rates supplied by it, will depend on the number of valves used and how these valves are distributed. The simplest alternative is to use direction on/off valves of the same size, but other combinations of valves can be used, such as power of two (1, 2, 4, 8 ...) and Fibonacci (1, 1, 2, 3, 5 ...) (LINJAMA *et al.*, 2003; LINJAMA, 2011; BELAN *et al.*, 2014). Figure 3.8 illustrates three different distributions of on/off valves

sizes using a DFCU with three valves. The valves of each DFCU are distributed in equal sizes (a), power of 2 series (b) and Fibonacci series, where all flow rates consider the same pressure differential.

Figure 3.8 - Distribution of discrete flow rate outputs: a) Valves with the same size; b) In power of two; c) In Fibonacci series.

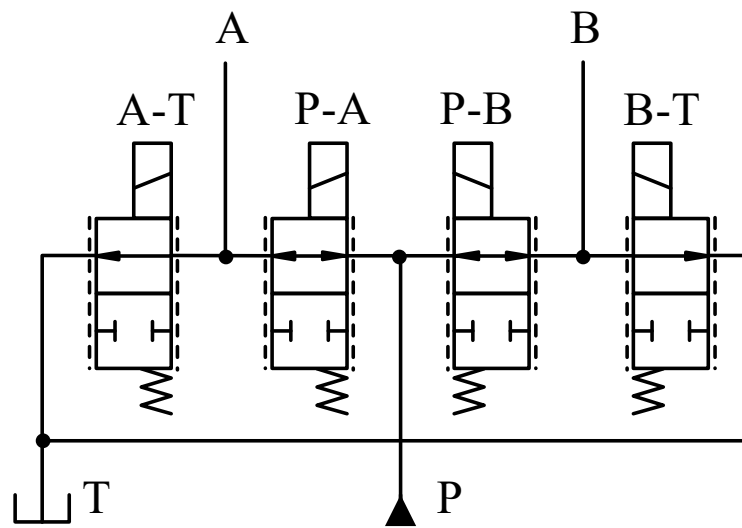


Source: By the author.

The results presented in Figure 3.8 show that using valves of the same size generates only three different flow rate levels. In addition, different valve combinations may provide the same output flow rate. This arrangement turns out not to be interesting from a control point of view, however, it is relevant in case of failure of one of the valves, where the system can work without significant loss of performance. By using the valve size setting at the power of 2, it is possible to obtain seven different discrete flow rate values for the system. This configuration allows good linearity of discrete flow values, improving system controllability. When using Fibonacci series valve sizes, a similar phenomenon occurs with the use of valves of the same size, where there is not only a reduction in the possible output values for the system, but also different valve combinations can provide the same output for the system.

An alternative of employing on/off valves in parallel connection is to replace common four way sliding spool directional valves, with DFCUs connected to form a similar arrangement, as shown in Figure 3.9.

Figure 3.9 – Four way hydraulic valve using DFCUs.



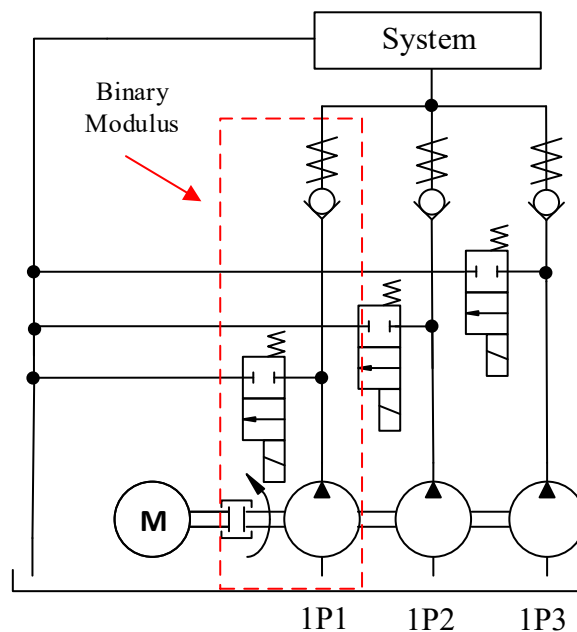
Source: Adapted from Linjama (2011).

According to Linjama & Vilenius (2003), the use of on/off valves in the digital parallel connection hydraulics, in order to replace the traditional directional valves, presents more control versatility. This is possible due the independently and simultaneously flow rate control through the ports P to A, P to B, A to T and B to T. For example, with the digital directional valve, the DFCU that connects the port P to A can be used with all valves opened and the DFCU that connects the ports B to T with only half of the valves opened, making it an interesting application for asymmetric actuators.

3.2.2. Digital pumps

In addition to digital valves, another approach for digital hydraulic systems is the use of digital pumps for the Primary Conversion Unit. According to Theissen *et al.*, (2013), a digital pump can be defined as an arrangement of several pumps with constant volumetric displacement, preferably coupled on the same axis, where each pump usually has different volumetric displacement rotating at a constant rotation frequency. However, in this thesis, another definition of a digital pump will be adopted, which consists as a fixed displacement pump where a directional valve is connected in its outlet port, which is responsible for directing the flow to the system or reservoir and a check valve, with the function of isolating the pump. This set of components can be called as a binary modulus. To increase the number of output flow rates for a digital pump, more binary modulus can be added in the same shaft. Figure 3.10 presents a hydraulic digital pump with three binary modulus.

Figure 3.10 – A digital hydraulic pump with three binary modulus.



Source: By the author.

From the circuit shown in Figure 3.10, pumps 1P1, 1P2, and 1P3 are connected on the same shaft to an electric motor with constant rotational frequency. Each pump is associated with an on/off valve at its outlet. By switching the on/off valves, it is possible to direct the flow rate of each pump to the reservoir or to the system, as required. When one of the pumps are not being required, the flow rate is direct to the reservoir at low pressure, which minimizes the volumetric losses. With the configuration of pumps shown in Figure 3.10 and using pumps with a volumetric displacement in power of two, it is possible to obtain seven discrete flow values that can be delivered to the system.

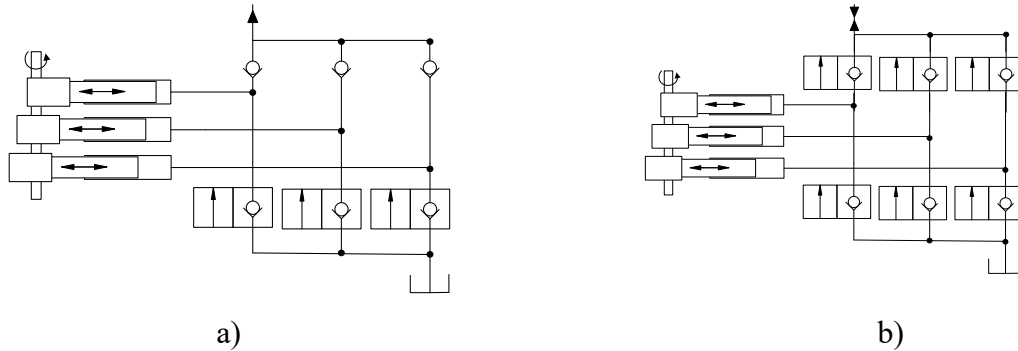
Pinto *et al.* (2016) point out that in systems that use variable volumetric displacement or variable rotational frequency, the effects of low lubrication of the pump at low flow rates must be taken into consideration because, in this working condition, the pumps work in a low volumetric efficiency range.

One of the advantages of using digital pumps in parallel arrangements is the use of constant displacement pumps, which are usually simpler and have a lower cost when compared to variable displacement or load-sensing pumps. In addition to these advantages, normally constant rotational frequency motors are used in this type of system, which avoids the use of frequency inverters, which are complex components and present high cost.

According to Linjama (2011), another way to implement digital pumps is the use of piston pumps. In this type of pump, each piston can be independently controlled by on/off

valves. The same author also points out that in this type of configuration, it is possible to use partial displacements of the pump and each piston can work in pump, idle, or motor mode. Figure 3.11 shows the hydraulic circuit of a digital piston pump.

Figure 3.11 – Digital piston pump: a) Pump mode; b) Pump and motor mode.



Source: Adapted from Linjama (2011).

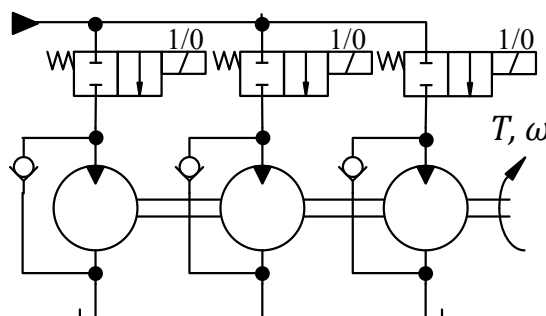
Nowadays, only the manufacturer of hydraulic components and systems Artemis commercially supplies pumps with these characteristics, where there are researches of its applications in wind turbines, as in the work of Rampen (2006).

In Chapter 4, Section 4.4, the use of a digital pump combined with multi-chambers hydraulic cylinders will be explained with more details.

3.2.3. Digital actuators

For the Secondary Conversion Unit, another type of component under study for use in digital hydraulic systems is the digital actuators. These types of components include digital cylinders and digital motors. In motor type digital actuators, two or more motors are coupled to the same shaft, where an on/off valve controls the input flow rate of each motor, as shows Figure 3.12.

Figure 3.12 - Motor type digital hydraulic actuators.

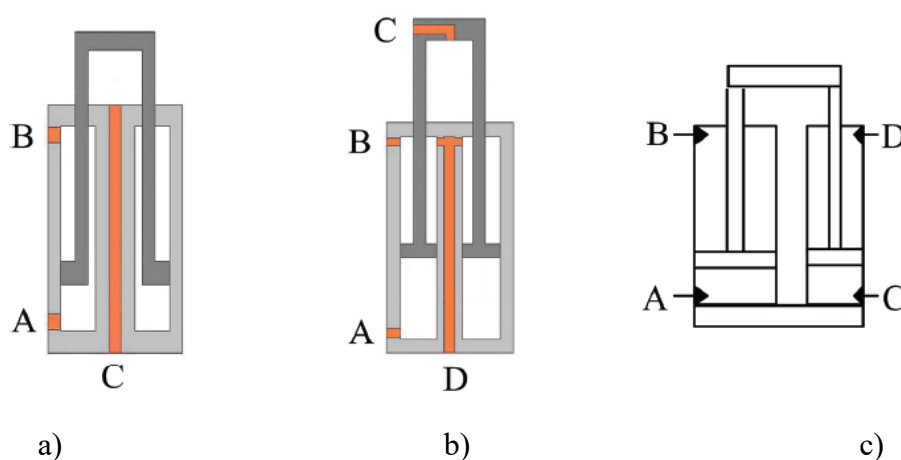


Source: Adapted from Linjama (2011).

In the configuration shown in Figure 3.12, the angular velocity transmitted by the shaft is controlled by combining the hydraulic motors, and then obtain different volumetric displacements. In the circuit shown in Figure 3.12, it is possible to obtain seven discrete output angular velocities values using motors with three different volumetric displacements. Digital hydraulic motors work similarly to digital pumps, but the number of researches in the area using digital hydraulic motors is smaller when compared to digital cylinders.

For the use of digital cylinders, multi-chamber cylinders with at least three chambers are used. Linjama (2011) points out that four-chamber cylinders, in the same body, is practically the maximum number of chambers possible. Dell'Amico (2013) uses a four-chamber cylinder in an excavator. This same author and Linjama (2011) quote that the number of discrete forces that can be obtained in multi-chamber actuators can be calculated as N^M , where N is the number of supply pressures and M the number of chambers. Figure 3.13 shows three different multi-chamber cylinders configurations.

Figure 3.13 - Multi-chambers linear cylinders: a) Three-chambers; b) Four-chambers; c) Parallel four-chambers cylinder.



Source: Adapted from Linjama *et al.*, (2009).

In Linjama *et al.* (2009) a multi-chamber linear cylinder with four different chambers and two different supply pressure levels is used, producing sixteen discrete force values, where its control is performed by a secondary technique. In this study, the authors report that the system using the digital cylinder achieved a 60% reduction in energy losses when compared to traditional load-sensing systems. In Belan *et al.* (2015), it is also studied a four-chamber linear digital actuator; however, three different supply pressure lines were used, which results in 81 discrete force values. In addition, the authors conducted a study of the design of the actuator areas in order to obtain a symmetric force distribution values for the backward and forward

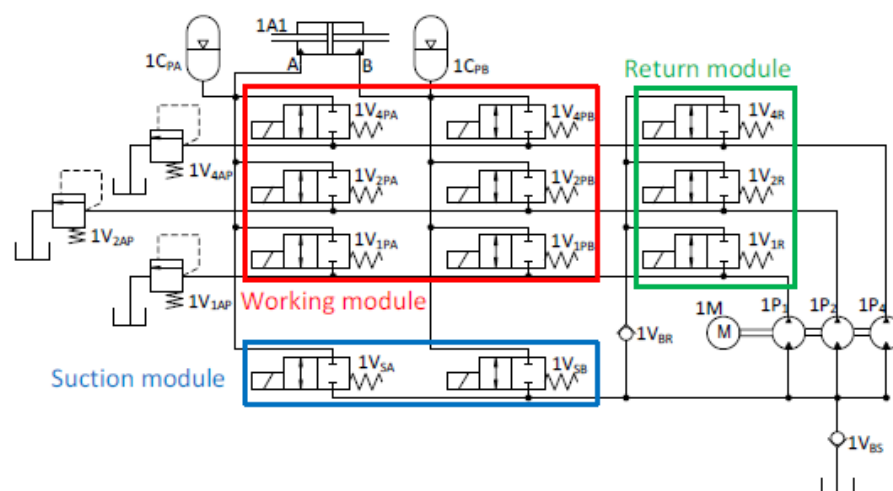
movements. Compared to traditional systems, Belan *et al.* (2015) achieved a reduction of energy losses around 80%. Houva *et al.* (2010) proposed another use of multi-chambers linear actuators, for application in mobile vehicles. In this study, the authors obtained a loss reduction of between 33 and 63%.

In addition to using multi-chamber linear cylinders in the same body or in parallel arrangements, as shown in Figure 3.13 item c, there is also the possibility of using cylinders in series, which allows the possibility of increase the number of chambers, and then, improve the system resolution. In Chapter 4, the digital system proposed in this thesis will be presented and the multi-chambers cylinders in series will be discussed with more details.

3.2.4. Applications for digital pumps, valves, and actuators

With the development of digital hydraulic components, the integration of these components together for the study of new hydraulic systems has increased significantly. In Locateli *et al.* (2014a) and Locateli *et al.* (2014b), a system using a digital pump coupled to on/off valves, which are connected directly to a hydraulic two chambers cylinder was developed. In these works, the authors conducted a study on the control of the actuator forward and backward velocities, through a non-restrictive control, with the use of on/off valves. Figure 3.14 presents the system using a digital pump and valves for velocity control.

Figure 3.14 – System using a digital pump and on/off valves for velocity control.

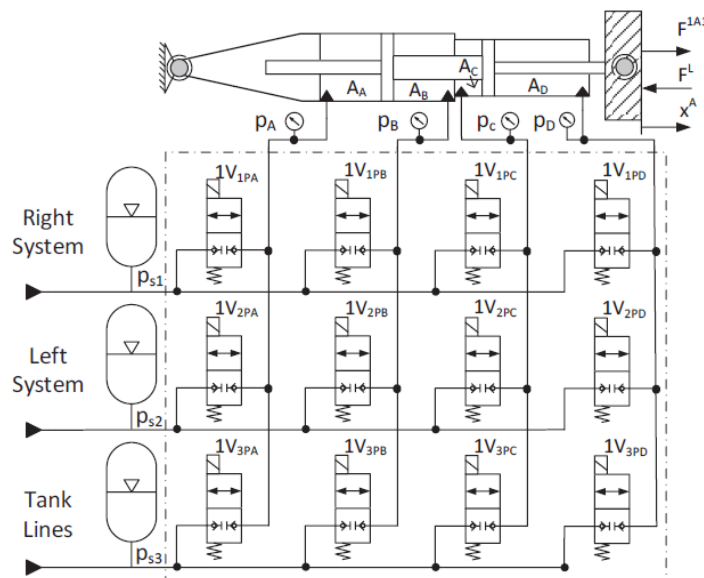


Source: Locateli *et al.*, (2014a).

In the configuration shown in Figure 3.14, each different combination that is possible to achieve by the digital pump can be selected in each actuator chamber by the on/off valves. Therefore, it is possible to obtain seven different supply flow rates and then, seven different

forward velocities and seven backward velocities. According to Locateli *et al.*, (2014b), the delay in the valve command signal affects the energy losses. However, the authors mention that this system presents a smooth response in the transition between different velocity levels. In Belan *et al.* (2015), a study on force control using on/off valves and a four chambers linear hydraulic cylinder was performed. In this study, the authors use twelve on/off valves to select three different pressure sources in the cylinder chambers. Figure 3.15 shows the hydraulic circuit studied by these authors.

Figure 3.15 – Digital hydraulic system using on/off valves and multi-chamber cylinder for force control.

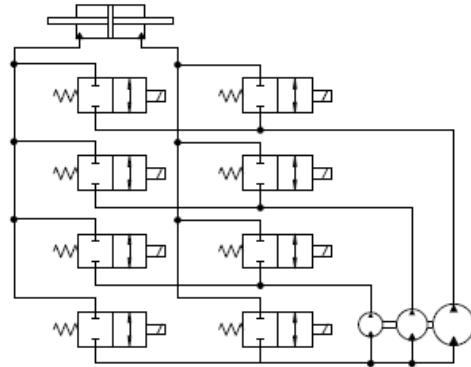


Source: Belan *et al.*, (2015).

This system is being developed for force control in aircraft actuators, with the purpose of reducing the energy losses of the aircraft hydraulic circuit. From the hydraulic circuit, that was designed by Belan *et al.* (2015), the authors obtained good dynamic responses for the system operating in position control and in force control. In addition, an energy loss reduction of 89% was achieved, when compared to conventional hydraulic systems already applied to the aircraft under study. Dell'Amico *et al.* (2013) proposed a configuration similar to that used by Belan *et al.* (2015). In this study, the authors used a system with digital hydraulic valves and a multi-chamber linear cylinder to control the force of an excavator's arm. According to Dell'Amico *et al.* (2013), the results obtained were promising, since the use of a simple control strategy can obtain relatively smooth behavior for the arm. The authors also point out that one of the major energy losses of this system is caused due to the compressibility of hydraulic fluid.

Heitzig & Theissen (2011) evaluate the use of a digital pump in closed-loop for application in a linear cylinder, as shown in Figure 3.16.

Figure 3.16 - Digital hydraulic system using a digital pump.



Source: Heitzig & Theissen (2011).

In the circuit shown in Figure 3.16, each pump can be independently selected for the cylinder chambers. Theissen *et al.* (2013) carry out a study on hydraulic circuits using a digital pump and valves, where the authors achieved a 38% reduction in the energy consumed by the digital pump, when compared to conventional pumps.

3.2.5. Final considerations about digital hydraulics

In this chapter, the main concepts about digital hydraulic systems were presented. From the researches conducted on this theme, it is evident the potential of using this technology in many different areas, such as mobile, naval, and aeronautics. In addition, in most cases of digital hydraulic systems, common components with low manufacturing and maintenance costs, such as seat on/off valves and fixed displacement gear pumps are used. However, digital hydraulic systems require a large number of these components, as for example in the system presented by Belan *et al.* (2015). In this system, the use of twelve valves is required. Consequently, with the large number of components that digital hydraulic systems require, there is a concern for the mass increase. However, due to the fact that digital hydraulic systems have better efficiency, other components can be better optimized, such as hydraulic fluid cooling systems, which may have smaller sizes and powers, and also the redundancy systems, due to the redundant nature of digital hydraulic systems.

Another factor to be emphasized is the need for the development of new hydraulic components, as is the case of the Artemis digital piston pump (RAMPEN, 2006), and the obtainment of faster response valves, with high flow rates. As mentioned in Section 3.1, there

are currently researchers developing faster valves (WINKLER *et al.* 2010; WANG & LI 2008; WANG & LI 2009; TU *et al.* 2009), however, most researches are in a prototype phase. One solution found to reduce valve response time is to use voltage boosters on the valve solenoids. In this type of device, an overvoltage is applied to the valve solenoid in a short period of time beyond its nominal voltage. This type of booster was used in Belan *et al.* (2016) research, where an overvoltage of 48 V for a few milliseconds was applied to a solenoid with a nominal voltage of 12 V. According to these authors, the valve response time was originally 19 ms, and with the booster, it was possible to obtain a response time of 3 ms. This type of technique allows conventional valves to have a shorter response time, making their use in digital hydraulic circuits feasible (BREGALDA & BELAN, 2015). However, the use of such devices may overload the valve solenoids, thereby reducing their lifetime.

Researches on digital hydraulics, according to Linjama (2011), has shown great effort and interest in this area, which means that this technology offers benefits compared to traditional hydraulic systems, such as (LINJAMA, 2011):

- Robust, simple and reliable components;
- Better performance due to faster valves;
- High degree of flexibility and programmability. However, the same can be achieved by traditional solutions;
- Unification of hydraulic components. For example, control software determines the system characteristics and not the valve spool;
- High efficiency in pumps and motors;
- New solutions are completely possible.

However, the same author highlights the challenges and disadvantages of using this new technology, such as:

- High noise and pressure pulsation;
- Durability and lifetime with the use of switched hydraulics;
- Physical size and price using parallel technology;
- Complex and unconventional control.

As mentioned by Linjama (2011), one of the biggest disadvantages of using digital hydraulic systems is pressure pulsation. This phenomenon occurs due to the fast switching of valves between low and high pressure levels, which can cause audible noise and vibration. To avoid this phenomenon, there are researches being carried out, including the works of Pan *et al.* (2012) and Pan (2012).

4. DIGITAL ACTUATOR DESIGN

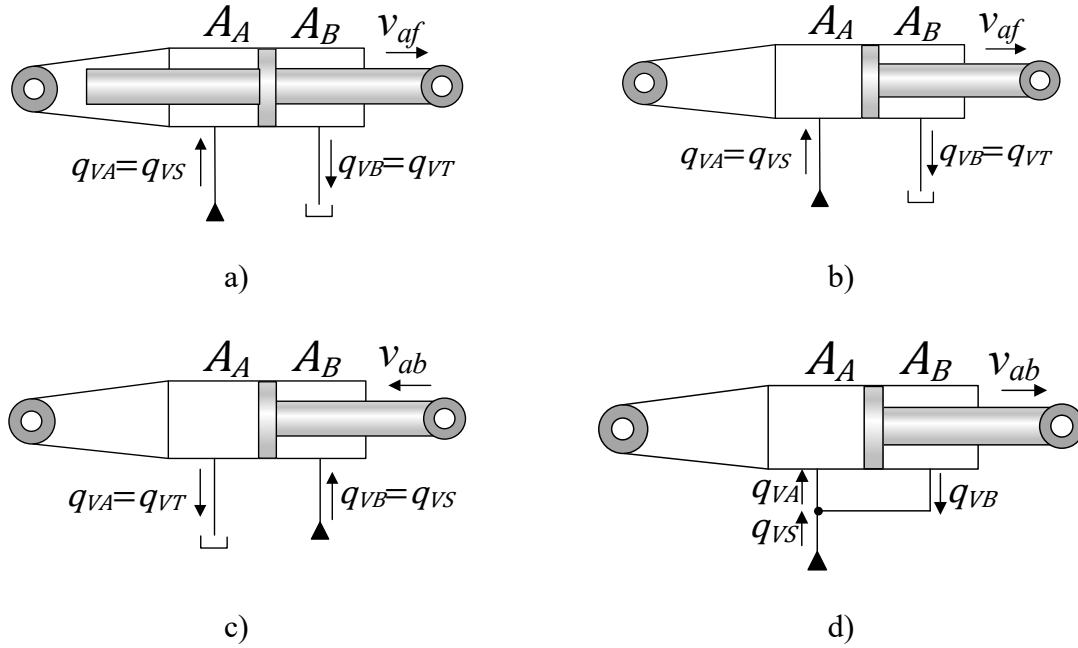
In this chapter, the design of the digital hydraulic actuator proposed using multi-chamber cylinders and a digital pump will be presented. As mentioned in Chapter 3, it will be described according to the classification proposed by von Linsingen (2013) and used by Belan *et al.* (2014). It divides digital hydraulic systems into four subunits, namely Storage and Conditioning Unit, Primary Conversion Unit, Secondary Conversion Unit, and Limitation and Control Unit.

4.1. SECONDARY CONVERSION UNIT

In this section, the secondary conversion unit design will be presented. In addition, the way of how the chamber combinations of a linear cylinder can determine the number of discrete velocities, which are possible to achieve, will be described. With the use of different flow sources, combined with the chambers of the cylinder, and with the possibility of regenerating the hydraulic fluid, the system velocity resolution can be improved. For position control, the improvement of the velocity resolution can increase the accuracy of the hydraulic positioning system.

Considering a simple linear cylinder with two chambers, the size of the areas defines the operation modes that can be implemented. If the areas A_A and A_B are equal (Symmetrical Cylinders), the actuator will have the same values for positive and negative velocities in steady-state, for the same supply flow rate (Figure 4.1a). For asymmetrical cylinders, as the areas A_A and A_B are different, the forward and backward velocities will be different (Figure 4.1b and Figure 4.1c). However, for this kind of cylinder, the regenerative mode can be also implemented, where the chamber with the smaller area (regenerative chamber), can be connected together with the chamber with the larger area, as shown in Figure 4.1d.

Figure 4.1 – Chamber combinations for a two-chamber linear cylinder. a) Symmetrical cylinder forward movement; b) Asymmetrical cylinder forward movement; c) Asymmetrical cylinder backward movement; d) Asymmetrical cylinder forward movement with the regenerative chamber.



Source: By the author.

For the symmetrical and the asymmetrical cylinders, without considering the possibility of using regeneration between chambers, the forward velocity v_{af} [m/s] in steady-state can be evaluated as

$$v_{af} = \frac{q_{VA}}{A_A}, \quad (4.1)$$

and for the backward velocity v_{ab} [m/s] as

$$v_{ab} = \frac{q_{VB}}{A_B}, \quad (4.2)$$

where q_{VA} [m³/s] and q_{VB} [m³/s] are the flow rate supplied for chambers A and B, respectively, and A_A [m²] and A_B [m²] are the areas of the chambers A and B, respectively. For these cases, the flow rate that is supplied for chambers A and B are equal to the supply flow rate q_{VS} [m³/s]. When the regenerative mode is used, the flow rate that is supplied for chamber A is calculated as

$$q_{VA} = q_{VS} + q_{VB}. \quad (4.3)$$

In steady-state, the flow rate that is delivered by the chamber B can be expressed as

$$q_{VB} = A_B v_{af}. \quad (4.4)$$

Therefore, substituting the equations (4.3) and (4.4) in Equation (4.1), the cylinder velocity v_{af} , in regenerative mode, can be expressed as a function of the supply flow rate and the cylinders areas, being

$$v_{af} = \frac{q_{VS}}{A_A - A_B}. \quad (4.5)$$

With the possibility of using the regenerative mode, more velocity values can be achieved for the cylinder using the same flow rate, improving the system resolution.

For an asymmetrical actuator with two chambers, the total number of chamber combinations, and consequently areas, is expressed according to

$$n_{cc} = C_2^1 + 1, \quad (4.6)$$

where, n_{cc} is the total number of chamber combinations. In Equation (4.6), the first term represents the chamber combinations taken one by one and the second term is related to the regenerative part. For a cylinder with two chambers, the set of chamber combinations, can be represented using the areas of the cylinder, being

$$A = \{A_A, A_B, A_A - A_B\}. \quad (4.7)$$

The symbol $A_A - A_B$ means an equivalent area value where the fluid presented in chamber A_B is being regenerated in the chamber A_A .

The evaluation of the total chamber combinations for a two-chamber hydraulic cylinder can be a simple process. However, digital hydraulics can require the use of multi-chamber cylinders, as presented in Belan *et al.* (2015), Dell 'Amico *et al.* (2018), and Heybroek & Sahlman, (2018).

If the number of the cylinder chambers increases, the number of chamber combinations also increases. For a cylinder with four chambers or more, some considerations should be applied. In a multi-chamber cylinder, all the chambers that are increasing the volume should receive fluid from the flow source at the same time. This condition is necessary to avoid cavitation. For to use the regenerative mode, the sum of the area values, which are increasing the volume, should be higher than the area values that are being connected in regenerative mode. For a hydraulic cylinder with four chambers, as the one shown in Figure 4.2, the following inequalities should be considered.

For the forward movement:

$$A_A + A_C > A_B, \quad (4.8)$$

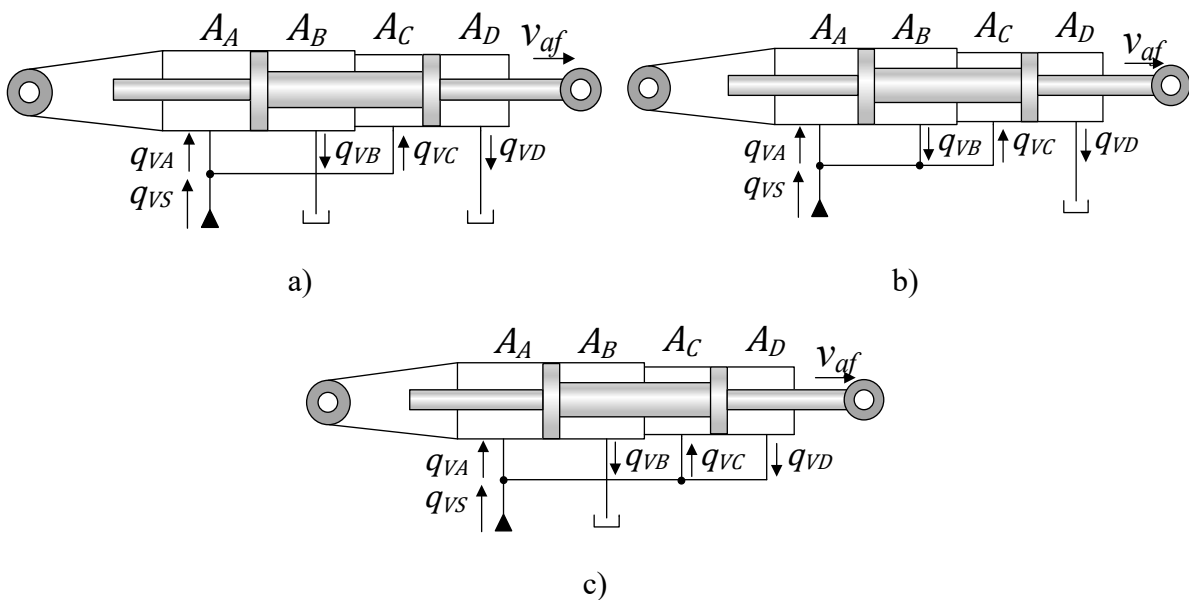
$$A_A + A_C > A_D. \quad (4.9)$$

For the backward movement:

$$A_B + A_D > A_A, \quad (4.10)$$

$$A_B + A_D > A_C. \quad (4.11)$$

Figure 4.2 – Chamber combinations on forward movement for a four-chamber cylinder. a) Without regeneration; b) Chamber B in regenerative mode; c) Chamber D in regenerative mode.

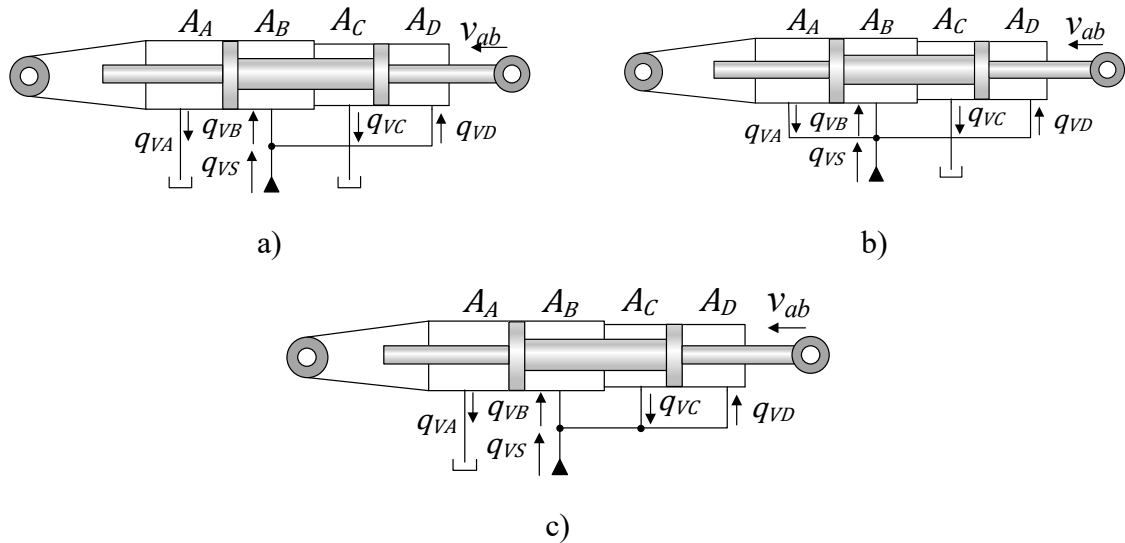


Source: By the author.

In Figure 4.2a, chambers A and C should receive fluid at the same time. If one of these chambers do not receive fluid, there is the possibility of cavitation due the expansion of their volumes. The chambers B and D are decreasing the volume, and in this case, they can be connected directly to the reservoir. In Figure 4.2b, the chamber B is in regenerative mode, where the fluid contained in its interior is absorbed by chambers A and C. For the case shown in Figure 4.2c, the chamber D is in regenerative mode, the cylinder works in an analogous way of the Figure 4.2b. The regeneration of the chambers B and D at the same time it not possible, because in this condition, all the chambers will have high pressure decreasing considerably the load capacity of the actuator, and in some cases as in symmetrical cylinders, the load capacity will be zero.

For the backward movement (Figure 4.3), the chambers B and D should always receive fluid from the supply system, also with the objective to avoid cavitation. For both chambers A and C operating in regenerative mode, the working principle is the same for the forward movement.

Figure 4.3 – Chamber combinations on backward movement for a four-chamber cylinder. a) Without regeneration; b) Chamber A in regenerative mode; c) Chamber C in regenerative mode.



Source: By the author.

As mentioned before, the chambers that are increasing the volume should receive fluid at the same time. The sum of the areas of these chambers can be represented as a resultant area A_r , which is associated with the lowest velocity value that the actuator can achieve without regenerative mode, considering the same supply flow rate. For the cylinder shown in Figure 4.2 and Figure 4.3, the resultant area for the forward movement (A_{rf}), is defined by

$$A_{rf} = A_A + A_C, \quad (4.12)$$

and for the backward movement (A_{rb}), by

$$A_{rb} = A_B + A_D. \quad (4.13)$$

For the total number of chamber combinations of a cylinder with four chambers, the resultant areas can be used isolated or in regenerative mode with the areas of the chambers that are against the movement. In a cylinder with only four chambers, a manual process can be done for the evaluation of all different combinations.

The total number of chamber combinations that can be used for the forward movement, in regenerative mode, can be evaluated as the combination of two areas taken one by one (C_2^1). This is possible due to only the areas A_B and A_D change in combination with the resultant

forward area A_{rf} . The total number of chamber combinations, for the forward movement n_{ccf} , can be expressed as

$$n_{ccf} = C_2^1 + 1. \quad (4.14)$$

The unitary term of the Equation (4.14) represents the combinations using the resultant forward area without regenerative mode (Equation (4.12)).

For the backward movement, the calculus of the chamber combinations (n_{ccb}) is similar when compared with the forward movement. In this case, the resultant area is A_{rb} and the areas that can be used in regenerative mode are A_A and A_C . Consequently, the backward total number of chamber combinations is expressed by

$$n_{ccb} = C_2^1 + 1. \quad (4.15)$$

Therefore, the total number of chamber combinations considering the forward and backward movements for a cylinder with four chambers is expressed by

$$n_{cc} = n_{ccf} + n_{ccb}, \quad (4.16)$$

or

$$n_{cc} = 2(C_2^1 + 1)., \quad (4.17)$$

For a cylinder with four chambers, all chamber combinations can be expressed as.

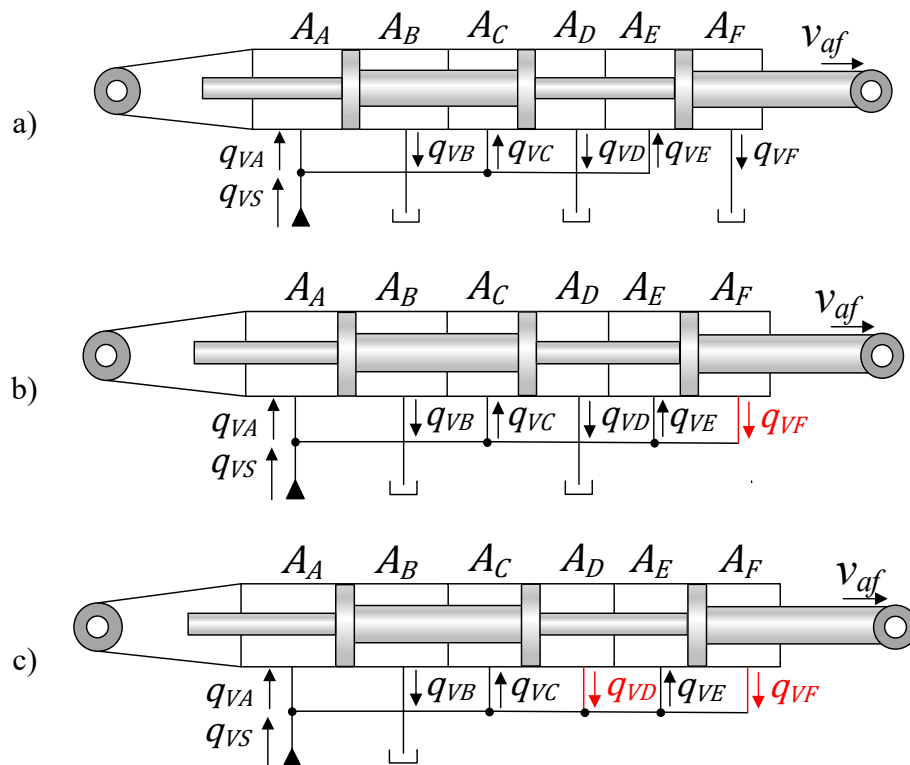
$$A = \{A_{rf}, A_{rb}, A_{rf} - A_B, A_{rf} - A_D, A_{rb} - A_A, A_{rb} - A_C\}. \quad (4.18)$$

One of the limitations of digital hydraulics is the system resolution. This resolution depends on the number of hydraulic components and the system operation mode. For instance, in Belan *et al.* (2015) a digital hydraulic cylinder with four chambers and three different pressure sources is used, where the system can achieve 81 discrete output force values. In Nostrani *et al.* (2019) the same cylinder with four chambers is used, but with three different flow sources, for velocity control. In this case, 28 discrete velocity values can be achieved without using chambers at the same time. For increase de system resolution, in force control, it is possible to increase the number of the cylinder chambers or increase the number of pressure sources. With four different pressure sources, the system can achieve 256 different force values. In velocity control, it is possible to increase the number of flow sources and also the number of the cylinder chambers. For instance, with four flow rate sources and a four-chamber cylinder without regeneration of chambers, the number of different possible velocity values is 60. However, in this kind of system, it is also possible to implement the regeneration of chambers. In Pynttäre *et al.* (2014), a four-chamber actuator is used combined with a digital pump for

velocity control, where the authors can achieve 106 different combinations of pumps and cylinder's areas.

As mentioned before, more chambers can be added to the actuator in order to improve the system resolution. Nevertheless, with the increasing of the number of chambers, the determination of the total combinations that can be achieved is not a simple process. For a six-chamber cylinder, the resultant areas for the forward and backward movements are composed of three chambers each. These resultant areas can be combined with the remaining chambers in the regenerative mode to achieve more chamber combinations and therefore, improve the system resolution. However, for cylinders with more than four chambers, the chambers that can be used in regenerative mode can be also combined together. Figure 4.4 presents some possible combinations for a six-chamber cylinder.

Figure 4.4 - Chamber combinations on forward movement for a six-chamber cylinder. a) Without regeneration; b) Chamber F in regenerative mode; c) Chambers D and F in regenerative mode.



Source: By the author.

As can be seen in Figure 4.4, for the use of the regenerative mode, the chambers that are decreasing the volume can be used individually (Figure 4.4b) or in combination (Figure

4.4c). For a six-chamber cylinder, as the one presented in Figure 4.4, the resultant areas for the forward and backward movements can be expressed, respectively as

$$A_{rf} = A_A + A_C + A_E, \quad (4.19)$$

$$A_{rb} = A_B + A_D + A_F. \quad (4.20)$$

In this type of cylinder, for the use of the regenerative mode, the chamber combinations that will operate in regenerative mode, the sum of their areas should be smaller than the sum of the resultant areas.

In the forward movement the total combination of chambers for a six-chamber cylinder is:

$$A = \{A_{rf}, A_{rf} - A_B, A_{rf} - A_D, A_{rf} - A_F, A_{rf} - (A_B + A_D), A_{rf} - (A_B + A_F), A_{rf} - (A_D + A_F)\}, \quad (4.21)$$

and for the backward movement

$$A = [A_{rb}, A_{rb} - A_A, A_{rb} - A_C, A_{rb} - A_E, A_{rb} - (A_A + A_C), A_{rb} - (A_A + A_E), A_{rb} - (A_C + A_E)]. \quad (4.22)$$

As can be seen, for a cylinder with six chambers, the chamber combinations that can work in regenerative mode are expressed in the combination of three chambers taken one by one and three chambers taken two by two plus one, or

$$n_{ccf} = C_3^1 + C_3^2 + 1. \quad (4.23)$$

The same equation can be used for the backward movement.

If a cylinder with more chambers, for instance with 8 chambers, the total number of chamber combinations can be expressed as

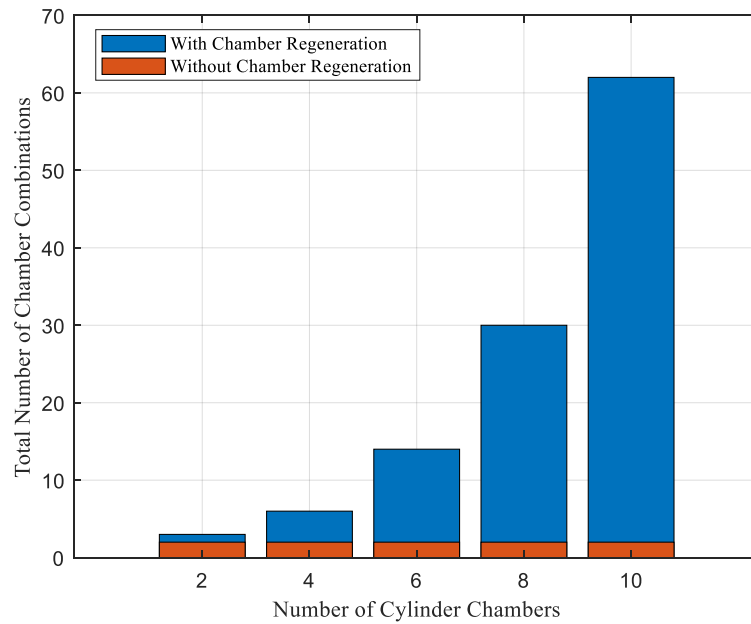
$$n_{cc} = 2(C_4^1 + C_4^2 + C_4^3 + 1). \quad (4.24)$$

Therefore, the total number of chamber combinations (n_{cc}) for a cylinder with n chambers, where n is an even number, is evaluated according to the Equation (4.25), being

$$n_{cc} = \begin{cases} C_2^1 + 1 & \text{for } n = 2 \\ 2 \left(\sum_{i=1}^{\frac{n}{2}-1} C_{\frac{n}{2}}^i + 1 \right) & \text{for } n \geq 4 \text{ where } n = 4, 6, 8 \dots \end{cases} \quad (4.25)$$

Figure 4.5 presents the results obtained from Equation (4.25).

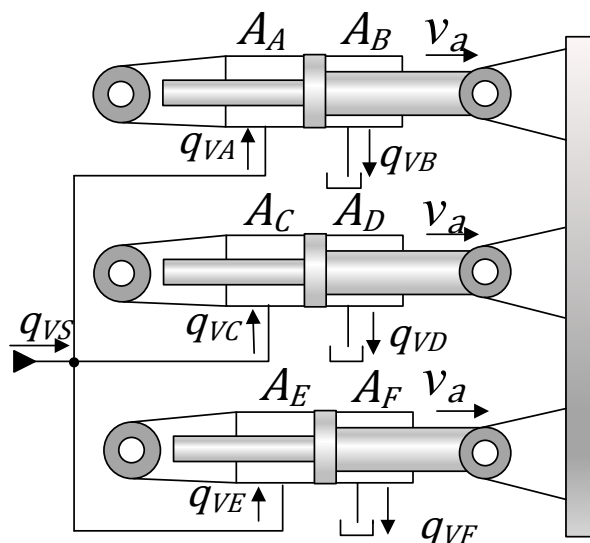
Figure 4.5 - Number of possible chamber combinations.



Source: By the author.

According to Equation (4.25), it is possible to increase the number of chamber combinations significantly, with cylinders with more chambers. Cylinders with four chambers are normally used in the aviation industry. These applications are necessary due to the high levels of redundancy that these systems should have, in order to increase the system safety. Cylinders with more than four chambers in the same body are not common, however, the application of cylinders with parallel connections is a good solution that can be applied easily, as presented by Figure 4.6.

Figure 4.6 - Actuator with six chambers.in parallel.

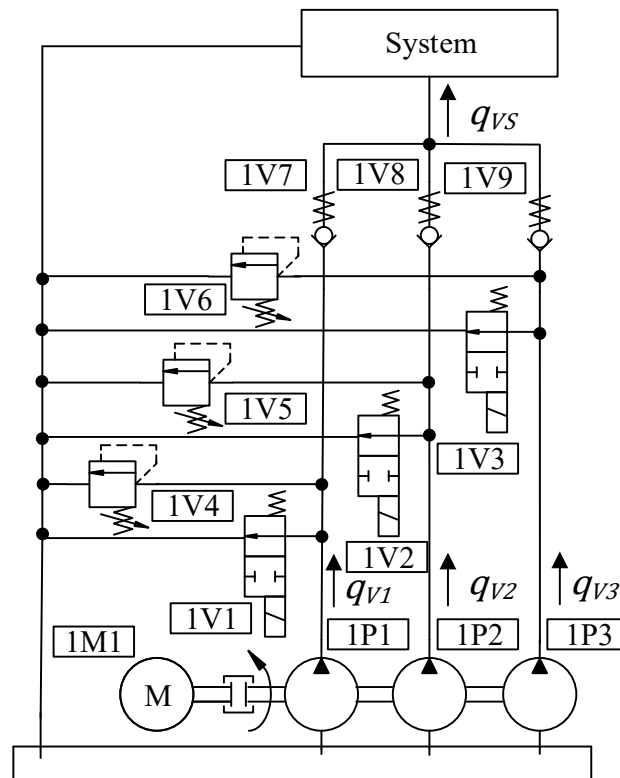


Source: By the author.

4.2. PRIMARY CONVERSION UNIT

As mentioned previously in Chapter 4, for the development of the digital actuator proposed in this doctoral thesis, a digital pump will be used for the primary conversion unit. In Figure 4.7, the hydraulic circuit of a digital hydraulic pump with three binary modulus is presented.

Figure 4.7 - Digital hydraulic pump circuit with three binary modulus.



Source: By the author.

In the digital pump presented in Figure 4.7, three binary modulus are used. However, the number of fixed displacements units can vary according to system design. The theoretical flow rate delivery by each pump depends on the volumetric displacement D [m^3/rad] and the rotational frequency ω [rad/s], being expressed as

$$q_V = D\omega. \quad (4.26)$$

With the use of a digital pump, the supply flow rate q_{VS} [m^3/s] delivered for the system is associated with the use of the different combinations of the binary modulus. The directional on/off valves 1V1, 1V2, and 1V3 are responsible for direct the pumps 1P1, 1P2, and 1P3 flow rate to the reservoir or to the system, respectively. These valves, for the case in study, are normally open. The normally open valves have the function of remain open in a case of a fault in one of the solenoids, keeping the pump at low pressure.

The relief valves, 1V4, 1V5, and 1V6 are installed in the outlet of the pumps 1P1, 1P2, and 1P3, respectively, in order to limit the maximum pressure, being a safety device. In normal operation conditions, these valves should not open, which avoid throttle losses. The check valves 1V7, 1V8, and 1V9 are necessary to isolate the pump lines and avoid pressure peaks that may occur in the system.

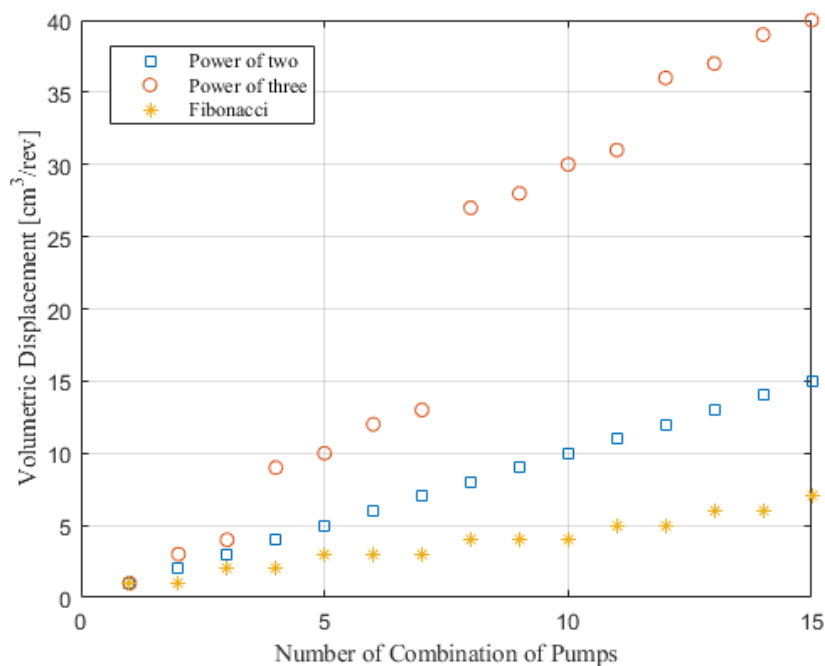
For an initial sizing of the pump volumetric displacements, different kind of mathematical series can be applied, as a power of two (1, 2, 4, 8) cm³/rev, power of three (1, 3, 9, 27) cm³/rev or Fibonacci (1, 1, 2, 3, 5) cm³/rev, for instance. The choice of the pump sizes to be used defines the distribution of the different flow rates that can be supplied by the digital pump for the system.

For a digital pump with p different binary modulus, the number of the total combinations of pumps that can be achieved is evaluated according to

$$n_{cp} = \sum_{i=1}^p C_p^i. \quad (4.27)$$

Figure 4.8 shows the possible combinations of volumetric displacements for a digital pump with four binary modulus with three different series of sizes,

Figure 4.8 - Displacement combinations for different sizes of pumps.



Source: By the author.

With the use of the pumps with sizes in the power of two, it is possible to obtain fifteen different displacement values that are well distributed, which means that for the point of view of the system control, this configuration has good linearity. When the Fibonacci configuration is used, some combinations can have the same volumetric displacement. This situation becomes a good alternative for the safety point of view since, in case of failure in one of the pumps, the system can still work properly. For the power of three configuration, the digital pump can supply a large range of flow rates. However, there are some high discontinuities between some displacement values, which can not be desired for system control.

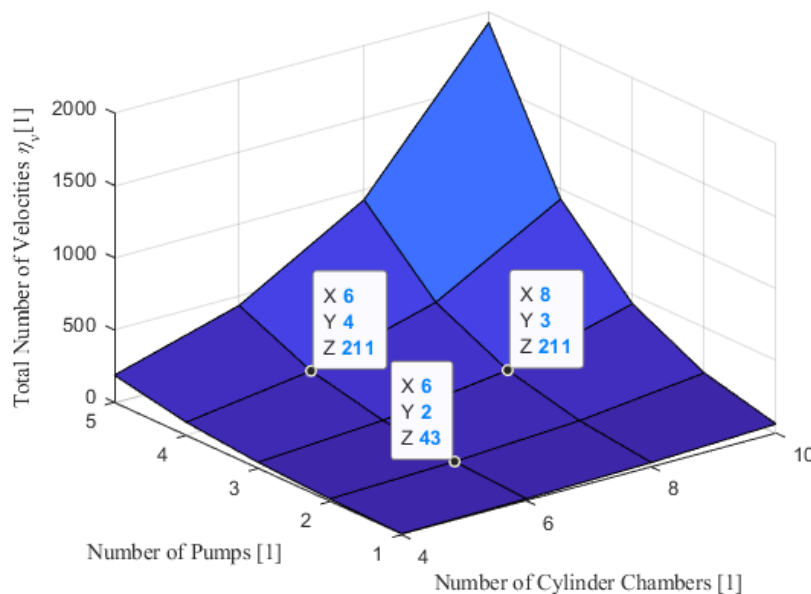
With the use of a digital pump combined with cylinders with multi-chambers, the total velocity values that the system can apply is given by

$$n_v = n_{cc}n_{cp} + 1, \quad (4.28)$$

where n_v is the total number of velocities for the actuator.

Figure 4.9 shows the total velocity combinations for different numbers of pumps and cylinder chambers, according to Equation (4.28).

Figure 4.9 - Total number of velocities for different number of pumps and chambers.



Source: By the author.

As can be seen in Figure 4.9, for a cylinder with ten chambers and a digital pump with five different binary modulus, the total number of velocities that the actuator can achieve is around 2000. Some different configurations can achieve the same numbers of velocity combinations. In these situations, some parameters should be taken into consideration, as the maximum velocity and the external load.

4.3. LIMITATION AND CONTROL UNIT

For the limitation and control unit, directional on/off valves were used. For each chamber of the multi-chamber cylinder, two valves are necessary. One valve is responsible for directing the flow rate from the digital pump to the cylinder chamber or connecting a specific cylinder chamber to another when it is operating in regenerative mode. The second valve has the function of directing the fluid from the chamber to the reservoir.

As the digital hydraulic system demands a high number of on/off valves, a nomenclature was created. In this way, the nomenclature of the valves, which connect the flow of the digital pump to the cylinder chambers or to the reservoir, was performed following the Vij pattern, where the index i represents when the valve is connecting the flow rate from the digital pump to the cylinder chamber (P), or the cylinder chamber to reservoir (R). The index j represents the chamber in which the valve is associated (A, B, C, D ...). Table 4.1 exemplifies the application of this nomenclature.

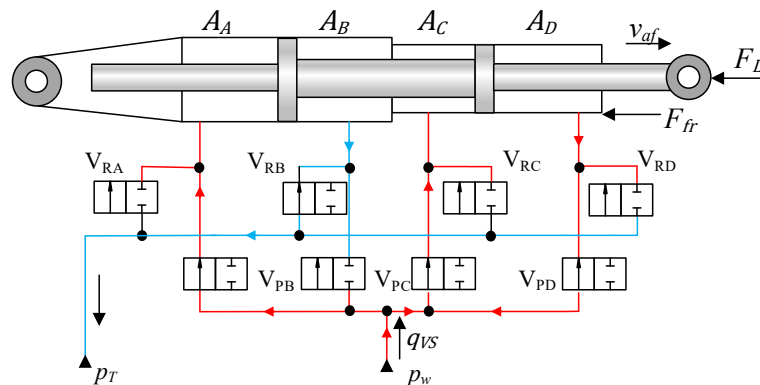
Table 4.1 – Nomenclatures of the limitation and control unit valves.

V_{RA} $i=R; j=A$	The valve that connects the chamber A of the cylinder to reservoir
V_{PB} $i=P; j=B$	The valve that connects the chamber B of the cylinder to the digital pump

Source: By the author.

Figure 4.10 presents a simplified circuit for the use of the limitation and control unit in a four-chamber cylinder, where the chamber D is in regenerative mode.

Figure 4.10 - Limitation and control unit connected in a four-chamber cylinder.



Source: By the author.

4.4. ANALYSIS OF THE MULTI-CHAMBERS CYLINDERS – VELOCITY AND PRESSURE

With the use of multi-chamber cylinders, different chamber combinations can be used and consequently, different resultant areas A_r , when compared with normal cylinders, as mentioned in Section 4.1. The velocity of the cylinder in steady-state depends on two different parameters, the supplied flow rate q_{VS} and the equivalent area A_e , being expressed as

$$v_a = \frac{q_{VS}}{A_e}. \quad (4.29)$$

The equivalent area A_e is dependent on the resultant area A_r and the regenerative area A_g , being defined as

$$A_e = A_r - A_g. \quad (4.30)$$

The regenerative area A_g is associated with the areas of the chambers which are in regenerative mode. The equivalent area A_e represents the area that is able to move a certain load, which depends on the maximum admissible pressure in the chambers. This area can assume different values, depending on the actuator movement direction (Forward A_{ef} and Backward A_{eb}).

For the actuator presented in Figure 4.2 and in Figure 4.3, the equivalent area, considering that the chamber D is larger than chamber B, which results in a maximum cylinder forward velocity, using the chamber D in regenerative mode, can be expressed according to

$$A_{ef} = A_A + A_C - A_D. \quad (4.31)$$

For the backward movement, considering that chamber A is larger than chamber C, the equivalent area for the backward movement is expressed as

$$A_{eb} = A_B + A_D - A_A. \quad (4.32)$$

For a four-chamber symmetrical cylinder with an area distribution according to Table 4.2, being A_a equals to $1.544 \times 10^{-3} \text{ m}^2$, and using a digital pump with three binary modulus with the displacement distributed in a power of two (Table 4.3), with a rotational frequency of 1800 rev/min, Figure 4.11 and Figure 4.12 show the actuator resultant velocity for the forward and backward movements, respectively.

Table 4.2 – Cylinder areas in the distribution of a power of two series.

Areas	Value
A_A	A_a
A_B	$A_a/2$
A_C	$A_a/2$
A_D	A_a

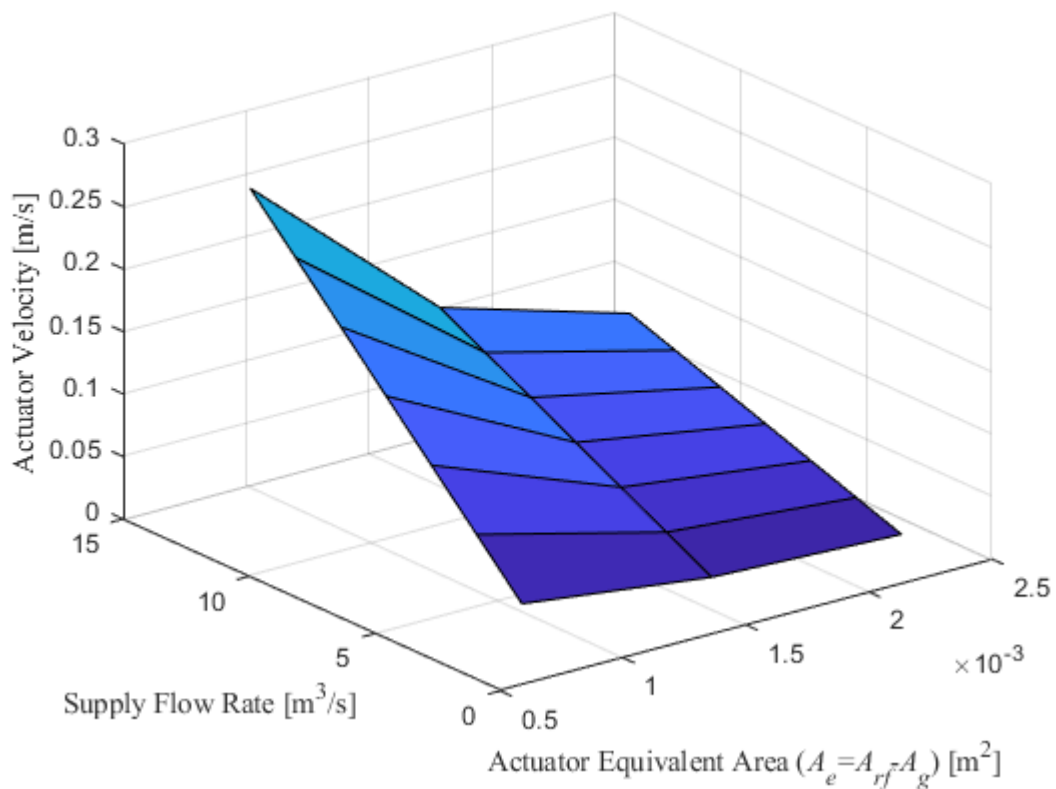
Source: By the author.

Table 4.3 – Digital pump displacements distribution in power of two series.

Volumetric Displacement	Value
D_1	$1 \times 10^{-6} \text{ m}^3/\text{rev}$
D_2	$2 \times 10^{-6} \text{ m}^3/\text{rev}$
D_3	$4 \times 10^{-6} \text{ m}^3/\text{rev}$

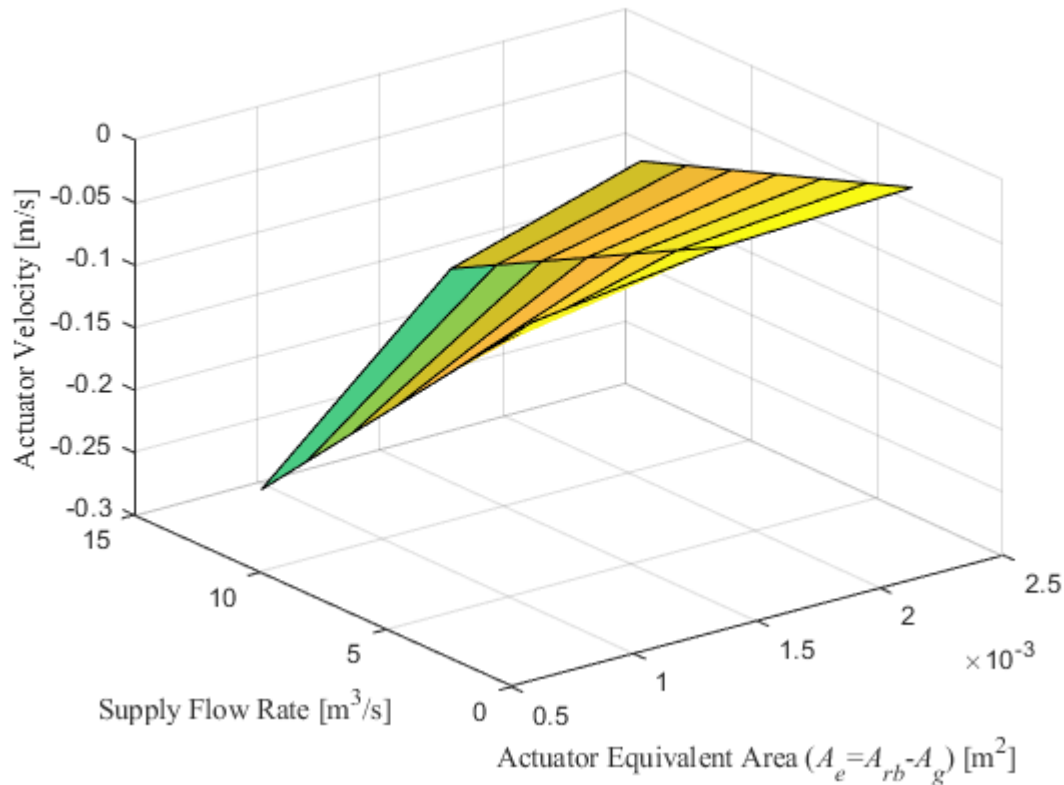
Source: By the author.

Figure 4.11 – Actuator forward velocity as a function of the supply flow rate and the equivalent area.



Source: By the author.

Figure 4.12 - Actuator backward velocity as a function of the supply flow rate and the equivalent area.



Source: By the author.

For the application of regeneration between chambers, one variable that should be taken into consideration, for the system design, is the working pressure at the cylinder chambers. When the system operates in regenerative mode, all chambers that are connected together will have the same pressure in steady-state. However, in this situation, the pressure tends to increase and the actuator load capacity becomes lower, when compared with the system working without regeneration. The reduction of the load capacity in regenerative mode is caused by the chambers that are decreasing the volume, which remains with high pressure.

Considering the cylinder with four chambers shown in Figure 4.2a, the movement equation (Second Newton's Law) for the actuator working without regeneration, in steady-state, can be expressed as:

$$(A_A + A_C)p_W - (A_B + A_C)p_T - F_L = M_T \frac{dx^2}{dt^2} + B \frac{dx}{dt}, \quad (4.33)$$

where, M_T is the total mass in movement [kg], B is the viscous friction coefficient [kg/s], F_L is the total load force [N] that considers the external actuator force and the friction force, p_W is

the working pressure [Pa] and p_T is the reservoir pressure [Pa]. Neglecting the spring force and considering the steady-state, the Equation (4.33) can be rewritten as

$$\frac{dx}{dt} = v_a = \frac{(A_A + A_C)p_W - (A_B + A_D)p_T - F_L}{B}. \quad (4.34)$$

When the system operates with A_D chamber in regeneration mode, the Equation (4.34) can be rewritten as

$$v_a = \frac{(A_A + A_C - A_D)p_W - (A_B)p_T - F_L}{B}, \quad (4.35)$$

where $(A_A + A_C - A_D)$ is related to the forward equivalent area A_{ef} , as presented in Equation (4.31). Therefore, using Equation (4.35), the working pressure can be expressed as

$$p_W = \frac{v_a B + F_L + (A_{rb} - A_g)p_T}{(A_{ef})}. \quad (4.36)$$

Equation (4.36) presents that the working pressure depends on the current actuator velocity (v_a), the forward equivalent area (A_{ef}), the resultant backward area (A_{rb}) and the regenerative area (A_g). With the increasing in the size of the regenerative area, the equivalent area becomes smaller, and therefore, the working pressure increases.

Based on the conclusions presented above, it can be observed that for digital hydraulics, some other different variables must be taken into consideration, when it is compared with conventional hydraulic systems, as the number of the cylinder chambers, the distribution of the cylinder areas, the number of the binary modulus in the digital pump and the distributions of the pump displacements. The number of the cylinder chambers combined with the number of the binary modulus of the digital pump define the total velocities that the actuator can achieve. The definition of the size of the digital pump and the cylinder areas describe the distribution of the total velocities available and the maximum load that the actuator can operate. Furthermore, some different combinations of areas and pumps sizes can result in the same velocity, but with different load capacities, when it is used pumps and areas with their sizes distributed in series.

Due to the different system parameters, which should be taken into consideration, guidelines for designing this kind of system will be discussed. According to Figure 4.8, different combinations of the volumetric displacement of each digital pump can produce different distributions of the resulting volumetric displacements that are available for the system. These

different arrangements can result on different distributions of the actuator velocities, according to its size of areas.

Considering two different digital pumps, with a volumetric displacement distribution according to Table 4.4 and two four chamber cylinders, with the areas distributed according to Table 4.5, Figure 4.13 shows the velocity distribution for different combinations of cylinders and digital pumps. The digital pump rotational frequencies were adjusted to keep the maximum velocity equal for all configurations.

Table 4.4 - Pumps volumetric displacement distribution, power of two, and power of three.

Volumetric Displacement	Series in Power of Two	Series in Power of Three
D_1	$1 \times 10^{-6} \text{ m}^3/\text{rev}$	$1 \times 10^{-6} \text{ m}^3/\text{rev}$
D_2	$2 \times 10^{-6} \text{ m}^3/\text{rev}$	$3 \times 10^{-6} \text{ m}^3/\text{rev}$
D_3	$4 \times 10^{-6} \text{ m}^3/\text{rev}$	$9 \times 10^{-6} \text{ m}^3/\text{rev}$

Source: By the author.

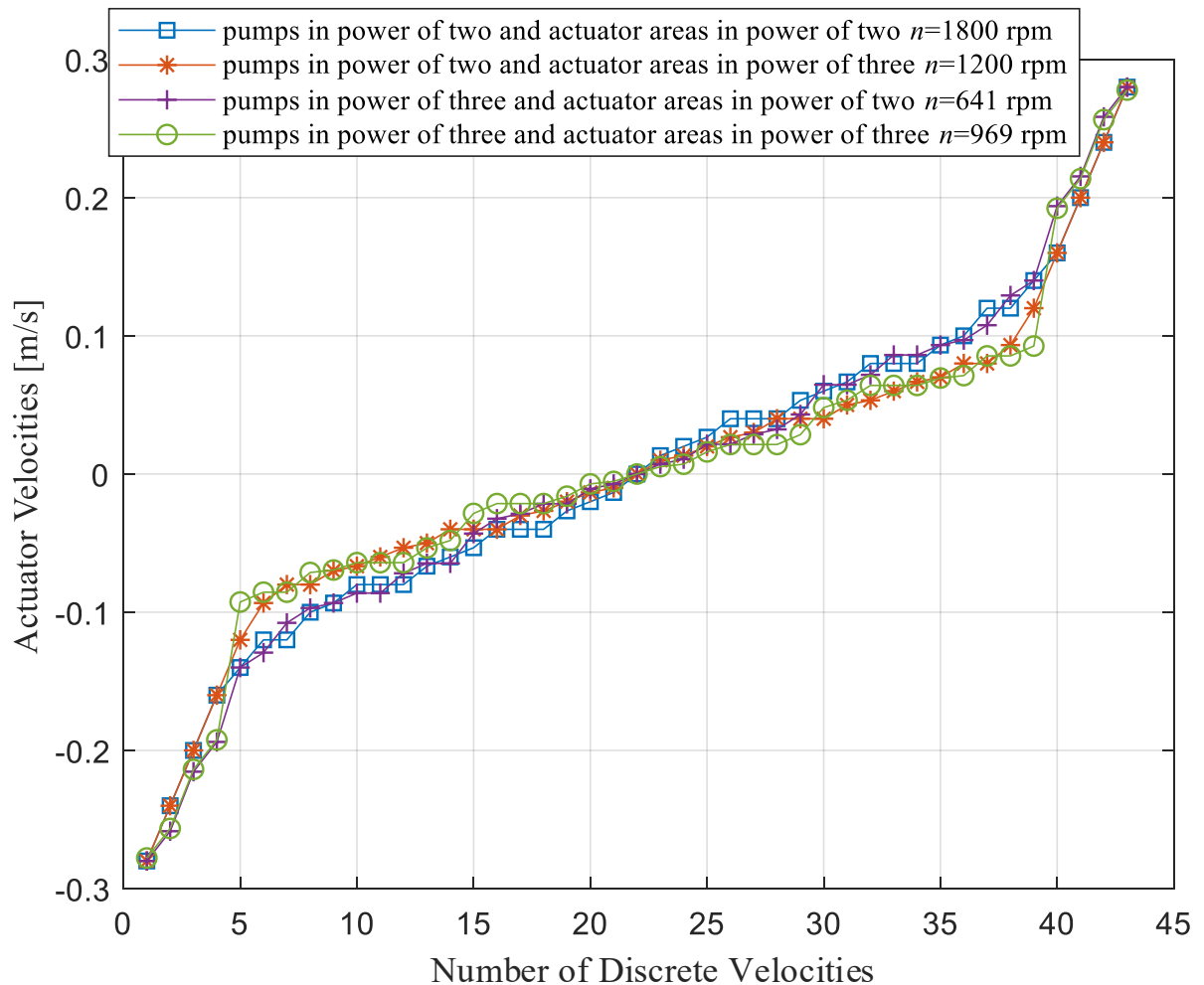
Table 4.5 - Cylinder areas distribution, power of two, and power of three.

Areas	Series in Power of Two	Series in Power of Three
A_A	$1.544 \times 10^{-3} \text{ m}^2$	$1.544 \times 10^{-3} \text{ m}^2$
A_B	$7.220 \times 10^{-4} \text{ m}^2$	$5.146 \times 10^{-4} \text{ m}^2$
A_C	$7.220 \times 10^{-4} \text{ m}^2$	$5.146 \times 10^{-4} \text{ m}^2$
A_D	$1.544 \times 10^{-3} \text{ m}^2$	$1.544 \times 10^{-3} \text{ m}^2$

Source: By the author.

As it can be seen in Figure 4.13, different combinations of cylinder areas and pump sizes can provide different velocities distributions. In addition, some different combinations of pumps and cylinder areas, for the same digital pump and areas distribution, can cause the same resultant velocity, which affects the system resolution. As shown in Equation (4.36), the working pressure in the chambers that are connected at the same time depends, although other parameters, on the actuator velocity, and the equivalent area. This fact means that the pressure, for the same velocity and the same load force, can achieve different values. For the system efficiency point of view, the digital pump should operate with a low output pressure to keep the internal leakage low, reducing the volumetric losses.

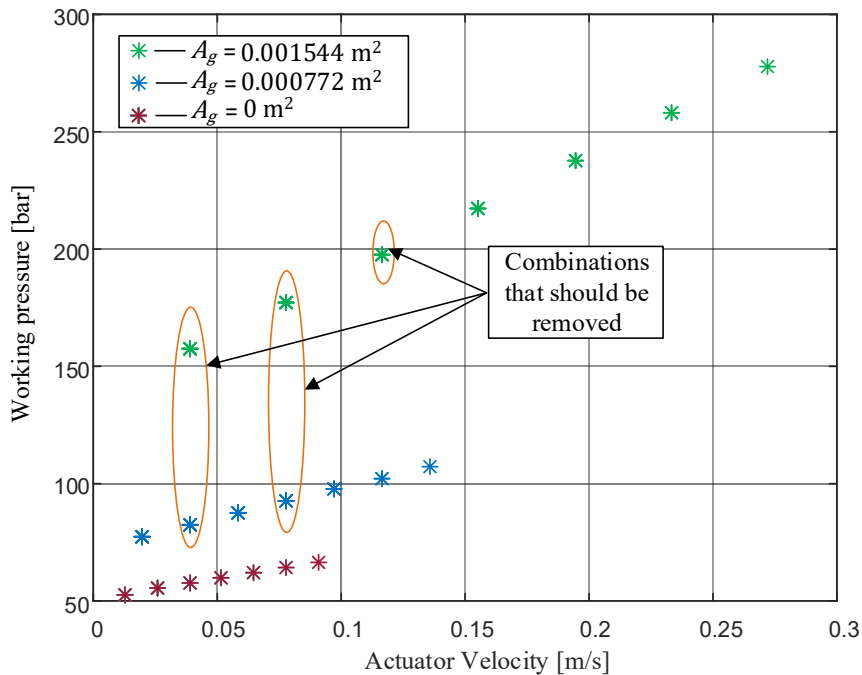
Figure 4.13 - Velocity distribution for different actuator and pump distributions.



Source: By the author.

To achieve the lowest system pressure value, for the same velocity, the equivalent actuator area should be the highest value as possible, which means that the regenerative area should have its value reduced. For a cylinder with four chambers with the areas distributed in a power of two series (Table 4.4) and using a digital pump with three binary modulus, where the volumetric displacements are also distributed in a power of two series, according to Table 4.4, and considering a rotational frequency of 1800 rpm, a load force F_L of 10000N, the reservoir pressure of 10 bar (1 MPa), and the viscous friction coefficient of 40000 kg/s, Figure 4.14 shows the actuator working pressure for the resulting discrete velocities.

Figure 4.14 - Actuator pressure according to velocity and regenerative area.



Source: By the author.

As can be seen in Figure 4.14, some velocity values can be obtained with more than one different combination of areas and pumps, using different regenerative areas. When it is used in the higher regenerative area, the pressure increases. For the system operation, when the configuration of the pumps and cylinder areas results in velocities that have repeated values, for different regenerative areas, the values that have the lowest working pressure should be preferred. This action is necessary in order to reduce the pump internal leakage for these points. However, as mentioned before, this action reduces the total velocities that are possible to obtain, affecting the system resolution.

4.5. CALCULUS OF THE CYLINDER AREAS AND THE SIZE OF THE PUMPS

For the system design, some parameters as the actuator maximum admitted velocity, external load, and working pressure should already be known as the system requirements.

Another challenger to design systems with a multi-chamber cylinder is to determine the values of each area individually, in order to obtain the better system performance and avoid combinations that provide the same resulting velocity. As shown in Figure 4.13, the cylinder areas distribution used combined with the pumps displacements in series of power of two or three, result in discrete velocity values that are not linearly distributed in the whole range.

Considering a hydraulic cylinder with four chambers, four variables should be determined, which are the areas A_A , A_B , A_C and A_D . Assuming that the cylinder is symmetrical, the size of the areas can be expressed as

$$A_A + A_C = A_B + A_D. \quad (4.37)$$

Equation (4.37) can be rewritten as

$$A_B = A_A + A_C - A_D, \quad (4.38)$$

$$A_C = A_B + A_D - A_A. \quad (4.39)$$

Comparing the equations (4.38) and (4.39) with the equations (4.31) and (4.32), the cylinder areas A_B and A_C are equal to the equivalent forward and backward areas, respectively. Considering that the maximum forward and backward velocities can be written as a function of the supply flow rate for the actuator forward (q_{vsf}) and backward (q_{vsb}) movements, being

$$q_{vsf} = \frac{A_{ef} q_{vsb}}{A_{eb}}. \quad (4.40)$$

For the digital pump, the maximum flow rate that can be achieved is the sum of the flow rate of each binary modulus. Considering that q_{vsf} can be expressed as a function of q_{vsb} , resulting

$$q_{vsf} = \alpha q_{vsb}, \quad (4.41)$$

where, α [1] is the flow coefficient. This coefficient represents that, for the same digital pump used as flow source, the total combination of pumps available for the forward and backward movement are different. In other words, for one movement, all combinations of pumps can be used and in the other direction, one or more pumps can be not used. This is necessary to avoid trivial solutions and save computation effort. In practical terms, all combination of pumps can be used for all movements, but the maximum positive and negative velocities will be different. Substituting Equation (4.41) in Equation (4.40), a relation between the forward and backward equivalent areas can be expressed as

$$A_{ef} = \alpha A_{eb}. \quad (4.42)$$

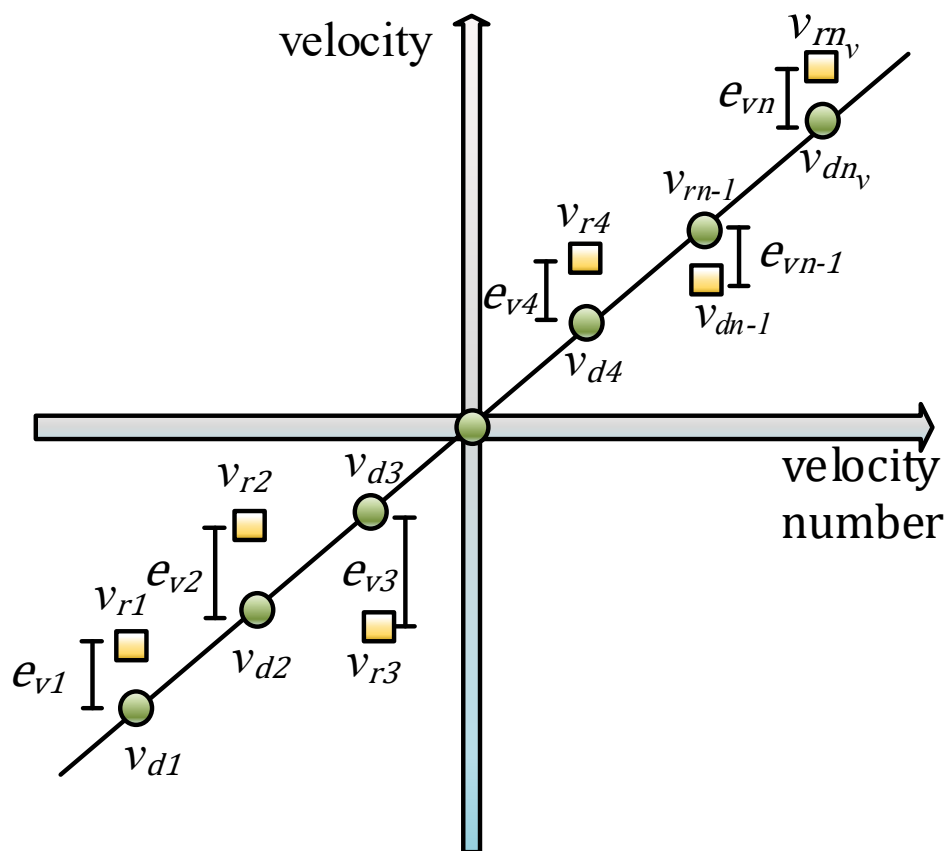
Substituting equations (4.39) and (4.40) in Equation (4.42) and assuming that $A_B = \alpha A_C$, the following equation is obtained.

$$A_A = A_D + \frac{A_C(\alpha^2 - 1)}{(\alpha + 1)}. \quad (4.43)$$

With equations (4.38), (4.39) and (4.43) some areas of the cylinder can be found analytically, as areas A_B and A_C . However, the areas A_A and A_D are mathematically dependent of each other according to Equation (4.43). Therefore, it is not possible to find all the areas, only using mathematical expressions. In order to overcome this bottleneck, other tools must be considered. Consequently, for the calculation of all areas, an optimization algorithm based in gradient was used. For the use of the optimization algorithm, an objective function should be defined. This function, for the case study, represents the desired discrete velocity distribution for the actuator. This distribution can assume different forms, depending on the application.

To achieve the velocity distribution as close as possible to the optimum distribution, the optimization algorithm optimizes the error between these two distributions at the minimum value possible. To exemplify this behavior, Figure 4.15 shows the error between the desired and the real velocity values.

Figure 4.15 - Error between the desired and real velocity values.



Source: By the author.

The total error (e_t) between the real velocity (v_r) and the desired velocity (v_d) can be expressed as

$$e_t = |v_{r1} - v_{d1}| + |v_{r2} - v_{d2}| + \dots + |v_{rn_v} - v_{dn_v}|, \quad (4.44)$$

and, therefore, the total error can be generalized as

$$e_t = \sum_{i=1}^{n_v} |v_{ri} - v_{di}|. \quad (4.45)$$

For the implementation of the optimization algorithm, the *fmincon* function provided by the Mathworks/MATLAB was used. In this function, some parameters must be given as input data, which depend on the design requirements, which are:

- The maximum actuator positive and negative velocities v_{a_maxp} , v_{a_minn} [m/s];
- The maximum actuator load force F_L [N];
- The maximum admissible working and reservoir pressures p_W , p_T [Pa];
- The estimated viscous friction coefficient B [kg/s];
- The area boundary conditions (equations (4.8), (4.9), (4.10) and (4.11));
- The number of the binary modulus in the digital pump;
- The pump rotational frequency ω_p [rad/s].

According to Mathworks/MATLAB, the implementation of the boundary conditions, which in the case of this thesis are equations (4.8), (4.9), (4.10) and (4.11), are inequalities in the form of

$$Ax \leq b. \quad (4.46)$$

The implementation of the equations (4.8), (4.9), (4.10) and (4.11) in the format of Equation (4.46), can be performed as a matrix, where the matrix A represents the areas coefficients, x the areas vector and b the inequalities. Therefore, the implementation of the boundary conditions for a cylinder with for chambers can be represented as

$$\begin{bmatrix} -1 & 0 & -1 & 1 \\ -1 & 1 & -1 & 0 \\ 1 & -1 & 0 & -1 \\ 0 & -1 & 1 & -1 \end{bmatrix} \begin{bmatrix} A_A \\ A_B \\ A_C \\ A_D \end{bmatrix} \leq \begin{bmatrix} 0 \\ 0 \\ 0 \\ 0 \end{bmatrix}. \quad (4.47)$$

For the evaluation of the equivalent area, the area A_B , using Equation (4.38), assumes the same value of the equivalent area. Moreover, using the definition of input parameters, substituting the Equation (4.38) in the Equation (4.35) and reorganizing the terms, the equivalent area A_e can be calculated as

$$A_e = \frac{v_{a_maxp} B + F_L}{(p_W - p_T)} \quad (4.48)$$

which represents the equivalent area that will result in the maximum actuator positive velocity v_{a_maxp} [m/s].

With the definition of the equivalent area and the maximum positive velocity, the maximum flow rate, which needs to be supplied for the actuator, can be obtained with the Equation (4.29). This value represents the total flow rate that must be supplied for the sum of all binary modulus of the digital pump.

The number of binary modulus depends on the number of different discrete velocity values that are needed for the system, which defines the minimum resolution between two different consecutive velocity values.

The actuator developed in this thesis is intended for the use in aircraft. According to Maré (2016), the power and dynamic needs for the aircraft actuators depend on the type of aircraft, as shows Table 4.6.

Table 4.6 - Examples of dynamic and load needs for aircraft.

Actuator Function	Typical Range	Aileron Airbus A320	Nose Landing Gear steering A320	Tiltrodor Boeing V22 OspreyMode Conversion
Stroke (mm)	20-700	44		1143
(degree)			± 75	
Speed (mm/s)	20-500	90 no-load		97
(degree/s)	10-90		20	
Force (kN)	20-350	44		80
(Nm)			7000	
Bandwidth (Hz)	1-20	≈ 1	≈ 1.5	3.2

Source: Adapted from Maré (2016).

As can be seen in Table 4.6, there is a huge variety of dynamic and load needs depending on the type of the aircraft. However, Maré (2016) mentions that, in normal operation conditions, the actuators operate far from the maximum force and velocity. For instance, in the aileron of the A320, the typical operation velocity is around $\pm 15\%$ of the total available velocity (MARÉ, 2016).

For a hydraulic positioning system considering a steady-state displacement x_{st} of 50 mm and an accommodation time t_s of 1 s, the natural frequency of the system, for a second order dynamic behavior, can be expressed as (DE NEGRI *et al.*, 2008; MURARO *et al.*, 2013)

$$\omega_n = \frac{6}{t_s}, \quad (4.49)$$

which results in 6 rad/s. The maximum positive velocity can be evaluated as

$$v_{a_maxp} = 0.37x_{st}\omega_n, \quad (4.50)$$

resulting on 0,111 m/s.

Combining Equation (4.50) in Equation (4.48) and considering a load force of 20 kN, the viscous friction coefficient B of 40000 kg/s, the working pressure of 20 MPa (200 bar) and the reservoir pressure of 1 MPa (10 bar), the equivalent area A_e results in $12,86 \times 10^{-4} \text{ m}^2$. Therefore, using Equation (4.29), the total supply flow rate can be calculated, resulting on $1,427 \times 10^{-4} \text{ m}^3/\text{s}$ [8.56 L/min].

Consequently, considering the maximum negative and positive velocities as -0.111 and 0.111, respectively with a resolution of 0.005 m/s and using a hydraulic cylinder with four chambers (six different equivalent areas can be used), the resulting number of different velocity values is equal to 43. Therefore, the number of the pump combinations necessary can be calculated according to Equation (4.28), resulting in 7 different combinations. In this case, a digital pump with three different fixed displacement pumps (three binary modulus) can be used (Figure 4.7). Table 4.7 shows the different combinations that are possible for this digital pump.

Table 4.7 - Digital pump combinations.

Pumps	Displacements [cm^3/rev]
Pump 1 (P ₁)	D_1
Pump 2 (P ₂)	D_2
Pump 1 (P ₁) and Pump 2 (P ₂)	$D_1 + D_2$
Pump 3 (P ₃)	D_3
Pump 1 (P ₁) and Pump 3 (P ₃)	$D_1 + D_3$
Pump 2 (P ₂) and Pump 3 (P ₃)	$D_2 + D_3$
Pump 1 (P ₁), Pump 2 (P ₂) and Pump 3 (P ₃)	$D_1 + D_2 + D_3$

Source: By the author.

With the definition of the digital pump, its rotational frequency, and the parameters of the multi-chamber cylinder, the optimization algorithm calculates all combinations that are

possible between areas and pumps. With all combinations, the algorithm attributes random values for the area A_D , in a defined interval, in order to calculate the area A_A (Equation (4.43)). In addition, the algorithm attributes random values, also in a defined interval, for the volumetric displacements D_1 , D_2 and D_3 for the digital pump in order to calculate the supplied flow rate.

For all interactions, the total error between the desired and the real velocity distributions is computed. When the error achieved its minimization, the algorithm stops and the volumetric displacement for the pumps and the areas of the cylinder are defined.

For the implementation of the optimization algorithm, Table 4.8 summarizes the total parameters used for the optimization of the areas and the size of the pump's displacements. The implementation of the optimization algorithm is summarized in APPENDIX C and its code is presented in APPENDIX D.

Table 4.8 - System parameters for the optimization algorithm.

Variable	Value
x_{st}	0.05 m
t_s	1 s
F_L	20000 N
ω_n	6 rad/s
v_{a_maxp}	0.111 m/s
B	40000 kg/s
p_W	20 MPa
p_T	1 MPa
A_e	$12.86 \times 10^{-4} \text{ m}^2$
ω_p	125.66 rad/s (1200 rpm)
α	1.2

Source: By the author.

With the use of the optimization algorithm, and considering a linear velocity distribution, the resulting cylinder areas and the volumetric displacement of the binary modulus of the digital pump, are presented in Table 4.9.

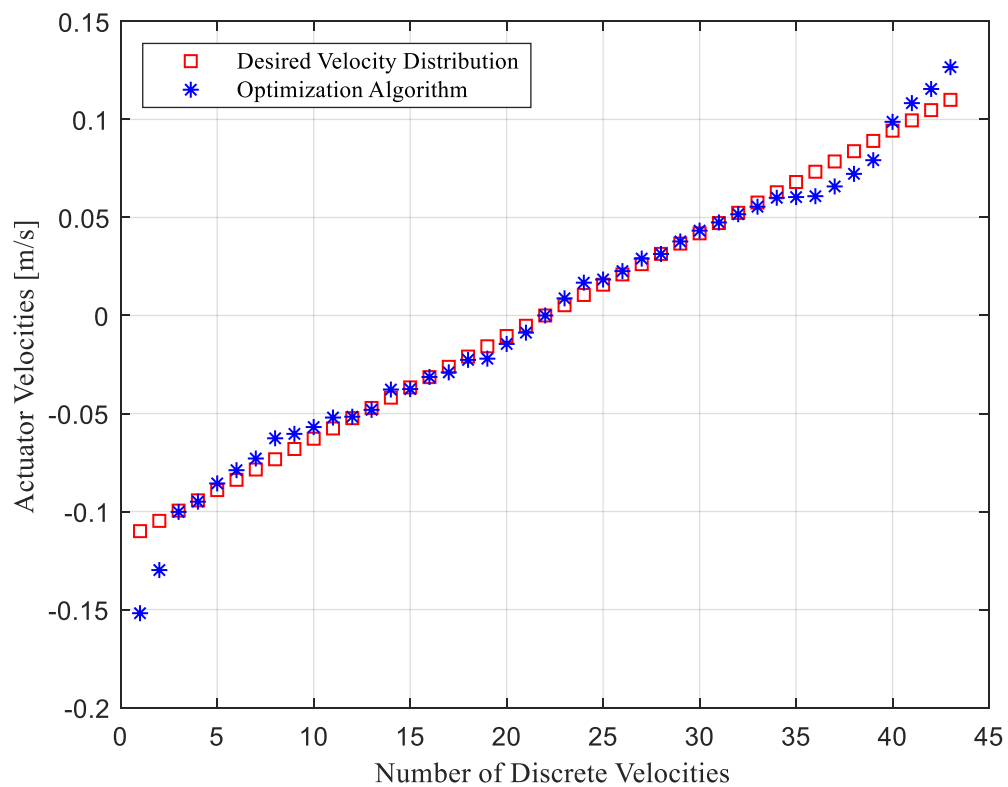
Table 4.9 - Optimized areas and volumetric digital pump displacements for a linear velocity distribution.

Actuator Areas	Value
A_A	$16.24 \times 10^{-4} \text{ m}^2$
A_B	$12.86 \times 10^{-4} \text{ m}^2$
A_C	$10.71 \times 10^{-4} \text{ m}^2$
A_D	$14.10 \times 10^{-4} \text{ m}^2$
Pump Displacements	Value
D_1	$1.18 \times 10^{-6} \text{ m}^3/\text{rev}$
D_2	$3.05 \times 10^{-6} \text{ m}^3/\text{rev}$
D_3	$3.91 \times 10^{-6} \text{ m}^3/\text{rev}$

Source: By the author.

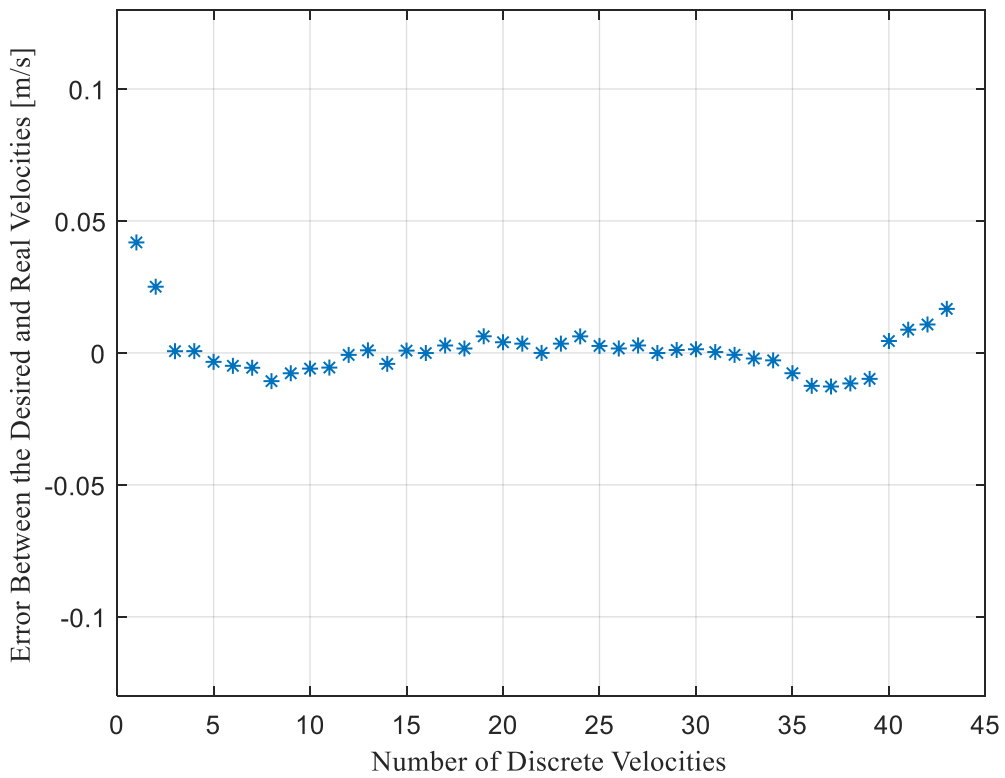
With the use of the results shown in Table 4.9, Figure 4.16, Figure 4.17, and Figure 4.17 present the obtained velocity distribution, the error between the desired and the resulting velocity, and the resulting system resolution, respectively. The resultant system resolution is calculated by the difference between two consecutive velocity values.

Figure 4.16 - Optimized velocity for a linear distribution.



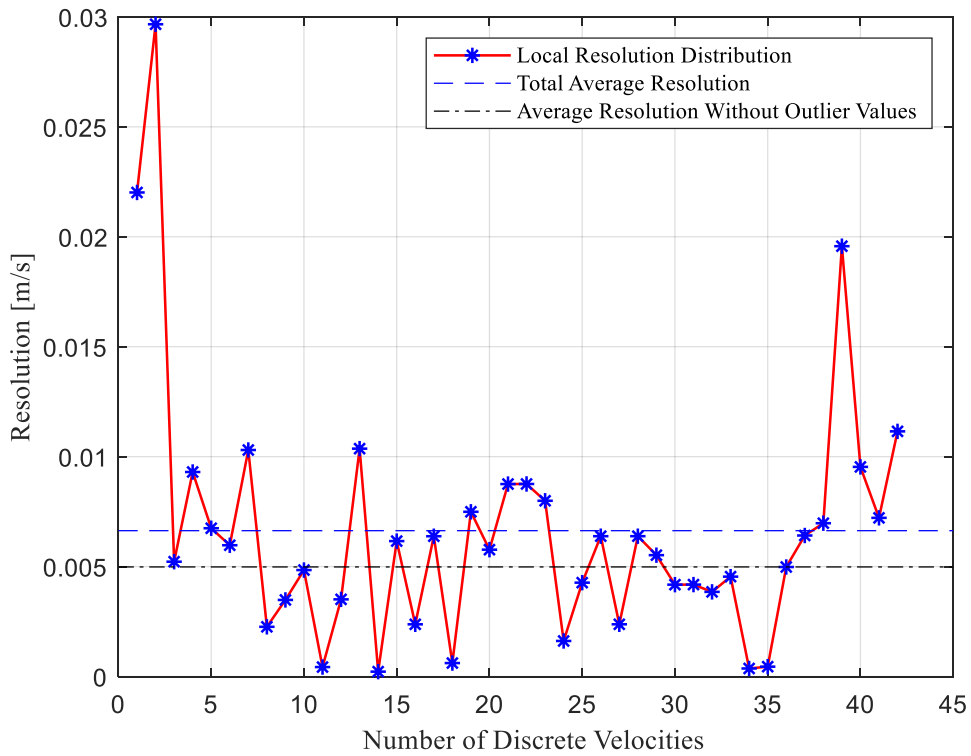
Source: By the author.

Figure 4.17 - Error between the desired and the resulting velocity for a linear distribution.



Source: By the author.

Figure 4.18 - System resolution for a linear distribution.



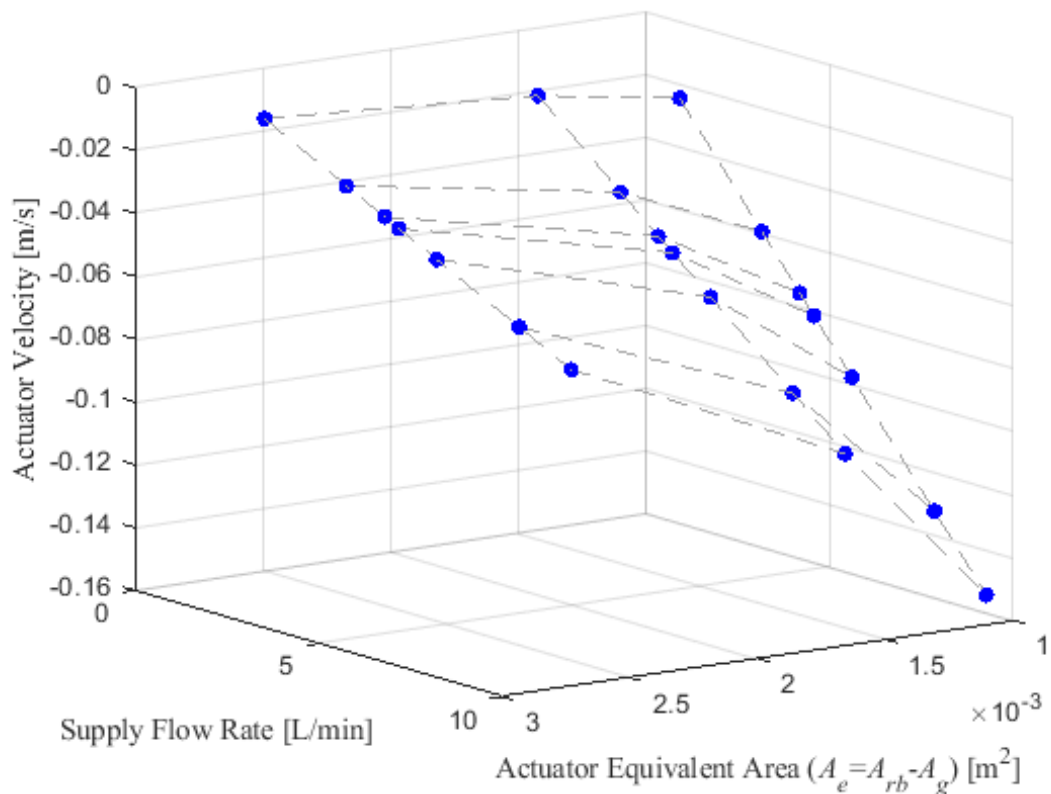
Source: By the author.

As it can be seen in Figure 4.16, the velocity values obtained from the optimization algorithm can follow the desired velocity distribution with satisfactory accuracy in a velocity range between -0.1 to 0.1 m/s, with a maximum error of 0.011 m/s. The maximum real negative velocity is higher, in modulus, than the positive one. This occurs due to the adoption of the α factor, which interferes in the size of the Area A_C and results in A_A value higher than all other areas (according to Equation (4.48)). However, the resulting actuator keeps being symmetrical ($A_A + A_C = A_B + A_D$).

The average system resolution is equal to 0.006 m/s, which is higher than the desired value. This occurs due to the high errors at the highest velocity values (Figure 4.17). Nevertheless, disregarding the outlier values, the average resolution is 0,0049 m/s, which is close to the desired value.

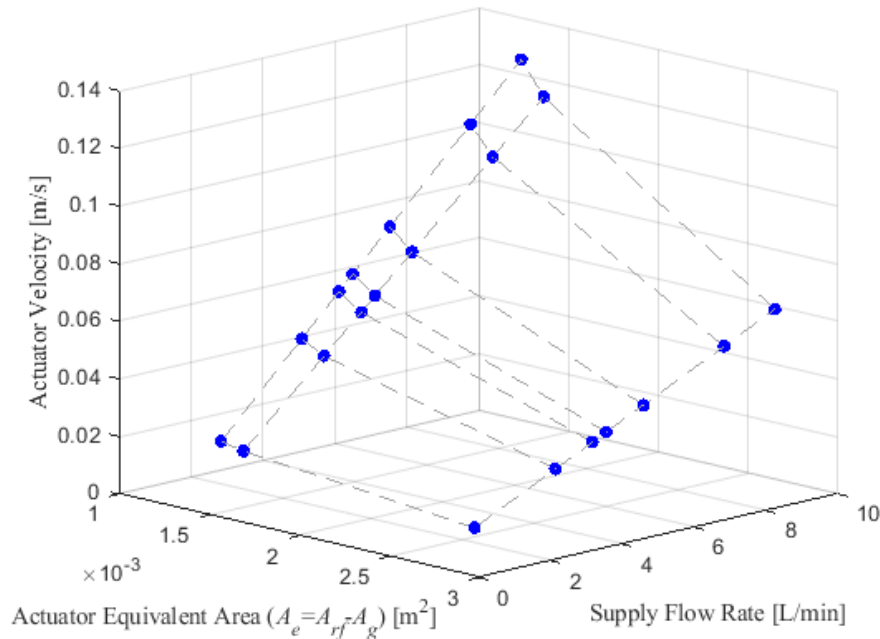
The velocity of the actuator, as mentioned in Section 4.4, depends on the supply flow rate and the equivalent area. Figure 4.19 and Figure 4.20 show the behavior of the actuator velocity with the variation of these parameters using the values presented in Table 4.8 and Table 4.9.

Figure 4.19 – Negative velocities as a function of the supply flow rate and the equivalent area.



Source: By the author.

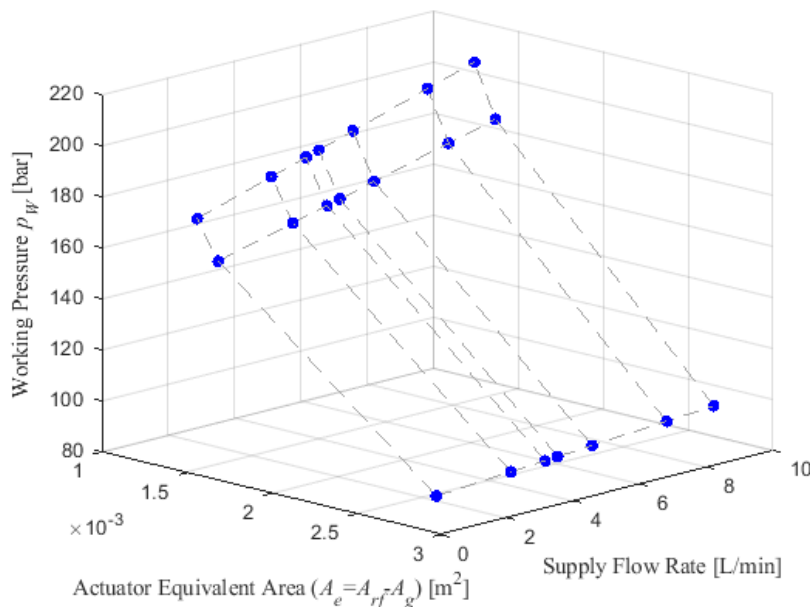
Figure 4.20 - Positive velocities as a function of the supply flow rate and the equivalent area.



Source: By the author.

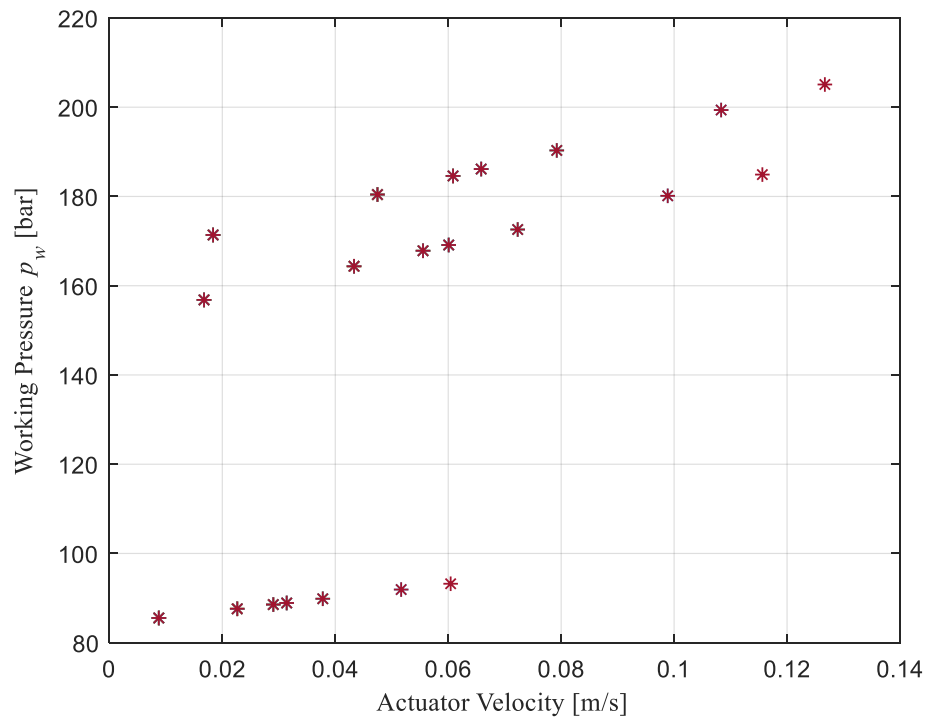
As can be noticed, with the increasing of the supply flow rate, for the same equivalent area the actuator velocity increases linearly. On the other hand, for the same supply flow rate, with the increasing of the equivalent area, the actuator velocity decreases. This is due to the higher values of equivalent areas, which have the smallest regenerative area, causing less gain of hydraulic fluid provided from the regenerative chamber. The behavior of the working pressure is presented in Figure 4.21 and Figure 4.22.

Figure 4.21 – Working pressure as a function of the supply flow rate and the equivalent area.



Source: By the author.

Figure 4.22 - Working pressure behavior for positive velocities.

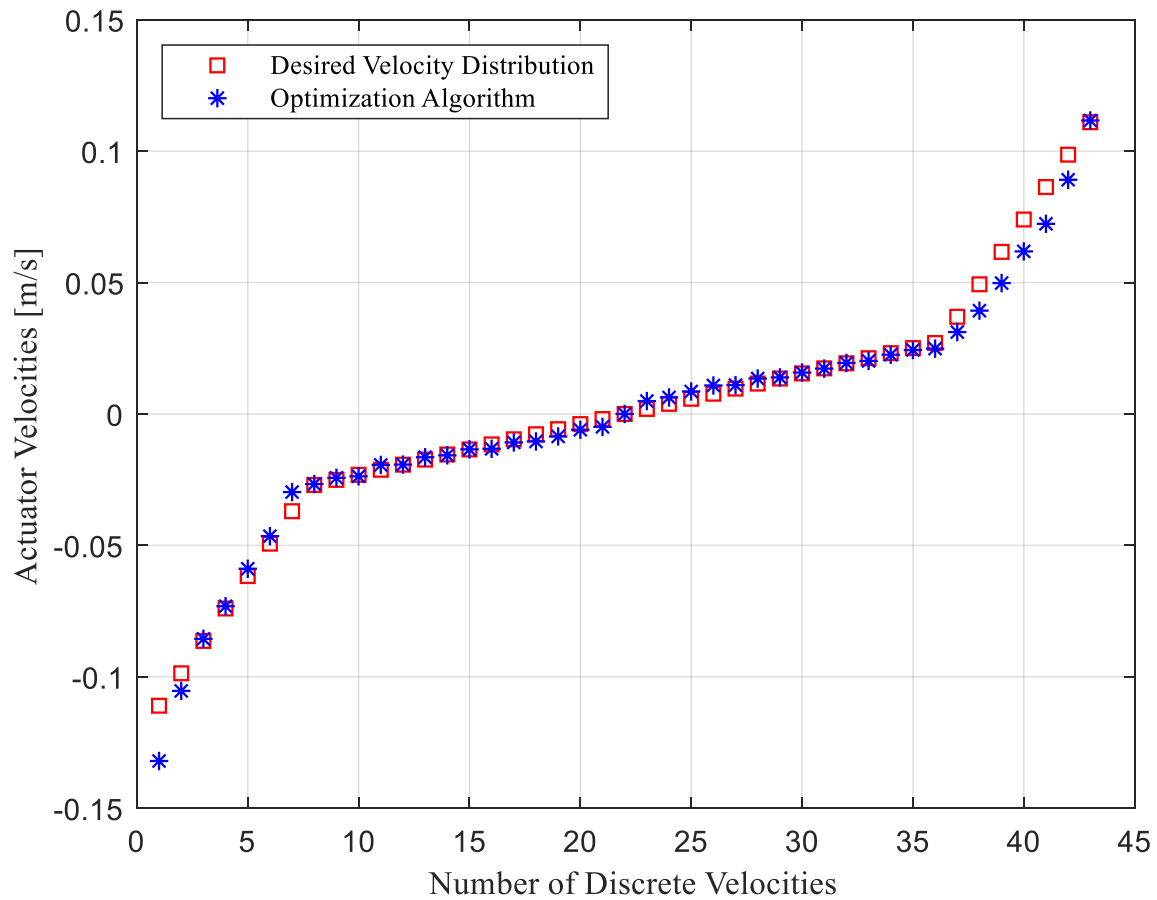


Source: By the author.

The results for the working pressure show that the maximum pressure occurs with the maximum supply flow rate and the minimum equivalent area. The minimum value for the equivalent area occurs when the chamber D is in regenerative mode, which implies in a high-pressure chamber against the actuator movement. Comparing the results presented in Figure 4.14 with the one obtained with the optimization algorithm (Figure 4.22), it is noticed that the optimization algorithm achieves different velocities using different equivalent areas in practically the entire range. Only the velocities close to the point 0.06 m/s have similar values. In this case, the velocities that have higher resultant pressure should be avoided.

Besides the implementation of a linear objective function for the calculus of the areas and the volumetric displacements of the pumps, others configurations can be also implemented, depending on the desired behavioral characteristics. Figure 4.23 presents the results obtained by the optimization algorithm for a nonlinear distribution considering the same parameters of Table 4.8. Table 4.10 present the resultant areas and pump volumetric displacements.

Figure 4.23 - Optimized velocity for a nonlinear distribution.



Source: By the author.

Table 4.10 - Optimized areas and volumetric pumps displacement for a nonlinear velocity distribution.

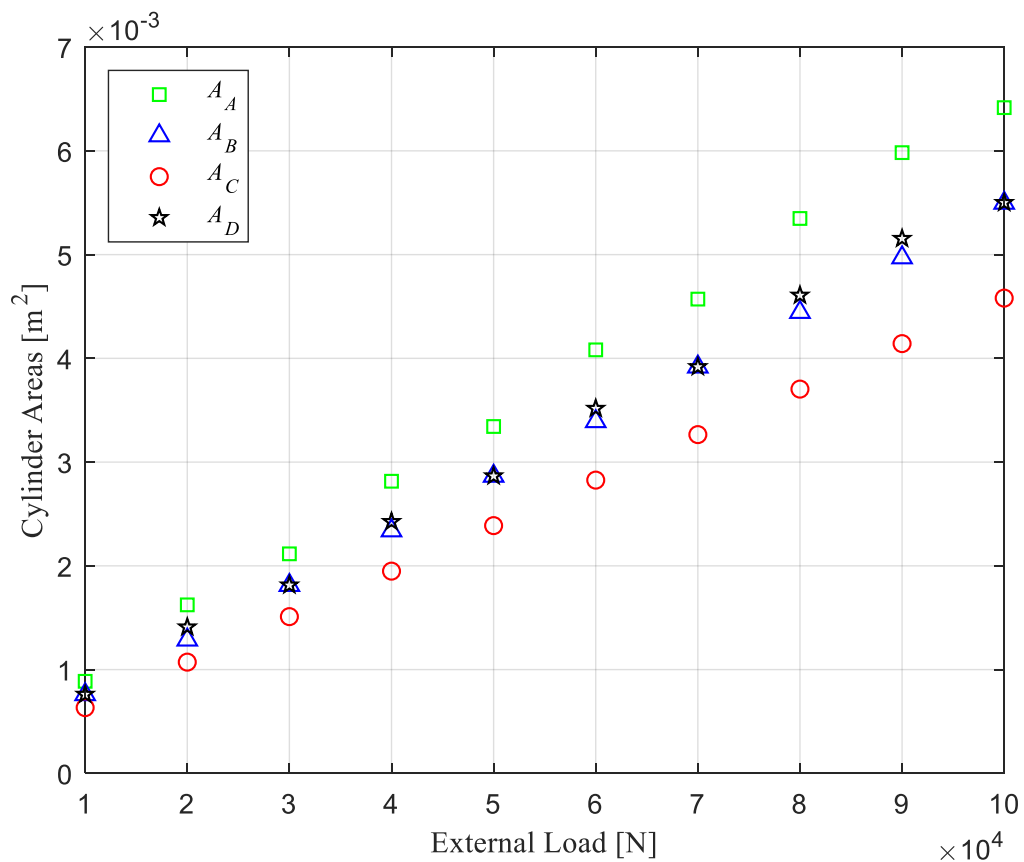
Actuator Areas	Value
A_A	$47.9 \times 10^{-4} \text{ m}^2$
A_B	$12.86 \times 10^{-4} \text{ m}^2$
A_C	$10.71 \times 10^{-4} \text{ m}^2$
A_D	$45.84 \times 10^{-4} \text{ m}^2$
Pump Displacements	Value
D_1	$1.44 \times 10^{-6} \text{ m}^3/\text{rev}$
D_2	$2.51 \times 10^{-6} \text{ m}^3/\text{rev}$
D_3	$3.18 \times 10^{-6} \text{ m}^3/\text{rev}$

Source: By the author.

As it can be seen by the results presented in Figure 4.23 and Table 4.10, the areas B and C have the same values when compared to the linear distribution. This is due to the restrictions imposed by equations (4.42) and (4.48). For the distribution presented in Figure 4.23, in order to compensate the velocity values between -0.025 e 0.025 m/s, required in the nonlinear distribution, the algorithm increases the values of the areas A and D. However, with the increasing of these areas, the actuator can achieve the maximum velocity required using the regenerative mode.

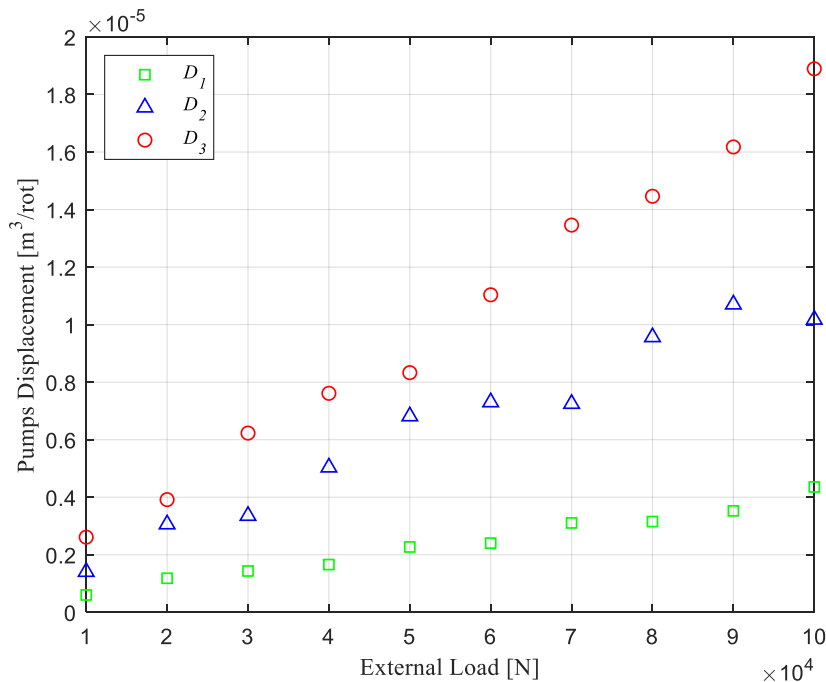
According to Equation (4.48), the external load F_L has a significant influence on the value of the equivalent area, and, consequently, in the size of the cylinder areas and the volumetric displacement of the digital pump. With the increasing of the external load force, the equivalent area also increases, and consequently the size of the digital pump. In Figure 4.24, the behavior of the size of the cylinder areas according to the external load is presented, and, in Figure 4.25, the volumetric displacement of the pumps.

Figure 4.24 – Cylinder areas for different external loads.



Source: By the author.

Figure 4.25 – Pumps volumetric displacements for different external loads.



Source: By the author.

4.6. FINAL CONSIDERATIONS OF CHAPTER 4

In this chapter, the guidelines for the design of a digital hydraulic actuator using multi-chamber cylinders and a digital pump were presented. In digital hydraulics, considering the topology of the actuator proposed in this thesis, there are many variables that must be taken into consideration for the actuator design, as the number of chambers, the number of binary modulus in the digital pump, the maximum positive and negative velocities, the external load and so on. The number of the chambers of the cylinder and the number of binary modulus present in the digital pump define the total number of different velocities that the actuator can achieve. The correct choice of the equivalent area implies in the maximum load that the actuator can achieve when the regenerative mode is being used.

As the evaluation of the areas of a cylinder with four chambers can be not realized analytically, a procedure using an optimization algorithm for the calculus of the cylinder areas and the volumetric displacements of the digital pump was presented. This algorithm takes into consideration the maximum positive and negative velocities, the external load, and the number of the chamber and binary modulus. With the use of the optimization algorithm, it is possible to obtain a better velocity distribution considering the desired velocity profile.

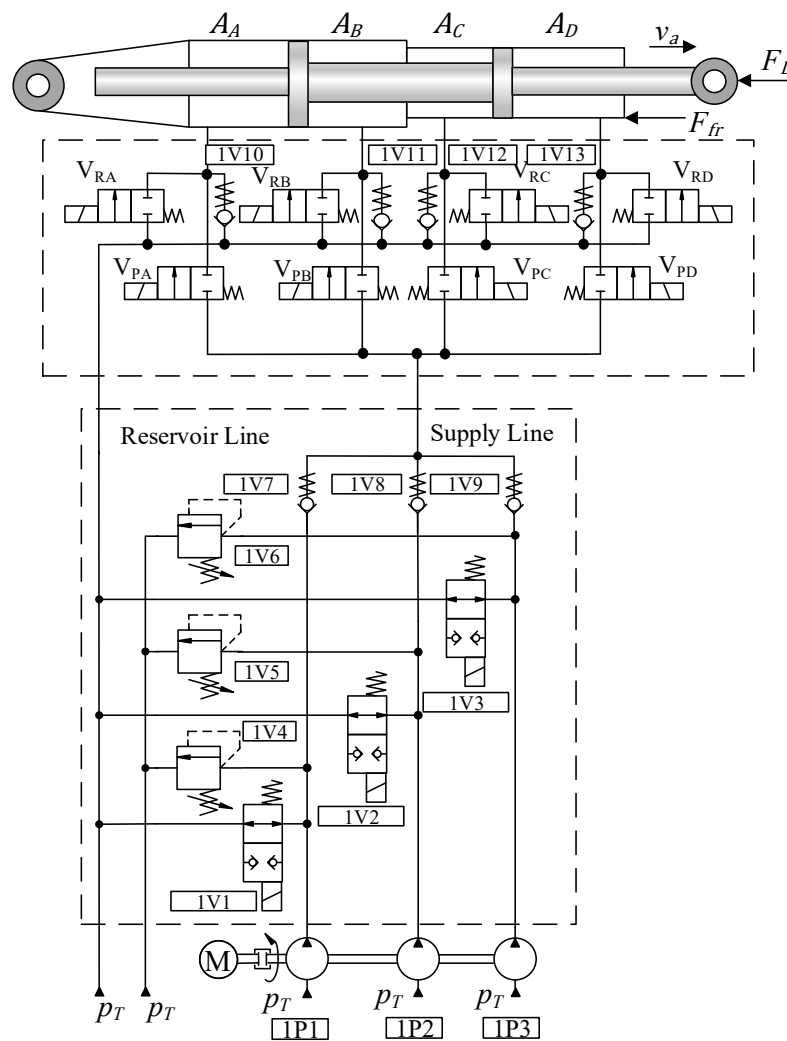
In order to verify the dynamic characteristics of the proposed actuator, in Chapter 5 an analytical model will be presented.

5. ACTUATOR MODEL

5.1. DIGITAL ELECTRO HYDROSTATIC ACTUATOR MODEL - DEHA

In this chapter, the actuator analytical model for the proposed actuator will be presented. The hydraulic circuit for the digital actuator is presented in Figure 5.1. The actuator proposed in this thesis, due to its similarity with the Electro Hydrostatic Actuators, where the pump and the cylinder comprise the actuator, was called Digital Electro Hydrostatic Actuator-DEHA.

Figure 5.1 – Proposed Digital Actuator – Digital Electro Hydrostatic Actuator.



Source: By the author.

The implementation of the model for the DEHA was carried out by the use of the software Hopsan 2.9.0 which was developed by the Department of Mechanical Engineering at the University of Linköping, Sweden. One of the advantages of this software is the possibility to perform co-simulation with MATLAB/Simulink, by exporting the model created for this

software. In addition, this software is open source, which facilitates its use for the academic community and provides expandability with the creation of new components by the users. Another important factor to be highlighted, for the justification of using the Hopsan software, is the partnership between LASHIP and the University of Linköping with the research group FLUMES. Besides the Hopsan software, some components were modeled using the software MATLAB/Simulink 2018 as the leakage curves of the pumps.

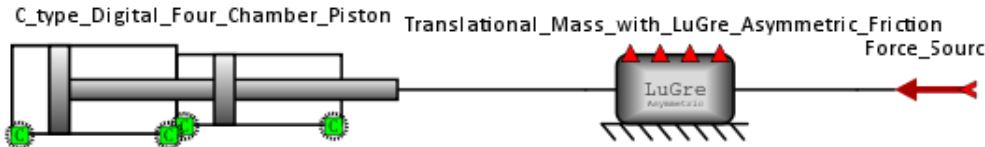
5.1.1. Cylinder model

For the modeling of the multi-chamber hydraulic cylinder, it was used an existing component in the Hopsan library, called *C_type_Digital_Four_Chamber_Piston*. The dynamics of the cylinder rod movement can be obtained through Newton's second law, being:

$$A_A p_A - A_B p_B + A_C p_C - A_D p_D - F_L - F_{fr} = M_T \frac{d^2 x}{dt^2}, \quad (5.1)$$

where p_A , p_B , p_C and p_D [Pa] are the pressures of chambers A, B, C, and D, respectively, A_A , A_B , A_C and A_D [m²] the areas of chambers A, B, C, and D, respectively, F_{fr} [N] the friction force, F_L the external load force [N] and M_T [kg] the total mass in movement. Table 5.1 presents the parameters for the multi-chamber cylinder.

Table 5.1 – Parameters for the multi-chamber cylinder.

Model Symbol		
 <p>The diagram shows a schematic of the multi-chamber cylinder model. On the left, a piston with four chambers (A, B, C, D) is shown. The piston rod is connected to a translational mass block labeled 'LuGre Asymmetric Friction'. A red arrow labeled 'Force_Source' points to the right, indicating the direction of the external load force.</p>		
Variable	Value	Unit
A_A	47.9×10^{-4}	m ²
A_B	12.86×10^{-4}	m ²
A_C	10.71×10^{-4}	m ²
A_D	45.84×10^{-4}	m ²
l	0.2	m
β_e	1.3×10^9	Pa
B	0.1	Ns/m
$V_{0A}, V_{0B}, V_{0C}, V_{0D}$	$6.8 \times 10^{-5}, 6.9 \times 10^{-5}, 6.8 \times 10^{-5}, 7.0 \times 10^{-5}$	m ³
$C_{LAB}, C_{LBC}, C_{LCD}$	$1 \times 10^{-16}, 1 \times 10^{-16}, 1 \times 10^{-16}$	m ³ /(sPa)

Source: By the author.

The parameters $V_{0A}, V_{0B}, V_{0C}, V_{0D}$, represent the dead volumes present in the chambers A, B, C, and D, respectively. The coefficients $C_{LAB}, C_{LBC}, C_{LCD}$ are constants related to the leakage that occurs between the chamber A to B, B to C and C to D, through the sealings. The friction force was modeled in the mass connected to the cylinder through the LuGre model, using the component *Translational_Mass_with_LuGre_Asymmetric_Friction*. The friction model will be presented in Section 5.1.1.1.

5.1.1.1 Friction force model

The friction force has a significant influence on the dynamics characteristics of hydraulic positioning systems. According to Viersma (1980), the friction force in hydraulic cylinders can cause losses of 10 to 15% of the supplied energy. Teixeira (2015) highlights that the magnitude of the friction force can achieve considerable values when compared with the external load.

According to Valdiero (2005), the friction is a nonlinear phenomenon, which demonstrates several nonlinear characteristics caused by the static friction, Coulomb friction, and the viscous friction. The same author also quotes that these frictions are the most present in the simpler friction models based on static maps. However, the friction is composed of more complex dynamics phenomenon as the Stribeck friction and so on (VALDIERO, 2005).

The effects of the friction force are dependents of several parameters, as the relative velocity between the surfaces, temperature, the direction of the movement, lubrication, wear of the surfaces, pressure in the chambers of the cylinder and the material of the sealings. (PERONDI, 2002, VALDIERO, 2005).

For the representation of the friction force presented in the multi-chamber cylinder used in the digital actuator, the LuGre model was applied, where the main equations are shown in APPENDIX B – Friction model equations.

To obtain the parameters of the friction model, experiments were carried out in the test bench developed in collaboration with the project of the DHA – Digital Hydraulic Actuator (BELAN, 2018).

The experiments consist of elaborate the static friction map, where a constant pressure is applied in the chambers A and C of the cylinder and a variable pressure in the chambers B and D. The constant and the variables pressures were applied using a controllable Hydraulic Power Unit presented at LASHIP. With this arrangement, the force applied can be controlled

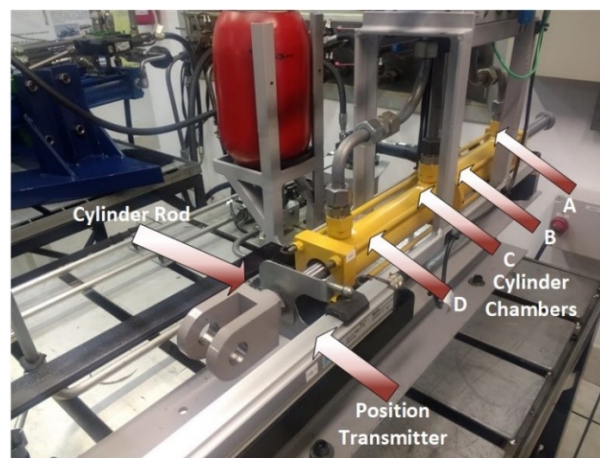
by the variation of the pressure of the chambers B and D, until a certain level, in which the cylinder starts to move, without any external load coupled in the cylinder rod.

The friction force can be estimated through the pressures in the chambers when the cylinder achieves the steady-state velocity, being.

$$F_{fr} = A_A p_A - A_B p_B + A_C p_C - A_D p_D. \quad (5.2)$$

Figure 5.2 presents the experimental apparatus for the obtention of the static friction map (The entire test bench will be presented in Chapter 6).

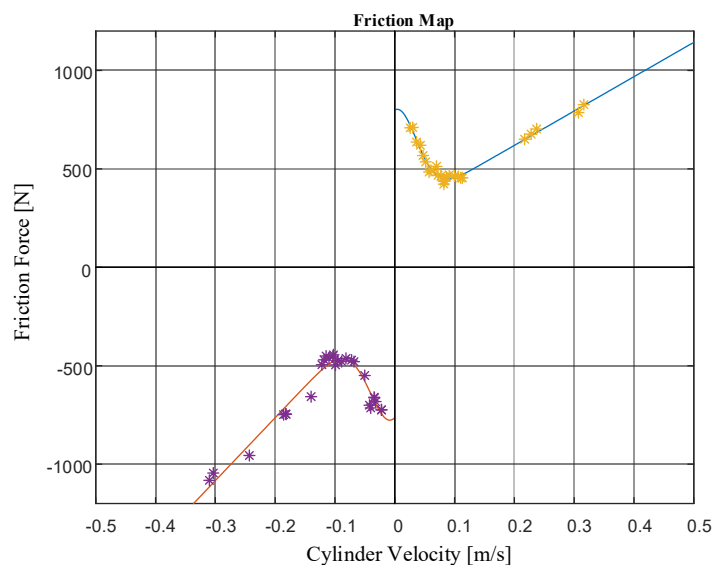
Figure 5.2 – Friction force test bench.



Source: By the author.

For the determination of the parameters presented in Equation (B.6), the nonlinear least squares method was used, where two curves were approximated through the points obtained by the experiments. Figure 5.3 shows the static friction force map.

Figure 5.3 - Static friction force map.



Source: By the author.

The identified friction force model parameters are presented in Table 5.2.

Table 5.2 - Friction force model parameters.

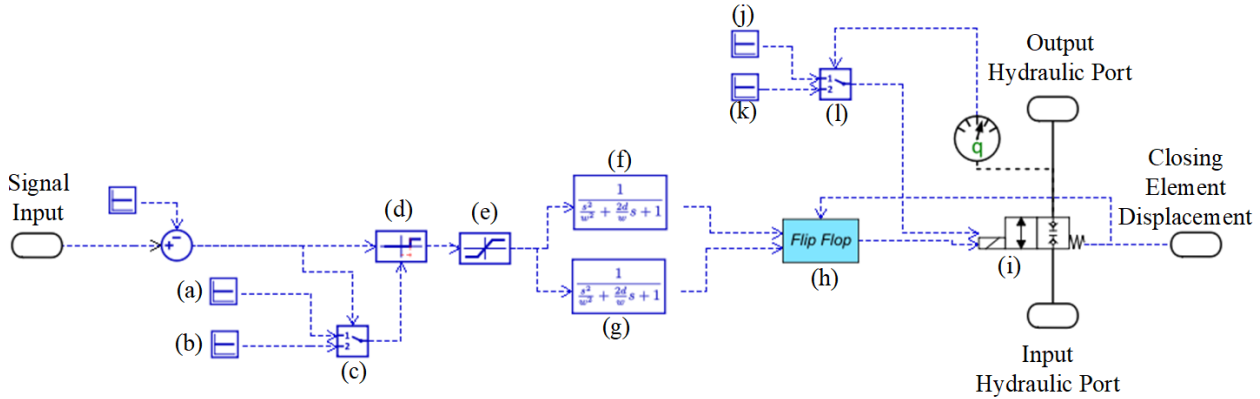
Positive Velocities		
Variable	Value	Unit
m	27	kg
σ_0	5×10^6	N/m
σ_1	0.1	kg/s
σ_2	1743.89	kg/s
F_S	798,96	N
F_C	270.72	N
v_S	0.05	m/s
Negative Velocities		
σ_0	5×10^6	N/m
σ_1	0.1	kg/s
σ_2	3195.67	kg/s
F_S	763.26	N
F_C	124.67	N
v_S	0.06	m/s
α_f	2	-

Source: By the author.

5.1.2. ON/OFF valves model

The on/off valves used in the limitation and control units were modeled using the component *digitalValve*. This model, which was used by Mantovani (2019), was previously developed by Belan (2018) based on the pre-existing model in the Hopsan library, called *2_2_Direction_Valve*. Figure 5.4 presents the digital valve for the application in the limitation and control unit.

Figure 5.4 – Normally closed digital valve.



Source: Adapted from Belan (2018), based in Mantovani (2019).

According to Belan (2018) and Mantovani (2019), the digital valve model developed is able to apply different dynamics characteristics for the valve opening and closing. In addition, different discharges coefficients can be applied depending on the flow rate direction.

According to Mantovani (2019), the valve model receives a digital input signal (0 to 1 or 1 to 0) through the *Signal Input* Port. This signal is sent for the block (d), which delays the input signal according to the opening or closing command. The magnitude of the delay is applied by the blocks (a) and (b), which are switched by the block (c), depending on the signal command.

As the input signal is digital and the model of the valve (i) receives the displacement of the valve closing element, the input signal is saturated by the block (d) until the maximum displacement of the closing element x_{vmax} [m].

The dynamics of the closing element movement is applied in the blocks (f) and (g). For the valve developed, a second order function was considered, represented as

$$X(s) = \frac{\omega_{n_{on}}^2}{s^2 + 2\xi\omega_{n_{on}}s + \omega_{n_{on}}^2} U_n(s), \quad (5.3)$$

where $X(s)$ is the closing element displacement, $U_n(s)$ the input signal, ξ [1] the damping factor, $\omega_{n_{on}}$ [rad/s] is the natural frequency for the opening movement. In the closing movement, the natural frequency is represented by $\omega_{n_{off}}$ [rad/s].

The *flip-flop* block (h) selects the dynamic of the closing element according to its opening and closing movement.

The flow rate through the valves can be expressed as (von LINSINGEN, 2013)

$$q_{vn} = c_d A_v \sqrt{\frac{2\Delta p}{\rho}}, \quad (5.4)$$

where, q_{vn} is the nominal flow of the valves [m^3/s], c_d is the discharge coefficient [1], A_v is the area of passage of the hydraulic fluid [m^2], Δp the pressure differential applied in the valves [Pa], and ρ the specific mass of the hydraulic fluid [kg/m^3].

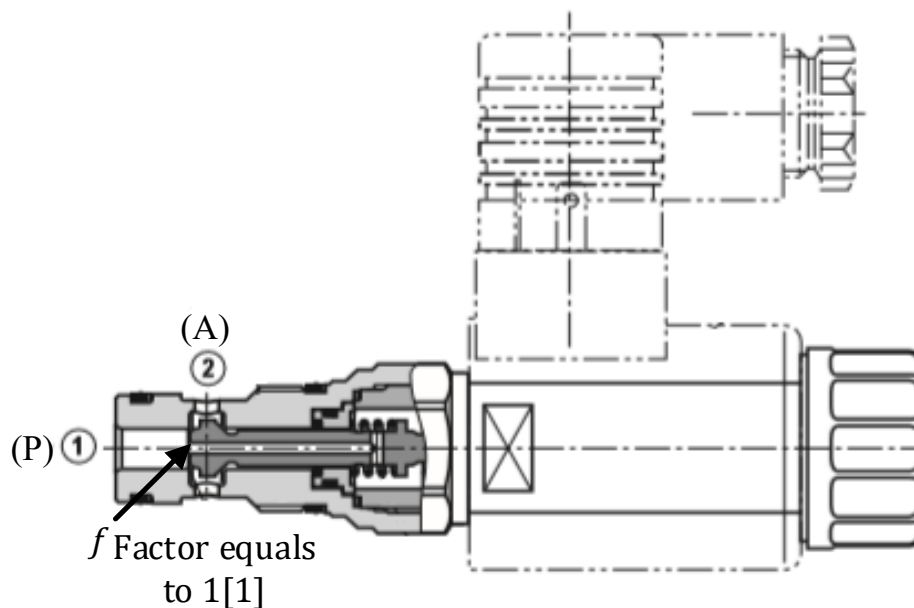
The model of the on/off valve presented in the Hopsan library uses more three different parameters for the evaluation of the area A_v , being the maximum closing element displacement x_{vmax} [m], the closing element diameter d [m] and the closing element diameter fraction coefficient f [1]. Therefore, the area of passage of the hydraulic fluid can be expressed as

$$A_v = \pi d x_{vmax} f. \quad (5.5)$$

The maximum displacement of the closing element represents the maximum opening of the valve. The fraction of the closing element diameter f represents the fluid passing fraction in relation to the diameter d of the fluid passing circumference.

The on/off valves modeled in the Hopsan library considers a sliding spool valve. However, the valves applied in the test bench (Chapter 6) are of the type of seat valves. According to Belan (2018), the Hopsan model does not consider the internal leakage present in sliding spool valves. Therefore, with the adjust of the closing element diameter d and the closing element diameter fraction f , the model can represent the seat valves, as the internal leakage does not occur in this kind of valves. For a seat valve, the closing element diameter fraction f can be considered equals to 1 [1], which means that all the perimeter of the closing element has flow when is opened and has sufficient pressure differential. Figure 5.5 shows the representation of the f factor for a seat valve.

Figure 5.5 – Representation of the f factor for a seat valve.



Source: Adapted from Bosch Rexroth KSDER valve catalog.

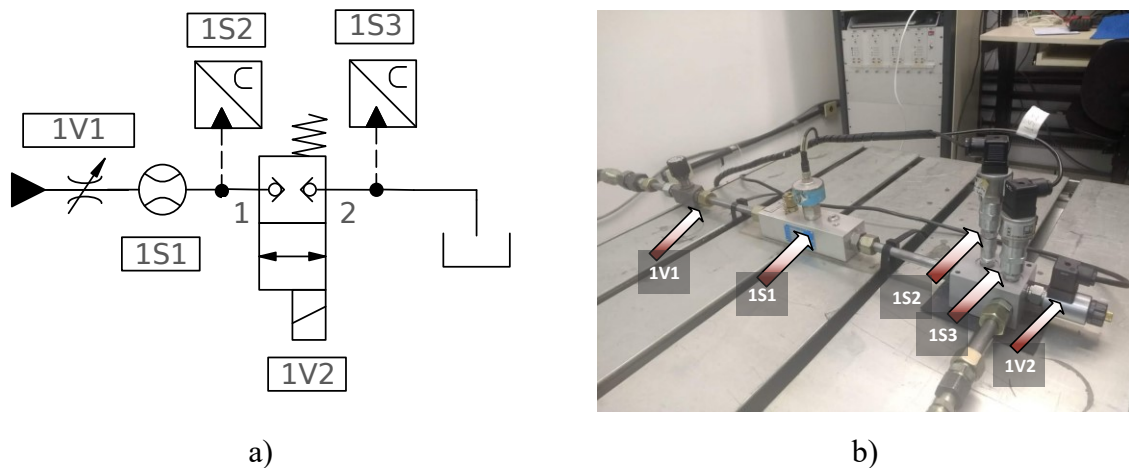
With the use of the blocks (j), (k) and (l) (Figure 5.4), it is possible to use different discharge coefficient according to the direction of the flow rate in the ports of the on/off valves (P to A or A to P - Figure 5.5).

For the modeling of the on/off valves presented in the primary conversion unit, the model was based in the valves of the limitation and control unit. However, the valves in the limitation and control unit, which means the valves that control the flow rate of the binary modulus of the digital pump, are normally opened. In this case, when the input signal changes the level 0 to 1, the valve closes and 1 to 0 the valve opens.

In addition to the dynamic behavior of the closing element of the valve for the opening and closing, the dynamic characteristics of the valve's solenoids were also implemented in the model. The solenoids on the valves take a certain amount of time to be energized, generate the magnetic field, and then, apply enough force so that the valve closing element begins the opening movement. This period of time was considered through the parameter t_{SOD} opening delay time. For the closing of the valves, a similar effect occurs. When the control signal commands the valve to close, the valve solenoid is de-energized. However, the magnetic field takes a certain time to weaken until the return spring starts closing the valve. This time is represented by t_{SCD} closing delay time. The opening and closing delay times were previously studied by Belan (2018) and Mantovani (2019).

For the determination of the limitation and control unit on/off valves parameters, an experiment was performed for evaluation of the valve's flow rate coefficient. The experiment consists in to apply different flow rates through the valves and measure the pressure drop.

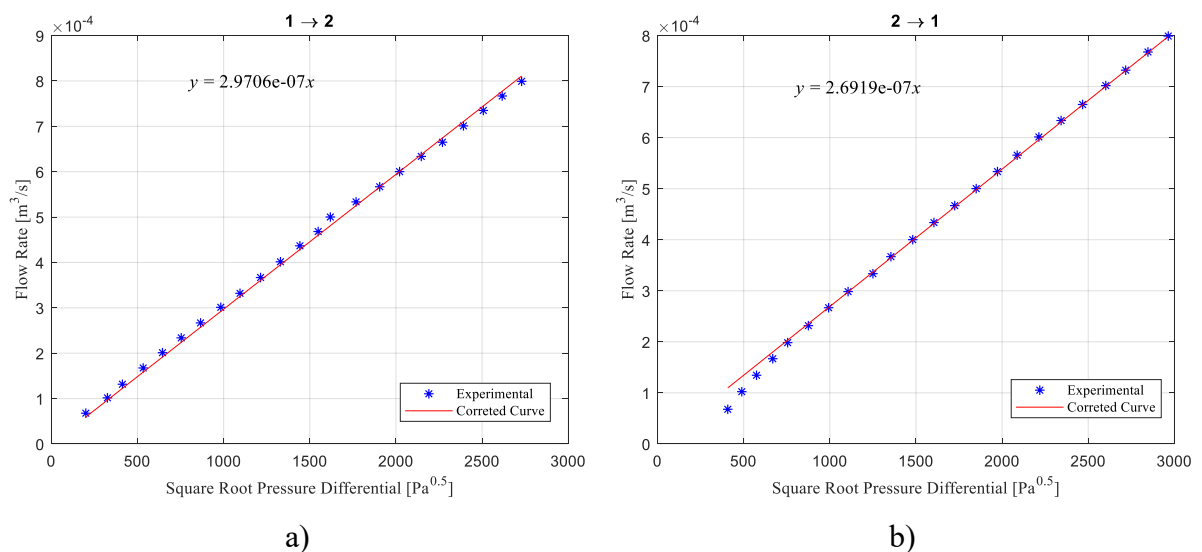
Figure 5.6 - On/Off valves flow rate coefficient experiments: a) Hydraulic circuit; b) Test bench.



Source: By the author.

With the valve opened, the flow rate was adjusted by the valve 1V1 and measured by the flow rate sensor 1S1. The pressure drop was measured by the sensors 1S2 and 1S3. The experiments were realized for both the valves flow direction, 1 to 2, and 2 to 1. The results are presents in Figure 5.7.

Figure 5.7 - On/Off valves flow coefficient experiments results: a) 1 to 2; b) 2 to 1.



Source: By the author.

With the results presented in Figure 5.7, the flow coefficient k_v can be obtained by the angular coefficient of the corrected curves, resulting in $2.970 \times 10^{-9} \text{ m}^3/(\text{sPa}^{0.5})$ for the ports 1 to

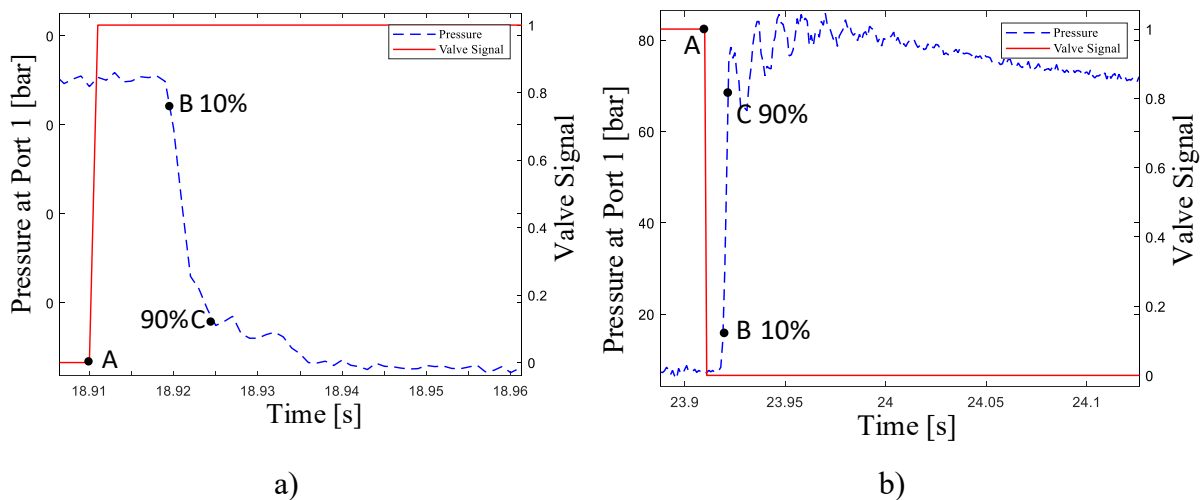
2 and $2.691 \times 10^{-9} \text{ m}^3/(\text{sPa}^{0.5})$ for the ports 2 to 1. With the determination of the flow rate coefficient, the area of the valves can be calculated as

$$A_v = \frac{k_v}{c_d} \sqrt{\frac{\rho}{2}} \quad (5.6)$$

For the evaluation of the dynamic response times of the on/off valves, another experiment was performed in the same test bench. The experiments consist in apply in the valve a flow rate value equals to 70% of the nominal value, which in the case in study is 20 L/min. The dynamic of the solenoid in the opening period t_{SOD} is obtained in the period of time between the application of the opening signal (point A) and the time when the pressure drops 10% of its value (point B) (BRIEDI *et al*, 2014), as shown in the Figure 5.8a. For the closing, the time t_{SCD} is obtained in a similar way (Figure 5.8b).

The time responses for the movements of the valve closing element (Opening t_{SOR} and Closing t_{SCR}) are estimated using the time period between the pressure achieves 10% to 90% of the steady-state values, points B and C (BRIEDI *et al*, 2014).

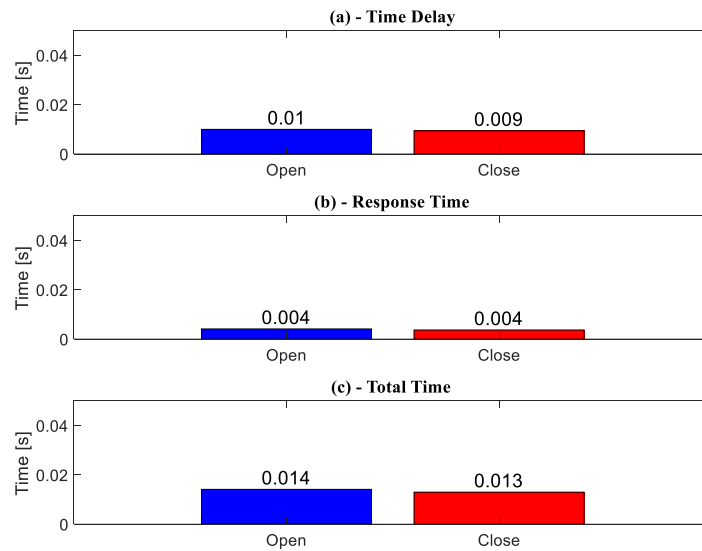
Figure 5.8 – Evaluation of the response times of the on/off valves.



Source: By the author.

The results obtained for the on/off valves in the limitation and control units are presented in Figure 5.9. The valves of the limitation and control unit have a booster to decrease the solenoid dynamics times. This booster will be better explained in Section 6.3.

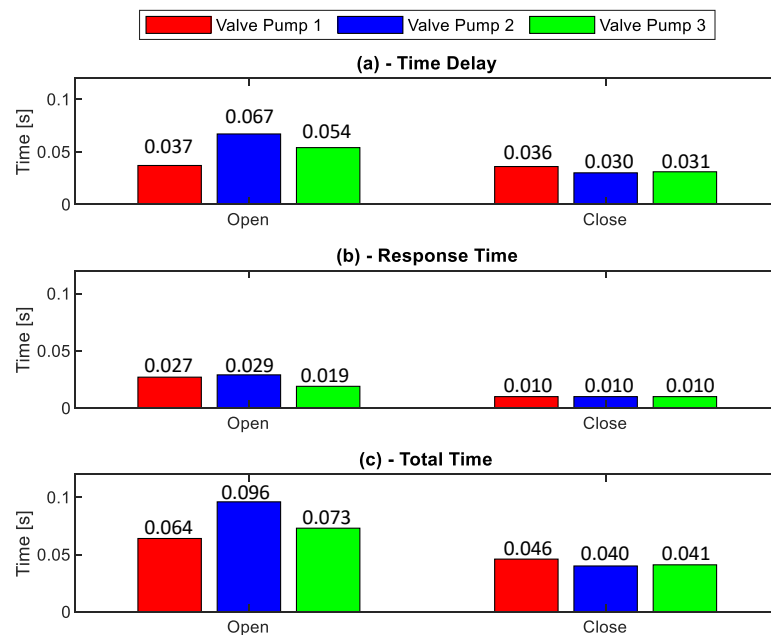
Figure 5.9 - Response times for the on/off valves in the limitation and control unit.



Source: By the Eng. Mantovani using the data from the author.

For the valves in the primary conversion unit, a similar experiment was carried out using the manifold block design for the application in the digital pump. In this case, the flow rate through the valves was limited by the flow rate produced by each binary modulus of the digital pump. In addition, the valves in the primary conversion unit do not have boosters, due to the limitations in the solenoids and in the boosters itself. Figure 5.10 presents the results obtained.

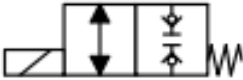

Figure 5.10 - - Response times for the on/off valves in the primary conversion unit.



Source: By the author.

As can be seen by the results presented in Figure 5.9 and Figure 5.10, the valves in the limitation and control unit are faster than the valves in the primary conversion unit. One of the reasons for this is the absence of boosters on the valves that control the digital pump. However, differences in the valve's construction can affect significantly the valves response times. The parameters of the on/off valves are summarized in Table 5.3.

Table 5.3 - On/Off valves parameters.

Model Symbol		Model Symbol	
			
Normally closed valves		Normally opened valves	
Variable	Value	Value	Unit
t_{SOD}	0.01	0.067	s
t_{SCD}	0.009	0.03	s
t_{SOR}	0.004	0.029	s
t_{SCR}	0.004	0.01	s
c_{d12}, c_{d21}	0.64, 0.69	0.67, 0.67	-
d	0.0063	0.0046	m
x_{vmax}	0.00045	0.001	m
f	1	1	-
ρ	870	870	kg/m ³
ω_{nv_on}	2000	206.9	rad/s
ω_{nv_off}	2000	600	rad/s

Source: By the author.

5.1.3. Check valves model

The check valves in the primary conversion unit, as mentioned in Section 4.2, are responsible to isolate each line of the binary modulus, which prevent the flow rate of one pump from being diverted to another. For the limitation and control unit, four check valves were added (Figure 5.1). These check valves have the function of avoiding the cavitation in the chambers of the cylinder.

The modeling of the check valves in the Hopsan software was carried out using the component *DynamicCheckValve*. This model is not present in the standard library of Hopsan.

The model presented in the standard library of the Hopsan does not consider the dynamics presented in the opening of the valve. Therefore, this aspect was added to the model.

The flow rate of the check valve can be represented according to


$$q_{vch} = k_{ch}\sqrt{\Delta p_{ch}}, \quad (5.7)$$

where q_{vch} is the flow rate through the check valve [m^3/s], k_{ch} is the check valve flow coefficient [$\text{m}^3/(\text{sPa}^{0.5})$] and Δp_{ch} is the pressure differential in the check valve [Pa]. For the opening behavior of the check valves, a second order dynamic was considered and implemented using a transfer function, being

$$Q(s) = \frac{\omega_{ch}^2}{s^2 + 2\xi_{ch}\omega_{ch}s + \omega_{ch}^2} q_{vch}(s), \quad (5.8)$$

where ω_{ch} is the check valve natural frequency [rad/s] and ξ_{ch} the check valve damping factor [1]. Table 5.4 presents the parameters used for the check valves. The parameters were obtained according to the components data catalog used in the test bench (Chapter 6).

Table 5.4 – Check valve parameters.

Model Symbol		
		
Variable	Value	Unit
q_{vch}	6.3×10^{-4}	m^3/s
k_{ch}	7.5×10^{-7}	$\text{m}^3/(\text{sPa}^{0.5})$
Δp_{ch}	7×10^5	Pa
ω_{ch}	314.15	rad/s
ξ_{ch}	0.7	-
p_{ac}	2×10^5	Pa

Source: By the author.

5.1.4. Digital pump model

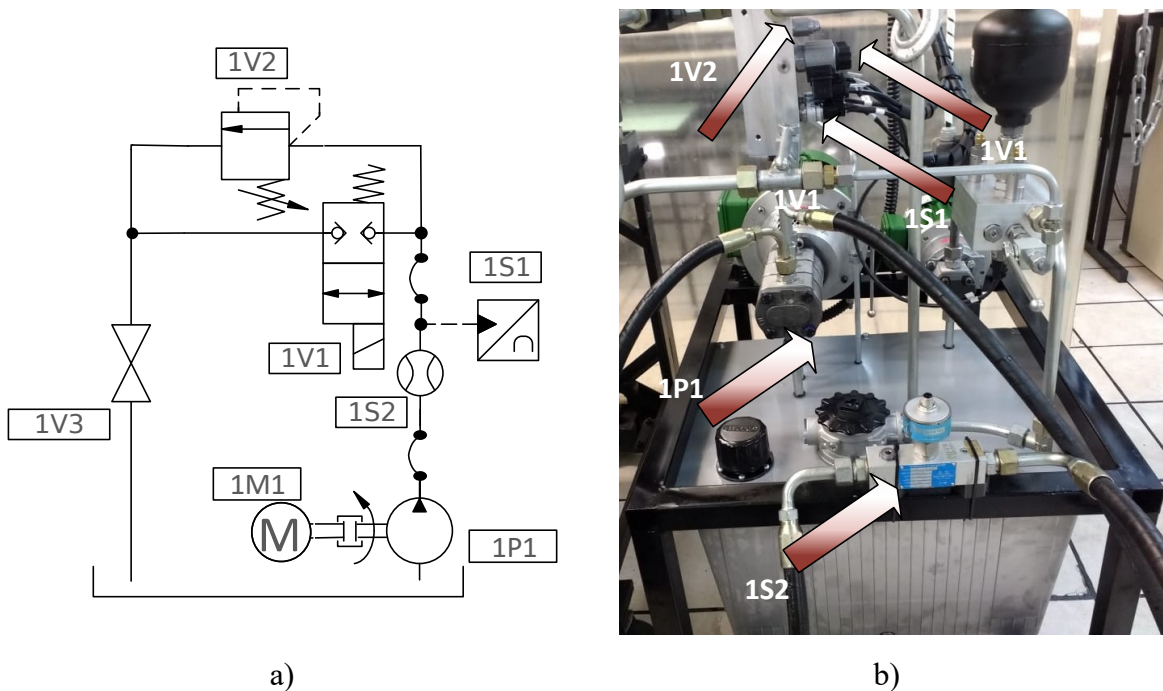
The fixed displacement pumps, which are used in the digital pump, were modeled using the component *Q_type_Fixed_Displacement_Pump*. The flow rate that is delivered by each pump, in steady-state without considering the leakages, can be calculated by the Equation (4.26). However, the hydraulic pumps have an internal leakage that should be taken into consideration in the model. The internal leakage of each pump was modeled adding an orifice in parallel of each pump (Figure 5.1). The leakage of the pumps can be evaluated as

$$q_{vpl} = k_{pl}\Delta p_{cl}, \quad (5.9)$$

where q_{vpl} is the leakage flow rate of the pumps [m^3/s], k_{pl} is the leakage coefficient [$\text{m}^3/(\text{sPa})$], and Δp_{cl} is the pressure differential applied at the pumps [Pa].

The leakage flow rate of the pumps was evaluated through experiments carried out in the test bench. The main objective of the experiments is to measure the real output flow rate q_{vpr} delivered by each pump for different output pressures. The experiments were carried out using the simplified hydraulic circuit present in Figure 5.11a. The hydraulic circuit present was simplified for a better understanding of the components that were used during the experiments for each pump (Figure 5.11b).

Figure 5.11 - Pumps internal leakage experiments.



Source: By the author.

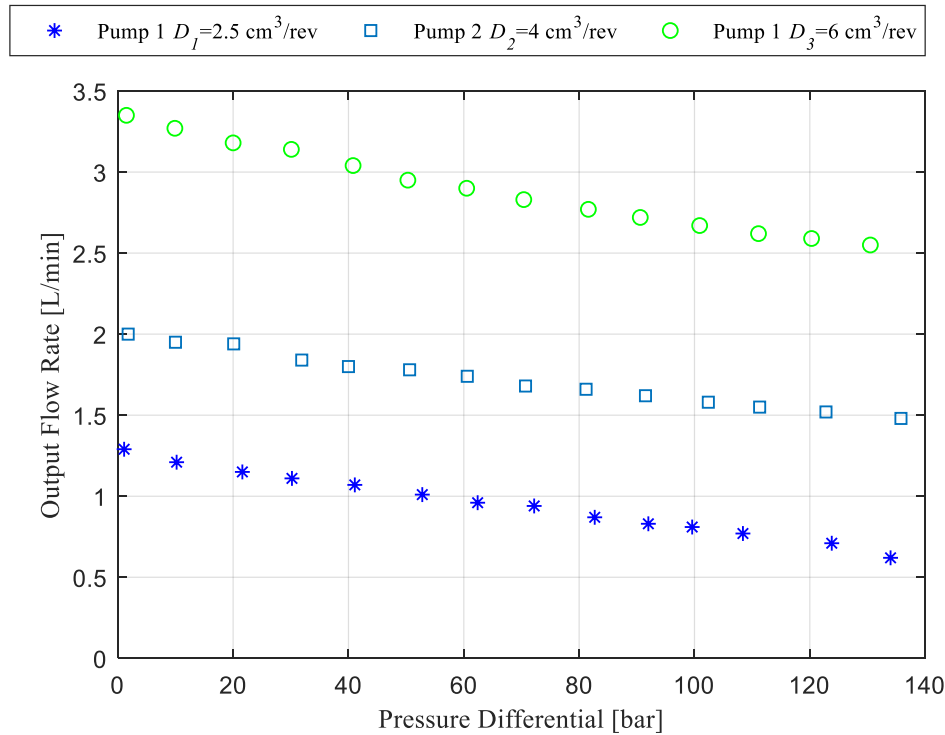
The sensor 1S2 (WEBTEC CT15) is a flow rate transmitter, which measures the real output flow rate of the pumps, and the sensor 1S1 (HYDAC HAD 844K-B-0250) the output pressure. The valve 1V1 is kept closed and the valve 1V3 opened throughout the experiment. The output pressure was adjusted by the relief valve 1V2.

With the results of the experiment, the leakage flow rate can be obtained as

$$q_{vpl} = q_V - q_{vpr}. \quad (5.10)$$

The results of the experiments are present in Figure 5.12, where the pumps were running at 600 rpm (the evaluation of the volumetric displacements of the digital pump used in the test bench will be presented in Chapter 6).

Figure 5.12 - Pumps delivered flow rate as a function of the output pressure.



Source: By the author.

As can be seen in Figure 5.12, the flow rate delivered by each pump is affected by the output pressure. This behavior is caused by the internal clearances presented in the components, which causes internal leakages.

For the implementation of the pump's leakage in the model, it was modeled as a laminar orifice in parallel to the pumps, as shown in Figure 5.17.

The leakage coefficient k_{vl} [m³/s(Pa)] can be expressed as

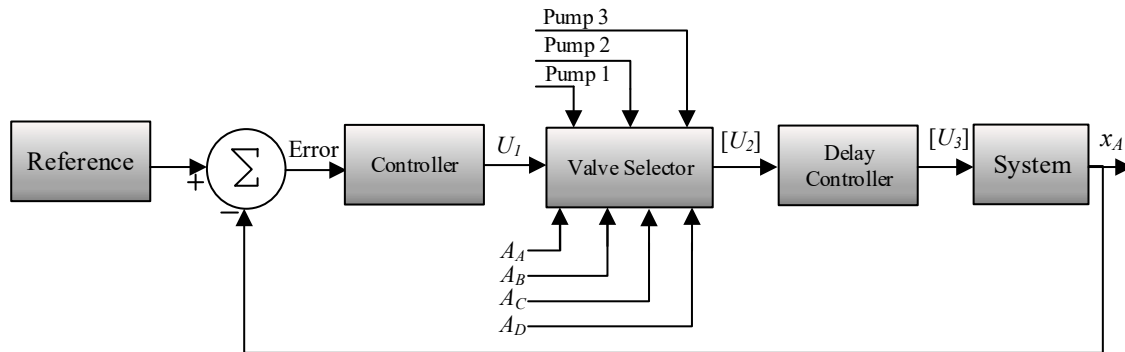
$$k_{vl} = \frac{q_{vpl}}{\Delta p}. \quad (5.11)$$

This coefficient is calculated in real-time by the model using the data present in Figure 5.12.

5.1.5. System control

In this section, the control strategy for the system in both open and closed loop will be presented. The system control was implemented using MATLAB/Simulink software., Figure 5.13 shows the schematic block diagram of the control system.

Figure 5.13 - System control block diagram.

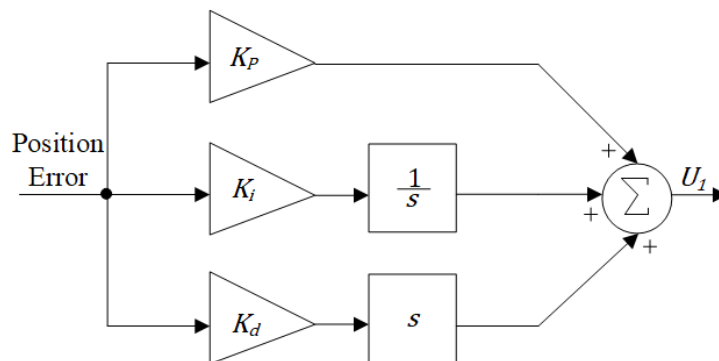


Source: By the author.

The operation of the system controller works as follows. When a reference signal is applied, it is compared with the actual position signal of the actuator x_A , generating an error. The generated error signal is then sent to the controller, generating the control signal U_1 . This signal represents the velocity that the cylinder must reach to achieve the reference position x_r . The signal U_1 is then sent to the valve selector which, together with the cylinder area and the combination of pumps of the digital pump, selects which valves should be activated or not, generating the signal $[U_2]$. The signal $[U_2]$ is then sent, for the delay controller. This controller has the purpose of synchronizing the on/off valves, due to their different dynamics for opening and closing. After the delay controller, the control signal is then sent to the system valves.

The controller used in the system is a PID controller. This type of controller was chosen due to its easy implementation. In addition, other studies using PI or PID controllers have obtained good results, as in Linjama *et al.* (2009), Belan *et al.* (2015), Dell'Amico *et al.* (2013). The PID controller is presented in Figure 5.14.

Figure 5.14 - PID controller block diagram.



Source: By the author.

From the pumps and areas used in the multi-chamber cylinder, the valve selector uses a matrix, where each column presents the combination of valves that must be activated to obtain the desired velocity value. In addition, if the velocity value is not equal to the values contained in the matrix, the selector chooses the velocity whose value is the closest to the required one. Figure 5.15 shows the matrix structure.

Figure 5.15 – Velocities matrix structure.

Interaction	i	25	27	---	29
Velocity [m/s]	v_d	0.0662	0.0937	---	0.1376
Switching Cost	c_s	0.2411	0.2136	---	0.1695
Pumps	Pump 1	1	1	---	1
	Pump 2	1	0	---	1
	Pump 3	0	1	---	1
Chamber A	V_{PA}	1	1	---	1
	V_{RA}	0	0	---	0
Chamber B	V_{PB}	0	0	---	0
	V_{RB}	1	1	---	1
Chamber C	V_{PC}	1	1	---	1
	V_{RC}	0	0	---	0
Chamber D	V_{PD}	1	1	---	1
	V_{RD}	0	0	---	0
Flow Rate [m ³ /s]	q_{vb}	0.00006	0.000083	---	0.00012
Area [m ²]	A	0.000907	0.000907	---	0.000907

16 x 43

Source: By the author.

In the matrix presented in Figure 5.15, the first row represents the velocity index and the second represents the velocity available in the system, which is calculated based on the cylinder areas and the pump's flow rate (Equation (4.29)). The third row represents the switching cost function, which is based on the one applied by Houva *et al.* (2017). This function is calculated with the difference between the desired velocity required by the PID controller and the velocity present the system, that is,

$$c_s = |v_{d(i)} - v_{ref}|, \quad (5.12)$$

where c_s is the switching cost factor [m/s], $v_{d(i)}$ is the velocity present in the matrix [m/s] and v_{ref} is the reference velocity calculated by the controller [m/s]. This function is related to the

selection of the velocity that will be applied for the system. Therefore, the switching cost factor calculates all the values for all the velocities present in the actuator, and select the one, which has the smaller cost, which represents the value closer to the one requested.

The rows four to six represent the status of the on/off valves for pumps one, two, and three, respectively. The rows seven to fourteen are responsible for the valves of the cylinder's chambers and the row fifteen and sixteen represent the flow rate and the area used for the calculus of the actuator velocity (row two).

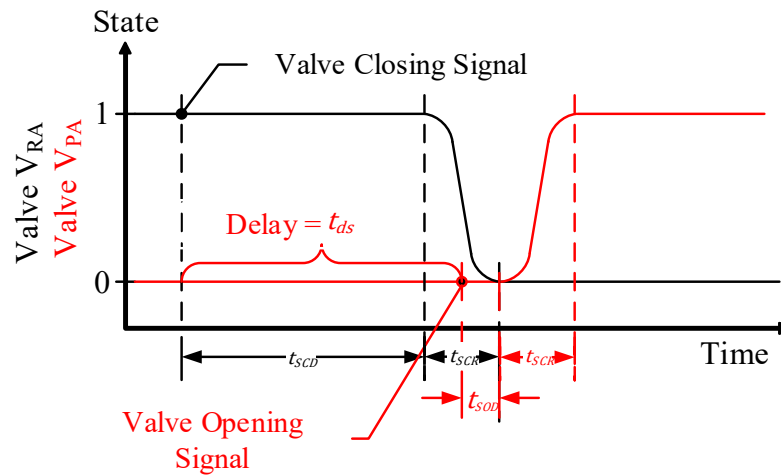
For the valve selector, three time intervals, dT_s , dT_v , and dT_{min} were implemented based on those used in Belan (2018). The dT_s is the time interval, in which the valve selector algorithm should operate according to the simulation sample time (1 ms). The dT_v defines the time that the combination valve matrix should be recalculated and the dT_{min} defines the minimum time interval for a valve combination change, which should be higher than the dynamics of the valves. It is necessary for the dynamics of the valves that need to be opened and closed, for a given velocity value, to be actually executed before applying the next velocity level. With the definition of the status of all valves for the desired velocity, the output signal from the valve selector is sent to the delay controller.

As mentioned in 5.1.2, there are four time intervals in the dynamics of the on/off valves that influence significantly the system behavior, being

- The time to energize the valve solenoid t_{SOD} ;
- The time to de-energize the valve solenoid t_{SCD} ;
- The opening valve closing element dynamics t_{SOR} ;
- The closing valve closing element dynamics t_{SCR} .

These parameters are necessary to define the valve's delay control signal. This delay is applied to synchronize the opening and closing of the valves of the same chamber. For instance, if the valve V_{RA} is opened and the valve V_{PA} is closed, if the controller requires that the valve V_{PA} should open, the control signal should be delayed, thus, allowing the valve V_{RA} to close before the opening of the valve V_{PA} . The delay controller behavior is presented in Figure 5.16.

Figure 5.16 - Delay controller.



Source: Adapted from Mantovani *et al.* (2018) and Mantovani (2019).

According to Mantovani (2019), the delay time t_{ds} that must be applied to synchronize the valves can be evaluated as

$$t_{ds} = t_{SCD} + t_{SCR} - t_{SOD}. \quad (5.13)$$

If the delay time applied to the valves is less than that calculated by Equation (5.13), the switching will occur in a short circuit, where the two valves remain open at the same time, in a certain period. If the delay time is higher than that calculated by Equation (5.13), the valve switching will occur where the chambers will remain confined for a period of time. According to Mantovani (2019), the short circuit between the switching of the valves improves the system performance, however, the energy efficiency is degraded.

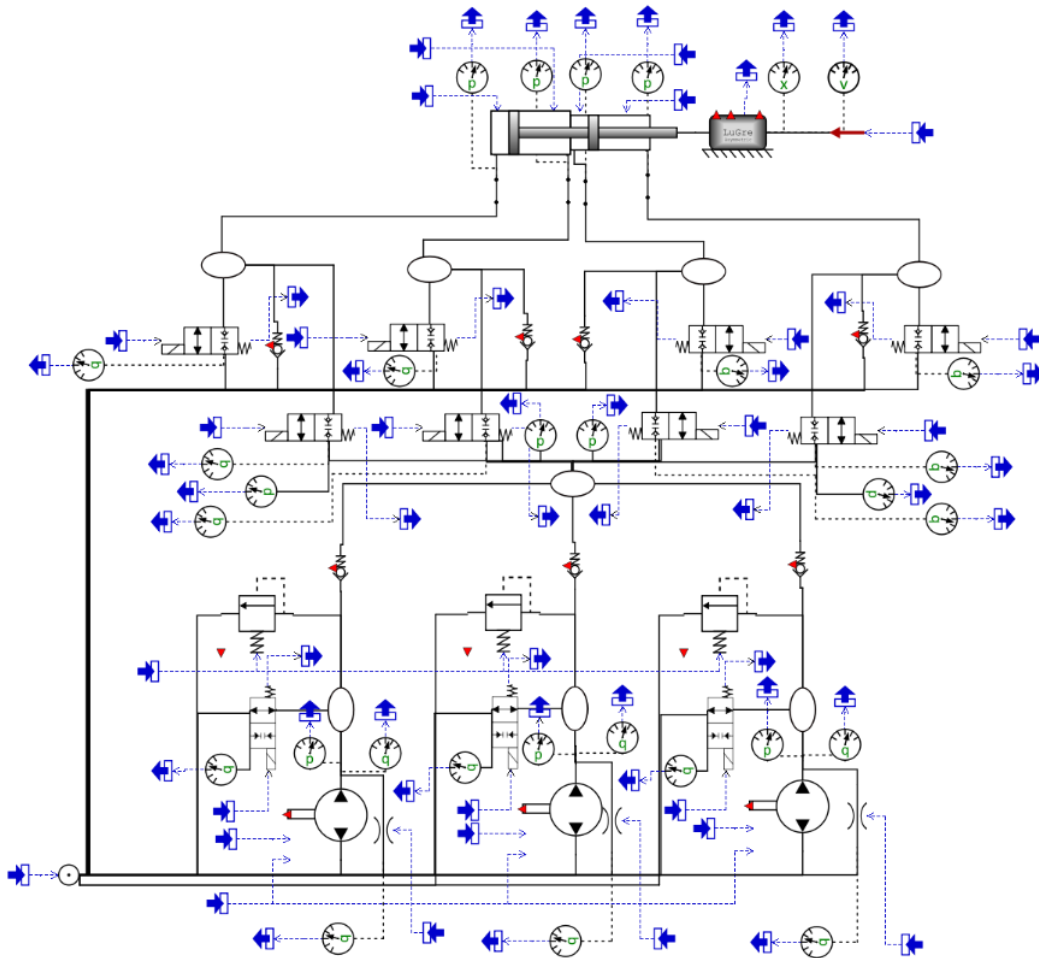
According to the results present in Figure 5.9 and Figure 5.10, the valves that control the limitation and control unit have a significant difference in the response times, when compared with the valves of the primary conversion unit. Therefore, there is the necessity to apply two different time delays, one for the primary conversion unit (t_{dsp}) and other for the limitation and control unit (t_{dsl}).

The minimum time between two consecutive change of velocities dT_{min} can be calculated as

$$dT_{min} = t_{SCD} + t_{SCR} + t_{ds}. \quad (5.14)$$

With the definition of the delay times for the valves in the primary and the limitation conversion units, the signal that comes out from the delay controller is sent for the system model, which in the case of this thesis was developed in the software Hopsan. The model developed in Hopsan is presented in Figure 5.17.







Figure 5.17 - DEHA Hopsan model.



Source: By the author.

Table 5.5 presents the components that are used for measurement and for the input and output signals.

Table 5.5 – Complementary components used in the Hopsan model.

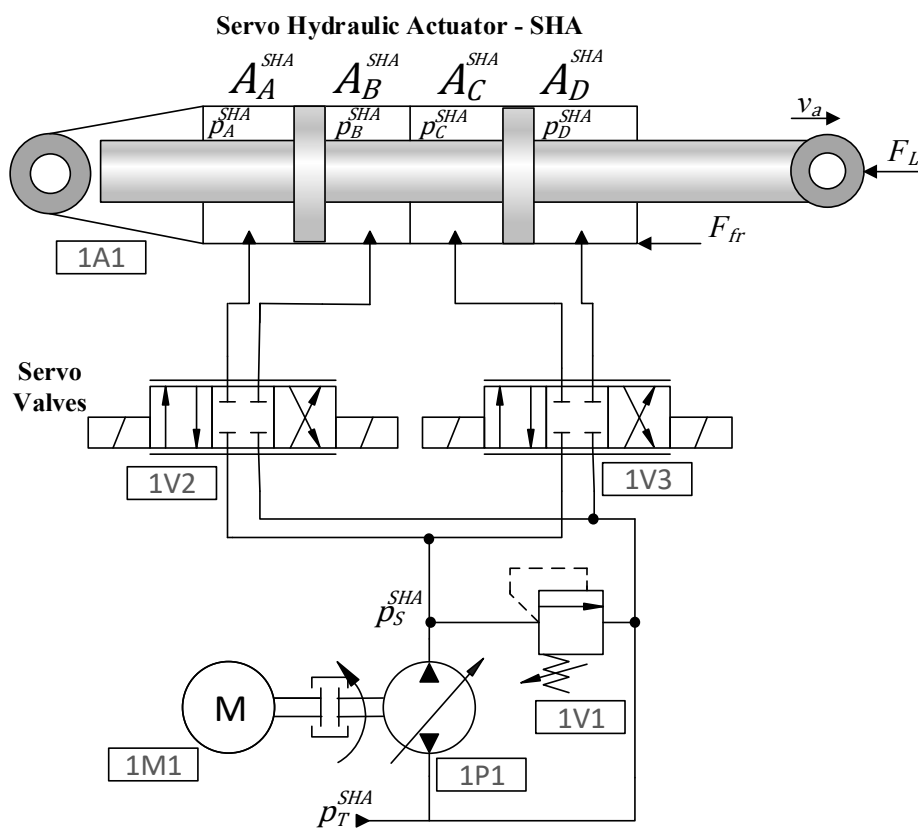
Symbol	Description
	Flow sensor
	Pressure sensor
	Displacement sensor
	Velocity sensor
	Input signal
	Output signal

Source: By the author.

5.2. SERVO HYDRAULIC ACTUATOR MODEL – SHA

In order to evaluate the energy consumption of the Digital Electro Hydrostatic Actuator – DEHA, two different models were developed. The first model consists of a Servo Hydraulic Actuator -SHA. This model is composed of a four-chamber hydraulic cylinder (1A1), two servo valves (1V2, 1V3), a variable displacement pump (1P1), a fixed rotational frequency electric motor (1M1) and a relief valve (1V1). The SHA system modeled is presented in Figure 5.18.

Figure 5.18 - Servo Hydraulic Actuator - SHA Model.



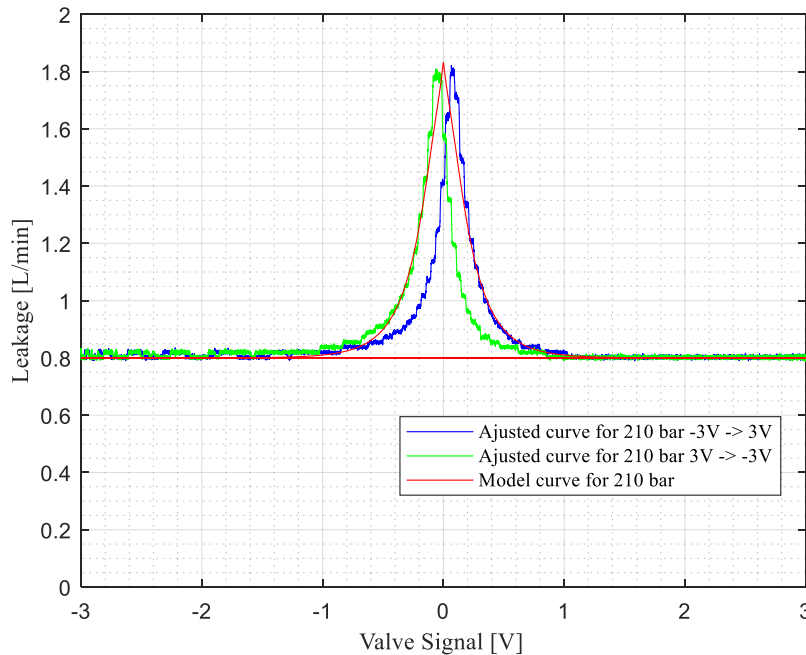
Source: By the author.

In the SHA, the two servo valves are used for the system redundancy, where in a fault of one of the valves, the actuator can keep operating with 50% of its force capacity. These servo valves present a sliding spool in their interior. With this configuration, there is a certain clearance between the spool and the valve's sleeve, which causes an internal leakage. This leakage must be supplied by the variable displacement pump in order to keep the system pressurized. However, when the cylinder is not moving, the pump must be set in a very low displacement, where the volumetric efficiency is degraded (PINTO *et al.*, 2016, MARÉ, 2016).

In order to implement the leakage of the servo valves in the model, Cruz (2018) developed a leakage model in Hopsan based on the experimental results carried out by the Eng.

Ivan Mantovani at the Laboratory of Hydraulic and Pneumatic Systems – LASHIP. The experiments were carried out using a servo valve from MOOG model 760 C263-A. The results of the leakage experiments are presented in Figure 5.19.

Figure 5.19 - Servo valves leakage.



Source: By the author using the data provided by Ivan Mantovani and Cruz (2018).

As can be seen in Figure 5.19, the total leakage of the valve in the center position is 1.8 L/min. In the extremity (-3 and 3 V), there is a leakage around 0.8 L/min, which is associated with the pilot stage of the servo valve. As the SHA, proposed in this thesis, has two servo valves, the total leakage of the system is 3.6 L/min. This means that the variable displacement pump should supply this amount of flow rate plus its internal leakage to keep the system pressurized.

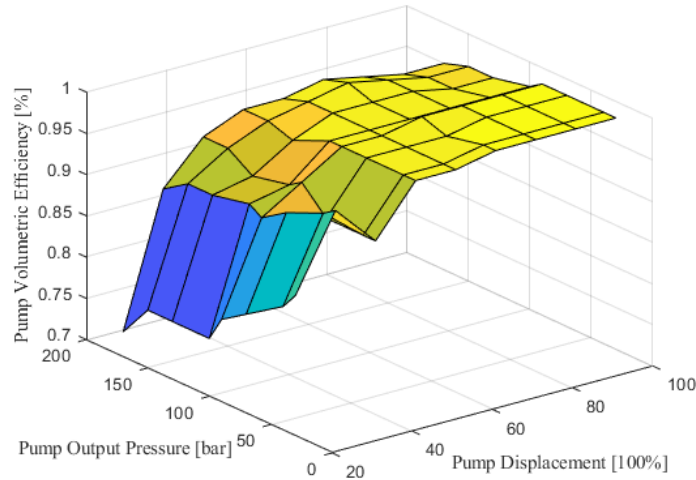
The variable displacement pump was modelled according to the Equation (5.15), being

$$q_{vp} = U_{Dv} D \omega, \quad (5.15)$$

where U_{Dv} [1] is the volumetric displacement control signal, which can assume values between 0 to 1.

For the implementation of the volumetric efficiency of the variable displacement pump, the results obtained by the experiments presented in Bravo (2017) were considered. With the experiments present by this author, an efficiency map considering the pump output pressure and the volumetric displacement was elaborated. The volumetric efficiency map is shown in Figure 5.20.

Figure 5.20 - Variable displacement pump volumetric efficiency map.



Source: By the author using the data provided by Bravo (2017).

In normal operation conditions, as in the steady-state flight of an aircraft, the variable displacement pump is set in low volumetric displacement, just to supply the pump internal leakage and the system leakage. As presented in Figure 5.20, in low values of volumetric displacement and high output pressure, the volumetric efficiency is considerably low, when compared with higher volumetric displacement values. In this situation, the losses in the pump become considerable.

In order to consider the effects of the volumetric efficiency of the variable displacement pump in the model, the pump leakage was modeled as a laminar orifice in parallel to the pump, where the pump leakage coefficient was calculated in real time using the data present in Figure 5.20 and the Equation (5.16).

$$k_{plv} = \frac{\omega_{np} D_{pv} U_{Dv} (1 - \eta_v)}{2\pi (p_s^{SHA} - p_r^{SHA})}, \quad (5.16)$$

where, ω_{np} is the pump rotational frequency [rad/s], D_{pv} is the pump maximum volumetric displacement [m^3/rev], U_{Dv} is the pump displacement control signal [1], η_v the volumetric efficiency, p_s^{SHA} is the pump output pressure for the SHA [Pa] and p_r^{SHA} is the reservoir pressure for the SHA [Pa]. The pump displacement control signal is calculated according to the actuator position error e [m] (Equation (5.17)).

$$\begin{cases} \text{if } 0 \leq e \leq 0.05 \rightarrow U_{Dv} = 13.038e + 0.3481 \\ \text{if } -0.05 \leq e < 0 \rightarrow U_{Dv} = -13.038e + 0.3481. \end{cases} \quad (5.17)$$

For the system using the variable displacement pump and the servo valves – SHA, the relief valve (1V3 - Figure 5.18) must remain closed, being only a safety device.

The areas A, B, C, and D of the SHA cylinder were calculated in order to achieve the same maximum force for the maximum positive velocity, when compared with the DEHA.

The dynamics of the valve and the pump volumetric displacement were considered as second order. Therefore, the natural frequency for the valve was considered as 1047.2 rad/s according to the data catalog and the displacement control with a natural frequency of 209.43 rad/s. The damping factor for both components is 0.9. The parameters for the SHA model are shown in Table 5.6.

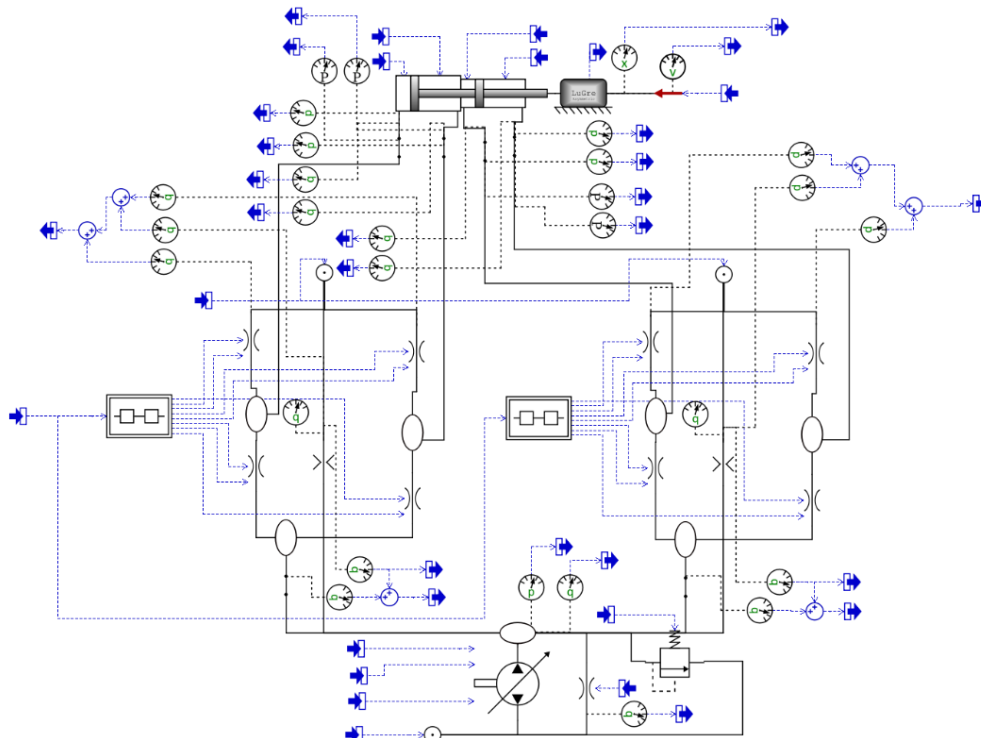
Table 5.6 - Parameters of the SHA.

Parameters	Value	Unit
A_A, A_B, A_C, A_D	453.5	mm ²
l	0.2	m
β	1.3×10^9	Pa
D_{pv}	6.15×10^{-6}	m ³ /rot
p_r^{SHA}	10×10^5	Pa
ω_{np}^{SHA}	125.66	rad/s

Source: By the author.

The model of the SHA developed in Hopsan is shown in Figure 5.21.

Figure 5.21 - SHA model developed in Hopsan.

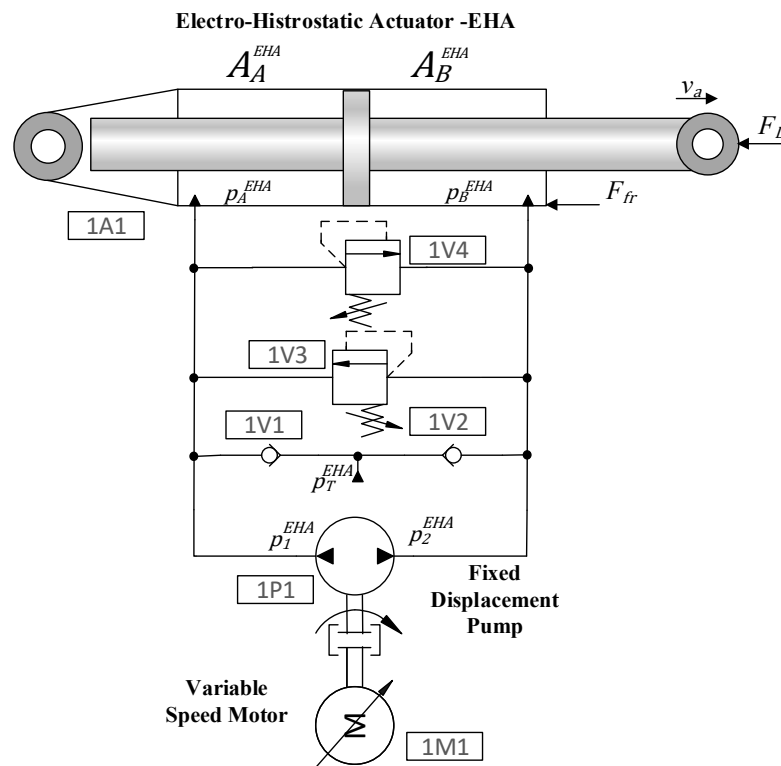


Source: By the author.

5.3. ELECTRO HYDROSTATIC ACTUATOR MODEL - EHA

Another actuator configuration that was considered and modeled for comparison of the hydraulic efficiency with the DEHA, was the electro hydrostatic actuator – EHA. In this actuator configuration, a fixed displacement pump (1P1) was modeled considering that its rotational frequency was controlled by an electric motor with variable rotational frequency (1M1). This fixed displacement pump is connected directly to the two chambers cylinder (1A1) and two relief valves (1V3 and 1V4) are used for limiting the pressure in the lines and safety reasons. The Electro-Hydrostatic Actuator is presented in Figure 5.22.

Figure 5.22 - Electro-Hydrostatic Actuator model.



Source: By the author.

The check valves 1S1 and 1S2 are used to isolate the pressurized reservoir, which is represented by a constant pressure source (p_T^{EHA}).

For the DHA position control, a PI controller was implemented, where the position error was converted, by a constant value (24000 rpm/m), in rotational frequency for the electric motor, and consequently for the pump. The dynamic of the variable rotational frequency electric motor was modeled considering a second order transfer function, where the natural frequency is 240 rad/s (this value is based on Xia (2012)).

The cylinder areas and the volumetric displacement of the pump were implemented in an analogous way of the SHA actuator, which takes into consideration the maximum external

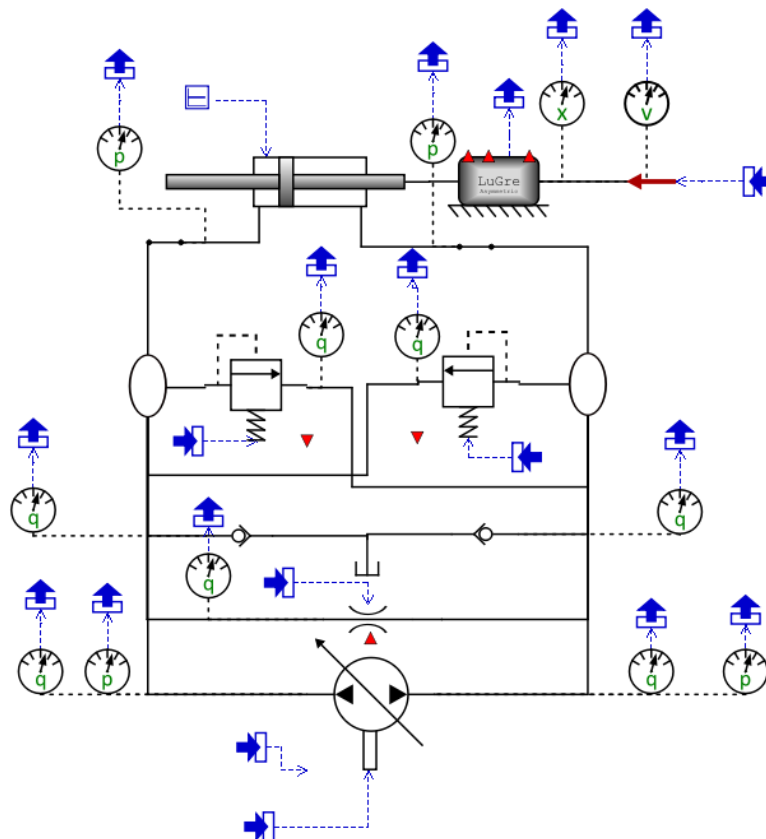
load, velocity, and pressure. The parameters of the EHA are shown in Table 5.7, and the EHA model developed in Hopsan is presented in Figure 5.23.

Table 5.7 - Parameters for the EHA actuator.

Variable	Value	Unit
A_A^{EHA}	0.907×10^{-5}	mm^2
A_B^{EHA}	0.907×10^{-5}	mm^2
l	0.2	m
V_{oA}	6.8×10^{-5}	m^3
V_{oB}	6.9×10^{-5}	m^3
β	1.3×10^9	Pa
D_p^{EHA}	6.15×10^{-6}	m^3/rot
p_r^{EHA}	10×10^5	Pa
ω_{np}^{EHA}	240	rad/s
ξ	0.9	0.9

Source: By the author.

Figure 5.23 - EHA model developed in Hopsan.



Source: By the author.

The internal leakage of the pump was modeled as an orifice in parallel of the pump, where the leakage coefficient was estimated using manufacture catalogs, which results in $13.44 \times 10^{-13} \text{ m}^3/\text{Pa}$.

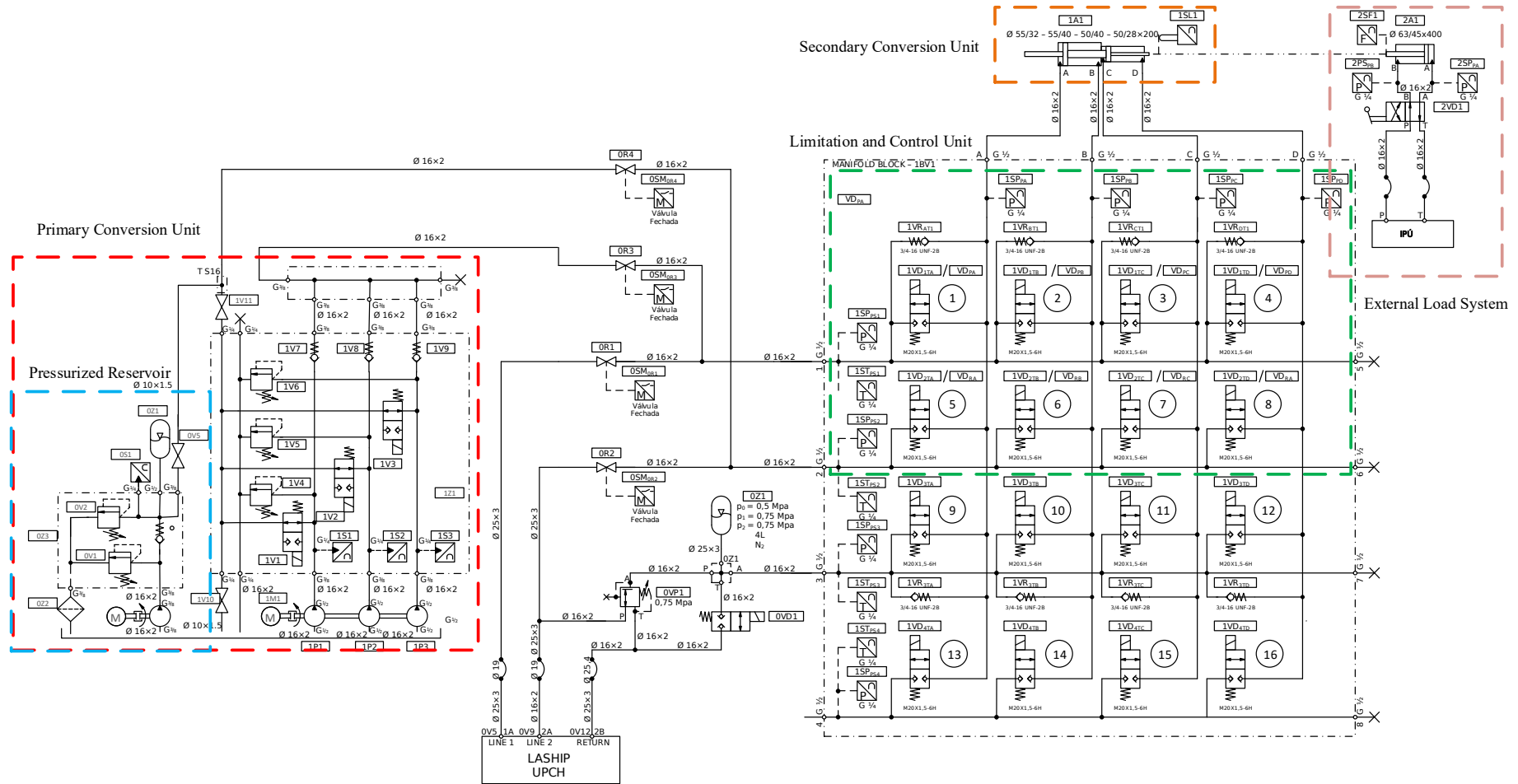
5.4. FINAL CONSIDERATIONS ABOUT THE ACTUATOR MODEL

In Chapter 5, the model of the components used in the Digital Electro Hydrostatic Actuator was presented. The model takes into consideration the components used in the test bench elaborated for the model validation. In addition, a model for the SHA and another model for the EHA were elaborated, with the purpose to being compared with the DEHA model. All the actuators (SHA, EHA, and DEHA) were modeled considering the same maximum load and maximum velocity. In Chapter 6, the test bench will be presented with more details.

6. TEST BENCH

In this chapter, the test bench developed during this thesis for the validation of the Digital Electro Hydrostatic Actuator model will be presented. This test bench contemplates two different concepts of actuators, the DHA and the DEHA, where the definition of which actuator is in operation is carried out by opening and closing some ball valves. The development of this bench was carried out with the support of the companies, Saab AB, Bosch Rexroth, Hydac, Medal, Wipro, Nova Electric Motors. In Figure 6.1 the complete hydraulic circuit diagram for the test bench is presented. In order to facilitate the understanding of the description of the components that comprise the test bench, they will be described separately through the primary conversion unit, limitation and control unit, and the secondary conversion unit.

Figure 6.1 - Hydraulic diagram of the test bench.

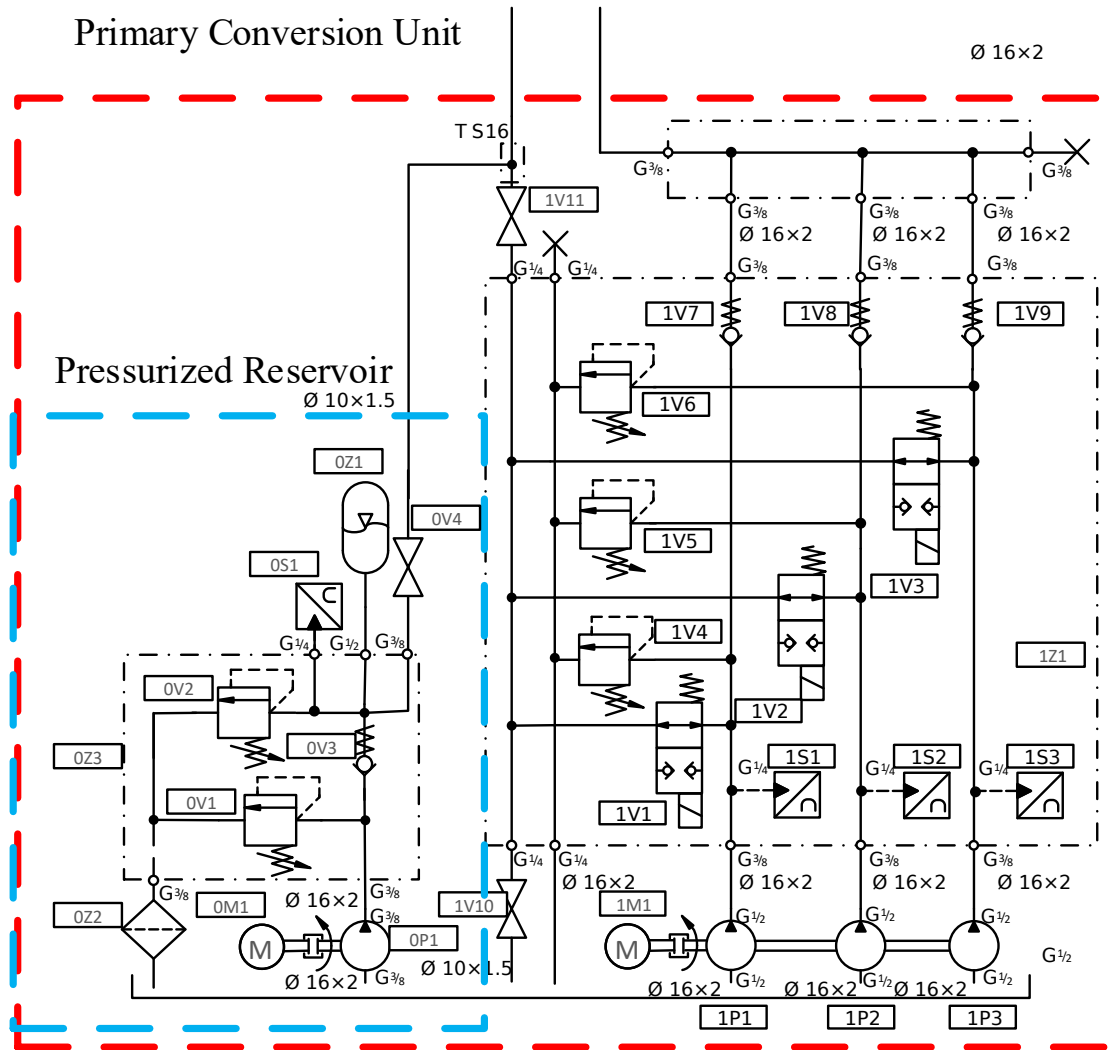


Source: By the author based in the circuit elaborated by Ivan Mantovani.

6.1. TEST BENCH PRIMARY CONVERSION UNIT

For a better understanding of the test bench, the primary conversion unit hydraulic circuit is presented in Figure 6.2.

Figure 6.2 - Test bench primary conversion unit hydraulic circuit diagram.



Source: By the author.

The multi-chamber cylinder used in the experiments is the same as the one used by Belan (2018) and Mantovani (2019). The areas of this cylinder were firstly designed for the implementation in the DHA - Digital Hydraulic Actuator, where three different constant pressure sources can be connected to the cylinder chambers. As a result, the choice of the volumetric displacements of the binary modulus (1P1, 1P2, 1P3), of the digital pump, take into consideration these areas. Therefore, the optimization algorithm was used only for the calculus of the volumetric displacement of the binary modulus. The results are shown in Table 6.1, where the rotational frequency is 600 rpm.

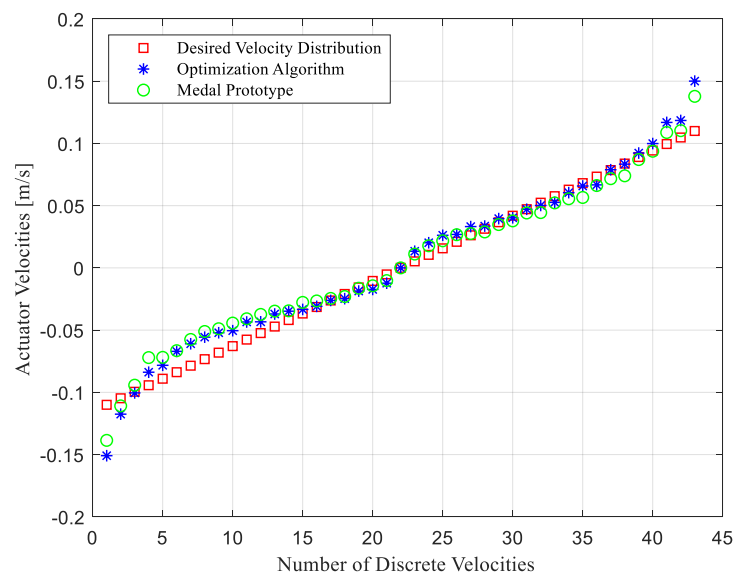
Table 6.1 - Pumps displacement for the test chamber multi-chamber cylinder.

Actuator Areas	Value
A_A	$15.44 \times 10^{-4} \text{ m}^2$
A_B	$11.02 \times 10^{-4} \text{ m}^2$
A_C	$7.07 \times 10^{-4} \text{ m}^2$
A_D	$13.44 \times 10^{-4} \text{ m}^2$
Pumps Displacements	Value
D_1	$3.01 \times 10^{-6} \text{ m}^3/\text{rev}$
D_2	$4.55 \times 10^{-6} \text{ m}^3/\text{rev}$
D_3	$6.05 \times 10^{-6} \text{ m}^3/\text{rev}$

Source: By the author.

From the results obtained through the optimization algorithm, it is not possible to find pumps with the exact values of volumetric displacements on the market. In this case, the closest values must be chosen. The national manufacturer of hydraulic pumps MEDAL supported the development of this thesis by manufacturing the pumps of the binary modulus with the volumetric displacements as close as possible to those required. In this case, the prototype developed and used in the test bench shows the nominal volumetric displacements of 2.5, 4, and 6 cm^3/rev for pumps 1P1, 1P2, and 1P3, respectively. Figure 6.3 presents the comparison between the optimization algorithm pump and the MEDAL prototype pump.

Figure 6.3 – Actuator velocities comparison for the optimization algorithm pump and the MEDAL prototype pump.



Source: By the author.

As can be seen by the results presented in Figure 6.3, the values obtained by the optimization algorithm and the ones provided by the Medal pump are very close.

With the definition of the volumetric displacement of the binary modulus, an electric motor (1M1) from Nova Motores, model ME-5086 T 7.5 cv IP-56 was used as a mechanical power source for the pump. This motor was controlled by a frequency inverter Micromaster 440 from Siemens, where the inverter frequency was adjusted in 20 Hz.

In the output line of each pump, there is a pressure transmitter 1S1, 1S2, and 1S3, that are responsible for measure the output pressure of the pumps 1P1, 1P2 and 1P3, respectively. In addition, the on/off valves 1V1, 1V2, and 1V3 are in charge for select if the pumps flow rate will be directed to the reservoir or to the system. The relief valves 1V4, 1V5, and 1V6 were installed for the system safety and the check valves 1V7, 1V8, and 1V9 are used to isolate the pump lines. The list of the components used in the primary conversion unit is shown in Table 6.2.

Table 6.2 – Hydraulic components of the primary conversion unit.

Component	Code	Response Time
Pressure Transmitter Hydac HDA 844K-B-0250-000	1S1, 1S2, 1S3	1.5 ms
Solenoid Directional Valve Hydac WSM06020V-01-C-N-0	1V1, 1V2, 1V3	-
Relief Valve DB06A-01-C-N-300F125	1V4, 1V5, 1V6	-
Check Valve Hydac RV08A-01-C-N-145	1V7, 1V8, 1V9	-
Prototype Digital Pump from MEDAL	1P1, 1P2, 1P3	-
Electric Motor Nova ME-5086 T 7.5 cv IP-56	1M1	-
Reservoir NG 70	1Z2	-

Source: By the author.

To emulate a pressurized reservoir, a pressurized reservoir unit was developed. This hydraulic unit is responsible for keeping the reservoir line with a certain level of pressure in the chambers of the cylinder that are connected to the reservoir, with the finality to avoid cavitation.

This unit is composed by one fixed displacement gear pump (0P1), an electric motor (0M1), two relief valves (0V1 and 0V2), one check valve (0V3), one ball valve (0V4), one accumulator (0Z1) and one hydraulic filter (0Z2). With the arrangement proposed for the pressurized reservoir unit, three different operation modes can be achieved using the ball valves 0V4, 1V10, and 1V11. If the valves 0V4, 1V10, and 1V11 remain opened, the system operates without a pressurized reservoir. If the valves 0V4 and 1V11 are kept opened and the valve 1V10

closed, the system operates with a reservoir pressure in the chamber of the cylinder and in the output of the digital pump. In the case of the valves 0V4 and 1V10 opened and the 1V11 closed, only the chambers of the cylinder are kept with reservoir pressure, and the output of the digital pump is kept in atmospheric pressure. Table 6.3 presents the components used in the pressurized reservoir unit.

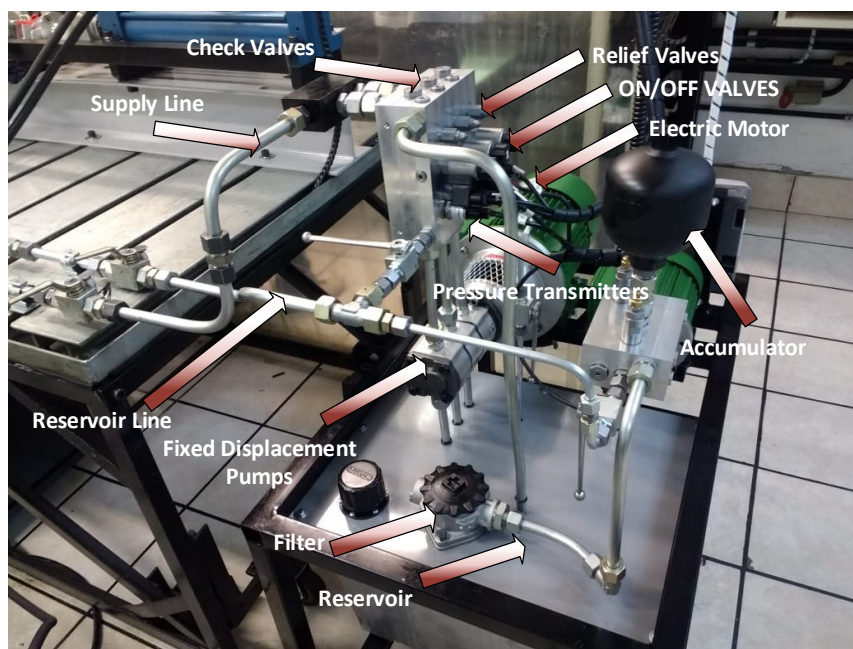
Table 6.3 - Hydraulic components of the pressurized reservoir unit.

Component	Code	Response Time
Pressure Transmitter Hydac HDA 844K-B-0250-000	0S1	1.5 ms
Fixed Displacement Gear Pump Hydac PGE101-160-RBQ1-N-3700	0P1	-
Relief Valve DB4E-01X-100P	0V1, 0V2	-
Check Valve Hydac RV08A-01-C-N-145	0V3	-
Electric Motor Nova ME-2050 T 0.5 cv IP-56	0M1	-
Filter RFM 165 BD XX A	0Z1	-
Membrane Accumulator SB0 210-0,75E1/112U-210AB07	0Z2	-
Ball Valve Hydac KHB-10SR-1112-03X-A-SW09	0V4, 1V10, 1V11	-

Source: By the author.

Figure 6.4 shows the test bench primary conversion and pressurized reservoir units.

Figure 6.4 - Test bench primary conversion and pressurized reservoir units.

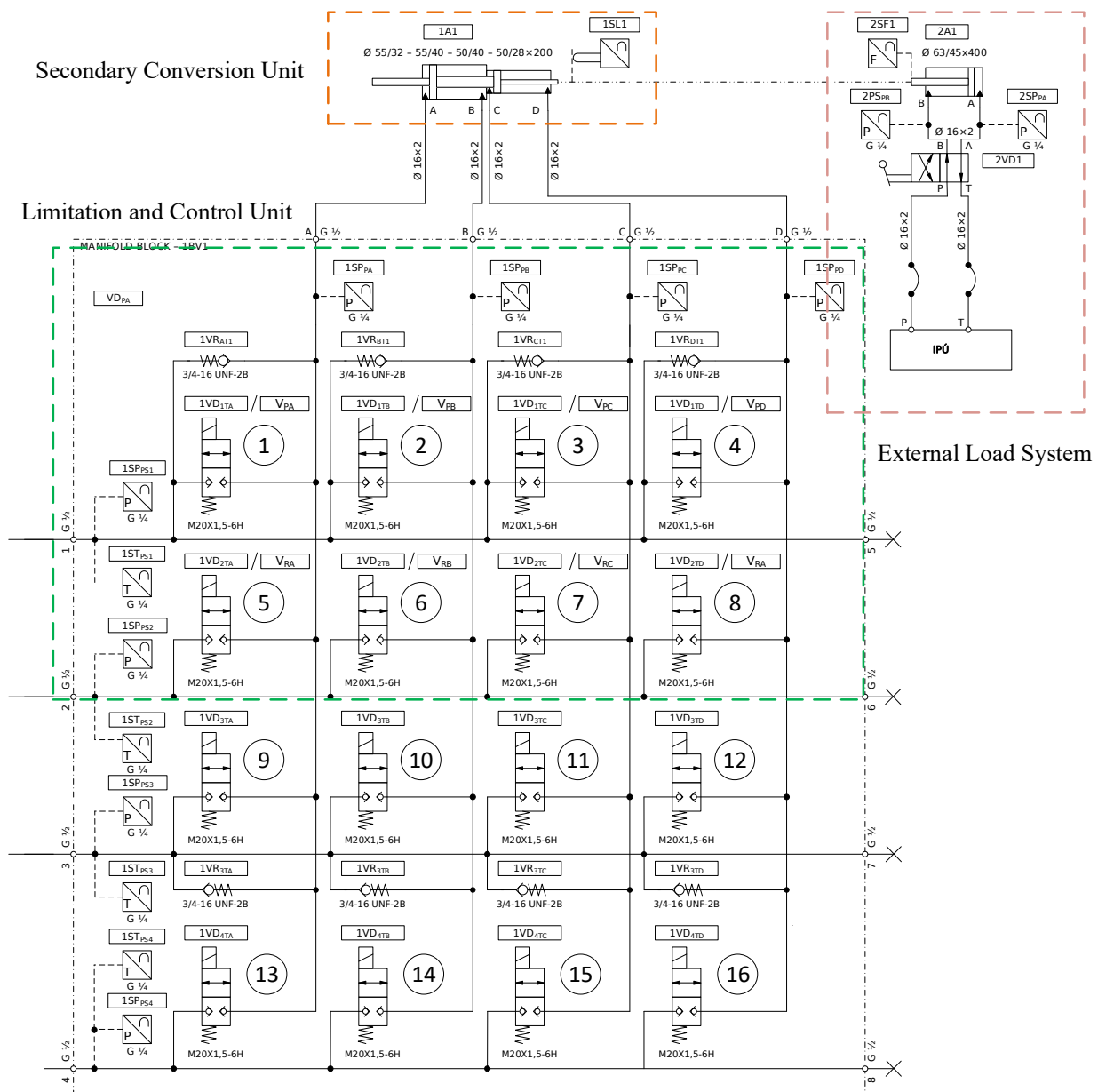


Source: By the author.

6.2. LIMITATION AND CONTROL UNIT AND SECONDARY CONVERSION UNIT

The hydraulic circuit of the limitation and control unit and the secondary conversion unit is present in Figure 6.5.

Figure 6.5 - Test bench limitation and control unit and the secondary conversion hydraulic unit circuit diagram.



Source: By the author based in the circuit developed by Ivan Mantovani.

As can be seen in Figure 6.5, there are sixteen on/off valves in the test bench. However, for the DEHA, only eight valves are necessary (1 to 8). The other eight valves (9 to 16) are used in the DHA and for future expansions.

In the limitation and control unit, all the on/off valves are from Bosch Rexroth model KSDER N with a maximum operating pressure of 350 bar, and a flow rate of 20 L/min in a

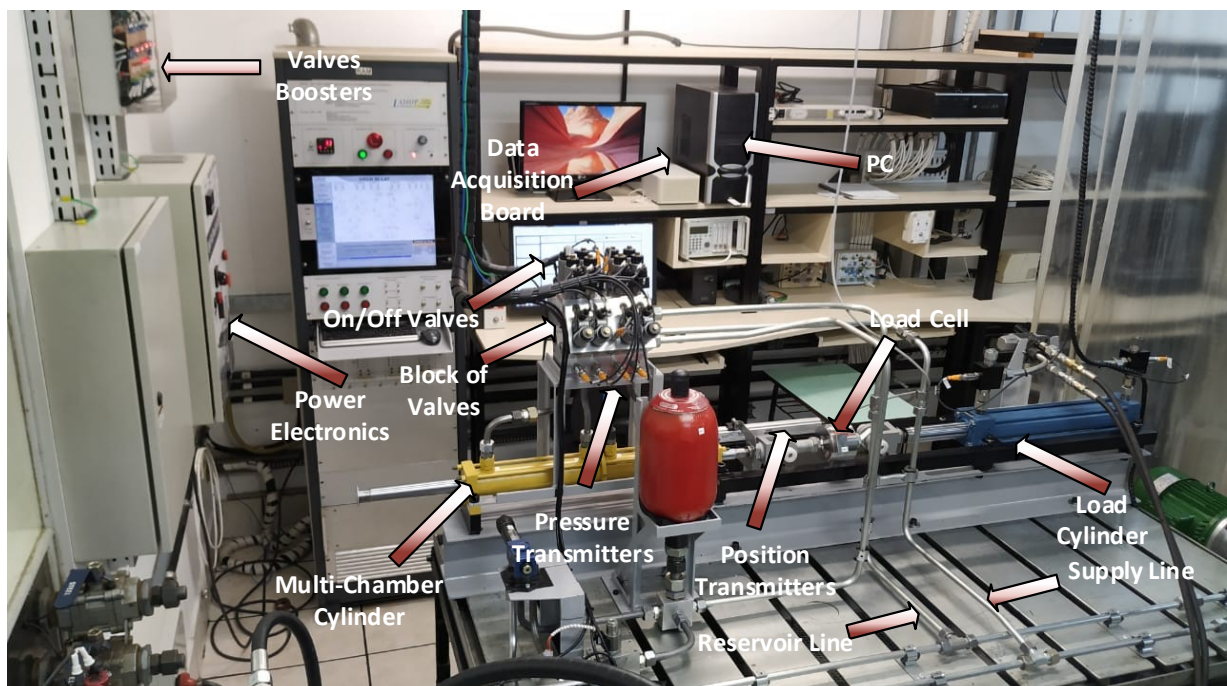
pressure differential of 20 bar. The solenoids of the valves are proportional CLASS H model 37-X-RY-Y 00 with a nominal input signal of 12V. Although the solenoids of the valves are proportional, they were used as on/off ones. The check valves are also from Bosch Rexroth model 04.31.20.00 56 Z 00.

The pressure transmitters are from IFM model PU5401 with a maximum pressure of 250 bar and a response time of 1 ms.

In the secondary control unit, a hydraulic linear cylinder with four chambers (1A1) was used. This cylinder corresponds to a special order and was developed by the manufacture WIPRO. The areas are presented in Table 6.1. This cylinder is attached to a position transmitter (1SL1) from BALLUFF model BTL5-A11-M0200 and to a load cell (2FS1) from HBM, model U2A, with a maximum load capacity of 50 kN, which is connected to the load cylinder (2A1) from the external load system.

The external load system is composed of an asymmetrical cylinder (2A1), a manual directional valve (2VD1) and two pressure transmitters IFM model PU5401. The hydraulic power source for the external load system is provided by the LASHIP hydraulic power unit IPU. Figure 6.6 presents the test bench for the limitation and control unit and secondary conversion unit.

Figure 6.6 - Test bench limitation and control unit and secondary conversion unit.



Source: By the author.

6.3. DATA ACQUISITION AND SYSTEM CONTROL

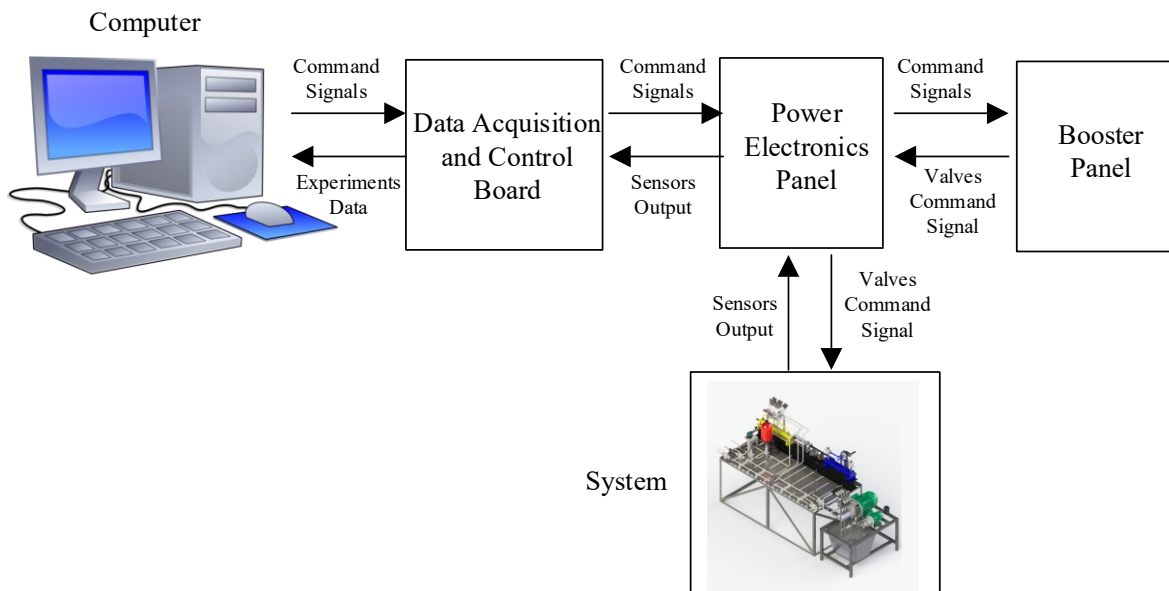
For the system control and data acquisition, a DSPACE DS PCC board was used for the data processing and the DS1103 board for the analogic to digital inputs and the digital to analogic outputs.

The control algorithmic was developed in the software MATLAB/Simulink 2007a and the system monitoring was carried out in the software Control Desk.

All data were collected through a PC that is connected to DSPACE using a DS817-03 PCI card. The PC features an Intel Core i5 2500K processor with 4 Gb / 1333 ddr3 RAM and 1 TB hard drive. All data were measured with a sampling time of 1 ms.

In Figure 6.7 a schematic diagram of the control system is presented.

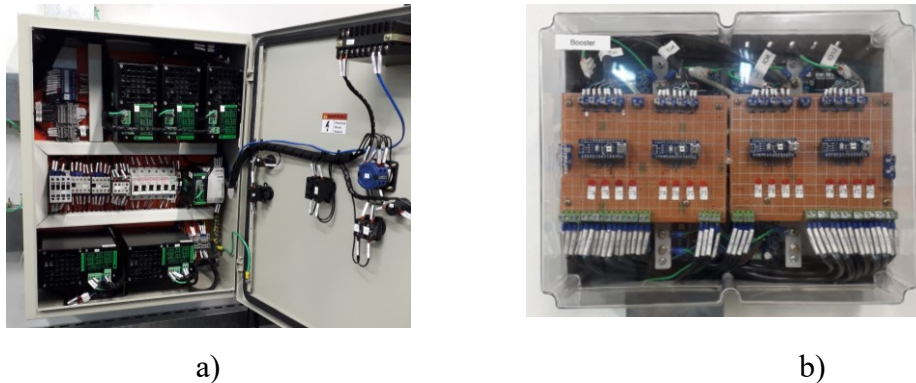
Figure 6.7 – Schematic diagram of the control system.



Source: By the author.

In Figure 6.7, the command signal from the user is sent by the computer to the control and data acquisition board. This board processes the command signal and sends the processed signal to the electronic panel, where the power electronics are located, such as power supplies and switches. The panel with the power electronics sends the opening and closing signals of the valves to the panel where the valve boosters are located. The output signal from the boosters is sent back to the power panel, which redirects the amplified signal for opening and closing of the valves of the system. The system, which in the present case is the DEHA, sends the signals read by the sensors back to the power panel. The signals from the sensors are, then, sent to the data acquisition board, where they are interpreted and viewed through the computer. In Figure 6.8, the power electronics panel and the booster panel are presented.

Figure 6.8 – a) Power electronics panel; b) Booster panel.

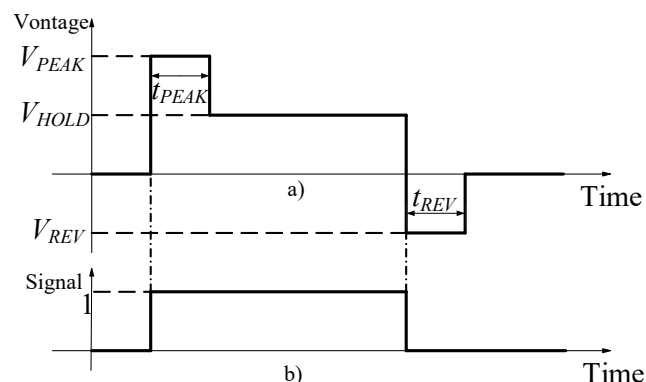


Source: By the author.

In order to improve the dynamic characteristics of the on/off valves, as mentioned in Section 5.1.2, a booster for the valves was developed. The conception of the booster was elaborated at LASHIP by the engineers Ivan Mantovani and Artur T. C. Gama and by the undergraduate students Pedro H. C. Costa and Thomas R de Souza. The booster is composed of an H bridge model bts7960 43a and it is controlled by an Arduino Mini.

To improve the dynamic characteristics of the on/off valves, the Peak-And-Hold technique was implemented. According to Breidi *et al.* (2014), this technique is based on applying a peak voltage higher than the nominal voltage of the solenoid valve, for a short period of time, and then applying a hold voltage just to keep the valve opened. In addition, a reverse voltage is applied at the shutdown of the valve to reduce the effects of the parasitic magnetic field and thus, speed up the valve closing (BREIDI *et al.*, 2014). Figure 6.9 presents the control signal for the booster.

Figure 6.9 - Booster control signal. a) Signal applied in the valve; b) Signal sent to the booster.



Source: By the author.

For the application of the booster, the peak voltage V_{PEAK} is 24 V, the hold voltage V_{HOLD} is 5 V and the peak t_{PEAK} and reverse t_{REV} times are 9 ms.

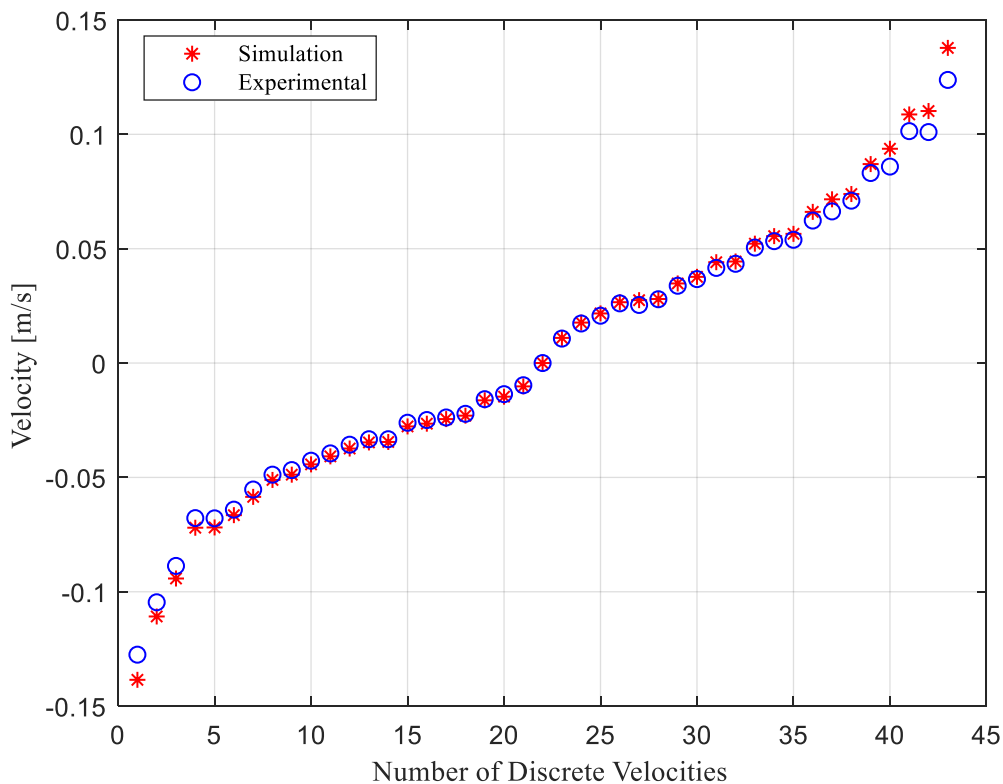
7. EXPERIMENTAL AND SIMULATION RESULTS

In this chapter, the results obtained by the experimental test bench and the mathematical model will be presented.

7.1. RESULTS FOR VELOCITY CONTROL

In order to verify the real velocities that the DEHA could obtain in the test bench, a velocity test was performed. In this test, an open loop velocity control was implemented, where a required velocity was given as an input signal to the system, and the real actuator velocity and the pressures in the chambers were measured. Also, in this test, the load actuator was not connected to the DEHA cylinder. Figure 7.1 presents the results obtained for the experimental and simulation velocities.

Figure 7.1 – Experimental and simulation velocities.

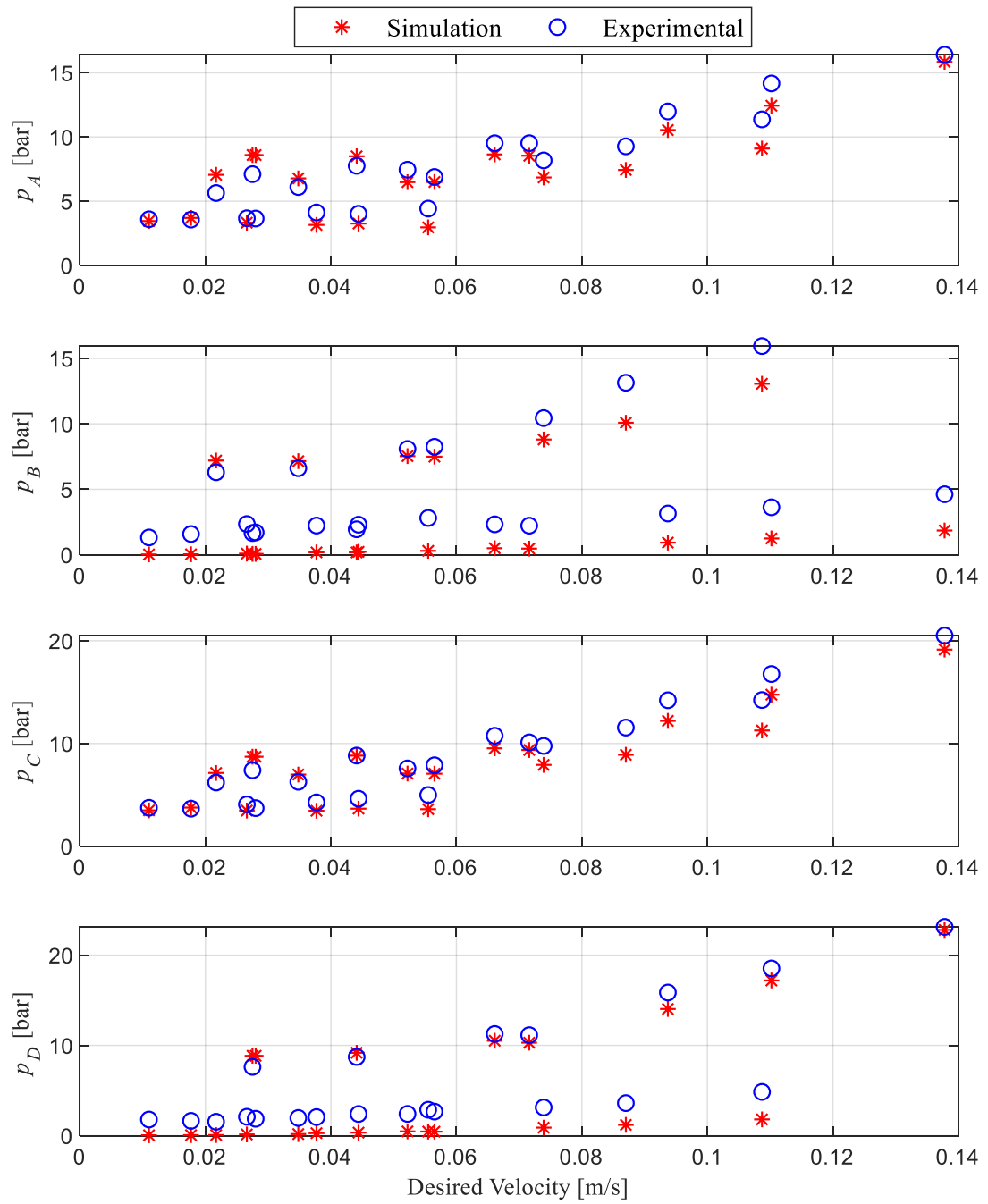


Source: By the author.

As can be seen in the results presented by Figure 7.1, the experimental results are very similar to the ones calculated by the simulation. The small differences in the velocity values are caused by the internal leakage in the digital pump.

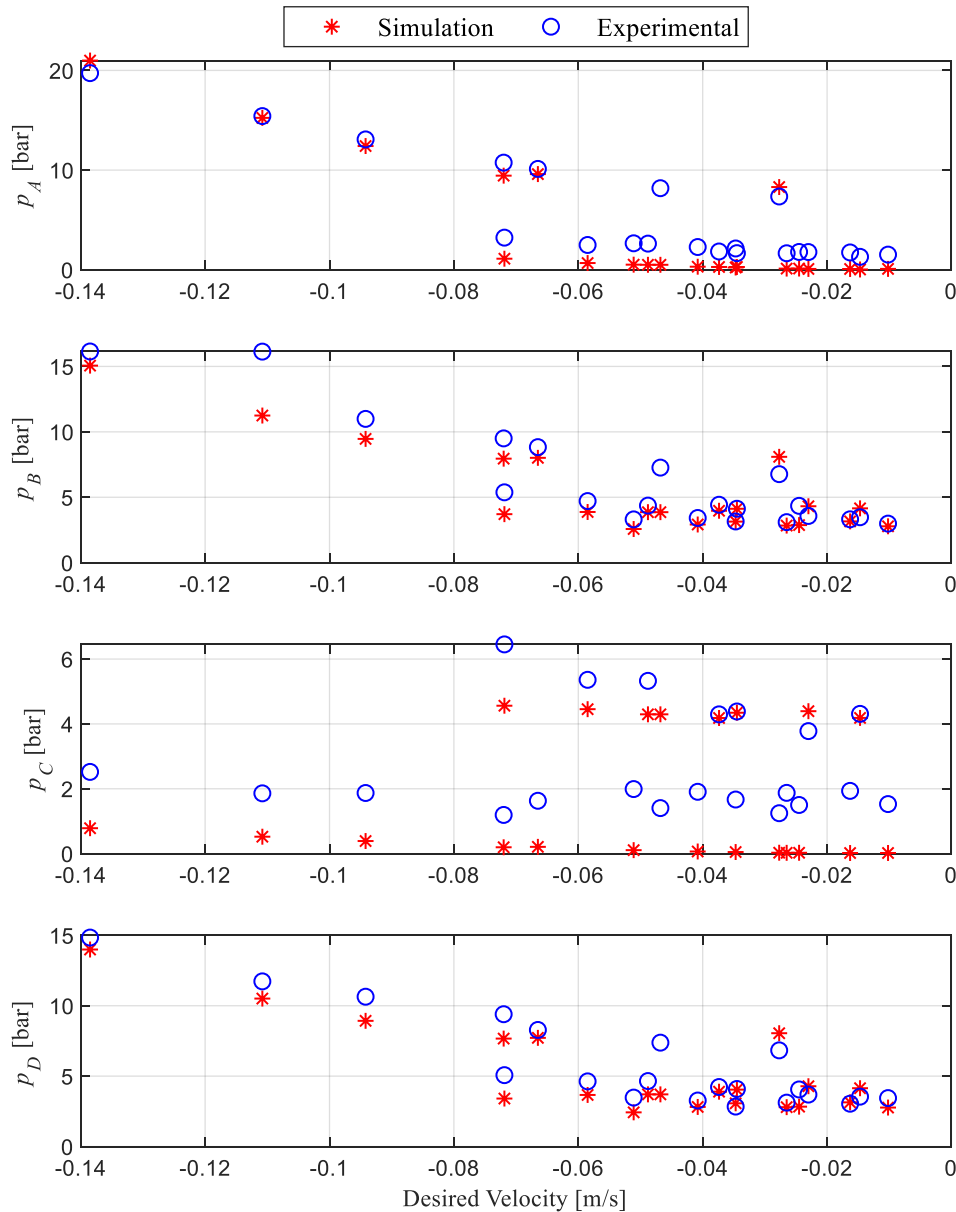
For the analyses of the pressures in the chambers of the cylinder, Figure 7.2 and Figure 7.3 show the results obtained for the positive and the negative velocities, respectively.

Figure 7.2 – Pressure in the chambers of the cylinder for positive velocities.



Source: By the author.

Figure 7.3 - Pressure in the chamber of the cylinder for positive velocities.



Source: By the author.

The results presented by Figure 7.2 and Figure 7.3 show that the points obtained by the simulation model follow the points obtained through the experiments. The differences between the simulation and the experimental points can be caused by the leakage in the digital pump, variations between the values of the parameters used in the friction force model and the real friction force, and non-modeled throttle losses.

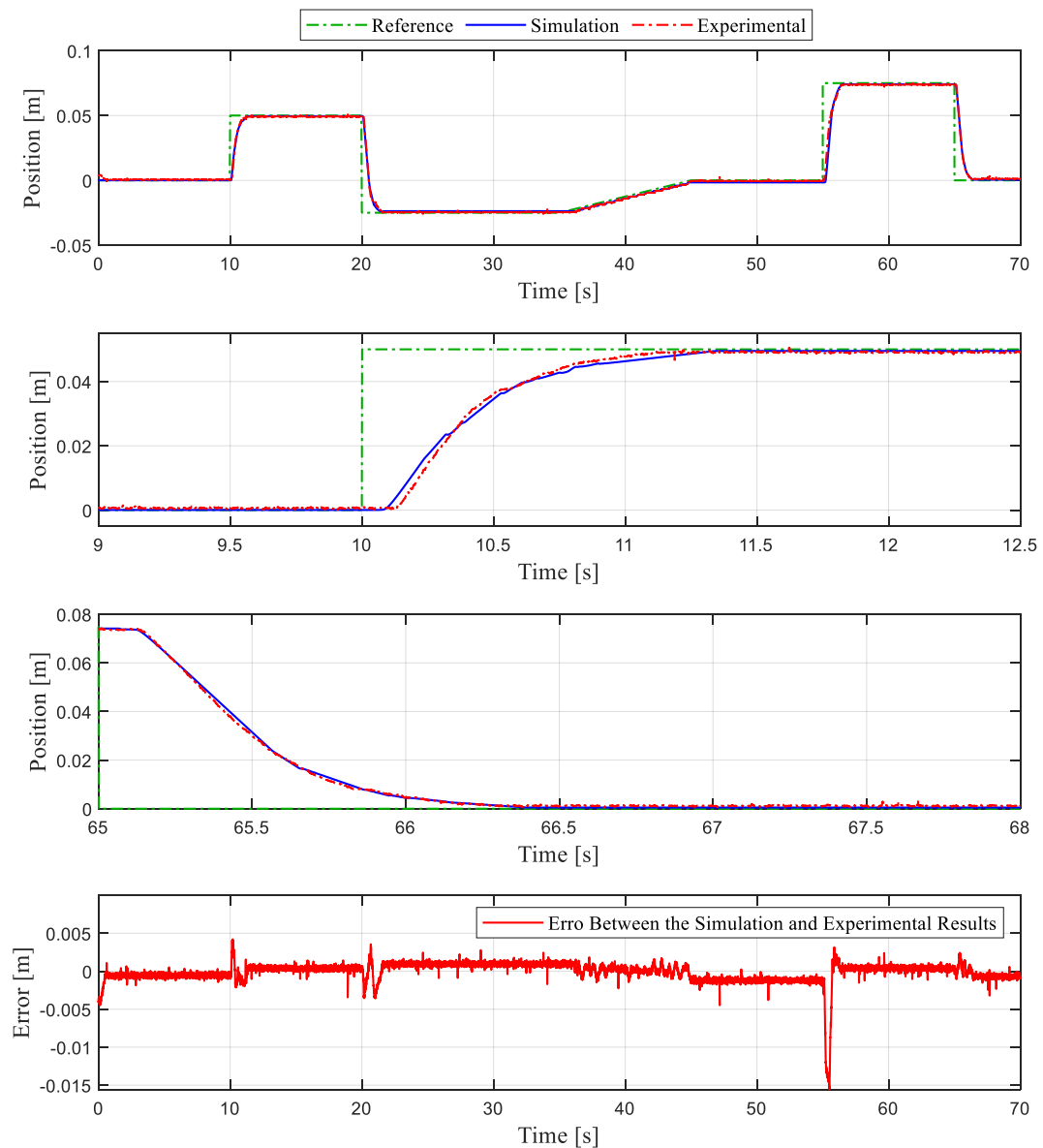
7.2. RESULTS FOR POSITION CONTROL

With the results obtained with the velocity experiments in the open loop, another experiment in a closed loop for position control was carried out. In these position control

experiments, the first one was realized without an external load, where the load cylinder was not attached in the DEHA cylinder.

For the experiment without load, the proportional gain used was 1 and the integral gain was 0. Besides, a gain of 2.75 1/s was implemented to convert the position error in velocity, which is obtained by dividing the maximum steady-state displacement (0.05 m) by the maximum real velocity (0.137 m/s). The dT_{min} is 144 ms, the t_{ds} for the valves of the limitation and control unit is 10 ms, and for the valves of the primary conversion unit is 37 ms, both applied in the closing of the valves. The reservoir pressure was considered 0 bar. The results for position control in these conditions are presented in Figure 7.4.

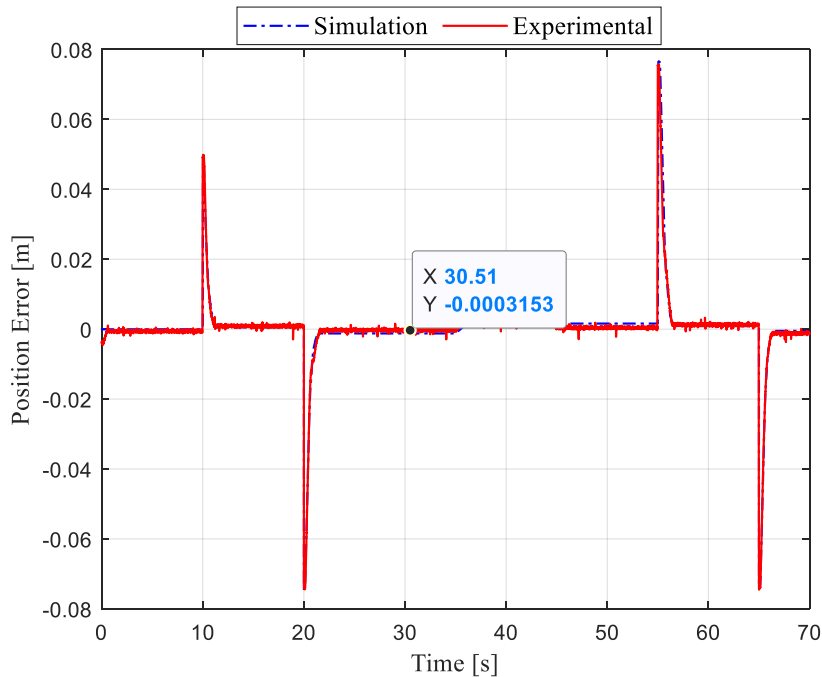
Figure 7.4 – Position response for position control without external load.



Source: By the author.

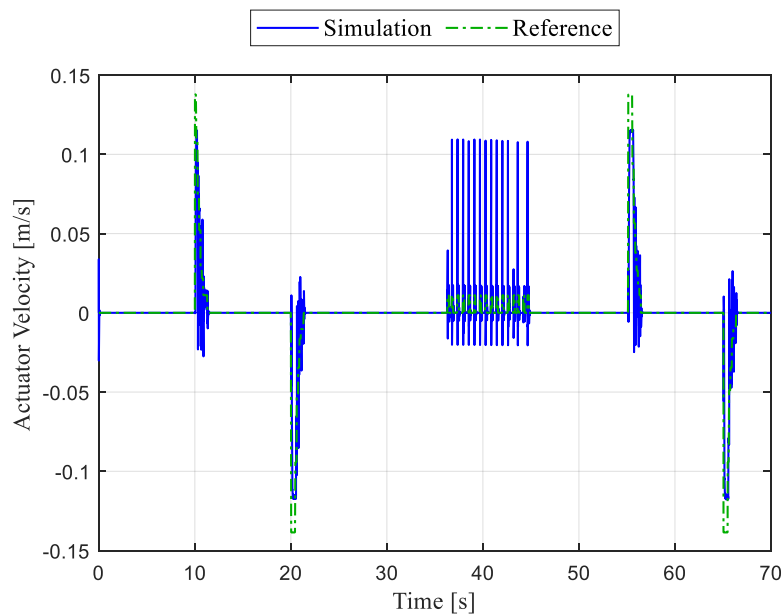
Figure 7.5 and Figure 7.6 present the position error and the velocity signal, respectively. In Figure 7.7, and Figure 7.8 the valve signal for the primary conversion unit and the output pressure of the pumps are shown, respectively. Figure 7.9, Figure 7.10, and Figure 7.11 present the signal for the valves in the limitation and control unit and the pressure in the chambers of the cylinder, respectively.

Figure 7.5 - Position error for position control without external load.



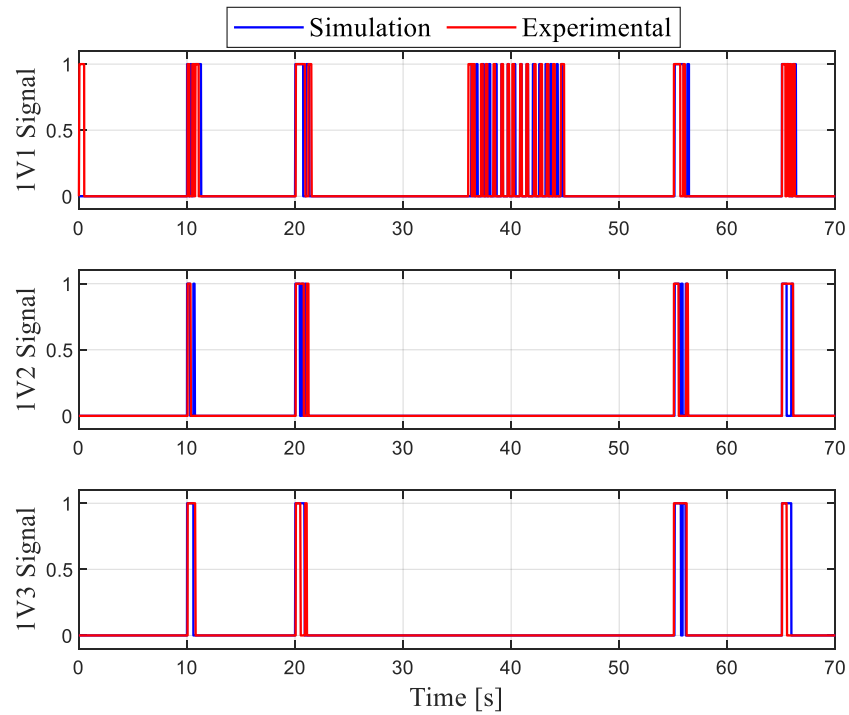
Source: By the author.

Figure 7.6 – Velocity signal for position control without external load.



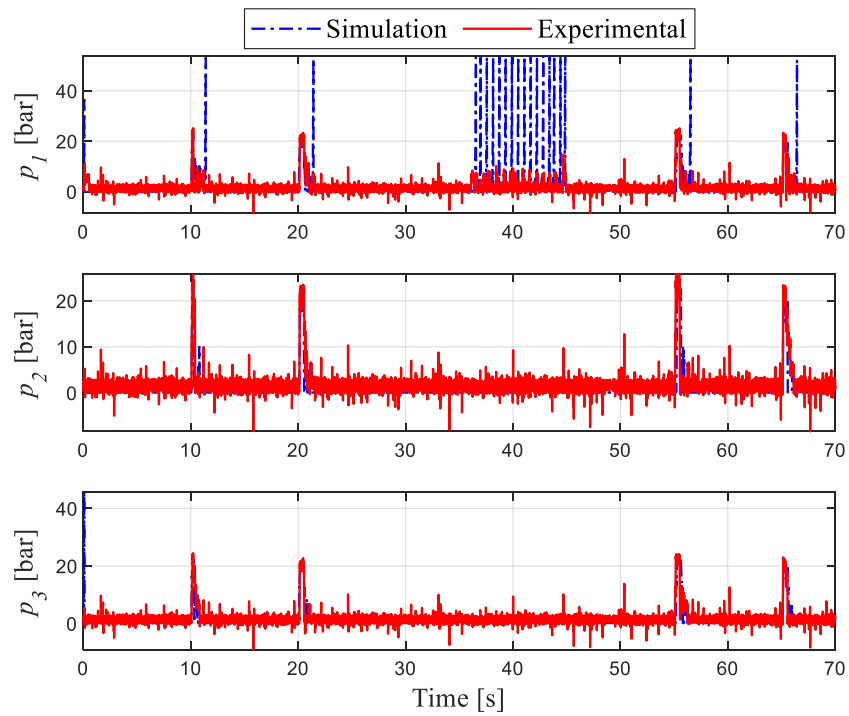
Source: By the author.

Figure 7.7 – Pump valve signals for position control without external load.



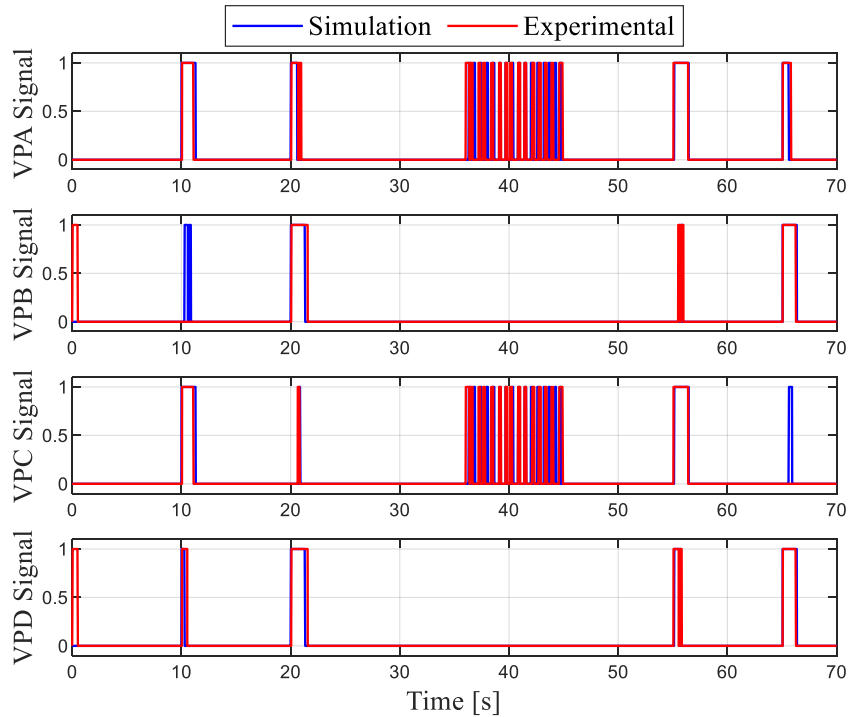
Source: By the author.

Figure 7.8 – Output pressure in the pumps for position control without external load.



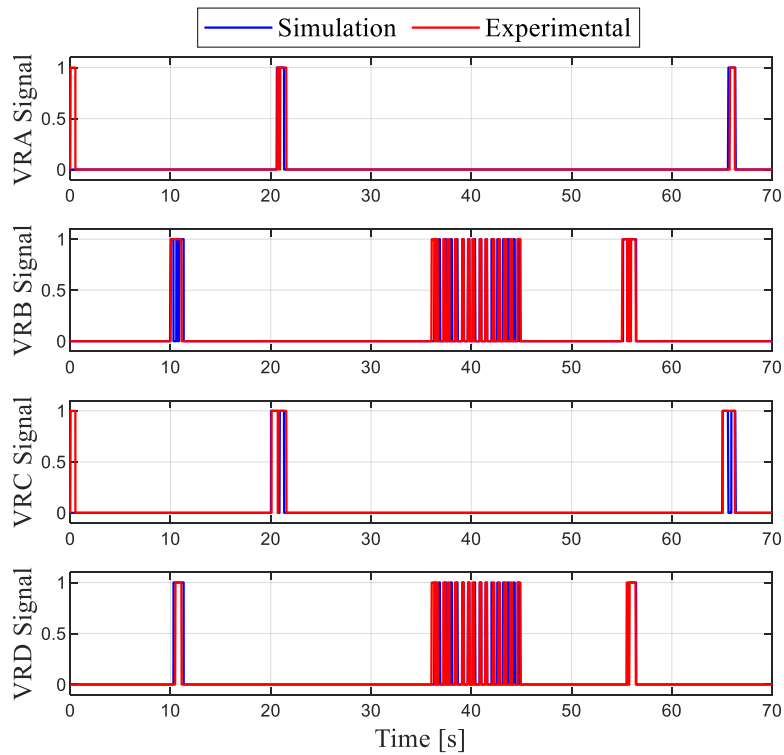
Source: By the author.

Figure 7.9 - VPs valves signal for position control without external load.



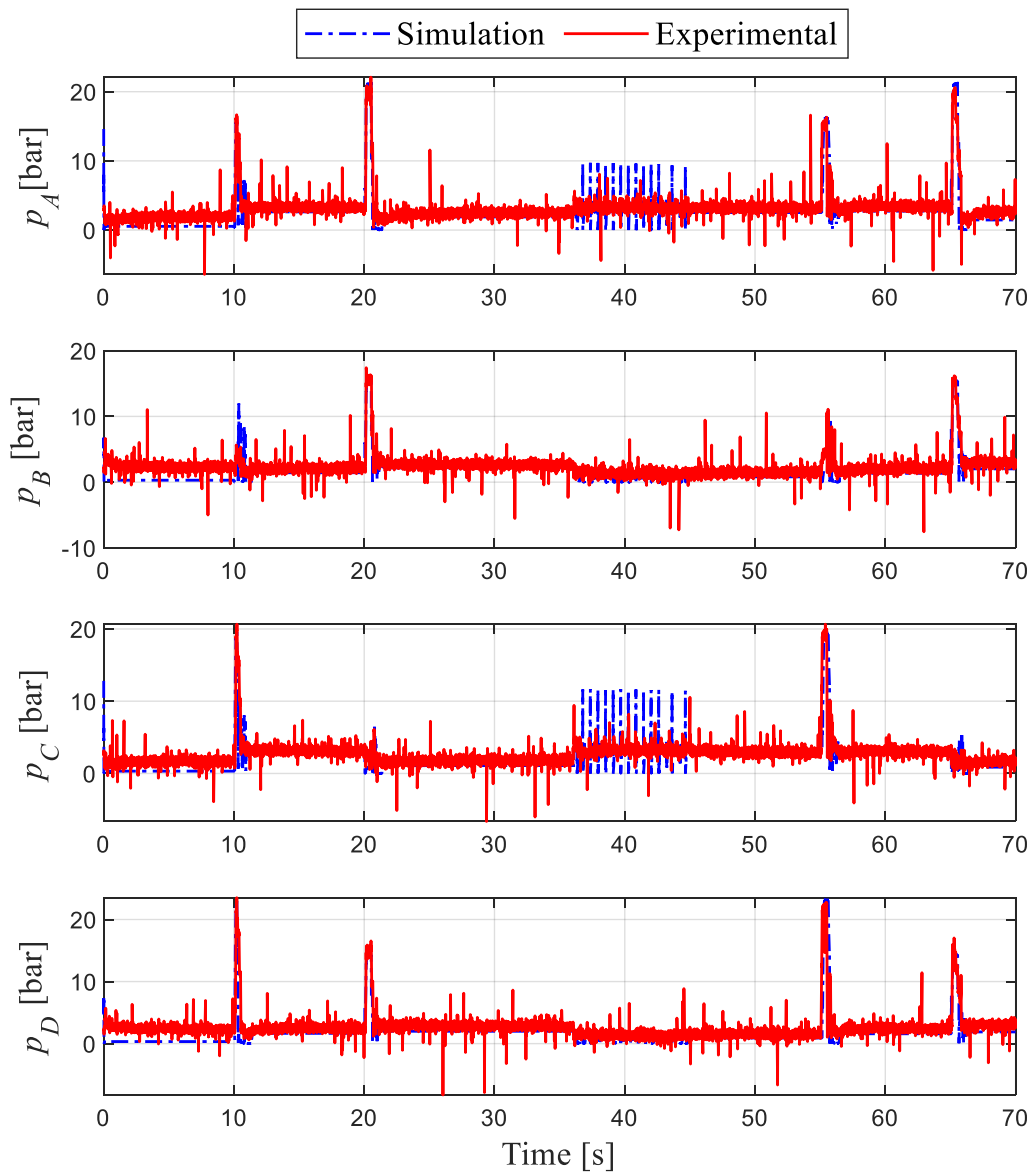
Source: By the author.

Figure 7.10 – VRs valves signal for position control without external load.



Source: By the author.

Figure 7.11 – Cylinder chambers pressure for position control without external load.



Source: By the author.

The results, for position control, presented in Figure 7.4 demonstrate that the model can represent the experimental results with good accuracy, where the position error in steady-state, Figure 7.5, is 0.31×10^{-3} m. When a step position input signal is applied in the system as for instance, in the time equals to 10 s and 65 s, both the experimental and simulation take a certain period of time to start to move, which is around 140 ms. This behavior is caused due the minimum time between switches dT_{min} , that is necessary to avoid excessive switching between valves due to their dynamics and intrinsic delays.

The signal applied in the on/off valves of the pumps 1, 2, and 3 of the digital pump, have also a similar behavior, as shows Figure 7.7. However, the number of switching is

different. This can be caused by the difference between the t_{SCD} , t_{SOD} , t_{SCR} and t_{SOR} of the valves used in the test bench and the values used in the model.

When the step input signal (time intervals of 10, 20, 55, and 65 s) all the pumps are used. In the time interval of 35 to 45 s, only pump 1 is required.

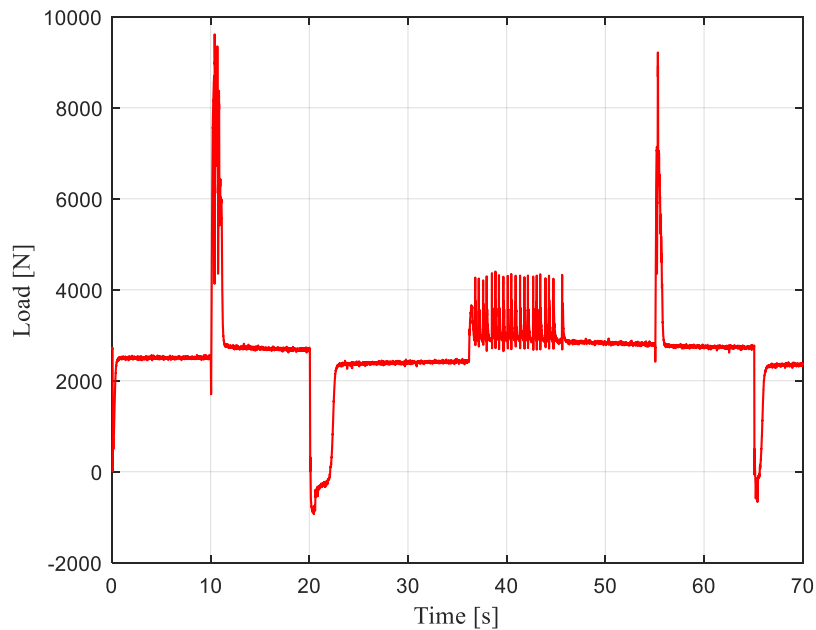
The experimental results for the output pressure of the pumps 1, 2, and 3 (Figure 7.8) feature with a noisy characteristic. This is caused by the frequency inverter that was used for controlling the rotational frequency of the digital pump, which was introducing a magnetic noise in all sensors used in the test bench. This noise was also present in Bravo (2017). Despite the noise in the values of the measured pressure, the values in steady-state for the experiments and the simulations present good concordance. In the pump 1, the pressure in the results of the simulation presents some peaks that are caused by the numerical error. These peaks do not occur in the pumps 2 and 3.

The signals for the valves that connect the pumps to the cylinder chambers VPs and the valves that connect the cylinder chambers to the reservoir also present good concordance between the experimental and the simulation results. In the period of time of 35 and 45 s, the flow rate of the digital pump is sent only for chambers A and C, without any regeneration. This corresponds to the smallest velocity available in the system.

The pressures in the chambers of the cylinder also present noise in the experimental curves. However, the values, when compared by the obtained in the simulation, present good concordance.

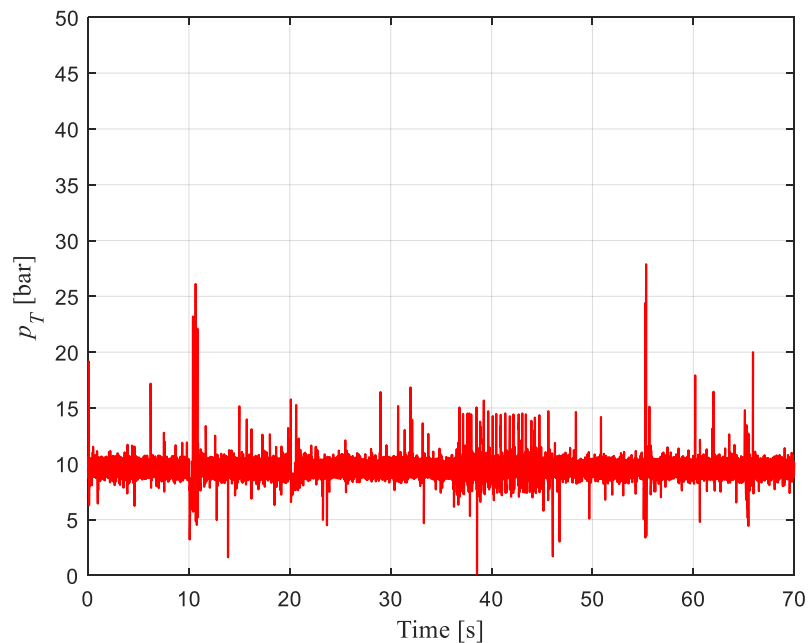
In addition to the experiments for position control without an external load, an experiment using a variable external load was also carried out. In this experiment, the load actuator was attached in the DEHA cylinder and the load was measured by the load cell 2SP1. The hydraulic power supply unit used in the load cylinder, IPU, was configured with a supply pressure of 30 bar (3 MPa). The reservoir pressure for the DEHA was set in 10 bar (1 MPa) by the pressurized reservoir power unit. Figure 7.12 presents the obtained profile for the external load and Figure 7.13 the reservoir pressure.

Figure 7.12 – External load.



Source: By the author.

Figure 7.13 – Reservoir pressure.

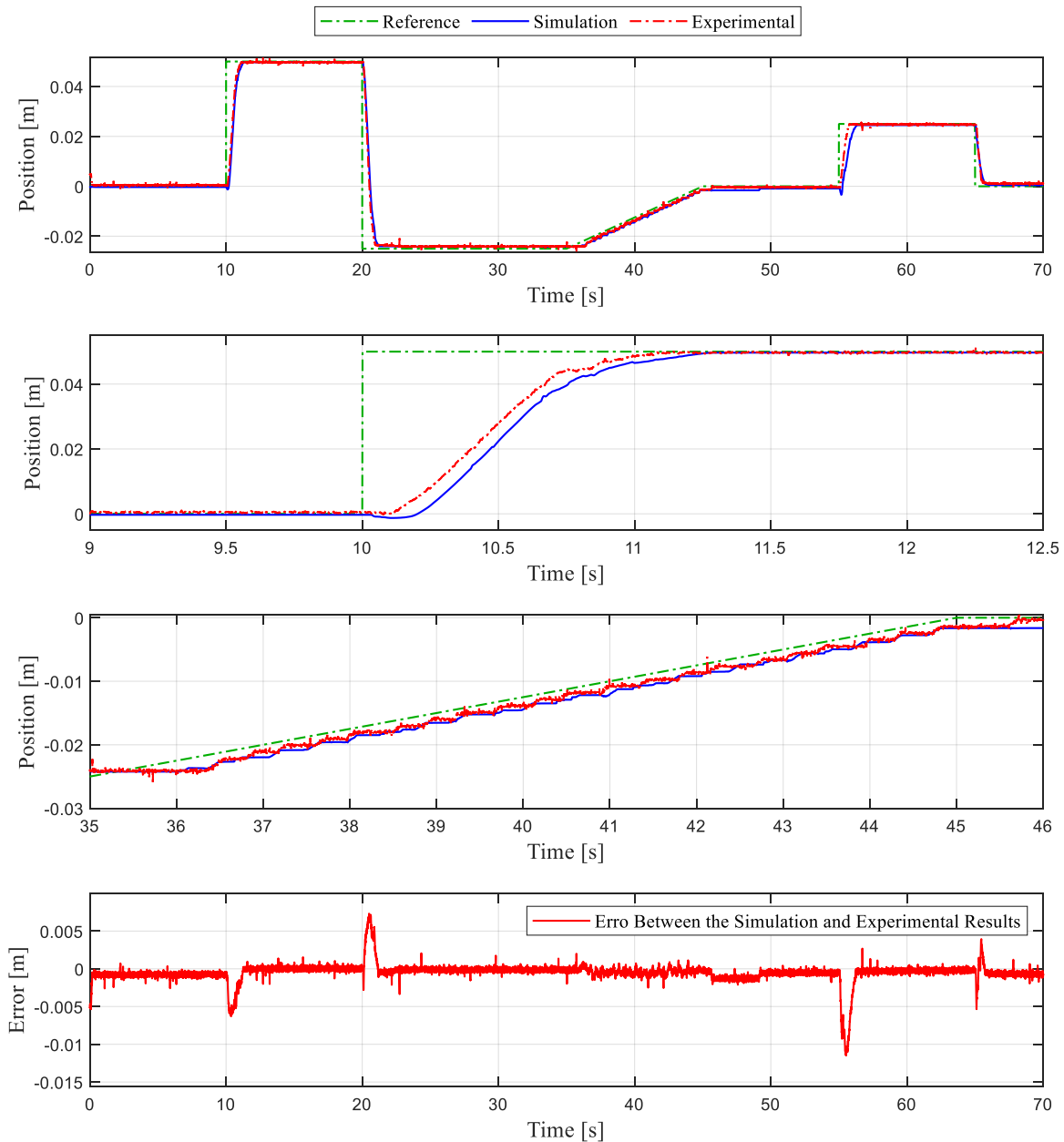


Source: By the author.

For the experiment with the external load, the proportional gain used was 1.2 and the integral gain was 0.01. The same gain of 2.75 1/s was implemented for convert the position error in velocity. The dT_{min} is 87 ms, the t_{ds} for the valves of the limitation and control unit is 1 ms, applied in the opening of the valves and for the valves of the primary conversion unit is 47 ms, applied in the closing of the valves. During the experiments was noticed that the friction

force was altered with the connection of the load actuator in the system. Therefore, for this experiment, the σ_2 was changed to 20000 kg/s for positive and negative velocities. Figure 7.14 presents the results obtained for position control, where the load profile shown in Figure 7.12 was given as an input signal for the model.

Figure 7.14 - Position response for position control with external load.

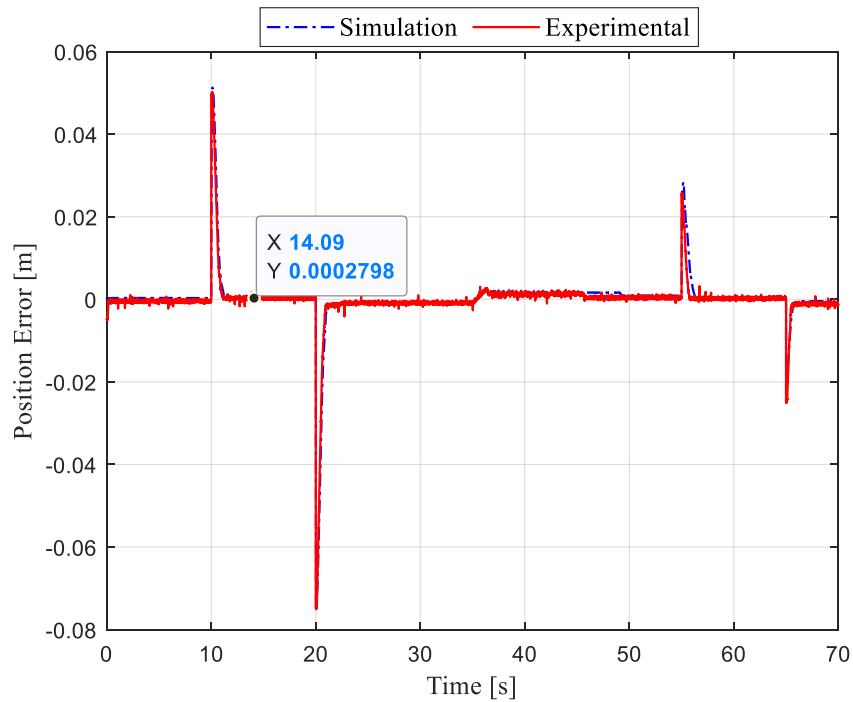


Source: By the author.

Figure 7.15 and Figure 7.16 present the position error and the velocity signal, respectively. In Figure 7.17, and Figure 7.18 the valve signal for the primary conversion unit and the output pressure of the pumps are shown, respectively. Figure 7.19, Figure 7.20, and

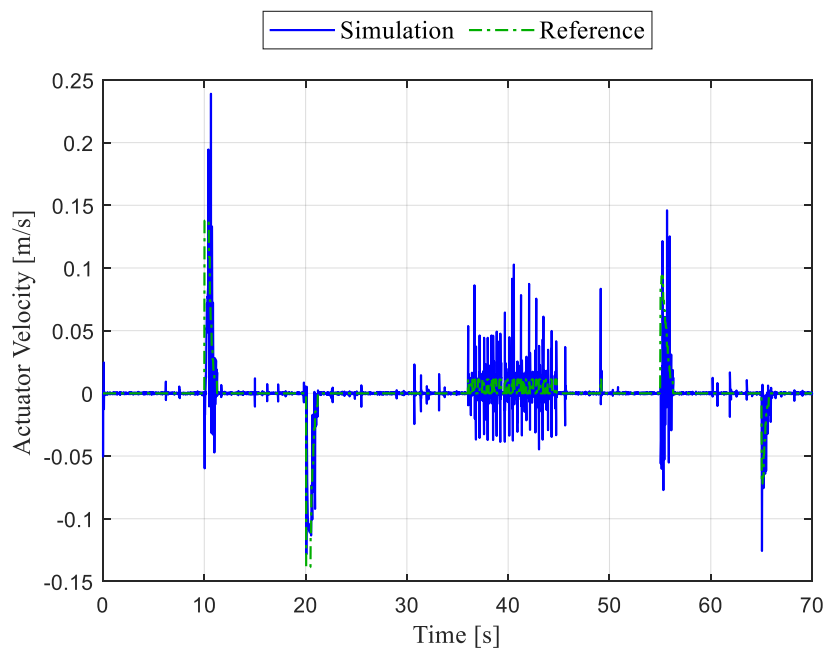
Figure 7.21 present the signal for the valves in the limitation and control unit and the pressure in the chambers of the cylinder, respectively.

Figure 7.15 - Position error for position control with external load.



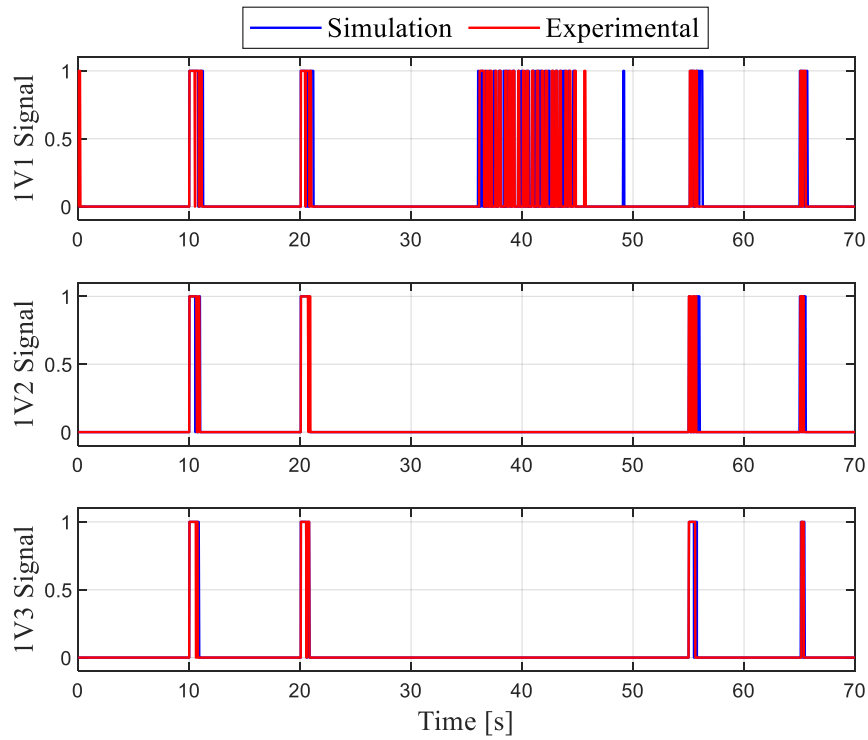
Source: By the author.

Figure 7.16 - Velocity signal for position control with external load.



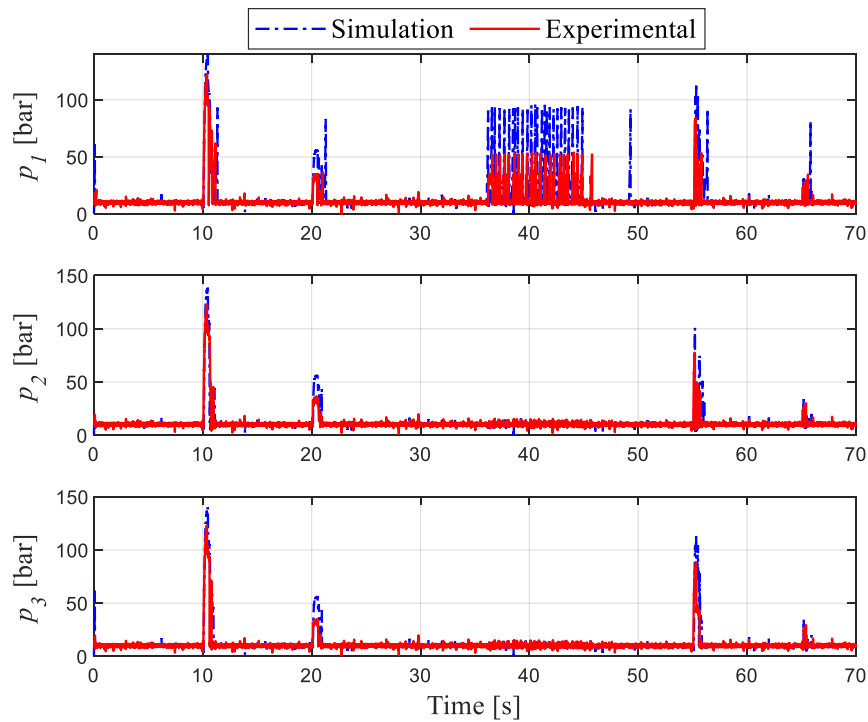
Source: By the author.

Figure 7.17 - Pumps valves signal for position control with external load.



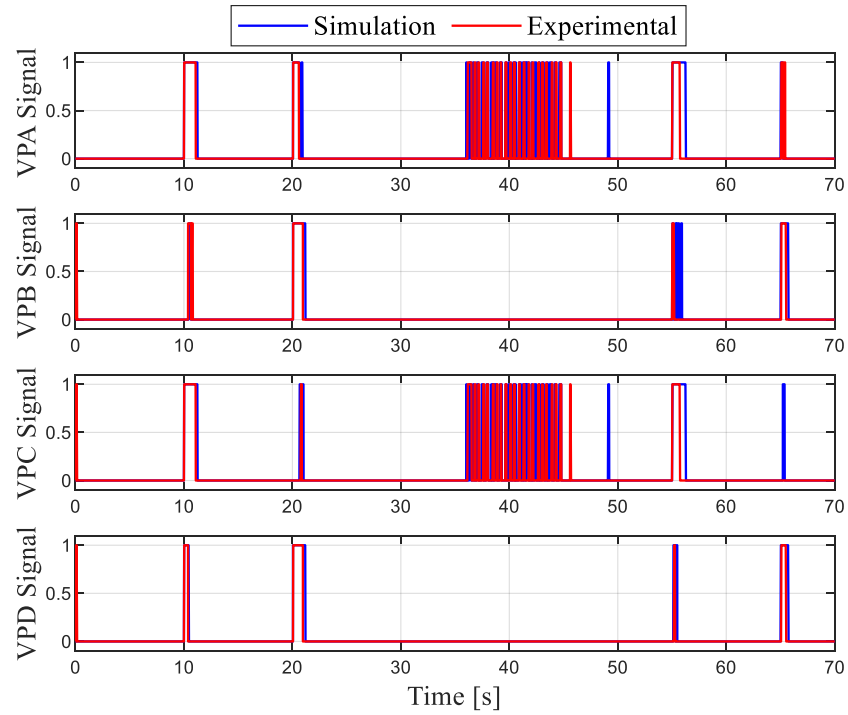
Source: By the author.

Figure 7.18 - Output pressure in the pumps for position control with external load.



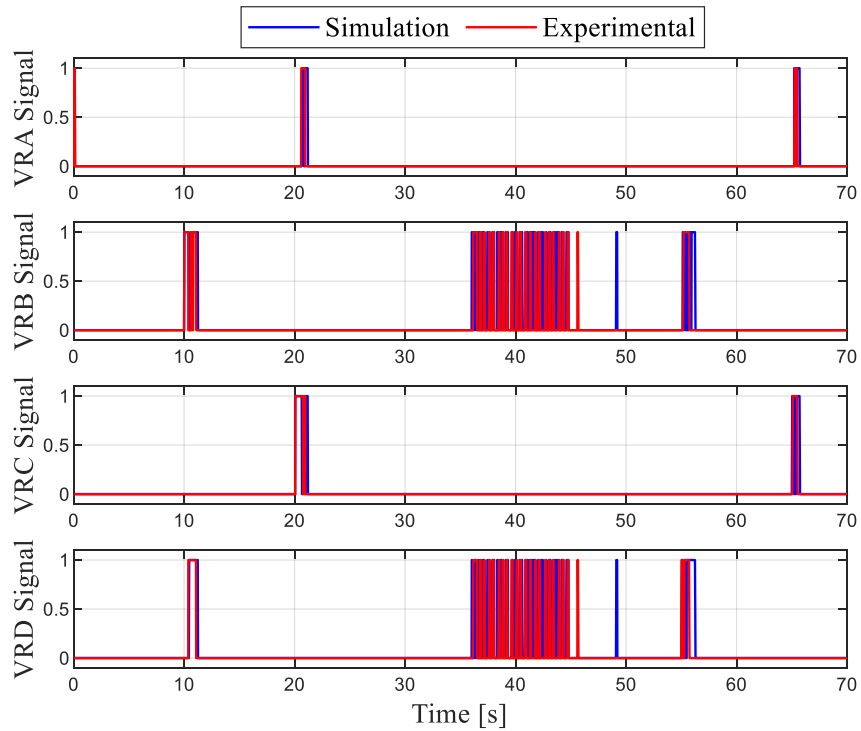
Source: By the author.

Figure 7.19 - VPs valves signal for position control with external load.



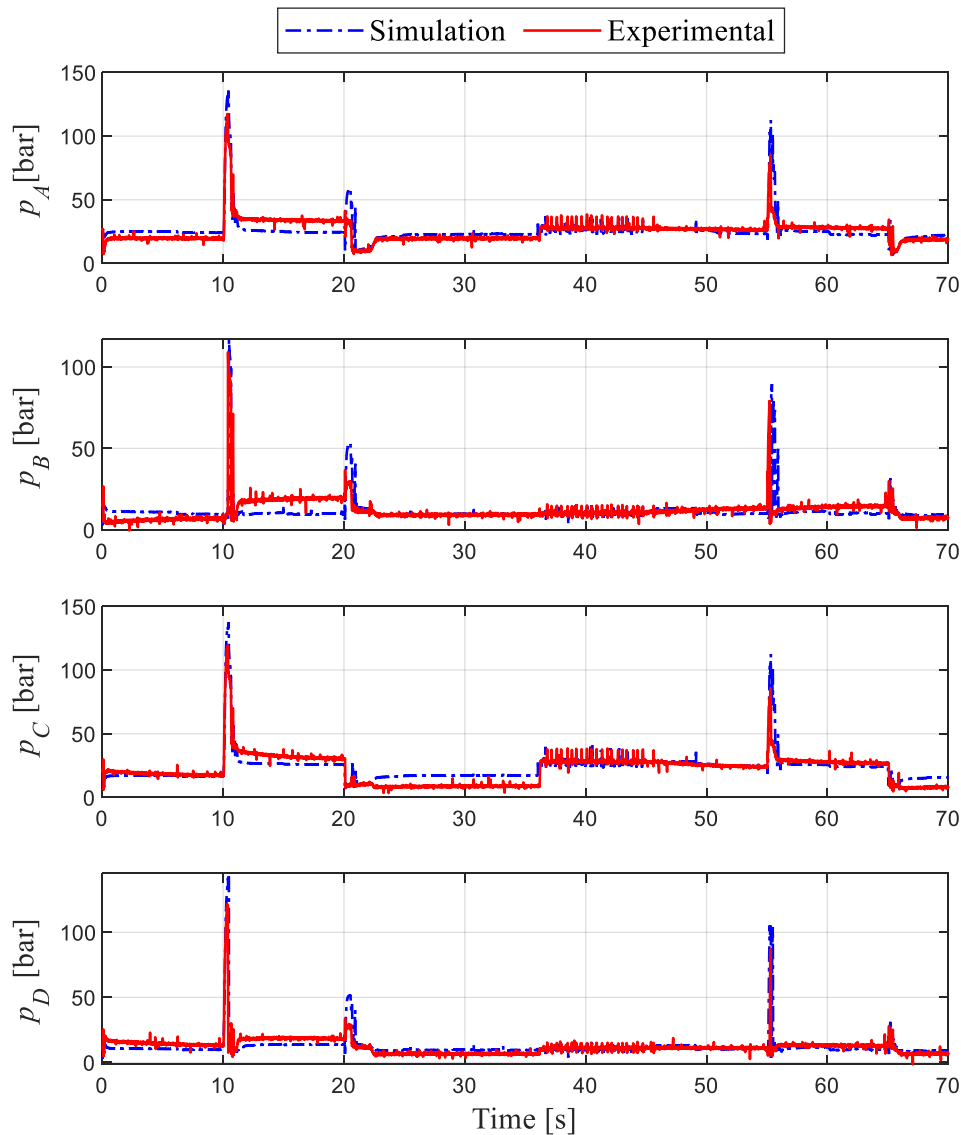
Source: By the author.

Figure 7.20 - VRs valves signal for position control with external load.



Source: By the author.

Figure 7.21 - Cylinder chambers pressure for position control with external load.



Source: By the author.

As can be seen by the results presented in Figure 7.12 and Figure 7.13, the load system can not keep the force at a constant level due to the limitations in the load control system. When the actuator receives a position step signal (Figure 7.14), the load force achieves a value around 10000 N.

The pressurized reservoir system can keep the pressure in the desired value. However, some pressure peak occurs due to the excess of fluid that returns from the cylinder to the reservoir unit.

In Figure 7.14, for position control, the results demonstrate that the model and the experiments can follow the position reference, with an error in steady-state of 0.27×10^{-3} m (Figure 7.15), however some oscillations occur due to the pressure peaks that are caused by the

switching of the on/off valves. In Figure 7.14, in the time period of 10 to 11.5 s, the experimental results take an accommodation time around 1.04 s to achieve an error of 2% of the steady-state value. The simulation results take an accommodation time of 1.21 s. As in the case of the experiments without external load, the dT_{min} also causes a delay for the cylinder to start the movement. In addition, there are a difference in the responses of the simulation and the experimental results. This can be caused by the leakage model, due to the errors that have been introduced in the flow transmitter used in the leakage experimenters, since it was working in a flow range near to its maximum error and also by differences in the dynamics of the valves used in the test bench, since they can have difference in the manufacturing process.

In the period of time of 35 to 45 s, a ramp signal is applied in the system. However, this ramp does not match with a velocity available in the system. In this situation, the controller chooses the closer velocity value available in the velocity matrix, causing the stair waveform response shown in Figure 7.14.

The signal for the on/off valves of the digital pump behaves similarly to experiments without external load. The pressure in the output of the pumps, Figure 7.18, presents a similar behavior for the simulation and the experiments. However, there are some pressure peaks in the simulation results, which do not occur in the experimental ones. This can be caused by retained air in the test bench circuit or by differences in the friction model and the real friction of the test bench.

For the pressures in the chambers of the cylinders, both results, simulation and experimental, present similar behavior, where the small differences can be also caused by retained air or differences in the friction model and the real friction.

With the comparison between the results obtained by the experiments and by the simulation model, the model can be considered validated and can be used for the calculation of the system efficiency, which will be presented in Section 7.3.

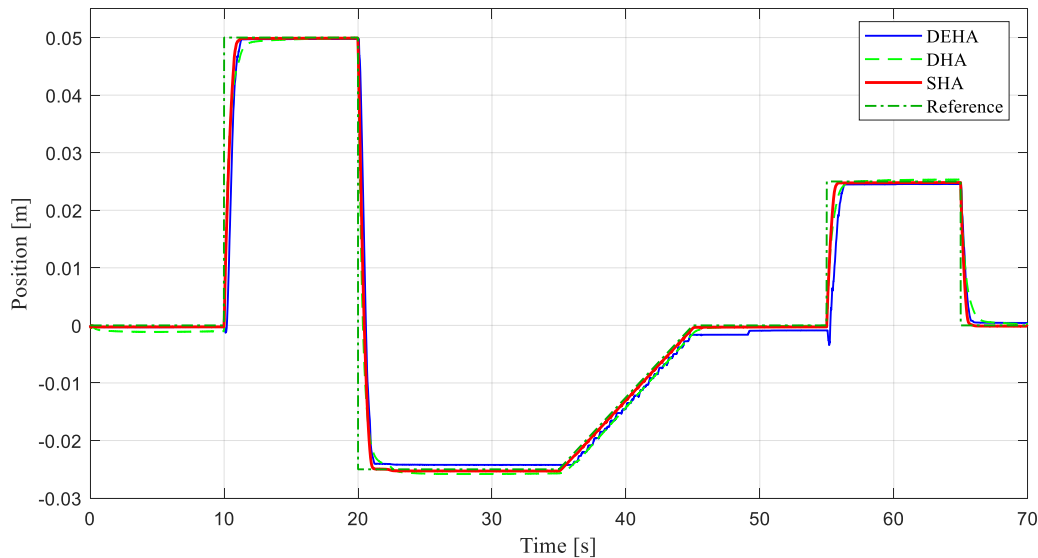
7.3. SYSTEM EFFICIENCY EVALUATION

In this Section, the analysis of the energy efficiency for the Digital Electro Hydrostatic Actuator DEHA will be presented. In addition, the energy efficiency for the Servo Hydraulic Actuator SHA and the Electro Hydrostatic Actuator EHA will be also analyzed, for comparison with the DEHA.

For the energy efficiency analysis, all the three different topologies of actuators were simulated in the same conditions, maximum load, maximum velocity. The parameters used in the SHA and the DHA were presented in sections 5.2 and 5.3, respectively.

In order to compare the dynamic responses of both systems, a position control simulation with all actuators topologies was carried out. The load applied in the system was presented in Figure 7.12. The proportional gain for the DEHA, SHA, and EHA is 1.2, 1, and 1.2, respectively. The integral gain for the DEHA, SHA, and EHA is 0.01, 0.01, and 0.05, respectively. Figure 7.22 shows the position responses for the DEHA, SHA, and EHA.

Figure 7.22 – Position responses for the DEHA, SHA, and EHA.



Source: By the author.

As can be seen by the results shown in Figure 7.22, all systems exhibit similar behavior for the position control. In this context, they can be used for the analysis of energy consumption and efficiencies.

In order to analyze the energy efficiency of the systems, the input hydraulic energy and the output hydraulic energy were calculated. The input hydraulic energy for the DEHA can be expressed as,

$$E_{i_DEHA} = \int_0^t (q_{v1}\Delta p_1 + q_{v2}\Delta p_2 + q_{v3}\Delta p_3)dt, \quad (7.1)$$

where, q_{v1} , q_{v2} and q_{v3} are the output flow rate, the Δp_1 , Δp_2 and Δp_3 the pressure differential of pumps 1, 2, and 3, respectively. The volumetric efficiency of the pumps is presented in Figure 5.12. For the SHA, the input hydraulic energy is calculated as

$$E_{i_SHA} = \int_0^t q_v^{SHA} (p_s^{SHA} - p_r^{SHA}) dt, \quad (7.2)$$

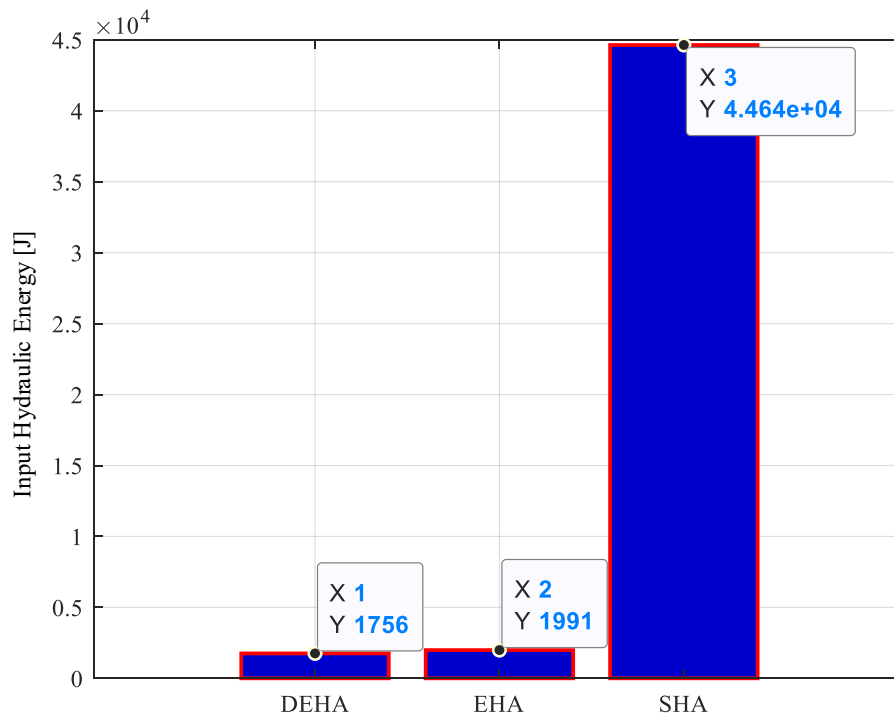
where, q_v^{SHA} , is the output flow rate of the variable displacement pump, the p_s^{SHA} the supply pressure and p_r^{SHA} the reservoir pressure.

For the EHA, the input hydraulic energy is expressed as

$$E_{i_EHA} = \int_0^t q_v^{EHA} (p_1^{EHA} - p_2^{EHA}) dt, \quad (7.3)$$

where, q_v^{EHA} , is the output flow rate of the variable rotational frequency pump, the p_1^{EHA} and p_2^{EHA} are the pressure in the ports 1 and 2 of the pump. The input hydraulic energy is shown in Figure 7.23.

Figure 7.23 – Input hydraulic energy.



Source- By the author.

In the results shown in Figure 7.23, the SHA input hydraulic energy is around 4.46×10^4 J, which is 25 times more when compared with the DEHA and with the EHA. This is caused by the leakage in the servo valves that the variable displacement pump needs to supply to keep the system pressurized and by the internal leakage of the pump. In the DEHA, when the pumps are not been used, the flow rate is directed for the reservoir, where the pressure drop in the pumps is almost zero, due to the pressurized reservoir. In the EHA, when the actuator is not

moving, the pump remains stopped and its internal leakage occurs with a reduced pressured drop since both chambers of the cylinder remain pressurized.

The output hydraulic energy for both systems can be calculated by the integral of the force produced by the actuator times its velocity. Therefore, the output hydraulic energy for the DEHA is expressed as

$$E_{o_DEHA} = \int_0^t (A_A p_A - A_B p_B + A_C p_C - A_D p_D) v_a dt. \quad (7.4)$$

In the SHA, the output hydraulic energy is expressed by

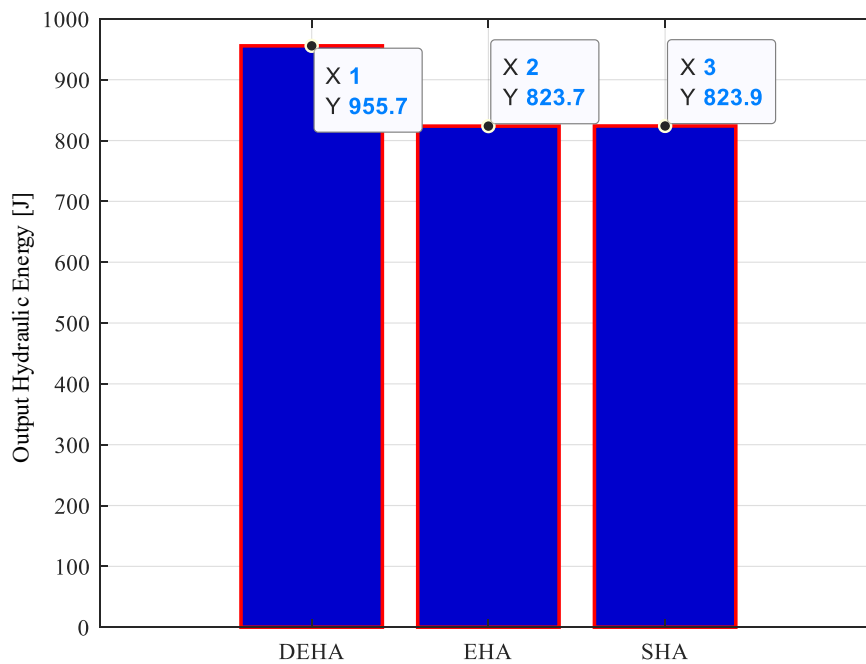
$$E_{o_SHA} = \int_0^t (A_A^{SHA} p_A^{SHA} - A_B^{SHA} p_B^{SHA} + A_C^{SHA} p_C^{SHA} - A_D^{SHA} p_D^{SHA}) v_a dt, \quad (7.5)$$

where, A_A^{SHA} , A_B^{SHA} , A_C^{SHA} and A_D^{SHA} are the areas and p_A^{SHA} , p_B^{SHA} , p_C^{SHA} and p_D^{SHA} the pressures for the chambers A, B, C, and D, respectively. For the EHA, the output hydraulic energy is calculated as

$$E_{o_EHA} = \int_0^{t_1} (A_A^{EHA} p_A^{EHA} - A_B^{EHA} p_B^{EHA}) v_a dt, \quad (7.6)$$

where, A_A^{EHA} and A_B^{EHA} are the areas and p_A^{EHA} and p_B^{EHA} the pressures for the chambers A and B, respectively. The output hydraulic energy is presented in Figure 7.24.

Figure 7.24 - Output hydraulic energy.



Source- By the author.

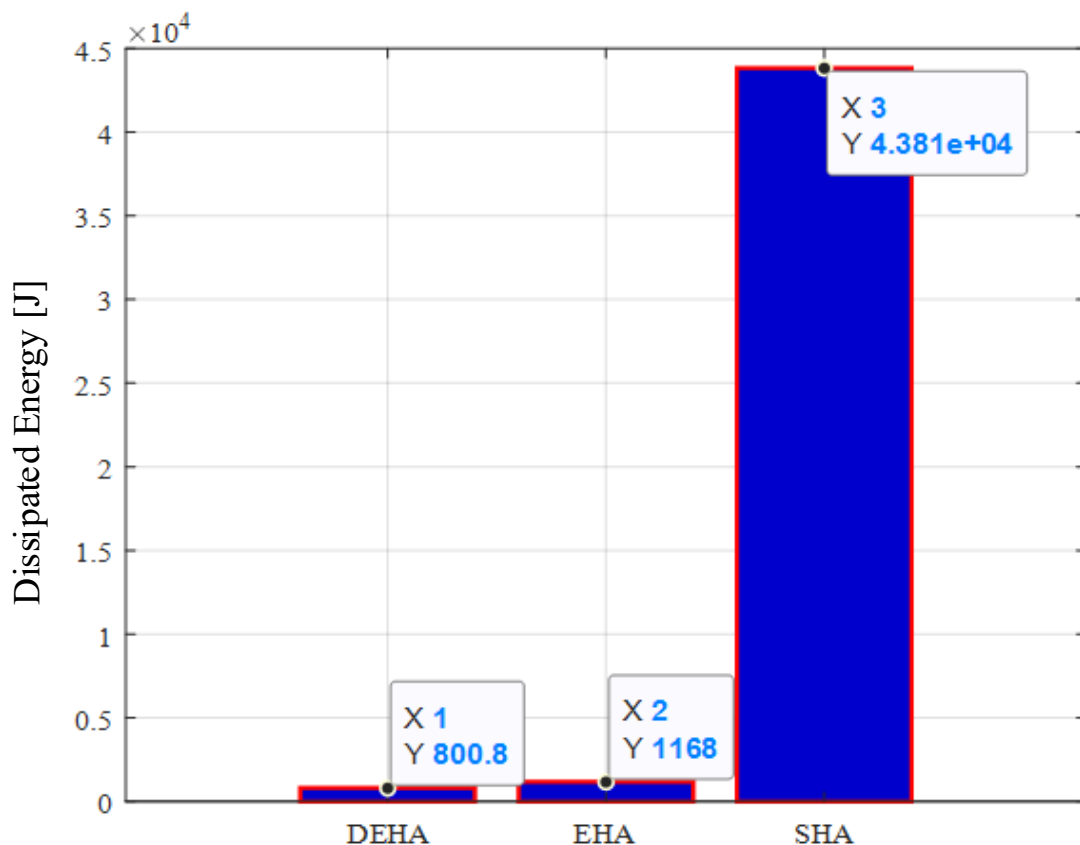
As can be seen by the results shown in Figure 7.24, the SHA and the EHA present an output energy with similar values. In the DEHA, there is a small difference around 132 J.

The dissipated energy can be expressed as

$$E_{dissipated} = E_{input} - E_{output}. \quad (7.7)$$

The results for the dissipated energy are presented in Figure 7.25.

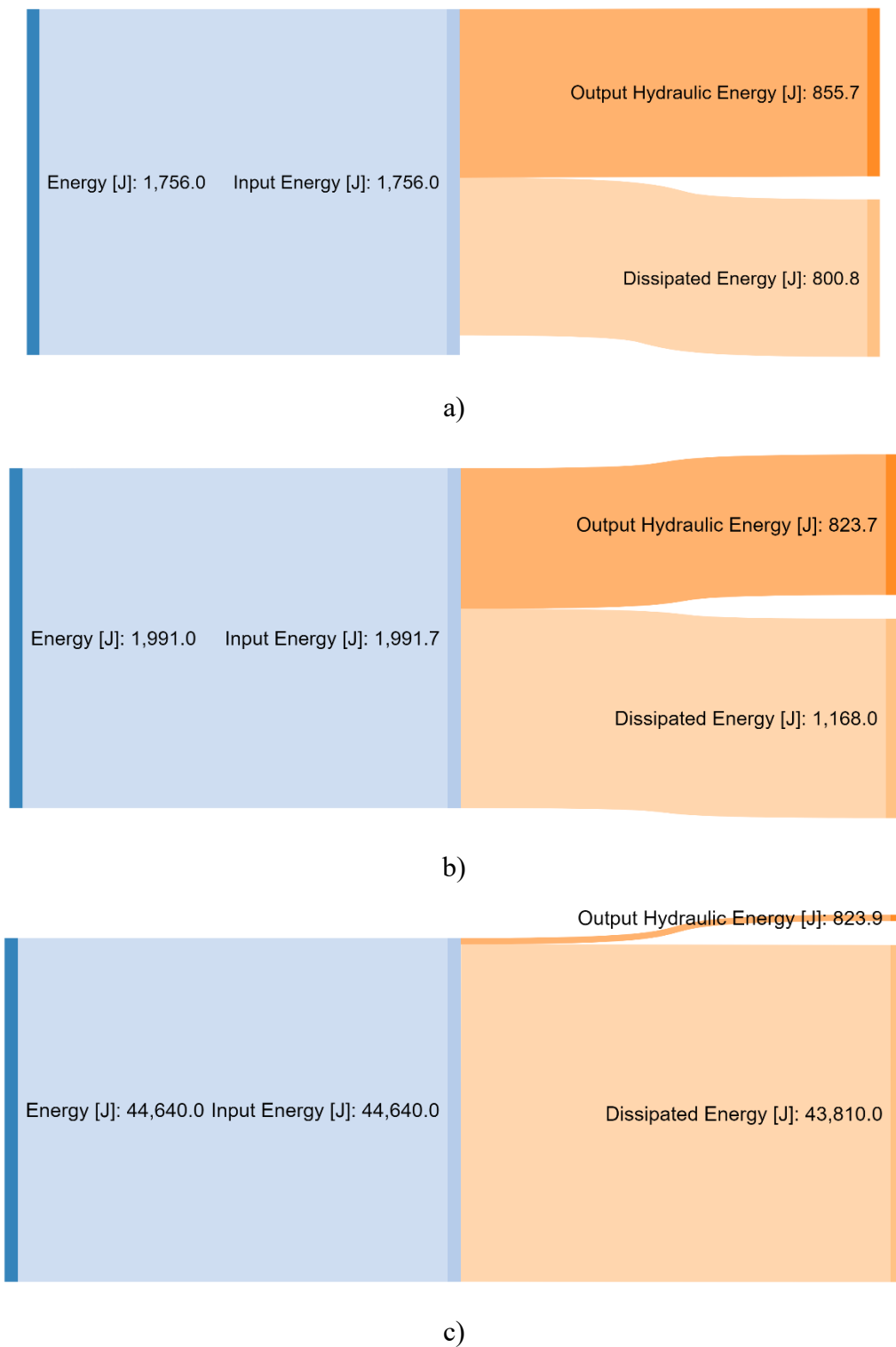
Figure 7.25 – Dissipated energy.



Source- By the author.

The results show that the SHA dissipates around 37 times more energy than the EHA and 54 times more than the DEHA. This dissipation of energy is converted in heat in the servo valves and in the variable displacement pump. As the DEHA and EHA dissipate less energy, the hydraulic fluid cooling system can be reduced saving weight for the aircraft. The results of the energy analysis for the DEHA, EHA and SHA are summarized in Figure 7.26.

Figure 7.26 – Input, Dissipated, Output Energies. a) DEHA, b) EHA, c) SHA.



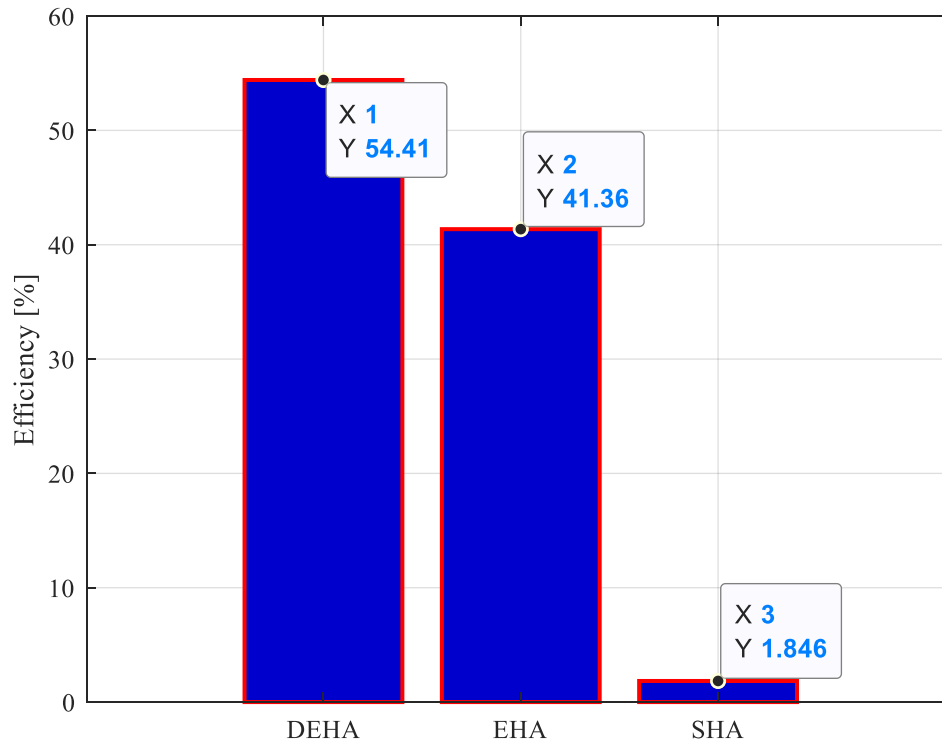
Source- By the author.

The efficiency of these actuators can be calculated as

$$\eta = \frac{E_{output}}{E_{input}}. \quad (7.8)$$

The results obtained for the efficiency of the DEHA, EHA, and SHA are present in Figure 7.27.

Figure 7.27 - Efficiency.



Source- By the author.

As can be seen, the DEHA has an efficiency of 54,41%, which is around 29 times higher when compared to the SHA topology and 1.31 times when compared with the EHA. As mentioned before, the high efficiency of the DEHA is caused due to when the actuator is not moving, the pumps in the digital pump are directed to the reservoir at low pressure, which reduces the leakage in the pumps and consequently the energy losses. In the SHA, for the same conditions, the pump is set in a low volumetric displacement, only supplying the servo valves leakage and keeping the system pressurized. In the EHA, the losses in this kind of actuator are also reduced, where the use of valves that throttle the flow is avoided. However, the main source of losses in the EHA can be associated with the internal leakage of the hydraulic components, as in the pump, which occurs at high pressure.

7.4. FINAL CONSIDERATION OF CHAPTER 7

In this chapter, the main results obtained by the model and by the simulation for the Digital Electro Hydrostatic Actuator – DEHA were presented. The results obtained by the

experiments and by the model have a good concordance, verifying that the model developed is able to predict the behavior of the system developed.

With the configuration adopted it is possible to control the velocity and position of a four-chamber cylinder using a digital pump with three binary modulus with an efficiency higher than 54% and with a performance similar to the conventional hydraulic actuators systems applied in aircraft, as the Servo Hydraulic Actuators – SHA and the Electro Hydrostatic Actuators – EHA, with a position error in steady-state of 0.27×10^{-3} m.

When the DEHA is compared with the SHA, the DEHA is around 29 times more efficient, where the low energy efficiency of the SHA is caused by the throttle losses that occur in the servo valves and by the losses due the internal leakage of the variable displacement pump in low volumetric displacements. In the DEHA, when the actuator is stopped, keeping the desired position, the output flow rate of the pumps is directed to the reservoir, where the pressure differential in the fixed displacement pumps of the digital pump becomes reduced.

8. CONCLUSIONS

In this thesis, a new topology of aircraft actuator for control of the primary and secondary control surfaces was presented. This topology is based in the Digital Hydraulics, which is a new technology for hydraulic systems that aims to increase the efficiency of hydraulic systems using nonrestrictive control techniques, avoiding the throttle losses.

For the design of the digital actuator proposed in this thesis, guidelines for the design of the actuator proposed were presented. The conception of the new actuator, for the primary conversion unit, is based on the use of a digital hydraulic pump, and for the secondary conversion unit, a multi-chamber cylinder. In the multi-chamber cylinder, two concepts of areas were created, the resultant area and the equivalent area. The resultant area is the sum of the areas that are increasing the volume. The equivalent area is the area responsible for the actuator to move a given load at a certain velocity. It is calculated by the resultant area subtracted the area being used in regenerative mode.

One of the characteristics of the use of the multi-chamber cylinder is the possibility of using the regenerative mode. In this mode, the chambers that are decreasing the volume can be connected in the chambers that are increasing the volume. It causes a booster of flow and increases the velocity of the actuator. With the increasing of the number of chambers for the cylinder, the determination of the number of different equivalent areas that can be obtained becomes a difficult task. In order to overcome this problem, a mathematical expression was developed. With this expression, the number of the different equivalent areas can be obtained only using the number of chambers of the cylinder.

The number of binary modulus in the digital pump, for the primary conversion unit, defines the number of flow rates that the digital pump can deliver. For the determination of the number of flow rates for a certain digital pump, another mathematical expression was developed. With the combination of the expression for the digital pump and for the multi-chamber cylinder, the total number of combinations of pumps and equivalent areas can be defined, and consequently the number of the different velocities that the actuator can achieve.

With the determination of the total number of velocities that are necessary and with the definition of the number of chambers of the multi-chamber cylinder, the total number of binary modulus for the digital pump that are necessary can be obtained using the expression developed.

For the calculation of the areas of the cylinder chambers, mathematical expressions for the maximum pressures considering the maximum velocity in steady state, and the external load were developed. The higher values for the pressure are achieved in the maximum velocity using the smaller equivalent area.

The size of the areas and the volumetric displacement of the pumps should be obtained in order to not achieve different combinations that could obtain the same velocity, which would affect the final resolution of the system. Therefore, an optimization algorithm was developed using an objective function, with the purpose to obtain the best possible velocity distribution. The algorithm allows the determination of the areas and volumetric displacements considering the maximum pressure in the chambers, the maximum velocity, and the external load. With the definition of these parameters, the maximum equivalent area can be determined.

For the elaboration of the actuator proposed in this thesis, a cylinder with four chambers was used in the secondary conversion unit. For the primary conversion unit, a digital pump with three binary modulus was used and for the limitation and control unit eight on/off valves. This configuration was denoted as Digital Electro Hydrostatic Actuator – DEHA due to its similarity with the Electro Hydrostatic Actuators where the pump and the cylinder comprise the actuator.

In order to compare the dynamics characteristics of the DEHA with the EHA and the SHA, a mathematical model using the software MATLAB/Simulink for the system control and Hopsan, for the modeling of the components, was elaborated. In addition, models for the EHA and SHA working in the same conditions of the DEHA were also developed. The model developed for the DEHA comprises the main dynamics that occur in the real components that were used in the test bench. The test bench was developed to validate the model, and it is the first of its kind using digital pumps and multi-chambers cylinder developed in Latin American that is known until the date of publication of this thesis.

The results obtained by the numerical and the experimental results demonstrate that it is possible to control the position of the actuator only by controlling the different combinations of pumps and chambers, where the position error in steady-state is 0.27×10^{-3} m. For a step input signal, the digital system takes a delay for start to move, which is caused by the delay controller. In addition, the small difference for the accommodation time between the design value and the one obtained in the experiments can be associated by the internal leakage of the binary modulus of the digital pump and differences in the dynamics of the valves used in the test bench and the parameters used in the model, since the valves can have differences in the manufacturing

process. As the digital pump used is a prototype, it still was not optimized for these operating conditions.

For the energy point of view, for an experiment lasting 70 s, the input hydraulic energy for the DEHA, EHA, and SHA are 1756 J, 1991 J, and 44.64 kJ, respectively. These values imply an energy reduction for the DEHA when compared to the SHA of 25 times. However, when compared with the EHA the values are equivalent. The dissipated energy, for the DEHA, EHA, and SHA are 800.8 J, 1168 J, and 43.73 kJ, respectively. With these results, the DEHA dissipates 54 times less energy when compared to SHA and 1,21 times when compared to EHA.

The energy efficiency for the DEHA is around 54%, being 29 times higher when compared to the SHA (1.84%), and 1.3 times when compared with the EHA (41.36%). The high efficiency of the DEHA is related with the reduction of the losses in the digital pump, when the cylinder is not moving, where the flow rate of the pump is directed to the reservoir at low pressure.

With the results obtained, the DEHA can be an interesting solution for the actuation of the flight control surfaces, where the power electronics that are necessary for control the rotational frequency of the pump in the EHA can be removed, since the digital pump run at constant rotational frequency. Besides, the cooling system for the hydraulic fluid can be reduced. These two actions can save weight for the aircraft. In addition, the systems that use digital hydraulics have an intrinsic redundancy, contributing to system safety. However, the DEHA is in its initial phase of research, and new improvements can be added in the future, as pumps with better volumetric efficiency and other control techniques, as fuzzy logic and neural networks. Finally, it is expected that the results obtained in this thesis for the DEHA could be used in other applications, such as in the mobile machinery industry.

8.1. FUTURE RESEARCHES

For future researches to continue the development of the Digital Electro Hydrostatic Actuator, the following studies are suggested:

- The evaluation of the application of two multi-chamber cylinders being controlled by the same digital pump, in order to control more than one control surface at the same time;
- A study of the on/off valves switching times for the systems that using constant flow sources;

- An analysis of the reliability of the digital system in the case of a failure in one or more binary modulus or one or more valves in the limitation and control unit;
- Carry out a study of the vibrations that occur in the system due the constant switching between high a low pressure levels and develop solutions to mitigate these effects;
- As the system proposed in this thesis has some continuous output values, as the cylinder position, but they are controlled with discrete values, as for instance by the combinations of the pumps and the cylinder chambers, the system can be treated as a hybrid system. In this context, a future study using sampled systems theory is proposed in order to verify others topologies of controllers and the analyses of the system stability.

9. REFERENCES

- ALLE, N., HIREMATH, S. S., MAKARAM, S., SUBRAMANIAM, K., TALUKDAR, A. Review on Electro Hydrostatic Actuator for Flight Control. *International Journal of Fluid Power*. Taylor & Francis. 2012.
- ALLEYNE, A., LIU, R. A simplified approach to force control for electro-hydraulic systems. *Control Engineering Practice* 8, 1347-1356, 2000.
- ÅSTRÖM, K. J., CANUDAS-DE-WIT, C. Revisiting the lugre model; stickslip motion and rate dependence. *IEEE Control Systems Magazine*, 28, 2008.
- BELAN, H. C., LOCATELI, C. C., ENDLER, L., PIERI, E. R. D., DE NEGRI, V. J. Aumento da eficiência energética em sistemas hidráulicos utilizando hidráulica digital. *Anais do XX Congresso Brasileiro de Automática*, Belo Horizonte, MG, 20 a 24 de setembro de 2014.
- BELAN, H., B., LOCATELI, C. C., LANTTO, B., KRUS. P., DE NEGRI, V. J., Digital Secondary Control Architecture for Aircraft Application. *The Seventh Workshop on Digital Fluid Power*, February 26-27, Linz, Austria, 2015.
- BELAN, H. C., FALLGATTER, R. H., BREGALDA, R. DE NEGRI, V. J., Técnicas de Dimensionamento e Implementação para um Sistema Hidráulico Digital. *COBEM Congresso Nacional de Engenharia Mecânica*. 2016.
- BELAN, C. H., *Sistemas de Atuação Hidráulicos Digitais para Aviões com Foco em Eficiência Energética*. Tese de Doutorado em Engenharia Mecânica. Universidade Federal de Santa Catarina. 2018.
- BENNETT, J. W., MECROW, B. C., JACK, A. G., ATKINSON, D. J. A Prototype Electrical Actuator for Aircraft Flaps. *IEEE Transactions on Industry Applications*, v. 46, n. 3, 2010.
- BENNETT, J. W.; ATKINSON, G. J.; MECROW, B. C.; ATKINSON, D. J. Fault-Tolerant Design Considerations and Control Strategies for Aerospace Drives. *IEEE Transactions on Industrial Electronics*, v. 59 n. 5, 2012.
- BOSCH REXROTH valve KSDER catalog <https://apps.boschrexroth.com/products/compact-hydraulics/ch-catalog/pdf/re18136-12_2011-10.pdf> Available in 2020.
- BOZHKO, S., HILL, C. I., Yang, T. *More-Electric Aircraft Systems and Modeling*. Wiley Encyclopedia of Electrical and Electronics Engineering. 2018.

BREGALDA, R., BELAN, H, C. Equipamento Eletrônico que Favorece a Utilização de Válvulas Convencionais em Aplicações Hidráulicas Digitais. 4º Simpósio de Integração Científica e Tecnológica do Sul Catarinense. 2015.

BRAVO, R. R. S., Sistema Hidráulico-Pneumático de Frenagem Regenerativa e Hibridização de Veículos Comerciais. Tese (Doutorado em Engenharia Mecânica) Universidade Federal de Santa Catarina, Florianópolis, 2017.

BREIDI, F. et al. The Impact of Peak-And-Hold and Reverse Current Driving Strategies on the Dynamic Performance of Commercial Cartridge Valves. ASME/BATH 2014 Symposium on Fluid Power & Motion Control. Bath, United Kingdom 2014.

BROWN, F.T. Switched reactance hydraulics: a new way to control fluid power. Proceedings of the national conference on fluid power. Chicago: National Fluid Power Association, p. 25–34, 1987.

BROWN, F.T., TENTARELLI, S.C., AND RAMACHANDRAN, S.A. A hydraulic rotary switched-inertance servo-transformer. Transactions of ASME: journal of dynamic systems, measurement, and control, 110, 144– 150, 1988.

CANUDAS-DE-WIT, C. *et al.* A new model for control of systems with friction. Automatic Control, IEEE Transactions on, v. 40, n. 3, p. 419-425. ISSN 0018-9286. 1995.

CAO, W., MECROW, B. C., ATKINSON, G. J., BANNETT, J. W., ATKINSON, D. J. Overview of Electric Motor Technologies Used for More Electric Aircraft (MEA). IEEE Transactions on Industrial Electronics, Volume 59. NO 9. September. 2012.

CRUZ, D. P. M. Análise de sistemas de atuação hidráulicos digitais para aviões com foco em eficiência energética. Dissertação de Mestrado. Universidade Federal de Santa Catarina - UFSC. Programa de Pós-Graduação em Engenharia Mecânica - POSMEC. Florianópolis, p. 142. 2018.

DAVIS, S. J., CALDEIRA, K. Consumption-Based Accounting CO₂ Emissions. Department of Global Ecology. Proceeding of the National Academy of Sciences. 2010.

DELL'AMICO, A., CARLSSON, M., NORLIN, E., SETHSON, M. Investigation of a Digital Hydraulic Actuation System on an Excavator Arm. 13th Scandinavian International Conference on Fluid Power - SICFP, Linköping, Sweden, 2013.

DELL'AMICO, A., SIMON, D., WARD, S., PINTO, L. P. G., LANTTO, B., DE NEGRI, V., KRUS. P., A Hybrid Digital-Proportional Hydraulic Actuation System for Aircraft Flight Control. 31st Congress of the International Council of the Aeronautical Sciences. Belo Horizonte, Brazil, September, 2018.

DE NEGRI, V. J., RAMOS FILHO, J. R. B., SOUZA, A. D. C. de. A Design Method for Hydraulic Positioning Systems. 51th National Conference on Fluid Power (NCFP), Las Vegas, USA. 2008.

DE NEGRI, V.J., WANG, P., JOHNSTON, D.N., and PLUMMER, A. Behavioural prediction of hydraulic step-up switching converters. International Journal of Fluid Power. Vol 15, No. 1, 1-9. 2014.

DE NEGRI, V. J., NOSTRANI, M.P., WANG P., JOHNSTON D.N., and PLUMMER, A. Modelling and analysis of hydraulic step-down switching converters, International Journal of Fluid Power, 2015.

EGGERS, B., RAHMFELD, R., IVANTYSYNOVA., M. An energetic comparison between valveless and valve controlled active vibration damping for off-road vehicles. Proceedings of the 6th JFPS International Symposium on Fluid Power. TSUKUBA. 2005.

FIORI, A. F. Modelagem Matemática da Dinâmica de uma Transmissão Mecânica do Tipo Fuso de Esferas de Um Robô Gantry. Dissertação de Mestrado Departamento de Ciências Exatas e Engenharias, Universidade Regional do Noroeste do Estado do Rio Grande do Sul, Panambi-RS, Brasil. 109 p. 2015.

GALLONI, A. Modelling and energy assessment of a switched inertance hydraulic system for pitch control. Iniversità degli studi di Modena e Reggio Emilia. Dipartimento di Ingegneria "Enzo Ferrari". 2015.

GARCIA, A., CUSIDÓ, J., ROSERO, J. A., OERTEGA, J. A., ROMETAL, L. Reliable Electro-Mechanical Actuators in Aircraft. IEEE A&E Systems Magazine, August. 2008.

GARG, G. C. A., LINDA, R. I., CHOWDHURY, T., Evolution of Aircraft Flight Control System and Fly-by-Light Flight Control System. International Journal of Emerging Technology and Advanced Engineering. Vol 3 Issue 12, December, 2013.

GÖSSLING, S. Sustainable Tourism Development in Developing Countries: Some Aspects of Energy Use. International Journal of Sustainable Tourism. 2010.

HEITZIG, S., THEISSEN, H. Aspects of digital pumps in closed circuit. The Fourth Workshop on Digital Fluid Power, Linz, Austria, 2011.

HEYBROEK, K., SAHLMAN, M. A Hydraulic Hybrid Excavator Based on Multi-Chamber Cylinders and Secondary Control – Design and Experimental Validation. International Journal of Fluid Power. 2018.

HOUVA, M., KARVONEN, M., AHOLA, V., LINJAMA, M., VILENIUS, M. Energy Efficient Control of Multiactuator Digital Hydraulic Mobile Machine. 7th International Fluid Power Conference. Aachen. 2010.

HUOVA, M., LINJAMA, M., KALEVI, H. Study of Energy Losses in Digital Hydraulic Multi-Pressure Actuator. The 15th Scandinavian International Conference on Fluid Power, SICFP'17, Linköping, Sweden, June 7-9, 2017.

INVANTYSYNOVA, M, Innovations in Pump Design – What are Future Directions. Proceedings of the 7th JFPS International Symposium on Fluid Power, TTOYAMA, September 15-18, 2008.

JÄNKER, P., CLAEYSSSEN, B., GROHMANN, B., CHISTMANN, M., LORKOWSKI, T., LELETTY, R., SOSNIKI, O., PAGES, A. New Actuators for aircraft and Space Applications. 11TH International Conference on New Actuators, Bremen, Germany, 9-11 June, 2008.

JIAN, F., MARÉ J. C., YONGLING, F. Modelling and Simulation of Flight Control Electromechanical Actuators with Special Focus on Model Architecting, Multidisciplinary Effects and Power Flows. Chinese Journal of Aeronautics. 2016.

KLEEMANN, E., DEY, D., RECKSIEK, M., The Development of a Civilian Fly by Wire Flight Control System. International Council of Aeronautical Sciences Conference. 2000.

KORNECKI, A. J., HALL, K., Approaches to Assure Safety in Fly-by-Wire Systems: Airbus Vs. Boeing. Conference on Software Engineering and Applications, November 9-11, MIT, Cambridge, MA, USA, 2004.

LINJAMA, M., LAAMANEN, A., VILENIUS, M. Is it time for digital hydraulics? The Eight Scandinavian International Conference on Fluid Power, Tampere, Finland, 2003.

LINJAMA, M. Digital fluid power-state of the art. The Twelfth Scandinavian International Conference on Fluid Power, Tampere, Finland. 2011.

- LINJAMA, M. Energy Saving Digital Hydraulics. Second Workshop on Digital Fluid Power, Linz, Austria, 2009.
- LINJAMA, M., VILENIUS, M. Digital Hydraulics – Towards Perfect Valve Technology. Technology. Digitalna Hidravlika, Ventil 14 // 2. pp. 138-148. 2008.
- LINJAMA, M., VIHTANEN, H. P., SIPOLA, A., VILENIUS, M. Secondary Controlled Multi-Chamber Hydraulic Cylinder. The 11th Scandinavian International Conference on Fluid Power, SICFP'09, June 2-4, Linköping, Sweden. 2009.
- LINJAMA, M., KOSKINEN, K. T., VILENIUS, M. Accurate Trajectory Tracking Control of Water Hydraulic Cylinder with Non-Ideal On/Off Valves. International Journal of Fluid Power. No. 1 p 7-16. 2003.
- LINSINGEN, I. V. Fundamentos de Sistemas Hidráulicos. 4ª ed. Florianópolis: Ed. UFSC, ISBN: 85-328-00646-8. 2013.
- LOCATELI, C. C., BELAN, H. C., DE PIERI, E. R., KRUS, P., DE NEGRI, V. J. Actuator Speed Control Using Digital Hydraulic Principles. Bath/ASME Conference of Fluid Power and Motion Control, Bath, United Kingdom, 2014a.
- LOCATELI, C. C., TEIXEIRA, P. L., DE PIERI, E. R., KRUS, P., DE NEGRI, V. J. Digital hydraulic system using pumps and on/off valves controlling the actuator. FPNI PhD Symposium on Fluid Power, Lappeenranta, Finland, 2014b.
- LOTFALIPOUR, M. R., FALAHI, M. A., MALIHE, A. Economic Growth, CO₂ Emissions, and Fossil Fuels Consumption in Iran. The International Journal of Energy. Elsevier. 2010.
- MANTOVANI, J. I., Otimização dos Chaveamentos entre Válvulas on/off em Atuadores Hidráulicos Digitais. Dissertação de Mestrado em Engenharia Mecânica. Universidade Federal de Santa Catarina. 2019.
- MANTAVANI, I. J., BELAN, C. H., DE NEGRI, V. J., Análise do Chaveamento entre Válvulas para Atuador Hidráulico Digital (DHA). XXII Congresso Brasileiro de Automática. 2018.
- MARÉ, J. C., Aerospace Actuators 1: Needs, Reliability and Hydraulic Power Solutions. John Wiley & Sons, Inc. 2016.
- MARÉ, J. C., Aerospace Actuators 2: Signal-by-Wire and Power-by-Wire. John Wiley & Sons, Inc. 2017.

MÁRTON, L. OSSMANN, D. Energetic Approach for Control Surface Disconnection Fault Detection in Hydraulic Aircraft Actuators. 8th Symposium on Fault Detection, Supervision and Safety of Technical Processes. Mexico City, Mexico. 2012.

MOIR, I, SEABRIDGE, A. Aircraft Systems: Mechanical, electrical, and avionics subsystems integration. 3rd Ed. John Wiley & Sons, Ltd. ISBN 978-0-470-05996-8. 2008.

MOOG. EPU – Electrohydrostatic Pump Unit – Controle Eletro-Hidrostático de Alta Performance Presentation. 2017.

MURARO, I., TEIXEIRA, P. L., DE NEGRI, V. J. Effect of proportional valves and cylinders on the behavior of hydraulic positioning systems. In: ASME/BATH Symposium on Fluid Power & Motion Control, Sarasota, FL. p.1 – 9. 2013.

NAAYAGI, R. T. A Review of More Electric Aircraft Technology. International Conference on Energy Efficient Technologies for Sustainability – ICEETS. 2013.

NEVES, S. A., MARQUES, A. C., FUINHAS, J. A. Is energy consumption in the transport sector hampering both economic growth and the reduction of CO₂ emissions? A disaggregated energy consumption analysis. The International Journal of the World Conference on Transport Research Society. 2017.

NIEDERMEIER, D., LAMBREGTS, A. A. Fly-By-Wire Augmented Manual Control – Basic Design Considerations. 28th International Congress of The Aeronautical Sciences. 2012.

NOSTRANI, M. P., Estudo Teórico-Experimental de um Posicionador Utilizando Hidráulica Digital de Chaveamento Rápido: Estudo de Caso em Bancada de Ensaio para Turbinas Eólicas. Dissertação (Mestrado em Engenharia Mecânica) Universidade Federal de Santa Catarina, Florianópolis, 2015.

NOSTRANI, M. P., GALLONI, A., RADUENZ, H., DE NEGRI, V.J., 2016. Theoretical and experimental analysis of a hydraulic step-down switching converter for position and speed control. The Eighth Workshop on Digital Fluid Power. Tampere. 2016.

NOSTRANI, M. P., GALLONI, A., RADUENZ, H., DE NEGRI, V.J., 2016. Design and Optimization of a Fast Switching Hydraulic Step-Down Converter for Position and Speed Control. The 15th Scandinavian International Conference on Fluid Power, SICFP'17, June 7-9, Linköping, Sweden, 2017.

NOSTRANI, M. P., DELL'AMICO, A., LANTTO, B., KRUS, P., DE NEGRI, V. J., An Aircraft Actuator Driven by Digital Hydraulic Pumps, Proceedings of the XV International Symposium on Dynamic Problems of Mechanics, Buzios, RJ, Brazil, .2019.

PAN, M., JOHNSTON, N., HILLIS, A. Active Control of a Pressure Pulsation in a Switched Inertance Hydraulic System Using a RectangularWave Reference Signal. Fluid Power and Motion Control. 2012.

PAN, M. Active Control of Pressure Pulsation in a Switched Inertance Hydraulic System. Thesis Submitted for the Degree of Doctor of Philosophy. Department of Mechanical Engineering. University of Bath, 2012.

PERONDI, E. A. Controle Não-Linear em Cascata de um Servoposicionador Pneumático com Compensação do Atrito. 196 p. Tese de Doutorado Programa de Pós-Graduação em Engenharia Mecânica, Universidade Federal de Santa Catarina, Florianópolis, SC, Brasil. 2002.

PINTO, L. O. G., BELAN. H. C, LOCATELLI, C. C., KRUS, P., DE NEGRI, V. J., LANTTO, B. New Perspectives on Digital Hydraulics for Aerospace Application. Aerospace Technology Congress. Solna. October 11-12, Stockholm. 2016.

POLLARD, F. H. Research Investigation of Hydraulic Pulsation Concepts. First Quarterly Progress Report (RAC-933-1), Republic Aviation Corporation, Farmingdal, L.I., N.Y., June 1963.

PYNTTÄRI, O. N. LINJAMA, M. LAAMANEN, A. HUHTALA, K. Parallel Pump-Controlled Multi-Chamber Cylinder. Symposium on Fluid Power & Motion Control. Bath. United Kingdom. 2014.

QIAO, G., LIU, G., WANG, Y., MA, S. A Review of Electromechanical Actuators for More/All Electric Aircraft Systems. Journal of Mechanical Engineering Science. 2017.

RAMPEN, W. Gearless Transmissions for Large Wind Turbines–The history and Future of Hydraulic Drives. Dewek Bremen, 2006.

ROBOAM, X. New trends and challenges of electrical networks embedded in “more electrical aircraft”. IEEE International Symposium on Industrial Electronics - ISIE, 2011.

RYDBERG, K. E. Energy Efficient Hydraulics – System Solutions for Loss Minimization. National Conference on Fluid Power. Linköping University. Linköping. Sweden. 2015.

SCHEIDL, R., LINJAMA, M., SCHMIDT, S. Is the Future of Fluid Power Digital? Proceedings of the Institution of Mechanical Engineers. Part I: Journal of Systems and Control Engineering, v. 226, n. 6, p pp. 721-723, ISSN 09596518. 2012.

SCHEIDL, R.; KOGLER, H.; WINKLER, B. Hydraulic Switching Control - objectives, concepts, challenges and potential applications. Magazine of Hydraulics, Pneumatics, Tribology, Ecology, Sensorics, Mechatronics, n. 1, ISSN: 1453 - 7303. 2013.

SLIWINSKI, J., GARDI, A., MARINO, M., SABATINI, R. Hybrid-Electric Propulsion Integration in Unmanned Aircraft. International Journal of Energy. 2017.

THEISSEN, H., GELS, S., MURRENHOFF, H. Reducing Energy Losses in Hydraulic Pumps. International Conference on Fluid Power Transmission and Control - *ICFP*, Hangzhou, China, 2013.

TEIXEIRA, P. L. Análise teórico experimental de prensa dobradeira hidráulica controlada por bomba-motor com velocidade variável. Dissertação de Mestrado Departamento de Engenharia Mecânica, Universidade Federal de Santa Catarina, Florianópolis-SC, Brasil. 154 p. 2015.

TERRENOIRE, E., HAUGLUSTAINE. D. A., GASSER, T., PENANHOAT. O. The Contribution of Carbon Dioxide Emissions from the Aviation Sector to Future Climate Change. Journal of Environmental Research Letters. 2019.

TRAN, X. Khaing, W., Endo, H., Yanada, H. Effect of friction model on simulation of hydraulic actuator. Proceedings of the Institution of Mechanical Engineers, Part I: Journal of Systems and Control Engineering, v. 228, n. 9, p. 690-698, 2014.

TSITA, K. G., PILAVACHI, P. A. Decarbonizing the Greek Road Transport Sector Using Alternative Technologies and Fuels. International Journal of Thermal Science and Engineering Progress. 2017.

TU, C. H., RANNO, B. M., DE VEM, J. D., WANG, M., LI, P. Y., CHASE, T. R., High Speed Rotary Pulse Width Modulated on/off Valve. Proceedings of ASME-IMECE. International Mechanical Engineering Congress and RD&D Expo. November 11-15, Seattle, Washington, USA. 2007.

TU, C. H., RANNO, B. M., WANG, M., LI, P. Y., CHASE, T. R., Modeling and Validation of a High-Speed Rotary PWM on/off Valve. Proceedings of ASME. Dynamic Systems and Control Conference. October 12-14, Hollywood, California, USA. 2009.

- UUSITALO, J. P., AHOLA, V., SOEDERLUND, L., LINJAMA, M., JUHOLA, M., KETTUNEN, L. Novel bistable hammer valve for digital hydraulics. *International Journal of Fluid Power*. N. 3, pp. 35-44. 2009.
- VALDIERO, A. C. Controle de Robôs Hidráulicos com compensação de atrito. Tese de Doutorado, Universidade Federal de Santa Catarina, Florianópolis. 157 p. 2005.
- van den BOSSCHE, D. More Electric Control Surface Actuation, A Standard for the Next Generation of Transport Aircraft. University of Bath, UK, September, 2004.
- van den BOSSCHE, D. The A380 Flight Control Electrohydrostatic Actuators Achievements and Lessons Learnt. 25TH International Congress of the Aeronautical Sciences. 2006.
- VIERSMA, T. J. Analysis, synthesis, and design of hydraulic servosystems and pipelines (Book). Amsterdam, Elsevier Scientific Publishing Co. (Studies in Mechanical Engineering., v. 1, 1980.
- VÍGOLO, V. Estudo Teórico-Experimental para Auxilio no Dimensionamento de Sistemas de Atuação Pneumáticos Dissertação de Mestrado Departamento de Engenharia Mecânica, Universidade Federal de Santa Catarina, Florianópolis-SC, Brasil. 170 p. 2018.
- WANG, S., TOMOVIC, M., LIU, H. Commercial Aircraft Hydraulic Systems. Shanghai Jiao Tong University Press Aerospace Series. Published by Elsevier Inc. 2016.
- WANG, F., GU, L., CHEN, Y. A continuously variable hydraulic pressure converter based on high-speed on-off valves. *Mechatronics*, v. 21, n. 8, p. 1298-1308. ISSN: 09574158, 2011.
- WANG, M., LI, P. Y., Event based Kalman filter observer for rotatory high speed on.off valve. American Control Conference. Seattle, Washington, USA, June 11-13, 2008.
- WANG, M., LI, P. Y., Duty Ration Control of a Rotary PWM Valve with Periodic Measurement Error. American Control Conference. St Louis, MO, USA, June 10-12, 2009.
- WARD, S. Digital Hydraulics in Aircraft Control Surface Actuation. Fluid and Mechatronic Systems Master Thesis. Linköping University. 2017.
- WINKLER, B., PLÖCKINGER, A., SCHEIDL, R. A novel piloted fast switching multi poppet valve. *International Journal of Fluid Power*. N. 3, pp. 7-14. 2010.
- XYLIA, M., SILVEIRA, S. On the Road to Fossil-Free Public Transport: The Case of Swedish Bus Fleets. *The International Journal of the Political, Economic, Planning, Environmental and Social Aspects of Energy*. 2016.

XIA, C. L. Permanent Magnet Brushless DC Motors Drive and Controls. WILEY. Tianjin University. China. 2012.

YANADA, H.; TAKAHASHI, K.; MATSUI, A. Identification of Dynamic Parameters of Modified LuGre Model and Application to Hydraulic actuator. JFPS International Journal of Fluid Power System, v. 3, n. 1, p. 1-8, 2010.

ZHANG, J., CHAO, Q., XU, B. Analysis of the Cylinder Block Tilting Inertia Moment and Its Effect on the Performance of High-Speed Electro-Hydrostatic Actuator Pumps of Aircraft. Chine Journal of Aeronautics. 2016.

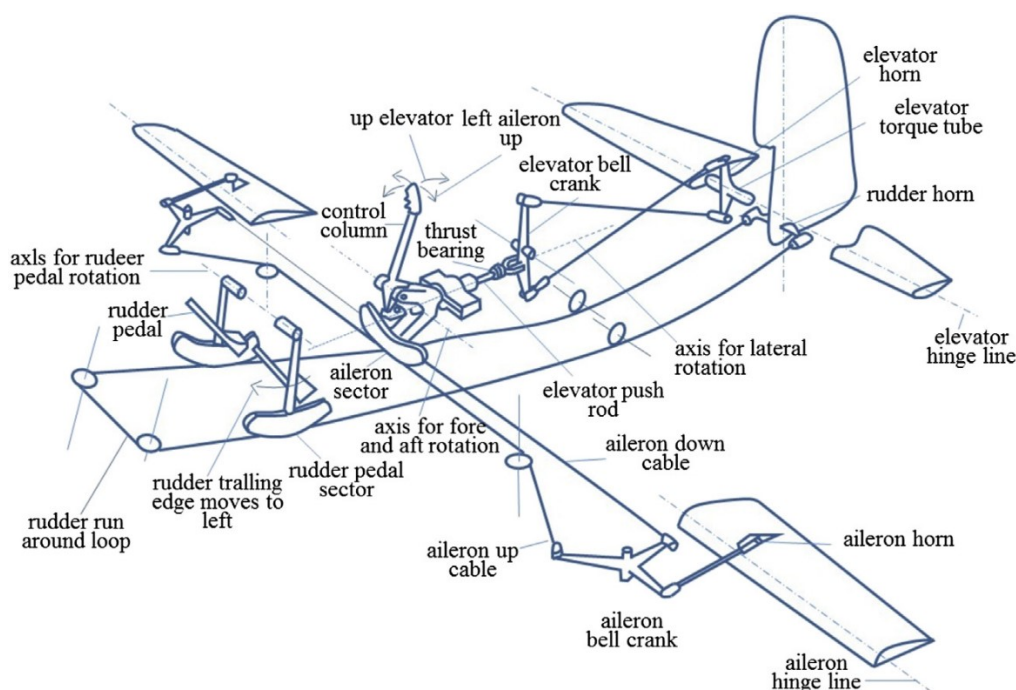
ZHANG, Y., ZHOU, Y. F. W. Optimal Control for EHA-VPVM System Based on Feedback Linearization Theory. 11th Conference Control, Automation, Robotics and Vision. Singapore. December 7-10. 2010.

ZIMMERMAN, J. D., PELOSI, M., WILLIAMSON, C. A., IVANTYSYNOVA, M. Energy Consumption of a LS Excavator Hydraulic System. International Mechanical Engineering Congress and Exposition. Seattle, Washington, USA, November 11-15, 2007.

APPENDIX A – Flight control systems

As mentioned in Chapter 2, the flight control systems (FCS) are extremely important for keeping the aircraft capable of flight in normal conditions or in failure situations. They can be defined as a mechanical/electrical system, which transmits the control signals that come from the pilot's commands and drives the control surfaces to realize the scheduled flight (WANG *et al.*, 2016). According to Moir & Seabridge (2008), the control of first biplanes was provided by warping the wings and control surfaces through wires attached to the flying controls in the cockpit. In these cases, the flight control system was purely mechanical, as can be seen in the example shown in Figure A.1.

Figure A.1 - Mechanical flight control system.



Source: Wang *et al.* (2016).

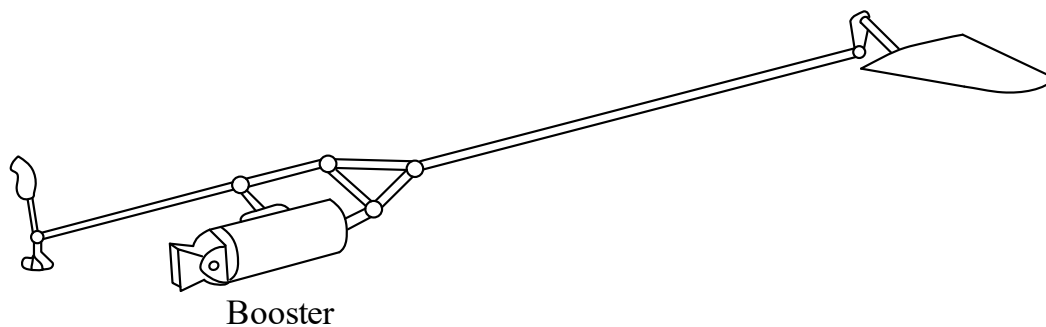
In the example shown in Figure A.1, the control of the flight control surfaces is afforded by using mechanical parts such as pushrods, tension cables, pulleys, counterweights, and others mechanisms, to transmit the pilot's commands to the control surfaces (WANG *et al.*, 2016; GARG *et al.*, 2013). For instance, when the pilot needs to move the rudder, the rudder pedals are activated, where the force applied by the pilot in the pedals is transmitted to the control surface through cables and connection links.

With the evolution of the aircraft over the decades, there was an increase of the aircraft velocity, weight and therefore, the aerodynamic loads through the control surfaces became

higher (MOIR & SEABRIDGE, 2008; WANG *et al.*, 2016). Consequently, the use of pure mechanical flight control systems became the aircraft difficult to fly, as mention Moir & Seabridge (2008) and Wang *et al.* (2016). Garg *et al.* (2013) also quote that with the increasing of the aircraft size, the complexity and weight of the mechanical flight control system increase considerably, and then being a limitation for this kind of systems.

In order to overcome this bottleneck, other technologies had to be developed and implemented in the flight control systems. The first solution implemented was the hydraulic systems. Wang *et al.* (2016) mention that the hydraulic boost appeared at the end of the 1940s, where the control surfaces forces are divided between the pilot and the boosting mechanism (Figure A.2 shows this kind of mechanism). In addition, Moir & Seabridge (2008) mention that the hydraulic systems today remain as the most effective source of power for control the primary and secondary control surfaces, undercarriage, braking, and anti-skid systems. Furthermore, according to Alleyne & Lui (2000), the main advantages of using hydraulic systems are the low weight/power ration and high dynamics behavior.

Figure A.2 - Mechanical actuator with a hydraulic booster.



Source: Adapted from Wang *et al.* (2016).

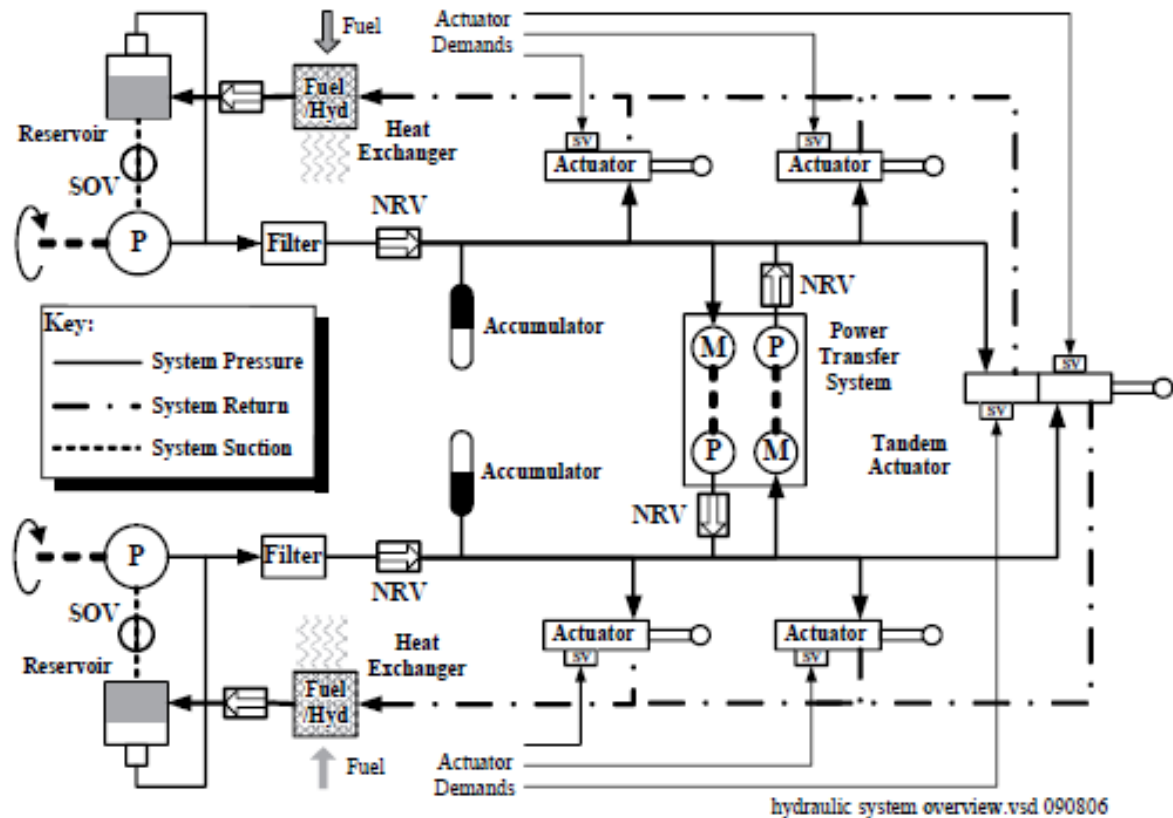
With the increase of the loads in the actuation systems of the aircraft, the use of hydraulic systems to control flight control surfaces has become increasingly common. According to Wang *et al.* (2016), the development of centralized hydraulic power units was realized since the 1950s. In this kind of arrangement, it is used a centralized hydraulic power unit, which is responsible to supply all actuators, and normally, it is composed of the hydraulic fluid reservoir, hydraulic pumps, valves, accumulators, heat exchangers, etc (WANG *et al.*, 2016).

Besides the control of the flight control surfaces, the hydraulic systems are also responsible for (MOIR & SEABRIDGE, 2008; WARD, 2017):

- Landing gear;
- Brakes;
- Steering;
- Cargo doors;
- Loading ramps;
- Passenger stairs.

In order to exemplify the application of the hydraulic systems in aircraft, Figure A.3 shows a simplified hydraulic circuit.

Figure A.3 - Aircraft simplified hydraulic system.



Source: Moir & Seabridge (2008).

As can be seen in Figure A.3, there is more than one hydraulic system, which works independently from each other. This system configuration is necessary to keep the aircraft safety standards. In the event of failure of one of the hydraulic systems, the power transfer system (PTS) is activated. When it is activated, the remaining hydraulic system supplies hydraulic power to both hydraulic systems. Furthermore, accumulators that are installed in the systems can operate as a backup flow rate source, in case of a pump failure. Wang *et al.* (2016)

quote that independent centralized hydraulic power units are necessary to ensure that a failure of a hydraulic system will not result in loss of control. Moir & Seabridge (2008) mention that, if flight safety is critical or its loss or degradation can be tolerated, these parameters will determinate the number of independent sources of hydraulic power.

In Moir & Seabridge (2008), it is mentioned that aircraft such as Airbus A320 and Boeing 767 feature three independent hydraulic systems. In the case of the A320, it has five hydraulic pumps, where the first hydraulic system consists of an engine driven pump (EDP). The second one consists of an electric motor driven pump (MDP), and another pump installed next to the RAT (Ram Air Turbine). The third system consists of EDP and MDP pumps (MOIR & SEABRIDGE, 2008). In Boeing 767, the fluid supply for the hydraulic systems consists of eight hydraulic pumps. Both the first and second hydraulic systems are each composed of an EDP type pump and a Demand Electric Motor Driven Pump (MP). The third one consists of two EDP type pumps, one ADP type (Air-Driven Pump), and the RAT pump (MOIR & SEABRIDGE, 2008).

In the earliest aircraft that used centralized hydraulic power units, the commands imposed by the pilots to the control surfaces were transmitted to the hydraulic system, to open and close hydraulic valves, through cables and mechanical levers (WANG *et al.*, 2016). With the use of flight control systems that use mechanical components to transmit the commands to the hydraulic actuator and then to the control surfaces, the implementation of redundant systems becomes difficult. Maré (2017) quotes that the Boeing 747-400 has more than 20 flight control actuators, which some of them are located more around 60 m away from the cockpit. Moreover, this kind of system can cause some undesirable dynamic behaviors, due to the dilation, structural, elasticity, and friction (MARÉ, 2017).

With the development of the hydraulic systems, where electronic systems were incorporated together with the hydraulic components, another technology was developed and implemented in the flight control systems, called Fly-by-Wire (FBW). This technology had its first appearance in the early 1970s (WANG *et al.*, 2016; GARG *et al.*, 2013). According to Garg *et al.* (2013), the Fly-by-Wire control systems replaces the conventional manual flight controls with electronic interfaces. For Kornecki & Hall (2004), a Fly-by-Wire is a computer based flight control system that replaces the mechanical link between the pilots and control surfaces with lighter electrical wires. Wang *et al.* (2016) highlighted that, with the introduction of the Fly-by-Wire systems, the aircraft flight performance improved. Kleemann & Recksiek (2000) quote some advantages of the Fly-by-Wire, as the reduction of weight and parts,

improvement of safety, for instance. However, Garg *et al.* (2013) highlighted that some disadvantages, as the susceptibility to electromagnetic interference and high intensity radiated field.

Nowadays, many civil aircraft implement the Fly-by-Wire as the Airbuses A319, A320, A330, A340, A380, and Boeing 777 and 787, being the A320 the pioneering aircraft with Fly-by-Wire technology (GARG *et al.*, 2013; NAAYAGI, 2013).

After the development of the Fly-by-Wire systems, another concept emerged for control the aircraft control surfaces, known as More Electric Aircraft – MEA (BENNETT *et al.*, 2010; CAO *et al.*, 2012; NAAYAGI, 2013). In this concept, the main goal is to replace the centralized hydraulic power units, which use conventional technologies and are known for their low efficiency, with more electric actuators. According to De Negri *et al.* (2014), the energetic efficiency of the hydraulic system is less than 50%. According to Bozhko *et al.* (2018), the MEA concept also aims the minimization of fuel consumption, and hence reduce cost and environmental impact.

In a typical civil aircraft, as the Airbus A320 and the Boeing 737, the electric power is around 11.5% of the non-propulsive power and around 0.5% of the engine power (BOZHKO *et al.*, 2018). In the results presented by the same authors, it can be noticed that the hydraulic system power is around 13.8% of the non-propulsive power and 0.6% of the engine power.

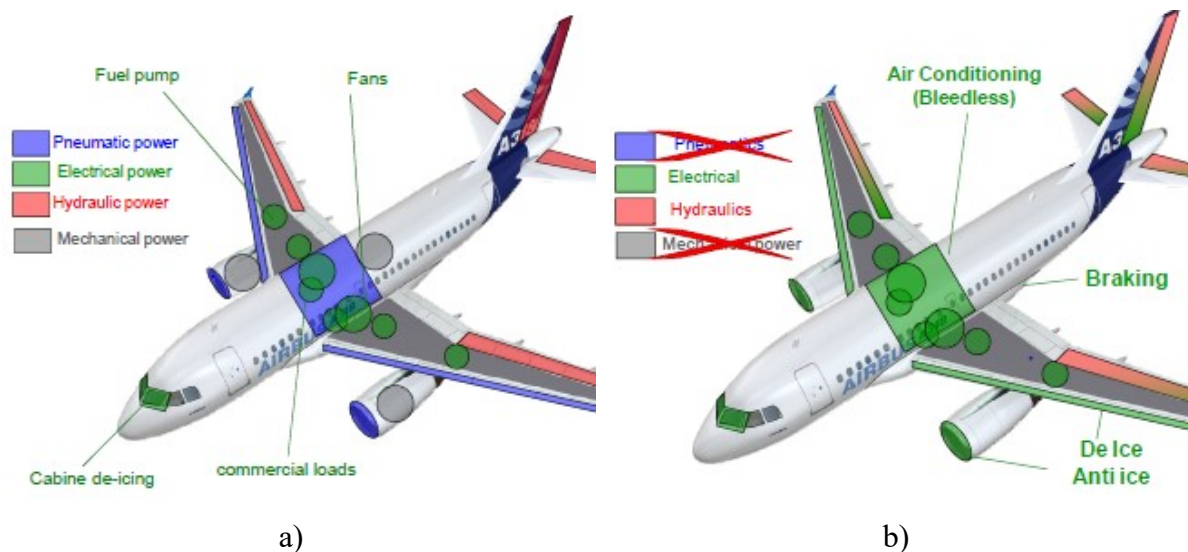
With the use of More Electric Aircraft concept, other benefits can be achieved, as quote Bozhko *et al.*, (2018).

- Reduce system weight;
- Ease of maintenance;
- Increase engine efficiency;
- Reduction of engine use on the ground;
- Controllability;
- Reconfigurability;
- Advanced diagnostics and prognostics.

The same authors also mention that the starting point of the More Electric Aircraft was the Airbus A380, although there were other attempts to create a more electric solution as the Vickers VC-10 in the 1950s (BOZHKO *et al.*, 2018).

According to Roboam (2011), the MEA concept can be exemplified according to Figure A.4.

Figure A.4 - More electric aircraft concept. a) Nowadays; b) Future tendencies.



Source: Adapted from Roboam (2011).

Figure A.4 shows that MEA aims the removal of pneumatic power systems and mechanical power systems. One of the major uses of pneumatic systems is to start the aircraft's main engines (MOIR & SEABRIDGE, 2008). In the MEA concept, this action can be provided by the use of electric motors. For mechanical power, something similar can occur. One of the uses of the mechanical power in the aircraft is to convert the engine power, through gearboxes, in hydraulic power. In the MEA concept, the gearboxes are replaced by electric motors connected directly to the hydraulic pumps. Figure A.4 also shows that, although the replacement of the pneumatic and mechanical power systems by electric power systems, the hydraulic systems are not completely removed. This fact can be explained by the high loads that the control surfaces are submitted, the high reliability of the hydraulic systems, and the necessity of the existence of a redundant or backup system.

The application of electrical systems to aircraft can bring other benefits, as well as increased efficiency, such as those listed by Bennett *et al.* (2012):

- Reduced maintenance due to the modular nature of these systems. A failed actuator can be removed without disassembling of sections along wings wingspan;
- Functionality increasing, because there is one individual actuator for each flap;
- Improved fault detection due to electronic monitoring that can be transmitted to the pilot;

- Wear and degradation can be monitored by the system control, allowing preventive maintenance;
- Mass reduction.

However, the same authors point out that, as there are more components acting in parallel, the systems end up becoming more complex, and thus, require levels of redundancy and fault tolerance that meet reliability requirements.

One of the key components for the introduction of the MEA concept is the Electro-Hydrostatic Actuator (EHA) (QIAO *et al.*, 2017, JIAN *et al.*, 2016, GARCIA *et al.*, 2008, WANG *et al.*, 2016). In this kind of actuators, a decentralized hydraulic power unit replaces the centralized hydraulic power unit (ALLE *et al.*, 2012).

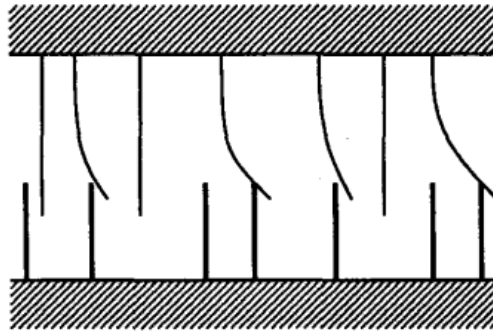
With the development and use of the Electro-Hydrostatic Actuators for the flight control surfaces, another concept for the flight control systems was developed, called Power-By-Wire (PBW). According to Maré (2017), Power-By-Wire actuators are powered by an electrical power source. For a Power-By-Wire using EHA, the electric power is converted in mechanical power by the electric motor, which is converted in hydraulic power by the hydraulic pump coupled in the electric motor, and the hydraulic power is converted in mechanical power to the hydraulic actuator. The main topologies of actuators that are used in aircraft control surfaces are presented with more detail in Section 2.2.

APPENDIX B – Friction model equations

As mentioned in Chapter 5, the friction of the multi-chamber cylinder was modeled according to the LuGre friction model. This model was firstly developed by Canudas-de-Wit *et al.* (1995), and the name of the model is a reference of the universities Lund and Grenoble, which participated in its development.

This model, according to Belan (2018), allows the representation of the effects that occur in the Stribeck region, the stick-slip, hysteresis, and micro displacements on the pre-slip region (ÅSTRÖM & CANUDAS-DE-WIT, 2008). According to Fiori (2015), the LuGre model is based on the micro deformations that occur in the surfaces in contact. When a tangential force is applied, the elastic bristles will suffer a deflection compared with springs (pre sliding region). With the increase of the deflection, the bristles will slip (FIORI, 2015; VÍGOLO 2018). In Figure B.1, the representation of the bristle deflections by the LuGre model is presented.

Figure B.1 – Representations of the bristles by the LuGre model.



Source: Adapted from Canudas-de-Wit *et al.* (1995).

According to Canudas-de-Wit *et al.* (1995), the friction force can be represented as

$$F_{fr} = \sigma_0 z + \sigma_1 \frac{dz}{dt} + \sigma_2 v, \quad (\text{B.1})$$

where v is the relative velocity, σ_0 is a coefficient related with the stiffness, the σ_1 a damping coefficient and the σ_2 the viscous coefficient. The variable z is denoted as the average deflection of the bristles (CANUDAS-DE-WIT *et al.*, 1995), and is calculated as

$$\frac{dz}{dt} = v - \frac{|v|}{g(v)} z. \quad (\text{B.2})$$

The function $g(v)$ is positive and depends on many parameters as the material properties, lubrication, and temperature (CANUDAS-DE-WIT *et al.*, 1995). In steady-state, the average deflection of the bristles can be approximated as

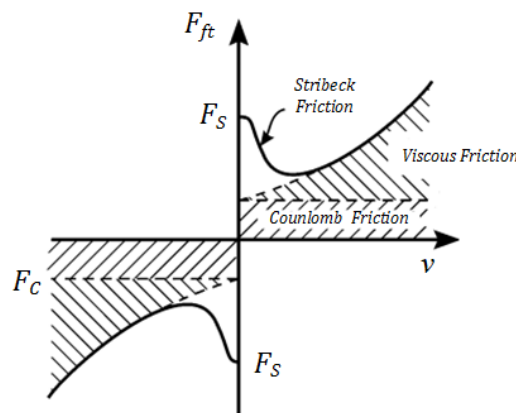
$$z = \frac{v}{|v|} \frac{1}{\sigma_0} g(v) = \operatorname{sgn}(v) \frac{g(v)}{\sigma_0}. \quad (\text{B.3})$$

The Stribeck friction can be parametrized of the using g function as

$$g(v) = F_C + (F_S - F_C) e^{-\left(\frac{v}{v_S}\right)^{\alpha_f}}, \quad (\text{B.4})$$

where F_C is the Coulomb friction, F_S the static friction, v_S the Stribeck velocity and α_f is an empiric parameter, which defines the Stribeck region (VÍGOLO, 2018). The relationship between the Coulomb, static, and viscous friction is presented in Figure B.2.

Figure B.2 – Friction characteristics in steady-state.



Source: Adapted from Valdiero (2005).

Using equations (B.1) and (B.2), the friction force in steady-state can be represented as

$$F_{fr} = g(v) \operatorname{sgn}(v) + \sigma_2 v, \quad (\text{B.5})$$

Vígolo (2018) mention that the Equation (B.5) takes into consideration the inversion of the sign using the function $\operatorname{sgn}(v)$, which would be valid for actuators with symmetric friction. However, this not occur in real actuators. Therefore, the Equation (B.5) can be rewritten for positive and negative velocities, considering an asymmetric friction, being (PERONDI, 2002; VALDIERO, 2005; TEIXEIRA 2015; VIGOLO; 2018)

$$F_{fr} = \begin{cases} F_{C_p} + (F_{C_p} - F_{C_p}) e^{-\left(\frac{v}{v_{sp}}\right)^{\alpha_{fp}}} + \sigma_{2p} v, & \text{for } v > 0 \\ F_{C_n} + (F_{C_n} - F_{C_n}) e^{-\left(\frac{v}{v_{sn}}\right)^{\alpha_{fn}}} + \sigma_{2n} v. & \text{for } v < 0. \end{cases} \quad (\text{B.6})$$

According to Teixeira (2012), the determination of the parameters σ_0 and σ_1 is less direct, since it is difficult to measure small displacements (μm) in mechanical systems. According to Belan (2018), a good approximation value for σ_1 is 0.1 kg/s, based on the results

obtained by Yanada *et al.* (2010) and Tran *et al.* (2014). Åström & Canudas-de-Wit (2008) mention that the σ_1 can be obtained according to (B.7). where a critically damped system is considered, thus

$$\sigma_1 = 2\xi\sqrt{\sigma_0 m} - \sigma_2, \quad (\text{B.7})$$

where m (kg) is the total mass in movement.

APPENDIX C – Optimization algorithm guidelines

In this appendix, the guidelines for the use of the optimization algorithm will be presented. As mentioned in Chapter 4, for the use of the optimization algorithm some parameters of the system should be already known, being:

- The maximum actuator positive and negative velocities v_{a_maxp} , v_{a_minn} [m/s];
- The maximum actuator load force F_L [N];
- The maximum admissible working and reservoir pressures p_W , p_T [Pa];
- The estimated viscous friction coefficient B [kg/s];
- The area boundary conditions (Equations (4.8), (4.9), (4.10) and (4.11));
- The number of the binary modulus in the digital pump;
- Moreover, the pump rotational frequency ω_p [rad/s].

With these parameters, the design process of the Digital Electro Hydrostatic Actuator can follow the procedure below.

For the design of the DEHA, the number of the chamber of the cylinder or the number of the binary modulus of the digital pump should be already known as a system requisite. Another important parameter is the system resolution, which will define the number of different velocities n_v that the actuator should achieve.

If the cylinder is already known and the number of different velocities, the Equation (4.25) should be used for the evaluation of the number of combinations of chambers n_{cc} . With this number and the number of different velocities, the Equation (4.28) should be used for the determinations of the number of combinations of pumps for the digital pump n_{cp} . With the determination of n_{cp} , the Equation (4.27) can be used for the determination of the number of binary modulus for the digital pump.

If the digital pump is already known and the number of different velocities, the Equation (4.27) should be used for the evaluation of the number combinations of pumps n_{cp} . With this number and the number of different velocities, the Equation (4.28) should be used for the determinations of the number of combinations of chambers for the cylinder n_{cc} . With the determination of n_{cc} , the Equation (4.28) can be used for the determination of the number of chambers for the cylinder. Following this procedure, it is possible to determinate the total number of chambers for the actuator and the total number of binary modulus for the digital pump.

With the determination of the number of the chambers for the cylinder, the number of binary modulus for the digital pump and the system parameters, these data can be given as an input for the optimization algorithm. After the calculation by the algorithm, the size of the cylinder areas and the size of the volumetric displacements of the pumps are determined.

APPENDIX D – Optimization algorithm code

In this appendix, the codes for the optimization algorithm will be presented. For run this algorithm, two files should be created. The first file should contain the following code:

```
clear all
global A1 A2 A3 A4 A1_4 y pp P B Ft pt int PP1 PP2 PP3
format long
clc
%%%%%%%%%%%%%%%%%%%%%%%%%%%%%%%%%%%%%%%%%%%%%%%%%%%%%%%%%%%%%%%%%%%%%%%%
%Pumps Rotational Frequency
rot=1200;
rot_s=rot/60;

% Initial Values for the Displacement of the Pumps

pp=[1 1 1]*1e-6*rot_s;

for jj=1:length(pp)
    P(jj)=factorial(length(pp))/(factorial((length(pp)-
    jj))*factorial(jj));
    size_m_Zeros_p=sum(P');
    m_Zeros_p=zeros(size_m_Zeros_p);
end

%Ideal Conditions of Velocities
%%%%%%%%%%%%%%%%%%%%%%%%%%%%%%%%%%%%%%%%%%%%%%%%%%%%%%%%%%%%%%%%%%%%%%%%
x1=43;
x2=1;
y1=0.111;
y2=-0.111;
a=(y1-y2)/(x1-x2);
b=y1-a*x1;
for iiii=1:x1
    x(iiii)=iiii;
    y(iiii)=a*x(iiii)+b;
end
%%%%%%%%%%%%%%%%%%%%%%%%%%%%%%%%%%%%%%%%%%%%%%%%%%%%%%%%%%%%%%%%%%%%%%%%

%%% Parameters

xrp=0.05; % Steady State Displacement [m]
ts=1; % Accomodation Time [s]
wn=6/ts; % System Natural Frequency [rad/s]
vmax=0.37*wn*xrp; % System Maximum Velocity [m/s]
F=20000; % Load Force [N]
B=40000; % Viscous Friction Coefficient [kg/s]
p1=210e5; % Working Pressure [Pa]
p2=10e5; % Reservoir Pressure [Pa]
Aea=(vmax*B+F)/(p1-p2); % Equivalent Area [m^2]
pt=p2;
Ft=F;
A2=Aea;
alpha=1.2; % Flow Coefficient
A3=A2/alpha;
A1_4=A3*((alpha^2-1)/(1+alpha));
```

```

%%%%%%%%%%%%%%%%%%%%%%%%%%%%%%%%%%%%%%%%%%%%%%%%%%%%%%%%%%%%%%%%%%%%%%%%
% Limits for the pumps volumetric displacement and the cylinder areas
%[A1, A2, A3, A4, D1, D2 D3]
lb = [0.0001, A2, A3, 0.0001, 0.1, 0.1, 0.1];
ub = [0.01, A2, A3, 0.01, 30, 30, 30];

% Initial guess for design parameters
%[A1, A2, A3, A4, D1, D2 D3]

x0 = [0, A2, A3, 0, 1, 2, 3];

% Vector for linear inequalities

A = [-1 0 -1 1 0 0 0; -1 1 -1 0 0 0 0; 1 -1 0 -1 0 0 0; 0 -1 1 -1 0 0 0; 0
1 0 -1 0 0 0; 0 0 0 0 1 -1 0; 0 0 0 0 0 1 -1];
b =[0; 0; 0; 0; 0; 0; 0];

% Vector for linear equalities

Aeq = [];
beq = [];

% Non linear constraints
nonlcon = [];

%% Call Optimization
int=0; % to count the iterations and store intermediate design sets

options_fmincon = optimoptions('fmincon','MaxIter',200,'TolFun',1e-
6,'DiffMaxChange',0.000001);
fmincon(@velocity_linearization_pumps_areas,x0,A,b,Aeq,beq,lb,ub,nonlcon,op
tions_fmincon);
% A4
% [A4,fval] =
fmincon(@velocity_linearization,x0,A,b,Aeq,beq,lb,ub,nonlcon,options_fminto
n);
% A4
A4-A2
Areas=[A1 A2 A3 A4] % Vector With the Values of the Areas
Pumps =[PP1 PP2 PP3] % Vector With the Values of the Pumps Displacements
int % Number of Interactions

```

The second file should contain the follow code:

```

function phi=velocity_linearization_pumps_areas(x)
global A A1 A2 A3 A4 A1_4 y pp P B Ft pt int PP1 PP2 PP3
A1=x(1);
A2=x(2);
A3=x(3);
A4=x(4);
PP1=x(5);
PP2=x(6);
PP3=x(7);
%
A1=A4+A1_4
Aea_verif=A1+A3-A4
Aer_verif=A2+A4-A1
Aa=1.5e-3

```

```

A=[A1 A2 A3 A4] ;

np=1;
mp=P(1);
rot=1200;
rot_s=rot/60;
pp=[PP1 PP2 PP3]*1e-6*rot_s;
for jj=1:1:length(pp)
    P(jj)=factorial(length(pp))/(factorial((length(pp)-jj))*factorial(jj));
    size_m_Zeros_p=sum(P');
    m_Zeros_p=zeros(size_m_Zeros_p);
end

for jjj=1:1:length(P)
    %Calculates Combinations Taken in jjj of pumps
    combos_p =combntns(pp,jjj);
    %Replaces Combinations in the Zero Matrix for pumps
    m_Zeros_p(np:mp,1:jjj)=combos_p;
    if jjj~=length(P)
        np=np+P(jjj);
        mp=mp+P(jjj+1);
    end
end
m_pumps=m_Zeros_p;
%%%%%%For the Forward Movement%%%%%%%%
for i=1:1:length(A)/2
    %Forward movement areas
    A_avan = A(1:2:end); % Take the Odd Positions of the Vector
    %Backward movement areas
    A_rec=A(2:2:end); % Take the Even Vector Positions
    % Resultant area for the forward movement
    Ar_avan=sum(A_avan);
    % Resultant area for the backward movement
    Ar_rec=sum(A_rec);
    % Calculation The number of Combinations referring to the number of
elements
    % desired
    K(i)=factorial(length(A)/2)/(factorial((length(A)/2-i))*factorial(i));
    %Calculate the size of the matrix of zeros
    size_m_Zeros=sum(K');
    %Makes the matrix of zeros
    m_Zeros=zeros(size_m_Zeros);
    m_Zeros_rec=zeros(size_m_Zeros);
end
n=1;
m=K(1);

for j=1:1:length(K)-1
    %Calculates Combinations Taken in j
    combos =combntns(A_rec,j); %For the positive velocities
    combos_rec=combntns(A_avan,j); %For the negative velocities
    %Replaces Combinations in the Zero Matrix
    m_Zeros(n:m,1:j)=combos;
    m_Zeros_rec(n:m,1:j)=combos_rec;
    n=n+K(j);
    m=m+K(j+1);
end
m_areas_feed_rec=m_Zeros_rec; % for the backward moviment

```

```

m_areas_feed=m_Zeros;
%Calculation of Regeneration Areas Forward Moviment
for z=1:1:length(m_areas_feed)
    zz(z)=z;
    m_areas_feed_sum(z,1)=sum(m_areas_feed(z,:)); %Regenerative areas
    m_areas_feed_sum_sort=sort(m_areas_feed_sum);
end
%Calculation of Regenerative Areas Backward Moviment
for zr=1:1:length(m_areas_feed_rec)
    zzr(zr)=zr;
    m_areas_feed_rec_sum(zr,1)=sum(m_areas_feed_rec(zr,:));
%Regenerative areas
    m_areas_feed_rec_sum_sort=sort(m_areas_feed_rec_sum);
end
%Calculation of the sum of the pumps
for w=1:1:length(m_pumps)
    ww(w)=w;
    m_pumps_sum(w,1)=sum(m_pumps(w,:)); %Sum of flow rates
    m_pumps_sum_sort=sort(m_pumps_sum); %Sum of ordered flow rates
end
%Calculation of the positive velocities
for Aa=1:1:length(m_areas_feed)
    Aaa(Aa)=m_areas_feed_sum_sort(Aa);
    for Q=1:1:length(m_pumps)
        Qa(Q)=m_pumps_sum_sort(Q);
        V(Aa,Q)=m_pumps_sum_sort(Q)/(Ar_avan-m_areas_feed_sum_sort(Aa));
        ps(Aa,Q)=(V(Aa,Q)*B+Ft+(Ar_rec-
m_areas_feed_sum_sort(Aa))*pt)/(Ar_avan-m_areas_feed_sum_sort(Aa));
    end
end
%Calculation of the negative velocities
for Aar=1:1:length(m_areas_feed_rec)
    for Qr=1:1:length(m_pumps)
        Vr(Aar,Qr)=-(m_pumps_sum_sort(Qr)/(Ar_rec-
m_areas_feed_rec_sum_sort(Aar)));
    end
end
for n=1:1: numel(V)
    V_total(n)=V(n);
end
for n_r=1:1: numel(Vr)
    Vr_total(n_r)=Vr(n_r);
end
Vel_total=[V_total Vr_total 0];
Vel_total_sort=sort(Vel_total);
%Condition to be minimized
phi=sum(abs(Vel_total_sort-y));
int=int+1;
end

```